DOCTORAL PROGRAM IN BIOMEDICINE

UNIVERSITAT DE BARCELONA

DISSERTATION:

TARGETING β-CELL DEATH IN TYPE 2 DIABETES:
The Effect Of Sodium Tungstate In Irs2 Knockout Mice

Presented by:

Joana Raquel Duarte Moitinho de Oliveira

Candidate for the degree of Doctor in Biomedicine

Under the supervision of:

Dr. Ramon Gomis de Barbarà

Dr. Sandra Rebuffat

This work was developed at the Diabetes and Obesity Research Laboratory, IDIBAPS-CEK, Barcelona 2013

IDIBAPS

FCT Fundação para a Ciência e a Tecnologia
MINISTÉRIO DA EDUCAÇÃO E CIÊNCIA

AGRADECIMIENTOS

“La verdadera ciencia enseña, por encima de todo, a dudar y a ser ignorante.” Miguel de Unamuno

Ha llegado el momento de agradecer a todos los que me acompañaran a lo largo de estos casi 5 años de aprendizaje intenso, tanto a nivel profisional como personal. En primer lugar, agradecerle a mi director de tesis Ramon Gomis. Primero por haberme dado la oportunidad de desarrollar mi trabajo sob su orientación y en su grupo. Me acuerdo que me dijo en la primera entrevista que todos tenemos derecho a tener una oportunidad para aprender y demonstrar lo que valemos, y le agradezco que a mí me haya concedido esa oportunidad. Segundo, le agradezco también por siempre haber fomentado el pensamiento crítico, haberme dado la libertad para dudar pero también haberme conducido a aclarar esas dudas y tomar decisiones cientificas, aunque algunas hayan resultado mejor que otras. Al fin y al cabo, supongo que equivocarse hace parte del proceso de aprendizaje. Quisiera agradecerle también a Anna Novials por coordinar el laboratório y recordarnos en los quefaz que nuestra investigación debe incorporar un punto de vista también clínico.

En segundo lugar, y como no podría dejar de ser, agradecerle a Sandra. También me acuerdo de la primera vez que la vi, y del buen feeling que tuve. A Sandra le tengo que agradecer toda la ayuda, apoyo y amistad que me ha dado. Su comprensión no tiene límites, así como su generosidad. Ademas, me ha enseñado muchísimo y me ha salvado la vida muchas veces, como suelo decir:D Las horas tardias que hemos compartido en el laboratorio, así como nuestros cafes de charlas profisionales/personales serán ciertamente de los mejores recuerdos que tendré de mi doctorado. En tercer lugar, quisiera agradecerle a Ainhoa porque me ha iniciado en el mundo de los animales y también me ha salvado la vida muchas veces:D Debo agradecerle porque siempre que pudo me prestó su ayuda, incluso fuera de su horário de trabajo. Por ultimo, y hablando de las personas que creo que mas directamente contribuiyeron para mi trabajo, le quiero agradecer a Rosa porque me ha ayudado muchisimo en este ultimo año de tesis que dicen ser el mas difícil. Le tengo que agradecer por escucharme y aconsejarme, transmitirme tranquilidad y confianza, ademas de contribuir para mi sanidad mental:D

Ahora me queda agradecer a todos los otros 30 miembros del laboratorio, lo que quiere decir que podría estar horas escribiendo:D En primer lugar, les quiero agradecer a Montse, Lisa y Katerina que empezaron al mismo tiempo que yo, y, por lo tanto, recorrimos caminos paralelos. Agradecerles por su amistad claro, y también porque compartimos vivencias muy similares y sentimientos muy parecidos a lo largo de estos años, ademas de muchas horas de laboratorio. Os deseo mucha suerte y mucho animo para concluir la tesis y seguir vuestro camino hacía donde deseáis. Despúes le quería agradecer a Rebeca, compañera de poyata, de las morfometrias interminables y de las dudas (supongo que nos habrán juntado por eso:D). Me alegro de nuestras charlas sinceras y de haber compartido contigo tanto lo bueno como lo malo, y te agradezco por tu actitud siempre positiva y tu apoyo. Finalmente, les quiero agradecer a los mas “jovenes”, aunque me da la sensación que ya

no son tan “jovenes”. A Elena, Rita, Hugo, Analu, Elaine, Lucia, Mariona y Silvia un “muito obrigada” por vuestro apoio incondicional y comprension. Nuestras sesiones terapeuticas de té fueron fundamentales para mantener los animos. The last but not the least, quisiera agradecerle a Marce por su disponibilidad en aclararme las famosas dudas, así como a Joan-Marc, Marc Claret y Pablo. A Belén por su ayuda de organización del grupo, a Kim por su ayuda con el ingles, y a Marta Julià. Ademas, quisiera agradecerles, porque hemos compartido muchos dias en el lab, y desearles mucha suerte a Sara, Yaiza, Marc junior, Alba Moreno, Alba Franquesa, Laura, Gemma, Miriam que ya no está, Eduardo, Marta, Carlos y Valeria.

Por ultimo, y muy especialmente, agradecer esta tesis a mi família, por lo que me cambiaré al portugués.

Sem dúvida que esta tese é dedicada à minha família, porque troquei 5 anos da sua companhia para a fazer e porque era neles que eu pensava nos momentos mais saudosos e difíceis da minha tese. Em primeiro lugar, tenho que agradecer aos meus queridos pais porque sou consciente do esforço diário que eles fizeram para que eu pudesse chegar até aqui; por terem sido exigentes e também compreensivos comigo, mas principalmente por me terem ensinado um princípio que creio fundamental: que sem trabalho nao se consegue nada na vida. Obrigado por me darem tudo o que eu sempre precisei, e não me darem tudo o que eu sempre quis; estes 5 anos de tese só foram possíveis graças a voçes. E claro, que seria de mim sem as minhas segundas mães, as minhas irmãs? Muito do que eu sou aprendi com elas, e não poderia ser de outra maneira porque são as minhas melhores amigas. Também queria dedicar esta tese às minhas 2 avós, que nunca tiveram as oportunidades que eu tive, e às minhas tias, uma porque me deu muito amor e a outra porque infelizmente e da pior maneira, me despertou a curiosidade pela ciência. Por último, e como não, dedicar-la e agradecer-lhe a Norberto, por ajudar-me a digerir certas amarguras do trabalho científico, por acompanhar-me sempre mas principalmente, por não me fazer perder nunca a perspectiva.

I INTRODUCTION

1 DIABETES MELLITUS

Diabetes Mellitus is a group of metabolic disorders characterized by high blood glucose levels resulting from defects in insulin secretion, insulin action, or both (Fonseca, 2009). The vast majority of cases of diabetes fall into two broad etiopathogenetic categories, type 1 diabetes (T1D) and type 2 diabetes (T2D), discussed in greater detail below.

Diabetes mellitus is one of the most common chronic diseases in nearly all countries, and both hyperglycaemia and diabetes are important causes of mortality and morbidity worldwide, through both direct clinical sequelae and increased mortality from cardiovascular and kidney diseases. The principal symptoms of overt diabetes are excess thirst, polyuria, hunger, unexplained weight loss, fatigue and blurring of vision. With rising overweight and obesity, the concern has risen about a global diabetes epidemic, with harmful effects on life expectancy and health-care costs. Indeed, the International Diabetes Federation (IDF) announced in 2011 that 336 million people worldwide now have T2D, and that the disease is responsible for 4.6 million deaths each year, approximately one death every seven seconds (Ashcroft and Rorsman, 2012). Diabetes is no longer restricted to the Western world, and the greatest increases in disease incidence in the next few decades are expected to be in China and India, which emphasize that there is currently fast-growing diabetes pandemic. This is a major healthcare problem because diabetes increases the risk of heart disease, stroke, and microvascular complications such as blindness, renal failure, and peripheral neuropathy. Consequently, it places a severe economic burden on governments and individuals: for instance, the cost of diabetes and its complications amounts to $612 million per day in the United States alone.

1.1 Prevalence of Diabetes Mellitus

Estimates of current and future diabetes prevalence have been published previously by the World Health Organization (WHO) or by the IDF (Wild et al., 2004).

The number of people with diabetes mellitus worldwide has more than doubled over the past three decades (Chen et al., 2012). According to a recent publication by Shaw et al., the world prevalence of diabetes in 2010 was about 6.4% of the population aged 20–79 years, affecting 285 million adults, and will increase to 7.7% corresponding to 439 million adults by 2030 with considerably disparity between populations and regions. Others estimated about 347 (uncertainty interval 314–382) million adults with diabetes in 2008, which is higher than the previous 285 million estimate for 2010 (Danaei et al., 2011).

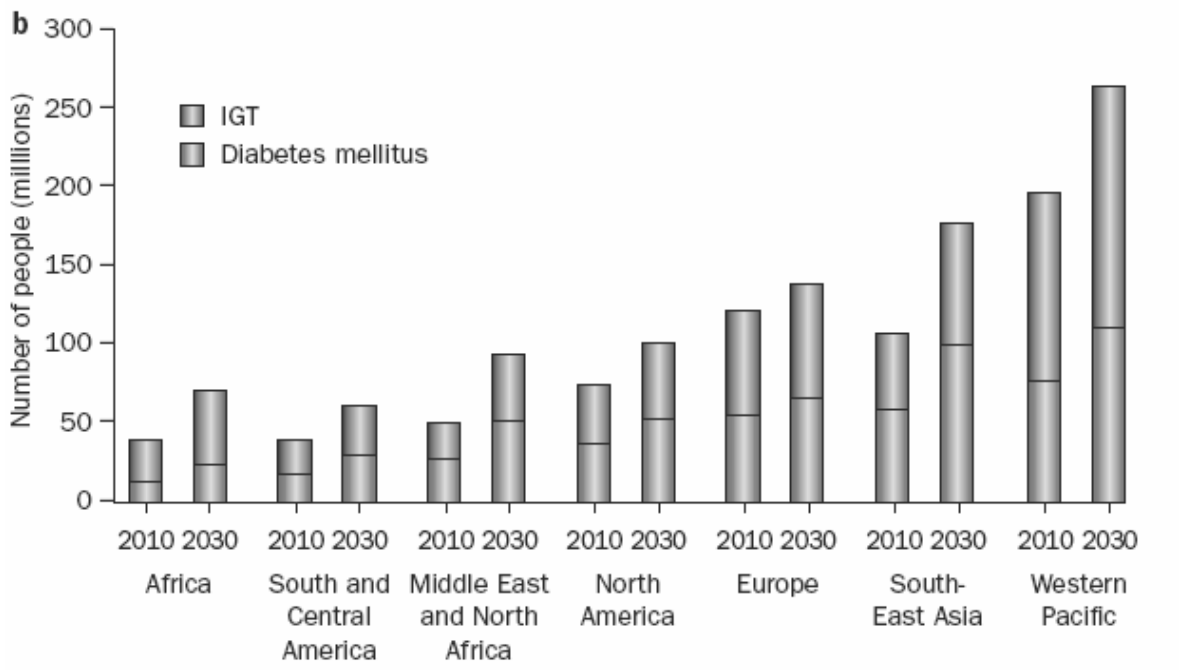

Figure 1. The number of people with diabetes mellitus and impaired glucose tolerance (IGT) (in millions) by region, among adults aged 20–79 years and for the years 2010 and 2030. Data courtesy of the International Diabetes Federation Diabetes Atlas (Chen et al., 2012).

As might be expected, the countries with the largest populations have the highest number of persons with diabetes (Table 1), (Shaw et al., 2010).

Table 1. Top 10 countries for numbers of people aged 20–79 years with diabetes in 2010 and 2030 (Shaw et al., 2010).

	2010		2030	
	Country	No. of adults with diabetes (millions)	Country	No. of adults with diabetes (millions)
1	India	50.8	India	87.0
2	China	43.2	China	62.6
3	USA	26.8	USA	36.0
4	Russian Federation	9.6	Pakistan	13.8
5	Brazil	7.6	Brazil	12.7
6	Germany	7.5	Indonesia	12.0
7	Pakistan	7.1	Mexico	11.9
8	Japan	7.1	Bangladesh	10.4
9	Indonesia	7.0	Russian Federation	10.3
10	Mexico	6.8	Egypt	8.6

According to the very recent cross-sectional population-based study, the prevalence of diabetes mellitus in Spain is 13.8%, with 6.8% having discovered diabetes during the study, and a higher prevalence in men than in women (Soriguer et al., 2012). More disturbing is that almost 30% of the studied population had some carbohydrate disturbance.

Additionally, in a recent Portuguese study aimed to determine the prevalence of T2D in Portugal, the results

were similar, as 11.7% of the Portuguese population presented diabetes, with a significant difference between men (14.2%) and women (9.5%), and 5.1% being undiagnosed (Gardete-Correia et al., 2010).
In summary, these estimates serve as a piece of evidence that diabetes is continuing to be an increasing international health burden.

1.2 Classification of Diabetes Mellitus

According to the American Diabetes Society (ADA), Diabetes Mellitus can be classified in four clinical classes (Fonseca, 2009):

1.2.1 Type 1 diabetes (T1D)

It results from β-cell destruction, usually leading to absolute insulin deficiency, and can be divided in two subclasses:

a) Immune-mediated diabetes: accounts for only 5–10% of those with diabetes, previously encompassed by the terms *insulin dependent diabetes, type 1 diabetes, or juvenile-onset diabetes*, results from a cellular-mediated autoimmune destruction of the β-cells of the pancreas. Individuals can often be identified by serological evidence of an autoimmune pathologic process occurring in the pancreatic islets and by genetic markers. Markers of the immune destruction of the β-cells include islet cell autoantibodies, autoantibodies to insulin, autoantibodies to GAD65 (Glutamic acid decarboxylase), and autoantibodies to the tyrosine phosphatases IA-2 and IA-2b. It commonly occurs in childhood and adolescence, but it can occur at any age. It has multiple genetic predispositions and is also related to environmental factors that are still poorly defined.

b) Idiopathic diabetes*:* only a minority of patients with T1D fall into this category, of those who do, most are of African or Asian ancestry. This form of diabetes is strongly inherited and lacks immunological evidence for β-cells autoimmunity.

1.2.2 Type 2 diabetes (T2D)

It is caused by an inadequate compensatory insulin secretory response in a context of resistance to the action of insulin.

This form of diabetes, which accounts for 90–95% of those with diabetes, was previously referred to as *non–insulin-dependent diabetes, type 2 diabetes, or adult onset diabetes*. It encompasses individuals who have insulin resistance and usually have relative (rather than absolute) insulin deficiency. At least initially, and often throughout their lifetime, these individuals do not need insulin treatment to survive. There are probably many different causes of this form of diabetes, but it is influenced by lifestyle factors, such as age and obesity,

and has also a strong genetic component.

Considerable progress has occurred over the last decade in our understanding of T2D, although all of the answers are not in yet. Figure 2 shows the main pathogenic factors to be discussed in this section and in sections 3 and 4 of introduction.

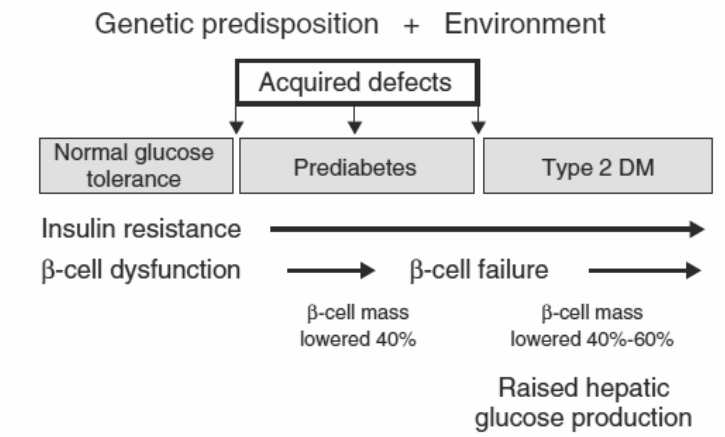

Figure 2. Proposed sequence of the key pathological features of type 2 diabetes.

a) Genetic predisposition

The fact that T2D has a genetic component is well known to clinicians by how it occurs in families, and by there being ethnic populations who are particularly high risk. Complex genetic determinants are widely considered to contribute to an inherent susceptibility to T2D. However, the pathogenesis of T2D is heterogeneous, and therefore, the contribution from individual genetic factors is modest. The genetic link was clearly shown by a famous study of identical twins in the United Kingdom that found essentially a 100% concordance rate for this disease— if one twin developed T2D, then the other one invariably developed it (Barnett et al., 1981). However, this kind of study provides no insight into how genetics act in the disease. Indeed, the genetic basis for this form of diabetes has been discovered by genome-wide association studies (GWAS), which facilitated a substantial and rapid rise in the number of confirmed genetic susceptibility variants for T2D. Since the GWAS for T2D identified novel susceptibility loci in 2007, approximately 40 T2D susceptibility loci have been identified so far in European and Asian populations (Table 2) (Imamura and Maeda, 2011). However, genetic insight into type 2 diabetes has been frustratingly elusive.

Many chromosomal hot spots have been identified in various populations are still under intense study to determine the genes involved. Also, many research groups are interested in various gene polymorphisms-common variations in the sequence of genes, sometimes in noncoding regions that may affect transcriptional regulation—that preliminary studies suggest may be linked to physiological differences. To date, however, most of them have proven to be unimportant after more rigorous study. Thus, specific answers are lacking as

to the genetic basis for T2D. It is almost certain the genetic basis for T2D and other common metabolic diseases is extremely complex—that a predisposition for the disease will require several genetic hits as opposed to just one. Also, it is generally assumed there will be many susceptibility genes for T2D, with enormous variability in different families and ethnic groups (Leahy, 2005).

Table 2. T2D susceptibility loci (Imamura and Maeda, 2011).

Year	Locus	Marker	Chr	Type of SNP	Association in the Japanese	Risk allele frequencey		Effect size odds ratio (95%CI)
						HapMap CEU	HapMap JPT	
2000	*PPARG*	rs1801282 [16]	3	Missense: Pro12Ala	Suggestive [65-67]	0.9	0.97	1.14 (1.08-1.20) [22-2
2003	*KCNJ11*	rs5219 [17]	11	Missense: Glu23Lys	Confirmed [67, 68]	0.47[a] [17]	0.34[a] [67]	1.15 (1.09-1.21) [22]
2006	*TCF7L2*	rs7903146 [6]	10	Intronic	Confirmed [14, 15, 42]	0.28	0.04	1.37 (1.28-1.47) [26]
2007	*IGF2BP2*	rs4402960 [22-24]	3	Intronic	Confirmed [36, 42, 67, 70]	0.3	0.3	1.17 (1.10-1.25) [26]
	WFS1	rs10010131 [69]	4	Intronic		0.67	0.97	1.11 (1.07-1.16)
		rs734312 [69]	4	Missense:Arg611His		0.65	0.84	1.08 (1.05-1.14)
	CDKAL1	rs7754840 [22-24]	6	Intronic	Confirmed [36, 42, 67, 70]	0.34	0.39	1.12 (1.08-1.16)
	SLC30A8	rs13266634 [20]	8	Missense:Arg325Trp	Confirmed [67, 70]	0.76	0.55	1.12 (1.07-1.16)][27]
	CDKN2A/B	rs10811661 [22-24]	9	125kb upstream	Confirmed [42, 67, 70]	0.8	0.52	1.20 (1.14-1.25)
	HHEX	rs1111875 [20]	10	7.7kb downstream	Confirmed [67, 70-72]	0.58	0.33	1.13 (1.08-1.17) [22]
	FTO	rs8050136 [23,24]	16	Intronic	Suggestive [67]	0.46	0.19	1.15 (1.09-1.22) [26]
	HNF1B	rs757210 [73]	17	Intronic	Confirmed [75]	0.45	0.24	1.12 (1.07-1.18) [27]
		rs7501939 [74]	17	Intronic		0.43	0.32	1.10 (1.06-1.15)
2008	*NOTCH2*	rs10923931 [26]	1	Intronic		0.09	0.03	1.13 (1.08-1.17)
	THADA	rs7578597 [26]	2	Missense:Thr1187Ala		0.87	0.99	1.15 (1.10-1.20)
	ADAMSTS9	rs4607103 [26]	3	38kb upstream		0.81	0.65	1.09 (1.06-1.12)
	JAZF1	rs864745 [26]	7	Intronic	Suggestive [76]	0.52	0.21	1.10 (1.07-1.13)
	CDC123/CAMK1D	rs12779790 [26]	10	Intergenic region		0.23	0.12	1.11 (1.07-1.14)
	KCNQ1	rs2237897 [36]	11	Intronic (intron15)	Confirmed [36]	0.93	0.61[a] [36]	1.41 (1.29-1.55)
		rs2237892 [37]	11	Intronic (intron15)	Confirmed [36, 37, 42, 75]	0.93	0.59	1.43 (1.34-1.52)
	TSPAN8/LGR5	rs7961581 [26]	12	Intergenic region		0.25	0.23	1.09 (1.06-1.12)
2009	*IRS1*	rs2943641 [77]	2	502kb downstream		0.61	0.93	1.19 (1.13-1.25)
	MTNR1B	rs10830963 [78]	11	Intronic		0.3	0.45	1.09 (1.06-1.12)
		rs1387153 [30]	11	Intronic		0.27	0.45	1.09 (1.06-1.11)
2010	*PROX1*	rs340874 [33]	1	2kb upstream		0.56	0.35	1.07 (1.05-1.09)
	BCL11A	rs243021 [27]	2	99kb downstream		0.48	0.7	1.08 (1.06-1.1)
	GCKR	rs780094 [33]	2	Intronic	Confirmed [75, 79]	0.61	0.43	1.06 (1.04-1.08)
	ADCY5	rs11708067 [33]	3	Intronic		0.77	1	1.12 (1.09-1.15)
	UBE2E2	rs7612463 [42]	3	Intronic	Confirmed [42]	0.86	0.84	1.19 (1.12-1.26)
	ZBED3	rs4457053 [27]	5	41kb upstream		0.26	0.023	1.08 (1.06-1.11)
	DGKB/TMEM195	rs2191349 [33]	7	Intergenic region	Confirmed [42]	0.48	0.73	1.06 (1.04-1.08)
	GCK	rs4607517 [33]	7	36kb upstream		0.2	0.2	1.07 (1.05-1.10)
	KLF14	rs972283 [27]	7	47kb upstream		0.55	0.71	1.07 (1.05-1.10)
	TP53INP1	rs896854 [27]	8	Intronic		0.44	0.32	1.06 (1.04-1.09)
	CHCHD9	rs13292136 [27]	9	234kb upstream		0.93	0.87	1.11 (1.07-1.15)
	CENTD2	rs1552224 [27]	11	5'UTR		0.88	0.96	1.14 (1.11-1.17)
	KCNQ1[b]	rs231362 [27]	11	Intronic (intron11)		0.52	0.86	1.08 (1.06-1.10)
	HMGA2	rs1531343 [27]	12	43kb upstream		0.12	0.12	1.10 (1.07-1.14)
	HNF1A	rs7957197 [27]	12	20kb downstream		0.85	1	1.07 (1.05-1.10)
	PRC1	rs8042680 [27]	15	Intronic		0.26	1	1.07 (1.05-1.10)
	ZFAND6	rs11634397 [27]	15	1.5kb downstream		0.64	0.09	1.06 (1.04-1.08)
	C2CD4A/B	rs7172432 [42]	15	Intergenic region	Confirmed [42]	0.58	0.58	1.13 (1.09-1.18)
	DUSP9	rs5945326 [27]	X	8kb upstream		0.22	0.32	1.27 (1.18-1.37)

[a] Data from references [b] This locus is thoght to be independent of the locus idenfiied by Japanese GWAS in 2008
References are in brackets

Interestingly, most of the known T2D susceptible variants appear to influence insulin secretion rather than insulin resistance. For instance, a large meta-analysis demonstrated that of 31 confirmed T2D susceptibility loci, 10 (MTNR1B, SLC30A8, THADA TCF7L2, KCNQ1, CAMK1D, CDKAL1, IGF2BP2, HNF1B, and CENTD2) were nominally associated with reduced HOMA-β and only 3 (PPARG, FTO, and KLF14) were associated with HOMA-IR. All loci identified in the Japanese GWAS, namely, KCNQ1, UBE2E2, and C2CD4A-C2CD4B were shown to be associated with decreased β-cell function in non-diabetic control groups. Prior to the accumulation of GWAS data, a genetic predisposition to insulin resistance had been considered to play the dominant role in development of T2D, especially in populations of European origin. The results obtained from GWAS, however, emphasize the crucial role of the pancreatic β-cells in the onset of T2D, and a genetic predisposition to reduced β-cell function may contribute more to the susceptibility to T2D.

b) T2D and Environment

An important concept is that the diabetes genotype typically causes only a predisposition for glucose intolerance (susceptibility). Whether one develops the diabetes phenotype depends on environmental factors, some obvious in how they act, others less so.

For instance, there is a positive association between obesity and lack of physical activity in the development of T2D (as expected), but also protection by not smoking and moderate alcohol intake. Also, many studies have shown an association between TV watching, high calorie diets, and lack of physical activity with risk of diabetes, i.e., our modern lifestyle, so it is not surprising that there is an explosion in the incidence of diabetes worldwide. What these predisposing factors share is an ability to negatively impact the glucose homeostasis system through worsening of insulin resistance or to impair β-cell function. Superimposing these factors onto a genetically compromised glucose homeostasis system raises the risk of progressing to hyperglycemia. It is the rapid emergence of these disadvantageous environmental factors that is causing the worldwide diabetes epidemic.

Concerning obesity, there is indeed a strong association to T2D, as 80% of the patients with this form of diabetes are obese, and develop some degree of insulin resistance. Patients who are not obese by traditional weight criteria may have an increased percentage of body fat distributed predominantly in the abdominal region. This form of diabetes frequently goes undiagnosed for many years because the hyperglycemia develops gradually and, at earlier stages, is often not severe enough for the patient to notice any of the classic symptoms of diabetes. Whereas patients with this form of diabetes may have insulin levels that appear normal or elevated, the higher blood glucose levels in these diabetic patients would be expected to result in even higher insulin values if their β-cell function is still normal. Thus, insulin secretion is defective in these patients and insufficient to compensate for insulin resistance.

c) Acquired Organ Dysfunction

The concept of the acquired defects is that, irrespective of the genetic and environmental factors in any individual patient, as they slip into glucose intolerance, the acquired organ abnormalities result in causing the common phenotype that characterizes the disease. Acquired defects refers to additional multi-organ defects related to glucose homeostasis that occur as the diabetes metabolic environment develops, for instance, beta-cell dysfunction, too much glucose production from the liver, and insulin resistance, which are the defects that the patients invariably present. This concept was first identified by studies that intensively treated persons with T2D to bring blood glucose values as close to normal as possible, and noted improved β-cell function, with later studies also showing some reversal of insulin resistance.

An enormous amount of research has focused on these acquired abnormalities, in particular the β-cell dysfunction. It was initially assumed the reversal effect after intensive glycemic therapy stemmed from the improvement in blood glucose level, and it was first termed glucose toxicity. Another suggestion relates to a different element of the diabetes phenotype, that the high triglycerides and free fatty acids that typically occur with T2D cause the acquired organ abnormalities, so-called lipotoxicity. The most recent idea proposes a combination of both elements, termed glucolipotoxicity. In summary, the acquired defects not only explain the multi-organ nature of the disease, but is also causative event in the transition from normal to abnormal glucose tolerance. As such, especially early in the disease, it is very important getting blood glucose values as close to normal as possible in order to maximize the reversal effect.

d) Insulin Resistance vs. β-Cell Dysfunction

One of the most controversial topics within the field of T2D over many years—is this a disease of insulin resistance or β-cell dysfunction? Both defects were invariably present when persons with T2D were investigated and also when persons with impaired glucose tolerance (IGT) were studied.

Large cross-sectional and natural history studies were performed in terms of the relative importance of β-cell dysfunction versus insulin resistance in this disease. They confirmed the findings of the earlier studies that insulin resistance occurs early in the disease, typically when glucose values are still within the normal glucose tolerance range. The reason is multifactorial—in some related to a genetic abnormality that affects insulin sensitivity, and others from lifestyle factors such as obesity, lack of exercise, high-fat diets, aging, etc. Thereafter, however, insulin resistance does not change much—once present, it remains present. Thus, it is not worsening of insulin resistance that causes blood glucose values to go from normal to IGT to diabetes, but worsening of β-cell function. The contributions of insulin resistance and β-cell dysfunction to the natural history of T2D is illustrated in sections 3 and 4 of the introduction.

1.2.3 Other specific types of diabetes due to genetic defects

a) In β-cell function: several forms of diabetes are associated with monogenetic defects in β-cell function. These forms of diabetes are frequently characterized by onset of hyperglycemia at an early age (generally before age 25 years). They are referred to as maturity onset diabetes of the young (MODY) and are characterized by impaired insulin secretion with minimal or no defects in insulin action. Abnormalities at six genetic loci on different chromosomes have been identified to date, being the most common form mutations on chromosome 12 in the hepatocyte nuclear factor (HNF)-1a (MODY1). A second form is associated with mutations in the glucokinase gene on chromosome 7p and results in a defective glucokinase molecule (MODY2). (Diagnosis and Classification of Diabetes Mellitus)
b) In insulin action: there are unusual causes of diabetes that result from genetically determined abnormalities of insulin action. The metabolic abnormalities associated with mutations of the insulin receptor may range from hyperinsulinemia and modest hyperglycemia to severe diabetes.

1.2.4 Gestational diabetes mellitus (GDM)

It is defined as diabetes or any degree of glucose intolerance diagnosed during pregnancy that is not clearly overt diabetes. Although most cases resolve with delivery, the definition applied whether or not the condition persisted after pregnancy and did not exclude the possibility that unrecognized glucose intolerance may have antedated or begun concomitantly with the pregnancy.

1.3 Diagnosis of Diabetes Mellitus

The diagnosis of diabetes has been based on glucose criteria, either the fasting plasma glucose or the 75-g oral glucose tolerance test. However, other factors were introduced as key for the diagnosis of diabetes, as described in table 3. For instance, the percentage of glycated hemoglobin, or HbA1c is a widely used marker of chronic glycemia, reflecting average blood glucose levels over a 2- to 3-month period of time (Fonseca, 2009).

Table 3. Criteria for the diagnosis of diabetes.

A1C ≥6.5%. The test should be performed in a laboratory using a method that is NGSP certified and standardized to the DCCT assay.*
OR
FPG ≥126 mg/dl (7.0 mmol/l). Fasting is defined as no caloric intake for at least 8 h.*
OR
2-h plasma glucose ≥200 mg/dl (11.1 mmol/l) during an OGTT. The test should be performed as described by the World Health Organization, using a glucose load containing the equivalent of 75 g anhydrous glucose dissolved in water.*
OR
In a patient with classic symptoms of hyperglycemia or hyperglycemic crisis, a random plasma glucose ≥200 mg/dl (11.1 mmol/l).

*In the absence of unequivocal hyperglycemia, criteria 1–3 should be confirmed by repeat testing.

The Expert Committee on Diagnosis and Classification of Diabetes Mellitus recognized an intermediate group of individuals whose glucose levels do not meet criteria for diabetes but were higher than those considered normal. This degree of hyperglycemia was sufficient to cause pathologic and functional changes in various target tissues, but without clinical symptoms, and may be present for a long period of time before diabetes is detected. During this asymptomatic period, it is possible to demonstrate an abnormality in carbohydrate metabolism by measurement of plasma glucose in the fasting state or after a challenge with an oral glucose load. Indeed, these people were defined as having impaired fasting glucose (IFG) [fasting plasma glucose levels of 100 mg/dl (5.6 mM) to 125 mg/dl (mM)], or IGT [2 h values in the oral glucose tolerance test of 140 mg/dl (7.8 mM) to 199 mg/dl (11.0 mM)]. Individuals with IFG and/or IGT have been referred to as having **pre-diabetes**, indicating the relatively high risk for the future development of diabetes. Impaired fasting glucose and/or impaired glucose tolerance can be observed as intermediate stages.

2 REGULATION OF GLUCOSE HOMEOSTASIS

Glucose is widespread in living organisms, in which, with proteins and fat, it completes the triad of the major metabolic fuels. As a metabolic substrate, glucose is present in organism essentially in its simple monomeric form (α-D-glucopyranose), and as a branched polymer of α-glucose named glycogen.

Despite periods of feeding and fasting, plasma glucose remains in a narrow range between 4 mM (75 mg/dl) and 7 mM (125 mg/dl) in normal individuals. A family of proteins residing in the plasma membrane can specifically and reversibly bind glucose molecules, and transfer them across cell membrane in both directions. They are the glucose transporters (Glut, or more generally solute carriers 2A or SLC2A).

Any given concentration of glucose in plasma is the result of simultaneous release of glucose into the circulation and uptake of glucose from the blood stream into cells. Thus, the stability in plasma glucose levels observed in a healthy adult depends on the normal regulation of insulin secretion from the pancreatic β-cells and the anabolic action of insulin on its target tissues. The control of the carbohydrate metabolism is a result of the crosstalk between several tissues (Saltiel and Kahn, 2001). However, as peripheral glucose uptake, hepatic glucose metabolism and impaired insulin secretion are most directly relevant actions to the clinical manifestations of diabetes (hyperinsulinemia and impaired glucose tolerance), this chapter will primarily focus on the regulation of glucose transport and hepatic metabolism, as well as on the secretion of insulin by the pancreatic compartment.

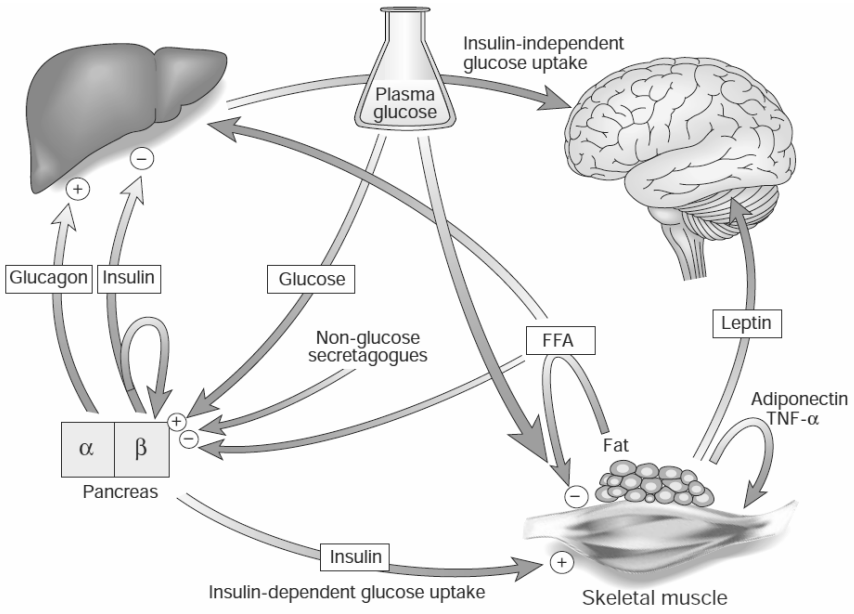

Figure 3. The crosstalk between tissues in the regulation of glucose metabolism (Saltiel and Kahn, 2001).

In mediating its pleiotrophic actions, insulin engages multiple networks of signal transduction molecules and a wide array of effector systems. Insulin alters activity of enzymatic pathways, subcellular localization of enzymes, and activation state of membrane transport systems by regulating the posttranslational modification, translation and degradation of proteins in cells, and by affecting gene transcription and expression. The insulin

action is initiated with specific binding to high-affinity receptors on the plasma membrane of target cells. The promulgation of insulin action can be viewed as a changing pattern of network interactions involving a web of signal molecules cascades and effector systems more than a linear cascade of sequentially interacting signal transduction molecules, which then engage specific effector systems. The final biological action represents the net synergism of the combined signaling pathways.

2.1 Role of peripheral tissues

Glucose transport is mediated through solute carriers referred to as the Glut family of facilitative glucose transporters, each with different tissue distributions, kinetic properties and sugar specificity (Garvey and Birnbaum, 1993; Khan and Pessin, 2002). The Glut4 protein is predominantly restricted to fat and muscle and responsible for insulin stimulated uptake. The rate-limiting step at which insulin stimulates uptake of glucose in muscle and fat is the translocation of Glut4 transporters to the plasma membrane.

Insulin increases glucose uptake in cells by stimulating the translocation of the glucose transporter Glut4 from intracellular sites to the cell surface in the classic insulin-sensitive tissues (adipocyte, brown fat, skeletal, heart and smooth muscle, Fig. 4) (Khan and Pessin, 2002). The activation of PI-3 kinase is critical for stimulation of Glut4 translocation to the plasma membrane, although a second pathway of insulin signaling originating from lipid rafts and resulting in the ultimate activation of a small G-protein, is also required for Glut4 translocation and glucose uptake (Khan and Pessin, 2002).

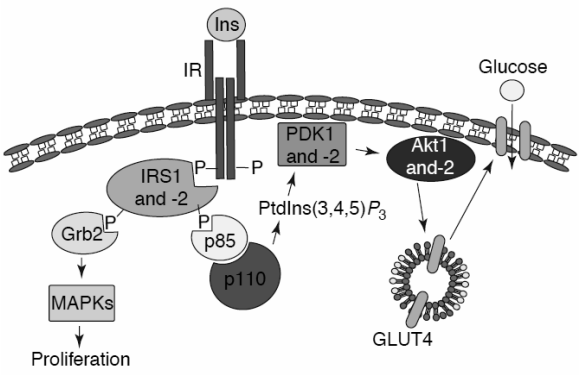

Figure 4. Insulin signaling chain of events regulating Glut4 translocation and glucose uptake in fat and muscle tissue (Thirone et al., 2006).

Up to 75% of insulin-dependent glucose disposal occurs in skeletal muscle, whereas adipose tissue accounts for only a small fraction (Thirone et al., 2006).

The role of specific tissues in the pathogenesis of diabetes has been explored using the Cre-lox DNA-recombination technology to create tissue-specific knockouts of the insulin receptor and Glut4. Despite the absence of diabetes in mice with a global knockout of Glut4, tissue-specific knockouts of Glut4 in muscle and fat have resulted in severely impaired glucose tolerance. Tissue-specific knockout of the insulin receptor has also produced surprising results. Despite recognition that insulin stimulates glucose uptake primarily in

muscle, mice with a knockout of the muscle insulin receptor have normal glucose tolerance. This occurs, at least in part, as the result of a shift of glucose uptake into fat, with subsequent increases in adipose tissue mass, circulating free fatty acids (FFAs) and triglycerides. Mice with a knockout of the fat-specific insulin receptor also have normal glucose tolerance, whereas the liver-specific insulin-receptor knockout shows both impaired glucose tolerance and decreased insulin clearance with marked hyperinsulinaemia.

2.2 Role of Liver

A primer function of the liver is contributing to the maintenance of blood-glucose homeostasis (Agius, 2008) by controlling the hepatic glucose balance through the:

1) rapid clearance of the glucose that reaches the liver via the portal vein after a meal (postprandial state);
2) controlled production of glucose in the basal state when an exogenous source of glucose is no longer available (glucose production);

Hepatic glucose production in normal subjects and in the fasted state occurs at a high rate, whereas in the fed state the rise in blood glucose leads to the consequent stimulation of insulin secretion from islet β-cells and the glucose production is stopped (Nuttall et al., 2008). The net rate of hepatic glucose production represents the balance between pathways that contribute to the formation of glucose (glycogenolysis and gluconeogenesis) and pathways that consume or store glucose (glycogen synthesis, glycolysis and the pentose monophosphate shunt). Tight control of these opposing pathways allows maintenance of glucose homeostasis in the fed and fasted states in normal subjects. The relative activities of these opposing pathways are controlled in large measure by the ratio of the pancreatic hormones insulin and glucagon. A low insulin/glucagon ratio in the fasted state favors glycogenolysis and gluconeogenesis, while a high insulin/glucagon ratio in the fed state favors glycogen synthesis and glycolysis. Insulin and glucagon controlled these pathways by activating/inactivating specific enzymes, which have different kinetic and allosteric properties from the corresponding isoenzymes that are expressed ubiquitously.

The important role played by impaired control of hepatic glucose balance in development of diabetes has motivated research into fundamental regulatory mechanisms involved in the control of liver glucose metabolism, which will be briefly described in this section.

2.2.1 Glycolysis

Glycolysis is a series of ten enzymatic reactions resulting in the conversion of glucose to pyruvate. Among the ten steps in the pathway, seven are catalyzed by enzymes with equilibrium constants that allow the reaction to proceed in either the “forward” (glycolytic) or the “reverse” (gluconeogenic) direction, depending upon physiological changes in the relative concentrations of the substrates and products of the reactions. The three other enzymatic steps, glucose phosphorylation by members of the hexokinase family (mainly hexokinase IV

or glucokinase in liver), the conversion of fructose-6-phosphate to fructose-1,6-biphosphate by phosphofructokinase (PFK), and the conversion of phosphoenolpyruvate to pyruvate by pyruvate kinase (PK) are considered to be essentially irreversible because of large release of free energy associated with these reactions. Regulation of glycolysis occurs primarily through modulation of the concentration and activity of the three enzymes that catalyze irreversible steps in glycolysis-glucokinase (GK), phosphofructokinase and pyruvate kinase. However, as glucokinase reaction is a limiting factor for glycogen synthesis from glucose in liver, more attention was paid to this enzyme.

a) Glucose phosphorylation by Glucokinase enzyme

Glucose phosphorylation in the liver is primarily catalyzed by **glucokinase** (hexokinase IV), which has a lower affinity for glucose and a higher catalytic capacity than the other members of its gene family, hexokinase I, II and III (Matschinsky, 2002). Glucose is its preferred substrate under physiological conditions, hence its widely accepted name glucokinase rather than hexokinase IV or D. In contrast, muscle and adipose cells contain mainly hexokinase II.

The transport of glucose into the liver cell is mediated by the bidirectional glucose transporter, Glut2, which is present in the membrane with high activity levels and maintains the intracellular glucose concentration in near-equilibrium with the extracellular concentration. Glut2 is not acutely controlled by insulin, and its transport capacity is not rate limiting for the hepatic uptake or release of glucose. This implies that the concentrations of glucose in the blood and in hepatocytes are the same, which enables the liver to function as a sensor of the blood glucose concentration (Bollen et al., 1998).

The enzyme glucokinase is both expressed in the liver and in pancreatic β-cells. It serves as a glucose sensor for insulin secretion in β-cells and glucose-sensory cells in the hypothalamus and gut. Collectively, these cells may be conceptualized as an integrated system of glucokinase-containing cells. Glucokinase operates as a monomer and phosphorylates glucose on carbon 6 with MgATP as the second substrate to form glucose-6-phosphate (G6P) (Matschinsky, 2002). The phosphorylation of glucose to glucose-6-phosphate is the first step of both glycolysis and glycogen synthesis.

In the liver, glucokinase is regulated by hormonal control of gene transcription and by rapid mechanisms that involve glucose-induced dissociation from a specific glucokinase-binding protein, the glucokinase regulatory protein (GKRP). The major role of glucokinase in the control of blood glucose is evident from the impaired glycogen synthesis in murine models of liver-specific knockdown of glucokinase and from the effect of glucokinase mutations on glucose homeostasis in human and animal models.

b) Phosphofructokinase

Another highly regulated reaction of glycolysis in liver is catalyzed by phosphofructokinase, which catalyzes the conversion of fructose-6-phosphate to fructose-1,6-biphosphate, with ATP serving as the phosphate donor. The most important allosteric regulator of phosphofructokinase activity in liver is fructose-2,6-biphosphate.

c) Pyruvate kinase

Pyruvate kinase catalyzes the last of the irreversible steps of glycolysis in liver. Like the other glycolytic enzymes, glucokinase and phosphofructokinase, transcription of pyruvate kinase is decreased by fasting or insulinopenic diabetes, and is increased in the fed state or by insulin injection.

2.2.2 Glycogen Metabolism

The mammalian cells are able to store glucose in the form of large polymers known as **glycogen** (Bollen et al., 1998). Glycogen is present in most cells in cytoplasmic granules that encase the enzymes that regulate its metabolism. In normal humans, the largest part of glycogen stores is in liver and skeletal muscle. The conversion of glucose into glycogen is one of the key pathways by which the liver removes glucose from the portal vein after a meal. Thus, liver glycogen serves as a reserve of glucose for extrahepatic tissues, which can be rapidly reconverted into glucose to maintain blood-glucose homeostasis. As a consequence, the level of hepatic glycogen changes considerably (between 1 and 100 mg/g) with the feeding condition. The transition from net degradation of glycogen in the fasting state to net synthesis in the postprandial state is regulated primarily by the blood-glucose concentration, as well as by the insulin/glucagon ratio and by a mechanism described as the 'portal signal' that involves autonomic innervation of the liver, and is activated by the glucose concentration in the portal vein.

In liver, glycogen can be synthesized via a *"direct" pathway*, involving transport of glucose from de blood and its phosphorylation to yield glucose-6-phosphate, or by an *"indirect" pathway* involving synthesis of glucose-6-phosphate from gluconeogenic precursors. Glycogen degradation, or glycogenolysis, is initiated by removal of glucose residues from the outer termini of the glycogen molecule. The metabolism of glycogen is controlled by irreversible cascades of enzymatic reactions that ultimately act upon the enzymes that catalyze glycogen synthesis (glycogen synthase) and degradation (glycogen phosphorylase, GP). For these two symmetric pathways, reverse phosphorylation/dephosphorylation cycles convert inactive enzymes into their active counterparts.

a) Glycogen synthesis (Glycogenesis)

Once glucose enters the hepatic cells, the first reaction is the ATP-dependent phosphorylation to glucose-6-phosphate, catalyzed by glucokinase enzyme as described above (Agius, 2008). The glucokinase reaction is a limiting factor for glycogen synthesis from glucose in the liver. In detail, glucose-6-phosphate is converted into glucose-1-phosphate by phosphoglucomutase, and then to UDP-glucose by UDP-glucose pyrophosphorylase. **Glycogen synthase (GS)** catalyses the transfer of glucosyl units from UDP-glucose to glycogen (Fig.5).

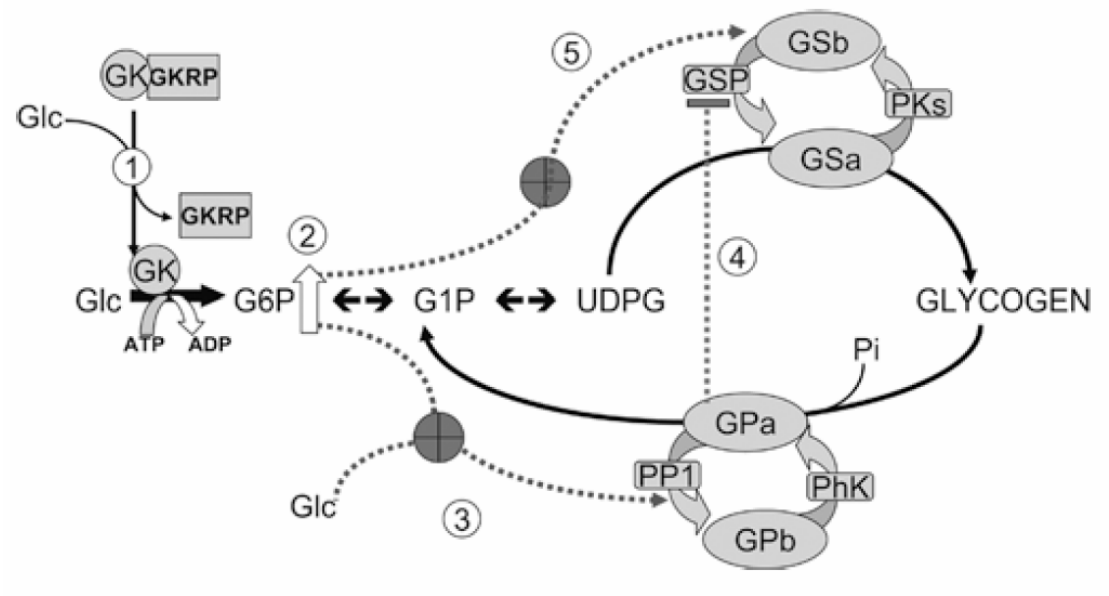

Figure 5. Conversion of glucose into glycogen in liver (Agius, 2008).

Glycogen synthase is tightly controlled by the reversible phosphorylation of multiple serine residues by various protein kinases as PKA (Protein Kinase A), phosphorylase kinase, AMPK (adenosine monophosphate-activated protein kinase), calmodulin-dependent kinase, GSK-3 (glycogen synthase kinase 3) and casein kinase-2, which causes its inactivation (Bollen et al., 1998). In contrast, dephosphorylation causes activation and is catalyzed by glycogen synthase phosphatase.

Progressive phosphorylation decreases the affinity for the substrate, UDP-glucose, and for the allosteric activator, glucose-6-phosphate. The activation state is conventionally assayed as the activity ratio in the absence/presence of glucose-6-phosphate, representing GSa (active glycogen synthase)/total enzyme [GSa + GSb (inactive glycogen synthase)] because the unphosphorylated form is active in the absence of glucose-6-phosphate, whereas the phosphorylated forms are dependent on allosteric activation by glucose-6-phosphate (Guinovart et al., 1979). Several studies have provided evidence for a correlation between the activity ratio of glycogen synthase and the cellular glucose-6-phosphate content during incubation of hepatocytes with various glucose concentrations and hexokinase inhibitors or during overexpression of glucokinase or glucose 6-phosphatase.

Glucagon and glucose, the major physiological stimuli for the inactivation and activation of glycogen synthase respectively, affect the phosphorylation level of many sites, suggesting the involvement of multiple protein kinases and/or protein phosphatases. Also, insulin promotes the dephosphorylation and activation of glycogen synthase by suppressing glycogen synthase kinase-3 (GSK3) activity. For instance, the activation of the insulin-signaling cascade activates protein kinase B (PKB/AKT), which phosphorylates and thereby inhibits GSK3, leading to the dephosphorylation of glycogen synthase by the glycogen-associated form of protein phosphatase 1 (PP1β.GM), and the stimulation of glycogen synthesis (Cohen and Goedert, 2004).

b) Glycogenolysis or glycogen degradation

Glycogenolysis is initiated by removal of glucose residues from the glycogen molecule and is catalyzed by the active form of **glycogen phosphorylase (GP)** (Fig. 4). GP catalyzes phosphorolytic cleavage of the α-1,4 bonds of the glucose polymer to form glucose-1-phopshate. Glucose-1-phosphate is then converted to glucose-6-phopshate. The activity of GP is regulated by allosteric effectors and by phosphorylation of a serine residue at the N-terminus by phosphorylase kinase, which converts the enzyme from unphosphorylated GPb into the active phosphorylated GPa (Fig. 4). Glucose is an important physiological regulator of GP in liver. It binds to the catalytic site and stabilizes the inactive T-conformation, resulting in enhanced dephosphorylation (inactivation). Consequently, GP has been classically regarded as the 'glucose sensor' for control of hepatic glucose production (Bollen et al., 1998). Glycogen degradation in liver is most active in fasting states, and the physiological goal is to deliver glucose to the circulation to support the needs of the brain and the central nervous system.

2.2.3 Gluconeogenesis

Gluconeogenesis is the metabolic pathway by which certain mammalian tissues, primarily liver and kidney, are able to synthetize glucose from carbon precursors such as alanine, pyruvate, lactate and glycerol (Nuttall et al., 2008). These precursors are converted to pyruvate, which is carboxylated to yield oxaloacetate, catalyzed by mitochondrial pyruvate carboxylase. Oxaloacetate is then converted to malate, which is transported out of the mitochondria, and reconverted to oxaloacetate. Finally, oxaloacetate is decarboxylated to yield the intermediate phosphoenolpyruvate by the enzyme **Phosphoenolpyruvate carboxylase (PEPCK)**, which is the rate-limiting step in gluconeogenesis, Phosphoenolpyruvate is converted to fructose-1,6-biphosphate via six enzymatic steps common to glycolysis. Fructose-1,6-biphosphate is the converted to fructose-6-phosphate by fructose-1,6-biphophosphatase enzyme, which is finally converted to glucose-6-phosphate. The terminal step of gluconeogenesis is the hydrolysis of glucose-6-phopshate to glucose, catalyzed by the glucose 6-phosphatase complex (Nuttall et al., 2008).

Insulin inhibits the production and release of glucose by the liver by blocking glycogenolysis and gluconeogenesis (Nuttall et al., 2008). Whereas glycogenolysis is regulated by rapid changes in the phosphorylation state of GP, gluconeogenesis is regulated by slower mechanisms through changes in gene expression. Insulin controls the activities of a set of metabolic enzymes by phosphorylation or dephosphorylation and also regulates the expression of genes encoding hepatic enzymes of gluconeogenesis. Importantly, it inhibits the transcription of the gene encoding PEPCK, and also the transcription of fructose-1,6-biphophosphatase and glucose-6-phosphatase. Gluconeogenesis is most active in the fasted condition or insulinopenic states, where the glucagon/insulin ratio rises, increasing the transcription of these genes in a gradual and coordinated manner. Also, in the fasted state, glucagon promotes lipolysis in adipose tissue, leading to an increase in circulating free fatty acids, which are transported to the liver mitochondria to suffer

oxidation. The products of fatty acid oxidation in the fasted state supply energy for the initial steps of gluconeogenesis that are energetically expensive.

2.3 Role of Pancreas

The pancreas is the organ responsible for the production of several hormones crucial for the maintenance of glucose homeostasis, including the insulin. It lies adjacent to the larger curvature of the stomach and is composed of the exocrine compartment composed by the acinar cells, which produces digestive enzymes that are drain into the duodenum via the pancreatic duct, and the endocrine compartment composed by the islets of Langerhans, which secretes hormones to the circulation (Steiner et al., 2010).

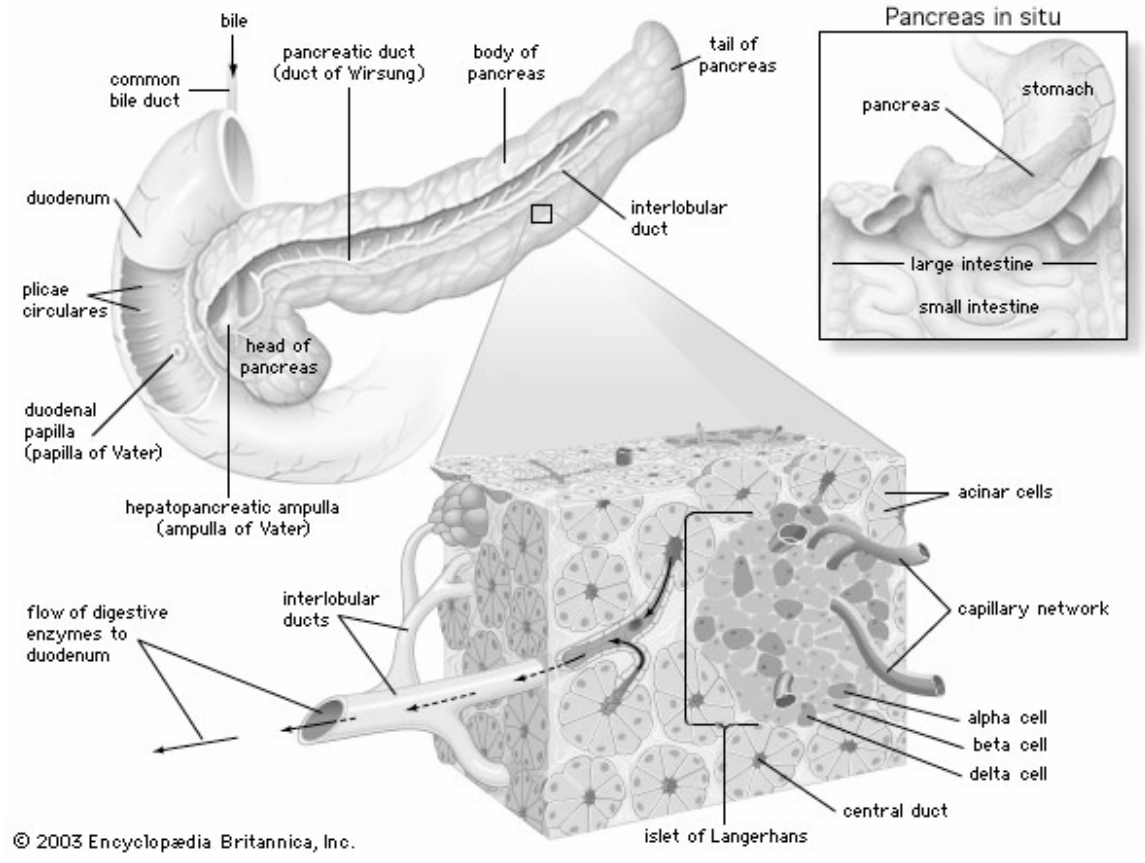

Figure 6. Structure of the Pancreas.

2.3.1 Morphology of the Pancreas

Anatomically, the pancreas is divided into three regions: the head, which lies adjacent to the duodenum; the body, which is the central part lying under the greater curvature of the stomach; the tail, the portion adjacent

to the spleen. The islets of Langerhans appeared to be distributed throughout the exocrine tissue, but remain relatively close to the ducts as a result of their embryological origin from the pancreatic ducts. Islet density is considered to be higher in the tail of the pancreas compared to the body region, but it is highest in the portion of the head.

The endocrine pancreas, which is 2-5% of the total pancreatic mass, is composed by the islets of Langerhans. These are highly vascularized micro-organs consisting of several endocrine cell types that function together to maintain glucose homeostasis.

2.3.2 Structure of the Islets of Langerhans

The islets of Langerhans consist of five main cell types (Steiner et al., 2010). The major hormone-secreting cell type is the β-cell, which secretes insulin. In rodent islets, β-cell represents 60–80% of total cells, and are predominating clustered in the core of α-cells. α-cells represent 15–20% of the cells of the islet and secrete glucagon. δ-cells are less than 10% of islet cells and secrete somatostatin, whereas pancreatic-polypeptide containing cells (PP-cells) and ε-cells (ghrelin) are very infrequent (<1% of cells). More than 90% of the endocrine cell mass is present in the islets but some isolated endocrine cells or small single cell clusters (defined as consisting less than five cells) are found in or adjacent to the ducts or scattered whining the exocrine tissue. However, it is unclear if these are functional units that can release hormones in response to a stimulus such as glucose. Current islet studies distinguish human islet architecture from that of rodents. In rodents, β-cells are located toward the center of the islet and surrounded by a mantle of non β-cells. However, human islets tend to contain fewer β-cells and more α-cells compared to rodent islets and have been described as maintaining a more scattered organization of endocrine cells (Fig. 7) (Cabrera et al., 2006).

Figure 7. Islet architecture varies between species (Cabrera et al., 2006).

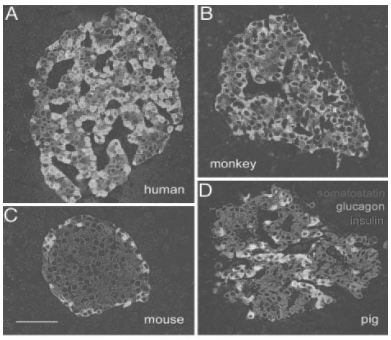

Interestingly, islet composition varies not only between species, but also within species (Fig. 8). Indeed, islet structure is not static but changes in response to normal physiology, including pregnancy, and pathophysiology states such as obesity and diabetes (Steiner et al., 2010).

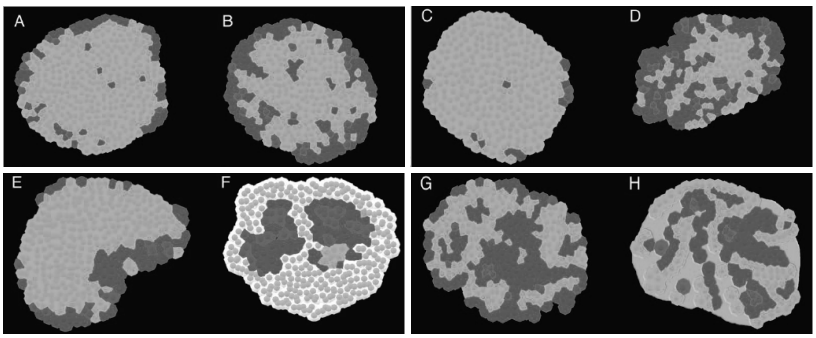

Figure 8. Murine and human islets display a wide array of morphologies under various physiological conditions. (A) Wild-type mouse (B) Pregnant mouse (C) ob/ob mouse (D) db/db mouse (E) Neonatal mouse (P14) (F) NOD mouse (G) Normal human (41 yr) (H) Type-2 diabetic human, cellular amyloid deposits in pink. α-cells (red), β-cells (green), and δ-cells (Szot et al.) (Steiner et al., 2010).

The endocrine cells are generally associated with blood vessels. Some studies point that 86% percent of the glucagon-immunoreactive and 77% of the insulin-immunoreactive cells were closely apposed to immunostained vascular endothelial and smooth muscle cells. These association with blood vessels is particularly important because allows that secretory granules docked at the plasma membrane can be released by exocytosis into the extracellular space, as a result of stimulus-secretion coupling (Cabrera et al., 2006). Insulin is stored in secretory granules and secreted by β-cells that are connected by tight junctions, which allows coordinated secretion from β-cells within an islet. Immature granules contain the precursor peptide proinsulin and in the mature granules, proteolytic cleavage results in separation of insulin, which forms crystals with zinc. Granule content of β-cells were estimated in 13 000 per cell in in the mouse (Rorsman and Renstrom, 2003). As a result of stimulus-secretion coupling, granules docked at the plasma membrane are released by exocytosis into the extracellular space, where the hexamer dissociates and insulin diffuses to the islets capillaries.

2.3.3 Regulation of insulin secretion

The cytoplasm of each β-cell is filled with insulin secretory granules and each granule stores about 200 000 insulin molecules. During glucose stimulation only a small proportion of the granules undergo exocytosis. In all mammals, including humans, the postprandial insulin secretion is regulated in a biphasic manner by nutritional and hormonal signals, but the primary regulator is glucose. Other secretagogues such as free fatty acids, amino acids or the incretin regulator glucagon-like peptide-1 (GLP1) serve as potentiators, requiring a threshold stimulatory level of glucose in the bloodstream before their effects are engaged. The β-cell rapidly adapts the rate of insulin secretion to fluctuations in the blood glucose concentration. Short-term changes in glucose concentration are controlled probably at the level of exocytosis of preformed insulin, whereas longer-term changes also involves changes in the transcription rate of the insulin gene, translation of the mRNA and processing of the proinsulin molecule into mature insulin.

The physiological regulation of insulin secretion from the pancreatic β-cells is now well understood (Bratanova-Tochkova et al., 2002; Henquin et al., 2002). Exocytosis of insulin granules requires an increase in intracellular calcium that results (at least in the case of glucose-stimulated insulin secretion, GSIS) almost entirely from calcium influx through plasmatic voltage-gated calcium channels. Their opening is controlled by the ATP-sensitive potassium channel, which links cell metabolism to the membrane potential. At low plasma glucose levels, this channel is open and K^+ efflux through the open pore keeps the membrane hyperpolarized, preventing electrical activity, calcium channel opening, calcium influx, and insulin secretion. An increase in plasma glucose levels leads to increased glucose uptake as in β-cells, as well as in hepatocytes, the concentration of glucose is rapidly equilibrated between the blood and β-cells. In rodents, the principal glucose transporter is Glut2, which transports glucose into the β-cells independently of insulin. In human β-cells the major glucose transporter is Glut1 but the role of Glut2 has been debated. Anyway, glucose equilibrates across the β-cells plasma membrane and is phosphorylated by glucokinase enzyme, ensuring efficient glycolysis that produces pyruvate (Fig. 9). Pyruvate preferentially enters the mitochondria and fuels the TCA cycle, resulting in the transfer of reducing equivalents to the respiratory chain and generation of ATP. ATP is then transferred to the cytosol, raising the ATP/ADP ration, resulting in closure of ATP-sensitive K^+ (KATP) channels. The increased membrane resistance (Rm) resulting from KATP channel closure allows opening of T type Ca^{2+} channels to depolarize the β-cell. This leads to activation of voltage-gated L type and P/Q type Ca^{2+} channels and Na^+ channels, which produces action potential firing. The associated Ca^{2+} influx triggers exocytosis of insulin granules. Sulphonylurea drugs (SU also stimulate insulin secretion by closing KATP channels, but they do so by binding directly to the K^+ channel, thus bypassing the metabolic steps. These drugs have been used for almost 60 years to treat T2D.

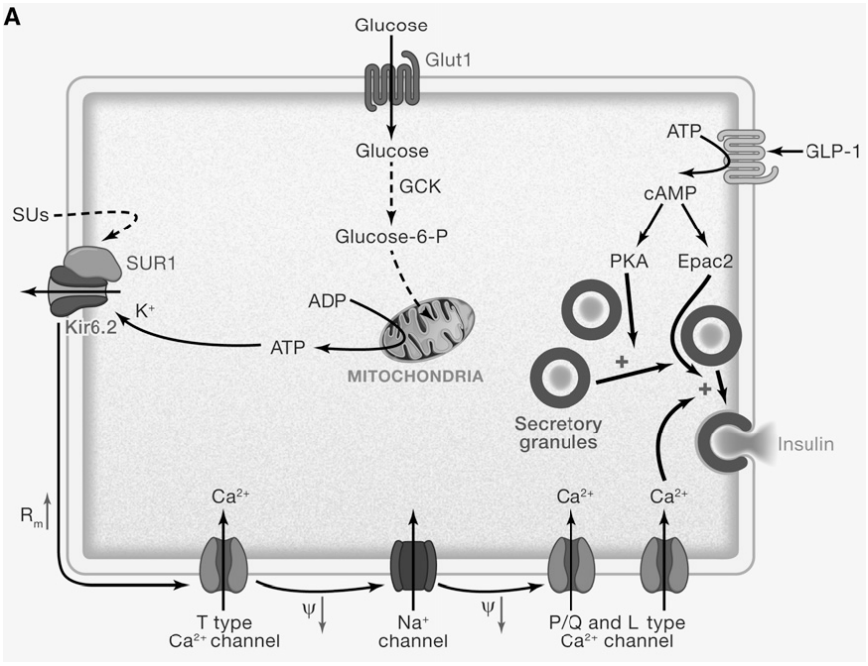

Figure 9. Stimulus-secretion coupling in human β-cell (Ashcroft and Rorsman, 2012).

The K_{ATP} channel-dependent mechanism, also known as the triggering signal, appears to be particularly important for the first, acute phase of insulin release that occurs in the first 10 minutes following glucose stimulation. However, blockade of Ca^{2+} channels abolishes both phases of insulin secretion, illustrating the absolute requirement for the elevation of cytosolic Ca^{2+} in the insulin release process.

The stimulation of insulin secretion by glucose is made in a biphasic manner: an immediate first-phase response and a second-phase response (Fig. 10) (Bratanova-Tochkova et al., 2002; Henquin et al., 2002; Rorsman and Renstrom, 2003). It has been proposed that the biphasic nature of insulin secretion reflects the existence of distinct functional pools within the β-cells. The first phase of the response consists of the rapid release of insulin and occurs within 2-5 minutes following glucose administration lasting approximately 10 minutes. It represents the rapid release if insulin that has already been synthesized and is stored in secretory granules that reside near the cell membranes and close to Ca^{2+} channels (readily releasable pool). The magnitude of the response depends on the amount of glucose that is administered and of the degree of insulin sensitivity. This first-phase response delivers insulin rapidly to the liver and is important in inhibiting hepatic glucose production.

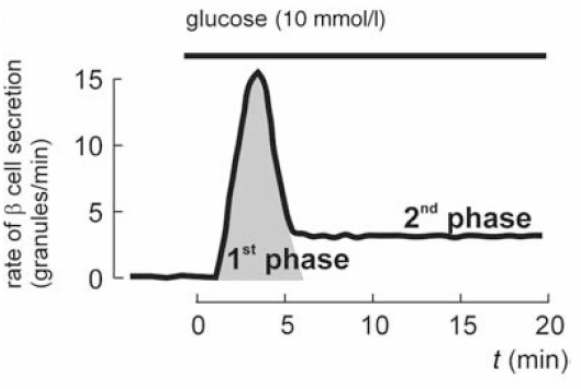

Figure 10. A Schematic of insulin secretion elicited by an increase of the extracellular glucose concentration to ≥10 mmol/l. Insulin secretion is triggered with a delay of ~1 min (the time needed for glucose to be metabolized) and then follows a biphasic time course (Rorsman and Renstrom, 2003).

Once this pool has been depleted, exocytosis proceeds at a much lower rate, possibly reflecting the physiological translocation of new granules to the release sites, producing the second-phase (Fig. 10). This phase continues as long as the glucose levels remains elevated and the insulin released depends primarily on insulin stores, but also comprises the release of newly synthesized insulin (Rorsman and Renstrom, 2003).

2.4 Overall of normal glucose homeostasis

Following nutrient ingestion, the delicate balance between endogenous glucose production and tissue glucose uptake is disrupted. Glucose concentration increases and therefore, β-cells secrete insulin to reduce blood glucose. Insulin increases glucose uptake in muscle and fat (85% in muscle and 5% in fat, which accounts for most of the insulin-dependent glucose), stimulates glycolysis and glycogenesis in muscle and liver while

inhibiting glycogenolysis and hepatic gluconeogenesis to preventing hyperglycemia (the liver changes from a state of glucose production to one of glucose storage). Insulin also stimulates de novo fatty acid synthesis in liver and adipose tissue and the mobilization of triglycerides from liver to adipose tissue. It also inhibits lipolysis and protein breakdown. Glucose uptake by the insulin-independent tissues such as the brain remains fairly constant (Fig. 11A) (Jitrapakdee, 2012).

If the glucose level falls too far, islet α-cells secrete glucagon, which stimulates the breakdown of glycogen to glucose in the liver and therefore increases blood glucose between meals. Glucagon stimulates fat mobilization from adipose tissue to skeletal muscle for energy production. Glycerol released from lipolysis, amino acids from muscle protein breakdown, and lactate generated from muscle and red blood cells (RBCs) are transported through the circulation to the liver where they serve as substrates for gluconeogenesis. Glucagon stimulates short-term production of glucose via glycogenolysis while it also stimulates long-term production of glucose via gluconeogenesis. Therefore, in fasting state, plasma glucose is maintained within the normal range. Glucose disposal in the fasting state occurs mainly by insulin-independent mechanisms, with the central nervous system accounting for approximately 80% and the rest 20% occurring in other tissues in an insulin-dependent mechanism, primarily muscle. The glucose produced by these two pathways provides fuel for RBCs and the brain (Fig. 11B).

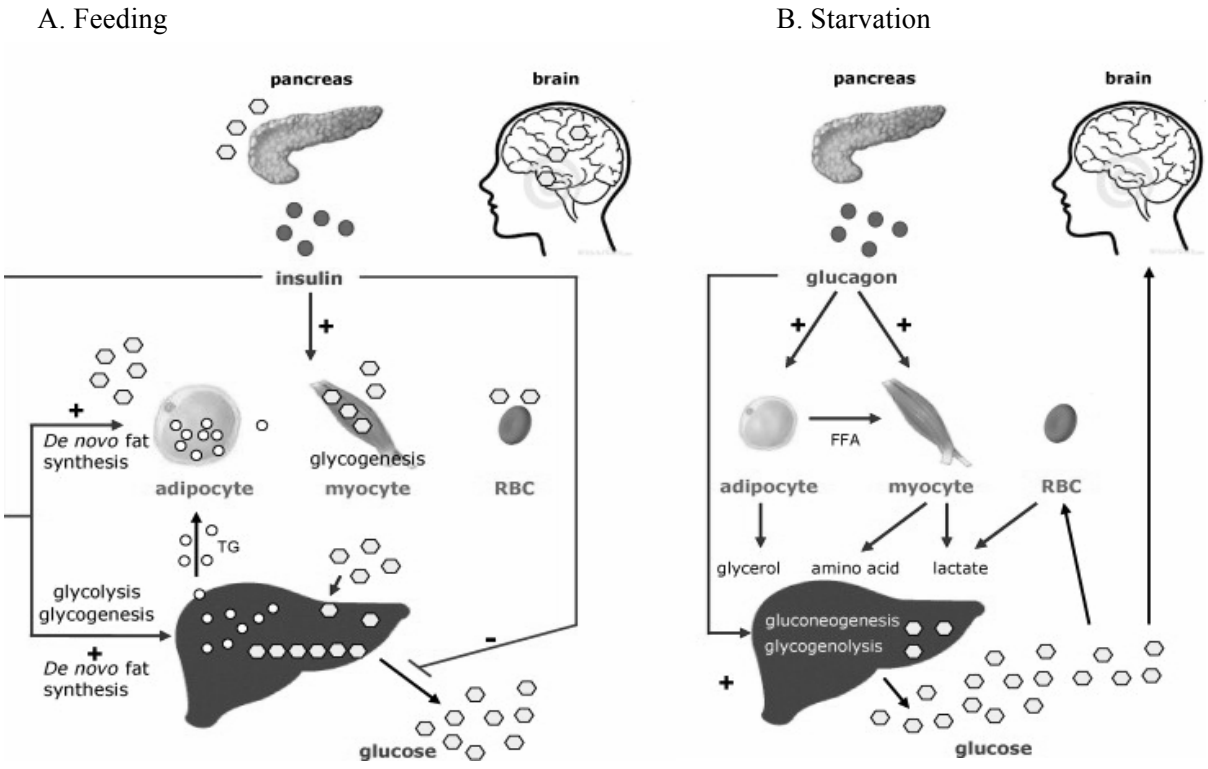

Figure 11. Hormonal regulation of fuel during feeding and starvation (Jitrapakdee, 2012).

3 PATHOPHYSIOLOGY OF TYPE 2 DIABETES

3.1 Glucose homeostasis in Type 2 Diabetes

As reviewed in the anterior section, the maintenance of normal whole body glucose homeostasis is dependent upon:

1) Insulin secretion;
2) Tissue glucose uptake
    (a) Peripheral (primarily muscle)
    (b) Splanchnic (liver plus gut)
3) Suppression of hepatic glucose production

Therefore, the maintenance of normal glucose homeostasis is dependent on a finely balanced dynamic interaction between tissue (muscle and liver) sensitivity to insulin, and insulin secretion. Even in the presence of severe insulin resistance, a perfectly normal β-cell is capable of secreting sufficient amounts of insulin to offset the defect in insulin action. Thus, the evolution of T2D requires the presence of defects in both insulin secretion and insulin action.

Therefore, type 2 diabetic individuals always present:

a) Insulin resistance involving mainly muscle and liver
b) Defects in insulin secretion

3.1.1 Insulin Resistance

Insulin resistance is defined as impaired insulin-mediated glucose clearance into target tissues. Both the liver and muscle are severely resistant to insulin in individuals with T2D (DeFronzo, 2004; Defronzo, 2009; Leahy, 2005). However, it is important to distinguish what is responsible for the insulin resistance in the basal or fasting state and what is responsible for the insulin resistance in the insulin-stimulated state.

a) Liver

Under basal or fasting conditions, the liver is the principal organ that produces glucose, which is used in an insulin-independent manner principally to meet the needs of the brain and other neural tissues. In T2D subjects, the rate of basal hepatic glucose production (HGP) is increased compared to nondiabetic individuals. The rise in HGP is correlated with increased fasting plasma glucose concentration in T2D subjects. The severity of dysfunction in terms of hepatic glucose balance is determined by the extent to which insulin concentration or action is impaired. Because insulin is a potent inhibitor of hepatic glucose production, hepatic resistance to the action of insulin must be present to explain the excessive output of glucose by the liver. Indeed, the overproduction of glucose by the liver occurs in the presence of increased fasting insulin levels,

indicating severe resistance to the suppressive effects of insulin on HGP. Thus, the inability of insulin to suppress hepatic glucose production is a key defect found in T2D individuals.

In addition to hepatic insulin resistance, multiple other factors contribute to accelerated rate of HGP including increased circulating glucagon levels and enhanced hepatic sensitivity to glucagon; lipotoxicity leading to increased expression and activity of phosphoenolpyruvate carboxykinase and pyruvate carboxylase and glucotoxicity, leading to increased expression and activity of glucose-6-phosphatase.

The glucose released by the liver can be derived from either glycogenolysis or gluconeogenesis. The majority of evidences support increased gluconeogenesis as the major cause of the increase in hepatic glucose production in T2D patients, but it is likely that accelerated glycogenolysis also contributes. Considerable evidence from both animals and human studies has implicated increased activity of PEPCK and Glucose-6Pase (gluconeogenesis) in the accelerated rate of hepatic glucose production in diabetic states. Also, the transcription of PEPCK gene is heavily regulated with the involvement of many transcriptional factors and has been reported to be upregulated in diabetic rodent models; other reports did not find upregulation of PEPCK in patients with T2D. Regarding glycogenolysis, and since glucose inactivates GPa, and thereby glycogenolysis, perturbations in the concentration of this metabolite may account for the decline in glucose effectiveness in diabetes.

By contrast, glucokinase activity was found to be decreased in morbidly obese subjects with diabetes, but elevated in newly diagnosed subjects with T2D. Hepatic glycogen synthesis, which is expected to parallel glucokinase activity, is decreased in subjects with type 2 diabetes or glucokinase mutations (MODY-2).

b) Muscle

In response to a physiological increase in plasma insulin concentration muscle glucose uptake increases linearly, reaching a plateau value. In contrast, in lean T2D patients, the onset of insulin action is delayed and the ability of the hormone to stimulate glucose uptake is markedly blunted, meaning that the primary site of insulin resistance during euglycemic insulin clamp resides in the muscle. Indeed, several studies demonstrated that muscle insulin resistance could account for over 85–90% of the impairment in total body glucose disposal in T2D subjects in the fed state.

In T2D subjects, the major muscle defect is impaired glucose transport into the cell and its phosphorylation, combined with defective storage as glycogen (De fronzo 2004). Instead of genetic defects in the glucose transport machinery or alternatively in the insulin receptor or its downstream cascade of factors, the current concept for muscle insulin resistance is the presence of defects in insulin signaling cascade.

In summary, insulin resistance involving both muscle and liver is a characteristic feature of the glucose intolerance in T2D individuals. In the basal state, the liver represents a major site of insulin resistance, with overproduction of glucose, which is the primary determinant of fasting hyperglycemia in T2D individuals. With eating failure of adequate insulin-mediated nutrient clearance into skeletal muscle combined with an

attenuated suppression of HGP cause the raised postprandial glycaemia, and contributes approximately equally to the disturbance in whole-body glucose homeostasis in T2D.

3.1.2 Defects in insulin secretion

Although the plasma insulin response to the development of insulin resistance is typically increased during the natural history of T2D (Fig. 12), this does not mean that the β-cell is functioning normally.
In healthy human subjects, as well as in animals, the insulin response to a meal normally occurs in a biphasic pattern, and the amount of insulin released is highly responsive to the prevailing glucose value. This biphasic pattern has an early phase, characterized by a rapid pulsatile pattern that appears to be intrinsic to the β-cells and occurs with a frequency of 6-10 minutes, followed by a gradually increasing phase of insulin secretion that persist as long as the hyperglycemic stimulus is present. As glucose tolerance moves from normal to minimally impaired, the insulin secretion that occurs within the first 30 min of eating (first phase) becomes markedly attenuated resulting in an elevated postprandial rise in glycemia (physiologic definition of impaired glucose tolerance). It is this postprandial hyperglycemia that causes the insulin secretion after the first 30 min (second phase) to be higher as a compensatory response. Indeed, studies examining subjects with impaired glucose tolerance or diabetes have demonstrated that not only the basal pattern of insulin release is disrupted but also the quantity of insulin released in response to a stimulus is diminished, principally the early response that occurs in the first 30 minutes of glucose ingestion (Perley and Kipnis, 1967). It has been suggested that in T2D subjects, the β-cells are unable to adequately sense or respond to fluctuations in glucose, and the onset of β-cell failure occurs much earlier and is more severe than previously appreciated (Gerich, 1998; Perley and Kipnis, 1967).

In summary, in individuals with T2D, both the first and second-phase responses to glucose are diminished, but the lack of the first phase response is an indispensable criteria for diabetes, being absent in all hyperglycemic individuals.

All together, impaired insulin secretion, decreased muscle glucose uptake, increased HGP, and decreased hepatic glucose uptake all contribute to the glucose intolerance in T2D individuals (Defronzo, 2009; DeFronzo, 2010; Leahy, 2005). However, the contribution of other tissues as pivotal in the pathogenesis of T2D cannot be disregarded and despite this thesis does not concern these other players, their contribution to T2D will be briefly described (Fig. 12).

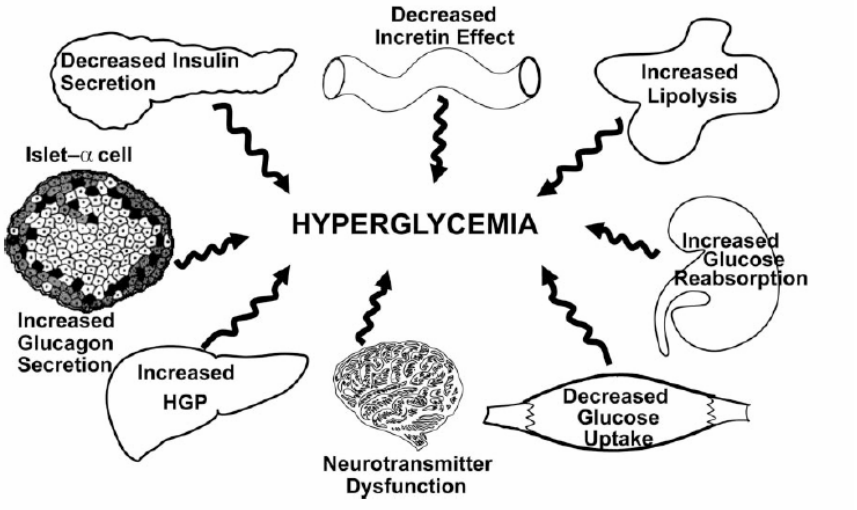

Figure 12. Several players are implicated in the pathogenesis of T2D (Defronzo, 2009).

Fat: Several evidences provide strong support for lipotoxicity and adipocyte insulin resistance in the pathogenesis of type 2 diabetes. Fat cells in intolerant or diabetic individuals are insulin resistant and have diminished capacity to store fat resistant, leading to elevation in the plasma FFA, causing muscle/ hepatic insulin resistance (stimulate gluconeogenesis) and impaired insulin secretion.

Gastrointestinal tissues: GLP-1 secretion by the L-cells of the distal small intestine is deficient, while GIP secretion by the K-cells of the more proximal small intestine is increased, but there is resistance to the stimulatory effect of GIP on insulin secretion. GLP-1 also is a potent inhibitor of glucagon secretion and the deficient GLP-1 response contributes to the paradoxical rise in plasma glucagon secretion and impaired suppression of HGP that occurs after ingestion of a mixed meal. Clearly, the gut is a major endocrine organ and contributes to the pathogenesis of type 2 diabetes.

Pancreatic α-cell: basal plasma glucagon concentration is elevated in type 2 diabetic individuals and contribute to the increased basal rate of HGP in type 2 diabetic individuals.

Kidney: The ability of the diabetic kidney to reabsorb glucose appears to be augmented by an absolute increase in the renal reabsorptive capacity for glucose. In diabetics, instead of dumping glucose in the urine to correct the hyperglycemia, the kidney chooses to hold on to the glucose.

Brain: Recent evidence suggests that the brain has a key role in the control of energy metabolism, body fat content and glucose metabolism. Neuronal systems, which regulate energy intake, energy expenditure, and endogenous glucose production, sense and respond to input from hormonal and nutrient-related signals that convey information regarding both body energy stores and current energy availability. In response to this input, adaptive changes occur that promote energy homeostasis and the maintenance of blood glucose levels in the normal range. Therefore, the central nervous system may be considered the conductor of an orchestra

involving many peripheral organs involved in these homeostatic processes. Defects in this control system are implicated in the link between obesity and T2D. Food intake is increased in obese subjects despite the presence of hyperinsulinemia and insulin being a powerful appetite suppressant. Nonetheless, it was postulated that the insulin resistance in peripheral tissues also extends to the brain. Whether the impaired appetite regulation by insulin in obese subjects contributes to or is a consequence of the insulin resistance and weight gain remains to be determined. Also, some information is now available in the literature concerning the control of the endocrine pancreas by the autonomic nervous system. Several studies have delineated the neuronal pathways that link the central nervous system with the autonomic innervation of the endocrine pancreas, which controls α-and β-cell secretion activity and mass.

3.2 Natural history of Type 2 Diabetes

The natural history of T2D has been observed in multiple populations (Caucasians, Native Americans, Mexican Americans, and Pacific Islanders) (Bergman et al., 2002; Lillioja et al., 1987; Martin et al., 1992) (Kahn, 2001). In all of these population studies, the development of T2D is closely associated with the presence of obesity. In these populations with individuals at high risk of develop T2D, the genetic background or other factors that makes them more susceptible to develop resistance to insulin resistance. This insulin resistance occurs early in the disease, typically when glucose values are still within the normal glucose tolerance range (Leahy, 2005). Thereafter, however, insulin resistance does not change much—once present, it remains present. It places a major stress on the pancreatic β-cells to augment their secretion of insulin to offset the defect in insulin action. Nevertheless, only a subset of obese, insulin-resistant individuals progress to T2D. Indeed, as long as the β-cells are able to augment their secretion of insulin sufficiently to offset the insulin resistance, glucose tolerance remains normal. However, with time the β-cells begin to fail and initially the postprandial plasma glucose levels and subsequently the fasting plasma glucose concentration begin to rise, leading to the onset of overt diabetes. Collectively, the insulin resistance in muscle and liver and β-cell failure has been referred to as the triumvirate (Defronzo, 2009) (Fig. 13).

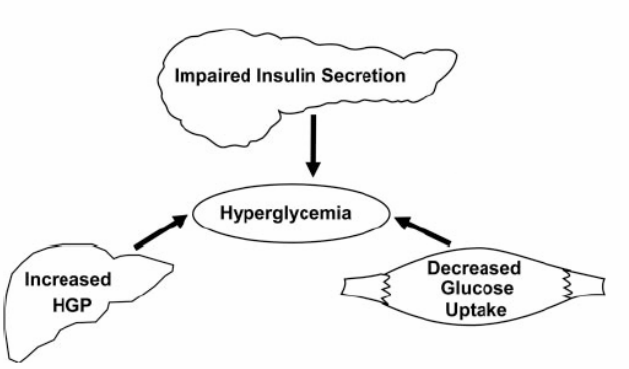

Figure 13. Pathogenesis of type 2 diabetes: the triumvirate. Insulin resistance in muscle and liver and impaired insulin secretion represent the core defects in type 2 diabetes (Defronzo, 2009).

The natural history studies of T2D invariably reported a biphasic pattern of β-cell function—hyperinsulinemia early on keeping blood glucose values normal to mildly impaired, and then a falling insulin level (so called β-cell failure) resulting in rising glycemia. This has been referred to as Starling's curve of the pancreas (Fig. 14).

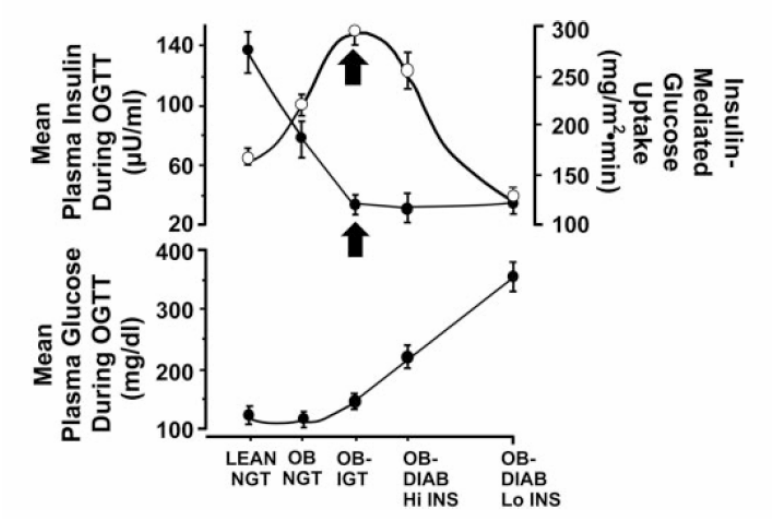

Figure 14. Natural history of type 2 diabetes and the Starling's curve of the pancreas (Defronzo, 2009).

As glycemia starts to rise, the acquired β-cell dysfunction occurs (defective first phase insulin secretion), and glycemia worsens even more, often leading to T2D. Thus, whereas insulin resistance is an important contributory pathogenic element in T2D, it is not worsening of insulin resistance that causes blood glucose values to go from normal to IGT to diabetes, but worsening of β-cell function. The current dogma is that the β-cell determines the level of glycemia in persons who are genetically at risk for T2D. The resultant hyperglycemia and poor metabolic control may cause a further decline in insulin sensitivity, but it is the progressive β-cell failure that determines the rate of disease progression (Fig. 15).

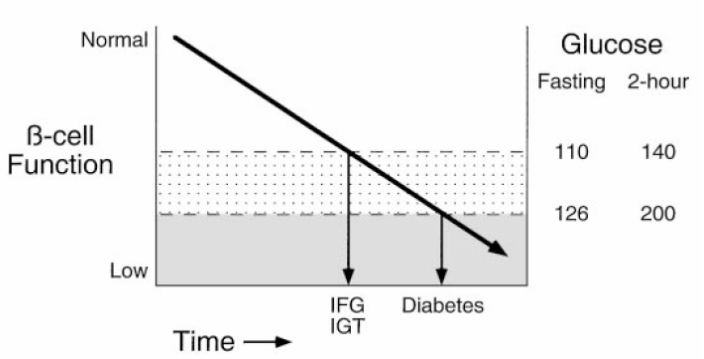

Figure 15. Model for the relationship between progressive β-cell dysfunction and deterioration of glucose tolerance (Kahn, 2001).

It was argued some years ago that the continued stimulation of an otherwise normal β-cell eventually causes it to become permanently dysfunctional, meaning that insulin resistance caused the β-cell failure through exhaustion. However, that concept does not fit the facts. Many highly insulin resistant subjects never get diabetes and only about a third of morbidly obese subjects develop diabetes. Also, the recent longitudinal data from the Pima Indians highlights the fact that β-cell function is enhanced in apparently healthy subjects as insulin resistance progresses. Also, puberty, pregnancy, and aging are times of profound insulin resistance—most of us do not get diabetes because our β-cells are able to continuously compensate. Thus, it seems that a necessary part of T2D is a compromised β-cell compensatory ability—many consider the disease to be a failure of β-cell compensation (Kahn, 2001; Leahy, 2005).

A well-known study is the one done with Pima Indians (population with the highest worldwide incidence of T2D), which shows the relationship between insulin sensitivity and insulin secretion (Weyer et al., 1999). All the subjects who started the study normally were glucose tolerant. Over the 5 years of the study, 17 went on to develop T2D (progressors) whereas 31 remained with normal glucose tolerance (nonprogressors). Note that the nonprogressors stayed on the curve throughout the study—they were insulin resistant because of obesity and likely genetic reasons, but remained normoglycemic because of perfect β-cell compensation (Fig. 16). In contrast, the progressors started below the curve—they already had evidence of β-cell dysfunction before the blood glucose level rose to the IGT range—and β-cell function continued to fall further off the curve as the level of glycemia worsened. These findings reinforce that β-cell function is the major determinant of blood glucose levels in persons who are at risk for T2D, and β-cell dysfunction occurs before blood glucose values rise into the prediabetes range.

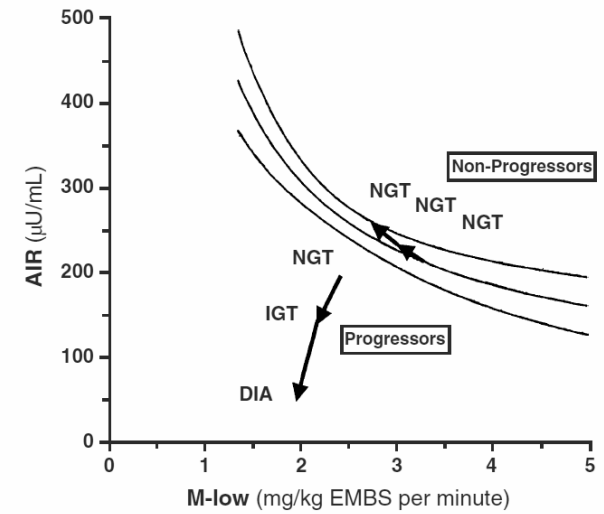

Figure 16. Relationship between a measure of insulin sensitivity on the x-axis and of insulin secretion on the y-axis. The curved lines show the normal relationship between these parameters which is usually termed the disposition index (Weyer et al., 1999).

In summary, multiple pathophysiological defects accounts to T2D appearance (Fig. 17). However, insulin resistance in liver and muscle and pancreatic β-cells are the most well demonstrated players implicated in the natural history of the disease. Although insulin resistance in liver and muscle are well established early in the natural history of the disease, T2D does not occur in the absence of progressive β-cell failure. This progressive decline in β-cell function precedes the development of hyperglycemia and continuous after the diagnosis of diabetes (Prentki and Nolan, 2006).

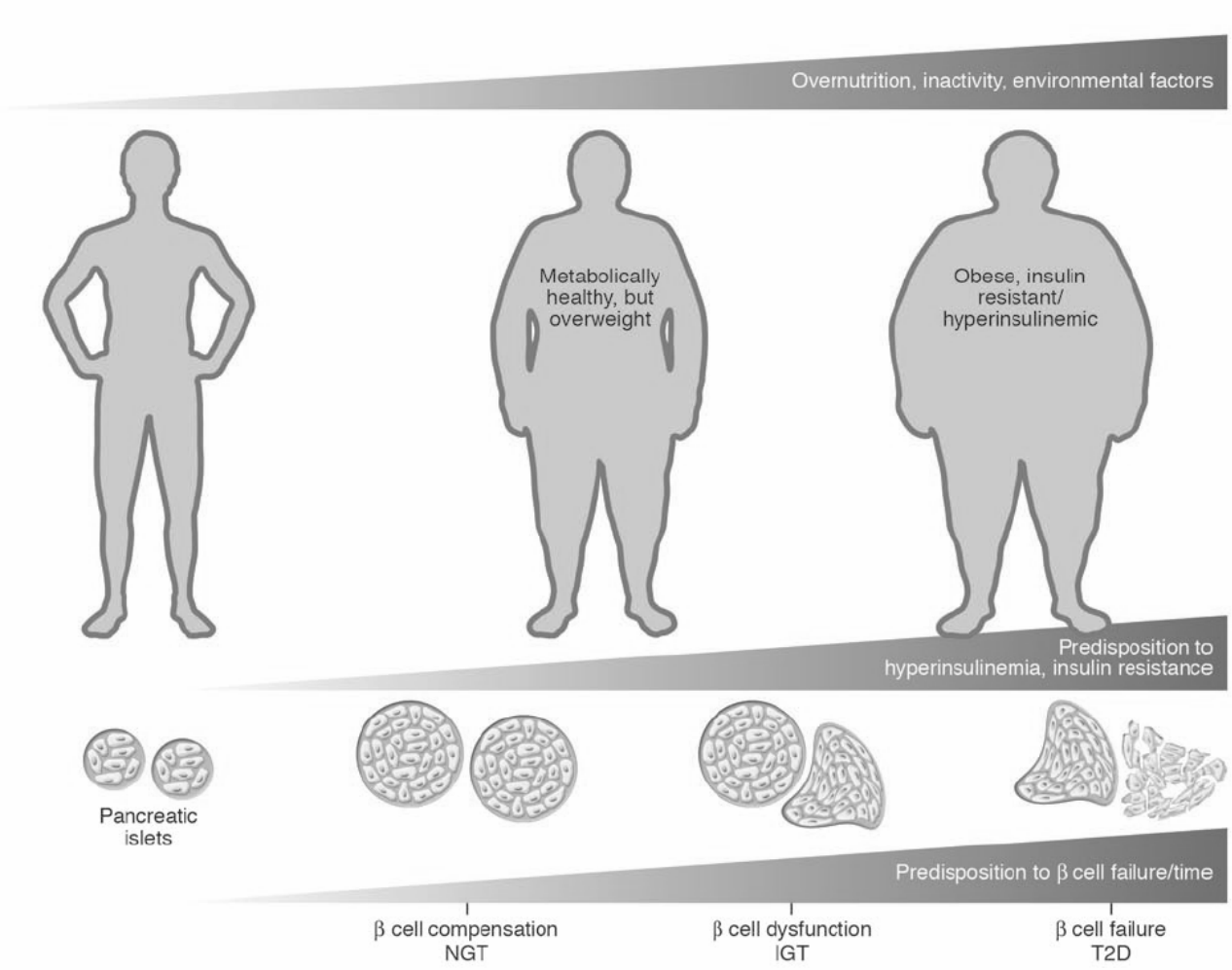

Figure 17. Islet β-cell failure and the natural history of T2D. β-cell dysfunction is the major determinant of progression from normoglycemia to diabetes (Prentki and Nolan, 2006)

4 β-CELL FAILURE AND β-CELL MASS IN TYPE 2 DIABETES

4.1 β-cell dysfunction

A progressive loss of β-cell function appears to be a critical component in the pathogenesis of T2D and to be a feature of the process of diabetes development (Karaca et al., 2009). Before the development of fasting hyperglycemia and the clinical diagnosis of diabetes, β-cell dysfunction manifest as abnormalities in insulin secretion and can be detected in groups at high risk of developing diabetes at a time when they do not have hyperglycemia and many still have normal glucose tolerance. Several studies have shown that the major defects are in the first phase of insulin response, but it also affects the second-phase, glucose potentiation, pulsatile insulin secretion, and the oscillatory pattern including an inability of glucose to synchronize with insulin secretion. In addition to these secretory defects, an inefficiency of proinsulin processing has also been demonstrated in individuals at high risk. The first phase serves a key role during food ingestion to prime the tissues for the coming nutrients. Experimental trials have shown that disrupting the first phase in healthy subjects causes glucose intolerance (Calles-Escandon and Robbins, 1987), and restoring the first phase in persons with type 2 diabetes improves postprandial glucose values (Bruce et al., 1988). Furthermore, an important discovery was the first phase was substantially restored following a period of intensive glucose control (Vague and Moulin, 1982) showing that this abnormality makes up the earliest form of acquired β-cell dysfunction. The current concept is that this β-cell defect not only occurs at the time of transition from normal glucose tolerance to IGT but is the key pathogenic event that causes that progression.

The loss of β-cell function appears to be also progressive and to continue after the onset of diabetes. As the hyperglycemia worsens over time, additional β-cell defects and deterioration of β-cell function occurs. This continued progression for many years after the onset of T2D has been shown to underlie the decline of clinical responses to oral agents in this disease. Intense investigation has been carried out in diabetic animals to understand the pathogenesis of these later stages of β-cell dysfunction. At least in animals, high levels of glycemia cause additional β-cell defects beyond the impaired glucose-induced insulin secretion that occurs at the earliest stage of the disease—additional defects in β-cell function as well as in β-cell viability.

4.2 Mechanisms for β-cell dysfunction

Although it is known that β-cell dysfunction is present early in the development of T2D and is progressive, the exact underlying molecular mechanisms leading to these defects are unclear. Several factors play important roles in the development of β-cell dysfunction that characterizes T2D (Fig.18) (Weir et al., 2009). Several mechanisms have been proposed, but none definitively proven for the human disease. Despite the goal of this thesis was not investigate the factors involved in β-cell dysfunction, a brief description of these factors is made in the following pages (Weyer et al., 1999).

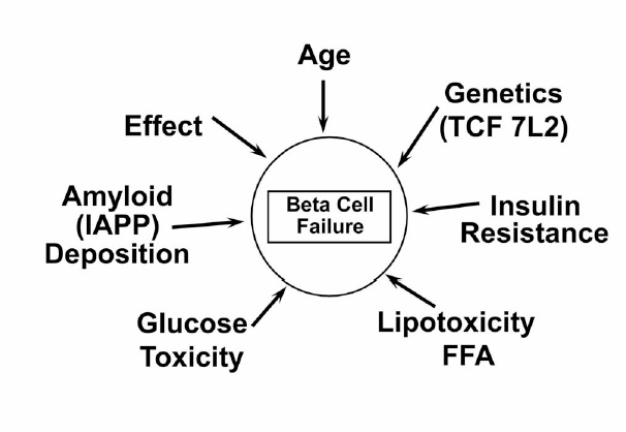

Figure 18. Etiology of β-cell failure in subjects with type 2 diabetes

Age: there is a progressive age-related decline in β-cell function, consistent with the well-established observation that the incidence of diabetes increases progressively with advancing age.

Genes: there is evidence for a genetic basis of the β-cell dysfunction. Moreover, a number of genes associated with β-cell dysfunction in T2D individuals have been recently described, as for example, the TCF7L2 gene.

Insulin resistance: it is commonly stated that the β-cells, by being forced to continuously hypersecrete insulin, eventually wears out. In this way, interventions aimed at enhancing insulin sensitivity are important. However, this explanation lacks a mechanistic cause. An alternate hypothesis is that the mechanisms that are involved in insulin resistance also cause β-cell failure, and considerable evidence exists for this hypothesis. For instance, the excess of fat deposition in liver and muscle cause insulin resistance and deposition in the β-cell leads to impaired insulin secretion and β-cell failure.

β-cell exhaustion: this descriptive term implies an indirect effect of hyperglycemia to impair β-cell function by causing a non-sustainable compensatory increase in insulin secretion that depletes some key substance for continued insulin secretion.

Lipotoxicity: The concept is that metabolic products from the excess fatty acids such as ceramides and precursors for oxidative stress impair insulin secretion and leads to β-cell failure and death.

Glucotoxicity: This concept implies a direct effect of an abnormally high glucose level to impair one or more key aspects of β-cell physiology and/or gene expression.

IAPP: hypersecretion of islet amyloid polypeptide (IAPP) and amyloid deposition within the pancreas were also implicated in the progressive β-cell failure.

Incretins: GLP-1 and glucose-dependent insulinotrophic polypeptide (also called gastric inhibitory polypeptide [GIP]) account for 90% of the incretin effect. In T2D, there is a deficiency of GLP-1 and resistance to the action of GIP, which have stimulatory effects on insulin secretion

In addition to the dysfunction of β-cell, it has been demonstrated that there is a decrease in β-cell mass in diabetes. Also, reductions in β-cells secretory capacity has been demonstrated to occurs in experimental models of T2D, in which reductions in islet mass have been produced.

In summary, it was demonstrated that, at the stage of IGT, individuals have lost over 80% of their β-cell function and that subjects with "pre-diabetes" have lost approximately half of their β-cell volume. Therefore, the progressive β-cell failure that characterizes T2D is likely to be a result of the combination of deterioration of β-cell function (defects in insulin secretion) and partial loss of β-cell mass.

4.3 β-cell mass is reduced in Type 2 Diabetes

The measurement of β-cell mass in humans is extremely difficult and must be done on autopsy specimens. A reduction in β-cell mass is considered to be a hallmark of T2D (Matveyenko and Butler, 2008). Recent reports conclude that β-cell mass is decreased in T2D, whereas others report no decrease in β-cell mass (Table 4). In fact, autopsy studies of patients with T2D have revealed a decrease in β-cell mass of 0–65% compared to body mass index-matched controls (Table 4) (Matveyenko and Butler, 2008). The reason for the discrepancy with the latter study is not known; however, a lack of appropriately matching subjects with T2D to weight-matched controls in many of the published studies can be the cause.

Table 4. Reported decrease in β-cell mass in several studies.

References	N (M/F)	BMI	Reported decrease in β-cell mass in T2DM
Rahier et al. 1983 [7]	4/4 lean T2DM ; 3/5 lean ND	Unknown	No significant difference between T2DM vs. ND
Kloppel et al. 1985 [3]	1/5 obese T2DM; 3/1 obese ND; 7/1 lean T2DM; 4/3 lean ND	29 ± 2 (obese T2DM); 30 ± 1 (obese ND); 21 ± 1 (lean T2DM); 20 ± 2 (lean ND)	~50% decrease in β-cell volume in obese T2DM vs. obese ND~60% decrease in β-cell volume in lean T2DM vs. lean ND
Sakuraba et al. 2002 [21]	10/4 lean T2DM; 10/5 lean ND	21 ± 3 (lean T2DM); 21 ± 3 (lean ND)	~30% decrease in β-cell mass vs. ND controls
Yoon et al. 2003 [5]	15/10 lean T2DM; 10/9 lean ND	22 ± 4 (lean T2DM); 23 ± 3 (lean ND)	~50% decrease in β-cell volume in patients with BMI < 25
Butler et al. 2003 [4]	17/21 obese T2DM; 9/10 obese IFG; 15/16 obese ND; 7/9 lean T2DM; 7/10 lean ND	38 ± 1 (obese T2DM); 37 ± 2 (obese IFG); 36 ± 1 (obese ND); 22 ± 1 (lean T2DM); 23 ± 1 (lean ND)	~50% decrease in β-cell volume in obese IFG vs. obese ND; ~65% decrease in β-cell volume in obese T2DM vs. obese ND; ~40% decrease in β-cell volume in lean T2DM vs. lean ND

Abbreviations: IFG, impaired fasting glucose; T2DM, type 2 diabetes; ND, non-diabetic; BMI, body mass index.

Part of the normal β-cell compensation to insulin resistance is an increase in the β-cell mass. Given that most persons with T2D are obese, it is crucial to match diabetic subjects and controls for obesity. A highly important recent study of a large number of weight-matched subjects with type 2 diabetes and controls showed a 40–60% reduction of β-cell mass in subjects with T2D (Butler et al., 2003) (Fig. 19). Interestingly, *Butler et al.* also showed that a group of individuals with impaired fasting glucose had a reduction of 40% in relative β-cell volume compared to obese non-diabetics (Fig. 19), suggesting that the deficit in β-cell volume and presumptive mass is an early process in the development of T2D and is likely of primary importance

rather than simply secondary to hyperglycemia (Butler et al., 2003). Thus, with the progression to overt diabetes, there was a further and significant loss of β-cell volume.

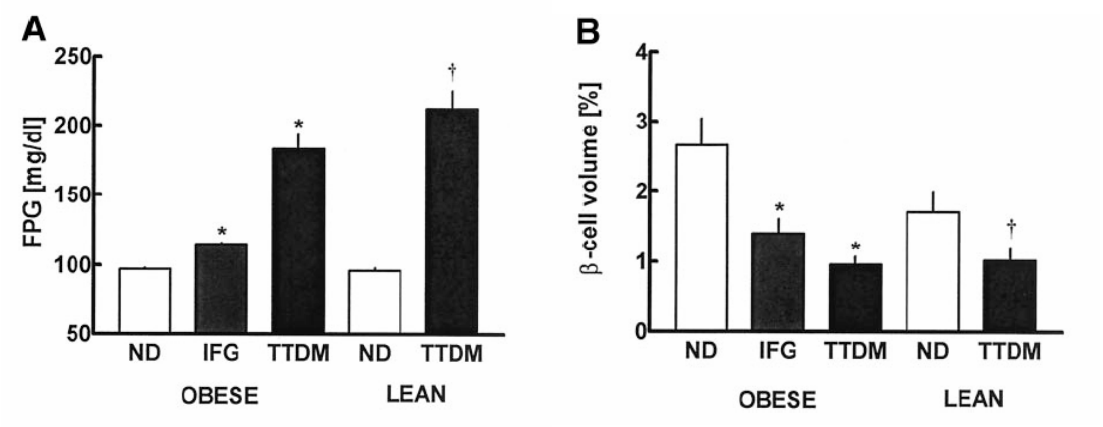

Figure 19. The mean FPG (fasting plasma glucose) concentration (A) and the mean relative β-cell volume (B) in obese (nondiabetic [ND], IFG (impaired fasting glucose), and diabetic subjects [TTDM]) and lean case (nondiabetic and type 2 diabetic subjects).

Although β-cell mass is reduced, no significant reduction in α, δ and PP-cells has been documented in T2D. But a higher relative proportion of α- to β-cells has been observed in T2D: α-cell mass is therefore disproportionately increased in T2D, despite this is not accompanied by an increase in α-cell mass. In the development of T2D, any reduction in β-cell mass has to be accompanied by a functional defect in β-cell function. Considerable current research is focused on trying to determine the pathogenic reason for the lowered β-cell mass in T2D, with the proposed mechanisms being indistinguishable from the proposed ones to β-cell dysfunction.

Finally, five stages of evolving β-cell dysfunction were proposed in the progression of diabetes (Fig. 20), each of which is marked by important and characteristic changes in β-cell mass, phenotype, and function (Weir and Bonner-Weir, 2004).

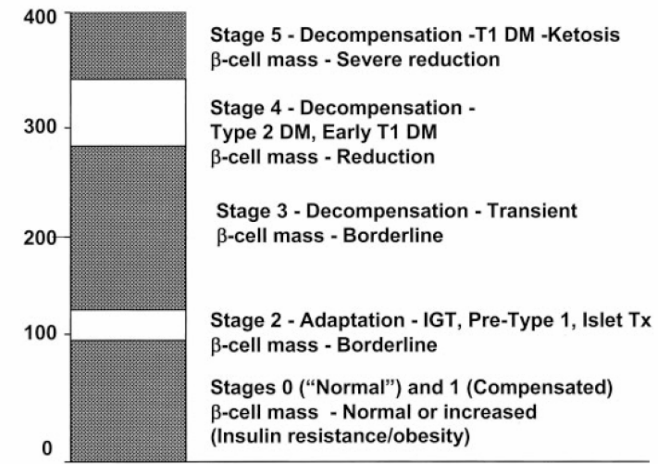

Figure 20. Five stages of evolving β-cell dysfunction in diabetes.

Stage 1 is best described as compensation: insulin secretion increases to maintain normal glucose levels in the face of insulin resistance resulting from obesity, physical inactivity, and genetic predisposition. Stage 2 occurs when glucose levels rise to levels of 5.0–6.5 mmol/l (89–116 mg/dl)—a stable state of β-cell adaptation. Stage 3 is an unstable period of early decompensation in which glucose levels rise relatively rapidly to stage 4, which is characterized as stable decompensation. Finally, there is the severe decompensation of stage 5 that represents profound β-cell failure with progression to ketosis.

5 HOW IS B-CELL MASS REGULATED?

Essentially, β-cell mass is governed by a constant balance between β-cell growth (replication from pre-existing β-cells, size of the cells and neogenesis (the emergence of "new β cells" from precursor cells or common pancreatic ductal epithelial cells) and β-cell death (mainly apoptosis) (Bouwens and Rooman, 2005) (Dickson and Rhodes, 2004).

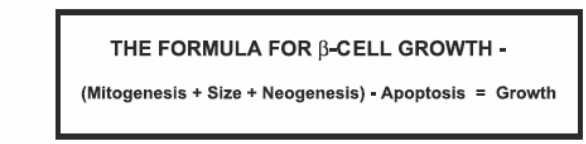

Figure 21. Major contributing factors that regulate β-cell mass. Change in β-cell mass is equal to the overall balance of cell growth from preexisting β-cells and the differentiation of cells from the common pancreatic ductal epithelium minus β-cell apoptosis.

A deficit in β-cells as found in T2D is likely to arise from many different causes including genetic predisposition affecting fetal/neonatal β-cell development, defects in the proposed cycle of turnover of islet cells in adults and cytotoxic events precipitating cell death. Most of this data have emerged from rodent studies and is difficult to translate into humans given the experimental limitations to obtain conclusive proof (Karaca et al., 2009).

In rodents, just after birth, there is a burst of islet cell replication, and then later, during weaning, there is a transient burst of neogenesis that supplements the increased β-cell replication. There is also some apoptosis during early life that parallels islet cell rearrangement, but this is minimal, so that the net effect is a marked increase in β-cell growth (Bonner-Weir, 2000b). Post weaning, as the young animal grows up, the rates of β-cell replication, neogenesis, and apoptosis all markedly trail off. In adult life, there remains a very slow turnover of β-cells with the estimated lifespan of a β-cell being approximately 60 days (Bonner-Weir, 2000a). About 0.5% of the adult β-cell population is undergoing replication, which is balanced by 0.5% of β-cells entering into apoptosis. There is also some rare instance of β-cell neogenesis, but little change in β-cell size, so that the net effect is that the β-cell mass stays relatively constant under normal circumstances in the adult.

5.1 β-cell mass plasticity

Despite being relatively constant under normal conditions, the β-cell mass has a remarkable ability to adapt depending on the metabolic homeostasis. This ability of the pancreatic β-cell mass to adapt to changes in the metabolic homeostasis caused by obesity and/or insulin resistance is called plasticity. In animal models, β-cell mass flexibly adapts to insulin requirement through disruption of the balance between β-cell growth and death. Conditions associated with increased demand for insulin including hyperglycaemia, insulin resistance, obesity and pregnancy result in larger β-cell mass in young rodents. This hypothesis of plasticity is less

evident in adult human islets as the degree of islet cell plasticity in adult man is low compared to that in rodents. Limited studies on postmortem pancreas in human pregnancy indicate a marginal increase (approx. 1.4-fold) in β-cell mass with no change in the islet or β-cell size compared to the larger expansion of islet mass in pregnant rats (two- to threefold). In addition, changes in β-cell mass in obesity/insulin resistance in humans are modest; β-cell mass in postmortem pancreas was shown to be 1.2- to 1.5-fold higher in patients with BMIs>30 kg/m2 compared to less obese subjects (Cnop et al., 2011).

5.1.1 Contribution of replication

Several studies performed in rodents have shown that increased rates of β-cell replication can contribute to compensatory increases in β-cell mass, for example in response to partial pancreatectomy or short-term glucose infusion. By contrast, replication of human adult islet β-cells has been estimated to be 10-fold less than that in adult mice and to be highest in children under the age of 5 years. Therefore, given the extremely low frequency of β-cell replication present in human islets compared with rodent islets, it appears that this important mechanism for regulation of β-cell mass in rodents is less important in humans. The relatively less importance of this pathway for regulation of β-cell mass in humans compared with rodents is consistent with the observation that obese mice develop very large islets, whereas in humans, islet size is minimally altered by obesity. Regarding the relative loss of β-cell mass in type 2 diabetes, β-cell replication was calculated in islets of obese and lean type 2 diabetic versus non-diabetic cases and appeared to have similar frequencies (Butler et al., 2003).

5.1.2 Contribution of neogenesis

The contribution of neogenesis in both normal conditions and during adaptation to stress has been debated, as the formation of new β-cells from precursor cells is a process that normally stops after birth. Numerous studies have implicated the pancreatic ducts as a source of new β-cells under regenerative conditions or after exposure to exendin-4 or beta cellulin (Juhl et al., 2010) (Demeterco et al., 2009).
However, no differences were reported in the percentage of exocrine duct cells positive for insulin in type 2 diabetic versus nondiabetic subjects, in either the lean or obese groups (Butler et al., 2003). Indeed, new islet formation from exocrine ducts and scattered single-cells was recently described in several pancreas specimens irrespective of obesity or diabetic status, consistent with recent and some much older studies in humans. This implies that the mechanism that enhances new islet formation in response to obesity is intact in humans with T2D. In animal models, both an acute decrease in β-cell mass (partial pancreatectomy) and hyperglycemia induce an increase in new islet formation. Patients with T2D had both a decreased β-cell mass and hyperglycemia, and therefore, it could be argued that there is a failure of compensatory increased new islet formation in T2D. However, the mechanisms that induce increased rate of new islet formation in response to a partial decrease in β-cell mass and hyperglycemia in rodents is not known, nor is it known whether such

adaptive changes occur in humans.

5.1.3 Contribution of apoptosis

The physiological occurrence of β-cell apoptosis has been shown *in vivo* during the involution of the β-cell mass in the post partum pancreas (Scaglia et al., 1995) and in a remodeling of the endocrine pancreas in the neonatal rat (Scaglia et al., 1997).

Since new islet formation, which is the predominant input into the β-cell mass in humans, appears to be intact in T2D, the mechanism for decreased β-cell mass in T2D should be increased β-cell apoptosis. In fact, β-cell loss in type 2 diabetes is accompanied by a marked increase in beta cell apoptosis, as shown in human pancreas autopsy specimens and in isolated islets. Specifically, *Butler et al* reported a 3-fold increased frequency of β-cell apoptosis in obese cases of type 2 diabetes and a 10-fold increased frequency in lean cases of T2D compared with the non-diabetic control cases (Fig. 22) (Butler et al., 2003).

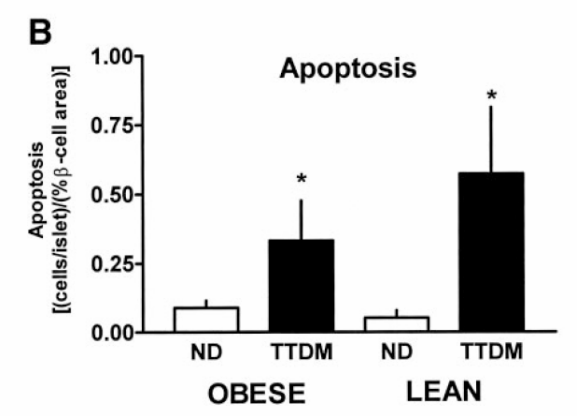

Figure 22: The frequency of β-cell apoptosis (B) normalized to relative β-cell volume in each case. ND, nondiabetic; TTDM, type 2 diabetes.

A universal observation in both humans and rodents is that decreased β-cell mass in T2D is accompanied by a marked increase in β-cell apoptosis that outweighs the rate of β-cell replication and neogenesis. Therefore, if the rate of new islet formation is sustained in patients with longstanding diabetes, this imply that if the increased rate of apoptosis present in type 2 diabetes could be inhibited, it should be possible to restore β-cell mass in these patients. Also, the relative contribution of β-cell loss versus β-cell dysfunction to diabetes onset remains an area of controversy. However, because cytotoxicity sufficient to induce β-cell apoptosis predictably disturbs β-cell function, it is naive to attempt to distinguish the relative contributions of these linked processes to diabetes onset. Currently, it is unclear what instigates an increased rate of β-cell apoptosis during the pathogenesis of T2D; however, both chronic exposure to elevated levels of fatty acids (lipotoxicity) and prolonged fluctuations of high circulating glucose levels (glucotoxicity) have a prominent influence.

In summary, relative β-cell volume, and therefore the presumptive β-cell mass, is decreased in both obese and

lean humans with T2D compared with their nondiabetic age- and weight-matched counterparts. Furthermore, humans with IFG have a decreased relative β-cell volume, suggesting that this is an early process and mechanistically important in the development of T2D. The mechanism for the decrease in β-cell mass to is increased frequency of β-cell apoptosis with the rate of new islet formation being unaffected. The implication for prevention of T2D is that strategies that avoid the increased frequency of β-cell apoptosis are most rational. Also, in people with established T2D, inhibition of this 3- to 10-fold increased rate of apoptosis may lead to restoration of β-cell mass since islet neogenesis appears intact.

5.2 Factors that govern β-cell mass

In the past few years, there have been novel insights into signal transduction mechanisms that control β-cell growth and survival. Interestingly, the components of these β-cell signaling pathways are the same as elements in insulin signal transduction pathways (Dickson and Rhodes, 2004). Multiple nutrients and growth factors stimulate growth and survival of existing β-cells acting via diverse intracellular signaling pathways (Lingohr et al., 2002). A list of such nutrients and growth factors are presented in Table 5. As a general trend, nutrients that stimulate insulin secretion and synthesis also increase β-cell mass.

Table 5. β-cell growth and survival effectors (Lingohr et al., 2002).

Adult β-cells			
Factors	**Effects**	**β-cell model**	
IGF-1	↑proliferation, ↑survival, ↑hypertropy	Islets, INS-1 cells, islet mass *in vivo*	[22,25–27]
IGF-2	↑proliferation, ↑survival	Islet mass *in vivo*, transgenic mice	[27–29]
Insulin	↑ ↓ proliferation	Transgenic insulin and receptor knockout mice	[30–32]
GH	↑proliferation, ↑survival, ↑hypertropy	Islets, INS-1 cells, islet mass *in vivo*, transgenic mice	[23,33–35]
Prolactin	↑proliferation, ↑hypertropy	INS-1 cells, pregnancy islet mass *in vivo,* transgenic mice	[33,35–37]
PL-1	↑proliferation, ↑hypertropy	INS-1 cells, pregnancy islet mass *in vivo,* transgenic mice	[37–39]
GLP-1	↑proliferation, ↑hypertropy	INS-1 cells, islet mass *in vivo*	[40,41]
GIP	↑proliferation	INS-1 cells	[42]
HGF	↑proliferation, ↑survival	Islets, INS-1 cells, islet mass *in vivo*, transgenic mice	[43–45]
PTHrP	↑survival	Islets, INS-1 cells 1, islet mass *in vivo*, transgenic mice	[46,47]
Betacellulin	↑proliferation	INS-1 cells 1, regenerating pancreas	[48–50]
NGF	↑proliferation, ↑survival	βTC6-F7 and INS-1 cells, islet β-cell monolayer	[51,52]
FGF	↑proliferation	INS-1 cells	[53]
PDGF	↑proliferation	Fetal rat islets, islet β-cell monolayer	[54,55]
Leptin	↑proliferation	MIN6-cells	[56]
Nutrients			
Glucose	↑proliferation, ↑ ↓ survival	INS-1 cells, islets, islet mass *in vivo*, (exposure time dependent)	[22,23,57–61]
Pyruvate	↑proliferation	INS-1 cells	[23]
Leucine	↑proliferation, ↑ survival	INS-1 and RINm5F cells, fetal rat islets	[62–64]
Glutamine	↑proliferation, ↑ survival	RINm5F cells, fetal rat islets	[62–64]
Fatty Acids	↓ proliferation, ↓ survival	INS-1 cells, islets, islet mass *in vivo*, (exposure time dependent)	[63,65–67]

5.2.1 Glucose

Glucose is the most physiologically relevant effector that increases rodent β-cell proliferation *in vitro* and *in vivo* (Lingohr et al., 2002).

Glucose is also the primary regulator of insulin secretion and insulin biosynthesis. The signaling pathways and mechanisms by which glucose stimulates β-cell growth and survival are not entirely understood but it is now

evident that it require activation of proteins in the insulin signaling pathway, as the insulin receptor substrate 2 (IRS2), a protein in the insulin/insulin like growth-factor I (IGF-I) signaling pathway (Assmann et al., 2009). Several pathways have been implicated as: autocrine effects of secreted insulin, dependent of Akt signaling; Induction of calcium signaling; Activation of the TSC2/mTOR signaling pathway, important regulator of β-cell mass and proliferation. However, these are relatively acute effects and, prolonged exposure of β-cells to significant elevations in glucose levels impaired proliferation and can evoke β-cell apoptosis leading to decreased β-cell mass (glucotoxicity).

5.2.2 Placental hormones

During pregnancy, placental hormones, especially placental lactogens, are mainly responsible for the changes in β-cell mass. These hormones stimulate β-cell proliferation in isolated islets, and β-cell mass is reduced 26–42% in receptor-deficient mice (Bouwens and Rooman, 2005).

5.2.3 Glucagon-like peptide-1

The gastrointestinal incretin hormone glucagon-like peptide-1 (GLP1) has been repeatedly reported to affect β-cell function, replication, apoptosis, and neogenesis (Wang et al., 2004). In obese hyperglycemic ob/ob mice, a GLP1 analog ameliorates glycemia and increases β-cell mass and β-cell replication. GLP1 delays the onset of diabetes in db/db mice, and in diabetic mice it lowers glycemia and increases β-cell mass through neogenesis from Pdx1-expressing ductal precursor cells (Stoffers et al., 2000).

The best characterized growth factors that increase β-cell growth, other than pregnancy hormones, are the Growth hormone, Insulin-like growth factors (IGF-I and II) and Insulin (Lingohr et al., 2002).

5.2.4 Growth hormone

The growth hormone receptor (GHR) is present on β-cells, and downstream signal transduction is via the JAK2–STAT5a/b signaling pathway, which acts as a transcription factor. GH can enhance the expression of cyclin D1 and D2, which is involved in progression of the cell cycle; this could therefore enhance β-cell mitogenesis. For comparison, STAT5 activation induces expression of the anti-apoptotic protein Bcl-xL and of members of the SOCS (suppressors of cytokine signaling) family (which inhibit cytokine receptor signaling); these might, therefore, play a role in β-cell survival.

5.2.5 Insulin and Insulin-like growth factors

Insulin and insulin-like growth factor I and II (IGF-I and II) are ubiquitous hormones that regulate growth and metabolism of most mammalian cells, including of the pancreatic β-cells (Fig. 23). The receptors for insulin and IGF-I are expressed ubiquitously and mediate the effects of these hormones. Most of the information

regarding insulin/IGF-I signaling pathways is derived from studies underlying the defects in insulin action in T2D. Insulin and IGF-I bind to distinct receptors but can each also cross-react with the other receptor. This makes it difficult to separate the specific effect of these peptides in β-cell growth (White, 2002)

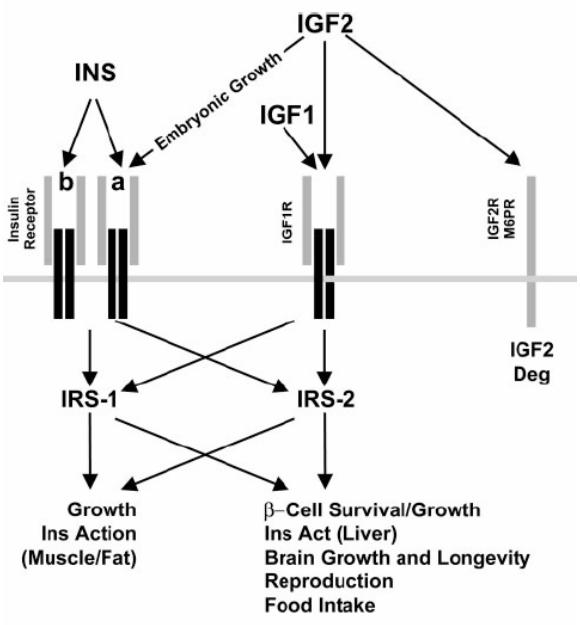

Figure 23. Diagram summarizing some of the physiological responses regulated by the insulin/IGF-signaling pathway (White, 2002).

6 MOLECULAR MECHANISMS THAT REGULATES PANCREATIC β-CELL SURVIVAL

6.1 The Insulin/IGF-signaling pathway

During ligand binding, insulin/IGF-I receptors become tyrosine phosphorylated through an autophosphorylation reaction of a regulatory region in the β subunit, which stimulates the intrinsic tyrosine kinase activity. The activated receptor engages and phosphorylates various cellular proteins on selective tyrosine residues, including the IRS protein family members (especially IRS2 in β-cells) and Shc, which serve as docking sites for various SH2 domain-containing effector elements. These include the p85 regulatory subunit of PI3K (phosphatidylinositide 3-kinase), Shp-2, Grb2, tyrosine kinases Fyn and Csk, adaptor molecules Crk and Nck, and PLCγ. Although the roles of each of these substrates are important, several works with transgenic mice suggests that many insulin responses, especially those that are associated with somatic growth and carbohydrate metabolism, are largely mediated through two IRS proteins, called insulin receptor substrates 1 and 2 (IRS1 and IRS2) (Myers and White, 1996; White, 2002). These IRS proteins play different but crucial roles in cellular processes that are important for the metabolism and growth of tissues, including β-cells, and comprises glucose transport and utilization, protein synthesis, cell growth, proliferation and antiapoptosis processes (Fig. 24) (Kulkarni, 2005).

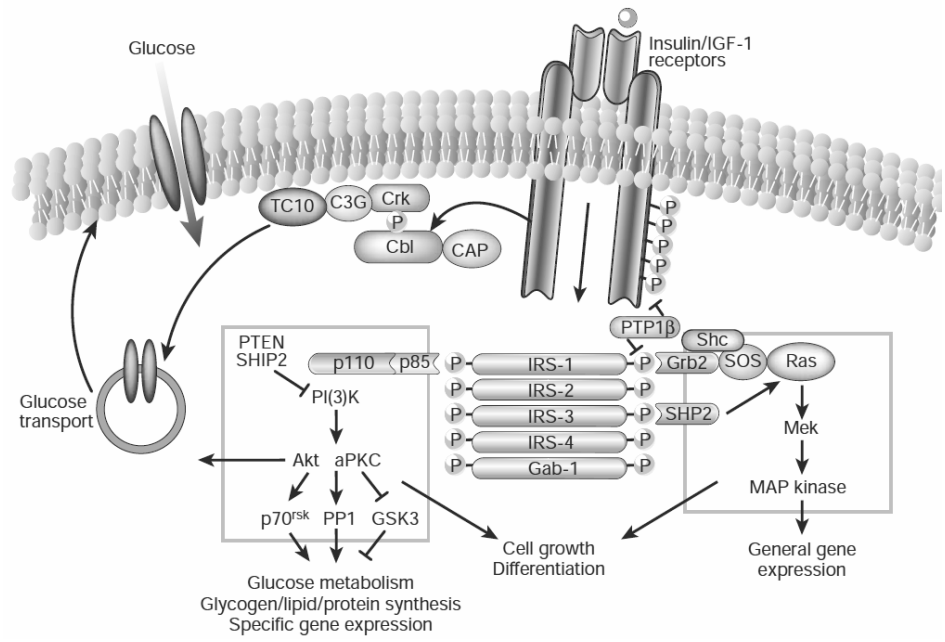

Figure 24. Signal transduction via IRS proteins in insulin/IGF action (Kulkarni, 2005).

Two main branches of the insulin/IGF-I signal transduction pathway, namely the MAPK and PI3K pathways, are well characterized (Manning and Cantley, 2007; Roskoski Jr, 2012).

Tyrosine phosphorylation of IRS-1/2 promotes association with the p85 regulatory subunit of PI3K, which, in turn, activates the p110 catalytic subunit. PI3K phosphorylates phosphatidylinositol PI (4,5) P2 in the β-cell plasma membrane to create phosphatidylinositol-3,4-bisphosphate and phosphatidylinositol-3,4-bisphosphate. Higher levels of PI (3,4,5) P3 attract serine kinases to the plasma membrane, including the phosphoinositide-dependent kinase (PDK1 and PDK2) and at least three protein kinase B (PKB) isoforms. Plasma membrane-associated PDK-1 or PDK-2 then phosphorylates PKB on Threonine 308 for partial activation, and subsequent phosphorylation at Serine 473 results in full PKB activation. PI3K-mediated increases in PI (3,4,5) P3 can also lead to activation of protein kinase C ζ (PKC), which can be further enhanced upon phosphorylation by PDK-1 and PKB. The activated PKB/Akt phosphorylates many substrates to control various biological signaling cascades, including glucose transport, protein synthesis, glycogen synthesis, cell proliferation, and cell survival, in various cells and tissues (Fig. 25) (Kulik and Weber, 1998; White, 1996; White, 1998; Yenush and White, 1997).

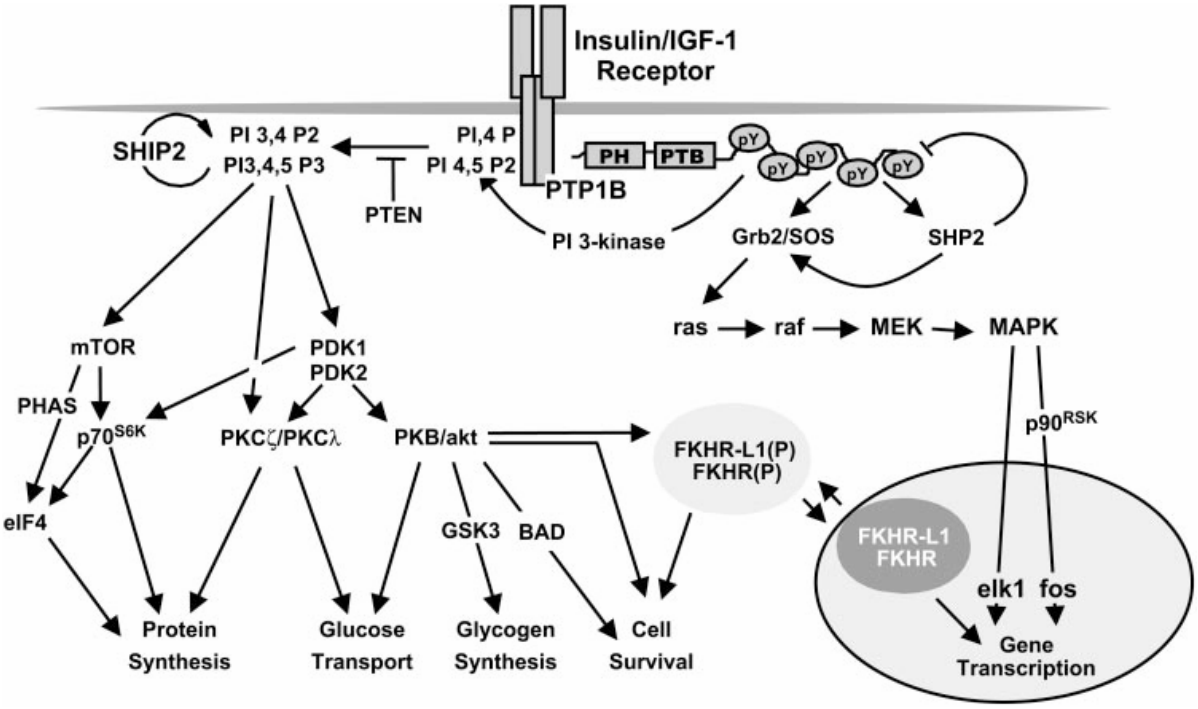

Figure 25. IRS protein-dependent insulin/IGF-I-signaling cascade (White, 2002).

A major contributing factor in the pathogenesis of T2D is an inadequate β-cell mass that is no longer able to compensate for insulin resistance and/or insulin-secretory demand, and this is associated with reduced β-cell mass and increased rate of β-cell apoptosis. In this regard, the insulin signaling in pancreatic β-cells, especially via PKB and mitogen-activated protein kinases (MAPK), plays a critical role in controlling β-cell growth and survival.

6.2 Akt/PkB effectors

Among the vast array of protein substrates, PKB phosphorylates GSK3 and FoxO, inhibiting their activity. By contrast, PKB-mediated phosphorylation activates the protein kinase mTOR, the apoptotic proteins BAD and Mdm2, the transcription factor CREB, and Rb, all of which might potentially influence β-cell mitogenesis, differentiation and/or survival (Manning and Cantley, 2007; Marte and Downward, 1997; Matheny and Adamo, 2009) (Lingohr et al., 2002) (Dickson and Rhodes, 2004).

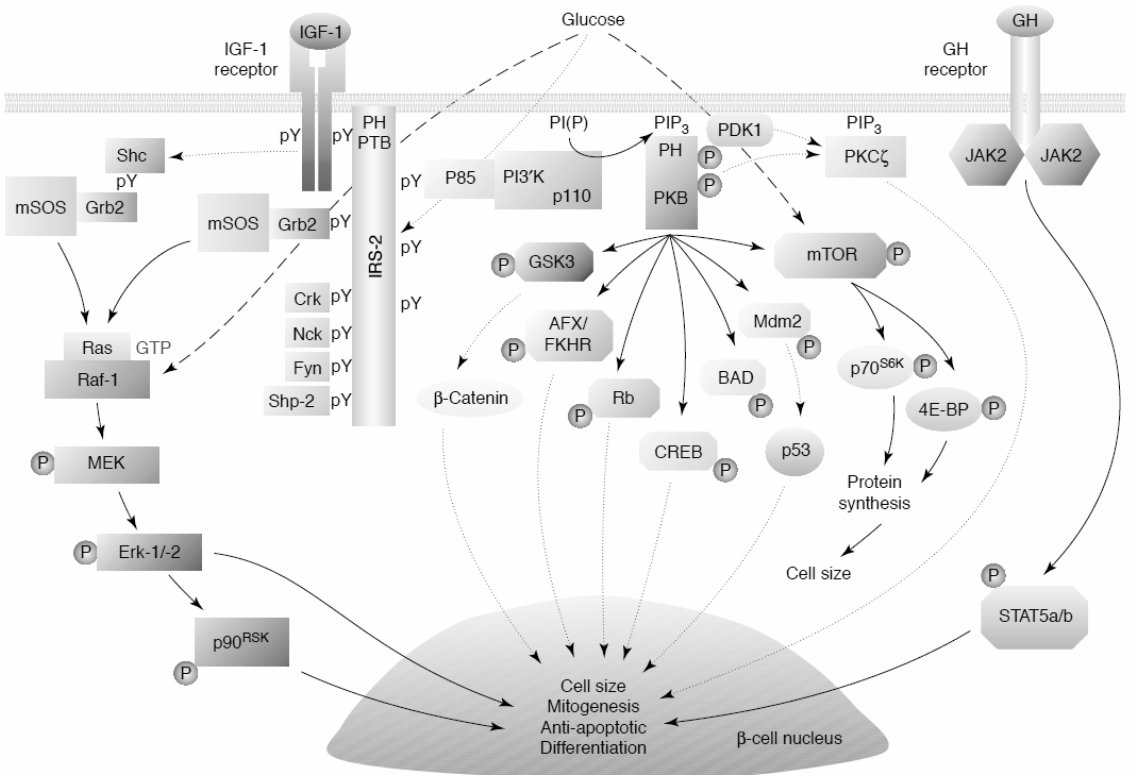

Figure 26. Insulin/IGF1 signal-transduction pathways and downstream Akt/PkB effectors in pancreatic β-cells (Lingohr et al., 2002).

1. PKB-mediated phosphorylation of **glycogen synthase kinase-3** (GSK3) has been shown in INS-1 cells. The consequences of GSK3 inactivation in β-cells are currently unclear, but it seems to participate in the control of general protein synthesis as GSK3-mediated phosphorylation inhibits eIF2-B, or cell differentiation as GSK3-mediated phosphorylation inhibits β-catenin transcriptional activity and/or association with cell adhesion molecules. These latter scenarios could contribute to β-cell hypertrophy and neogenesis (Manning and Cantley, 2007) .

2. It has been considered that **FoxO** (forkhead box-containing protein, O sub-family) proteins are phosphorylated by PKB at three residues; resulting export of FoxO from the nucleus to the cytoplasm, negatively regulate FoxO transcriptional activity. FoxO proteins inhibit cellular proliferation through

induction of cell cycle inhibitors, such as p27Kip1 and p21waf1. Therefore, its inhibition by PKB can lead to decreased expression of cell cycle inhibitors and promotion of cell proliferation. At the β-cell level, FoxO also inhibits β-cell growth through suppression of Pdx1 transcription (Kitamura and Ido Kitamura, 2007).

3. The **mTOR** (mammalian target of rapamycin) activation leads to phosphorylation activation of p70S6K and 4EBP, upregulating protein synthesis and, in turn, positively influencing β-cell size (Manning and Cantley, 2007) .

4. PKB phosphorylation of **Rb** (retinoblastoma) protein, possibly promotes cell proliferation via downregulation of the cyclin-dependent kinase inhibitor p27kip and/or upregulation of G1-phase cyclins (Manning and Cantley, 2007).

5. The transcription factor cAMP response element binding protein, **CREB,** has also been identified as a target for several signaling pathways mediated by growth factors, and Akt/PKB has been shown to phosphorylate CREB on serine 133. CREB is a positive regulator of Bcl-2 expression, as the promoter region of Bcl-2 contains a cAMP response element (CRE) site; also, up-regulation of Bcl-2 expression has been identified as a critical mechanism by which growth factors promote cell survival. Thus, it seemed that Akt activation through PI3K could mediate improve cell survival by regulation of Bcl-2 expression (Pugazhenthi et al., 2000).

6. Another mechanism that promotes cell survival is PKB-mediated phosphorylation of **Mdm2** (E3 ubiquitin-protein ligase), which results in translocation of this protein to the nucleus where it sequesters the p53 tumor suppressor protein, blocks p53 transcriptional activity and decreases p53 levels. As a consequence, cell survival is promoted (Lingohr et al., 2002).

7. Akt/PKB has also been shown to promote cell survival by growth factors against several apoptotic stimuli. One mechanism by which Akt prevents apoptosis is through phosphorylation of the pro-apoptotic protein **Bad (**Bcl-2-associated death promoter) on Ser-136 (Datta et al., 1997). Interaction of Bad with outer mitochondrial membrane (OMM)-associated Bcl-2 and Bcl-XL leads to disruption of OMM integrity and cytochrome c release, which promotes apoptosis through the mitochondrial intrinsic death pathway (Gross et al., 1999; Martinou and Youle, 2011). By contrast, phosphorylated Bad dissociates from Bcl-2/Bcl-XL and associate with cytosolic 14-3-3 proteins, away from mitochondrial membranes. Bcl-2/Bcl-xL complexes prevent the activation of caspase-9, therefore impending the intrinsic apoptotic pathway. Interestingly, PKB-induced phosphorylation of procaspase-9 is also anti-apoptotic and prevents proteolytic activation of procaspase-9. If any of these PKB-mediated, anti-apoptotic mechanisms occur in β-cells, then β-cell survival would be increased (Manning and Cantley, 2007).

6.3 MAPK effectors

Insulin and IGF-1 can also promote cell survival through activation of Map kinase pathway (Lingohr et al., 2002) (Fig. 27). Indeed, increased phosphorylation of the extracellular signal-related kinases-1 and -2 (Erk-1 and -2) members of the MAPK family, was observed in islets and β-cell lines after stimulation with insulin/IGF-1. The effector element Grb2 is associated with the Ras guanine nucleotide exchange factor mSOS. When the Grb2–mSOS protein complex is recruited to tyrosine-phosphorylated IRS2 and/or Shc docking proteins, the guanine nucleotide exchange activity of mSOS is activated; this loads Ras with GTP, resulting in Ras activation. By specific association with activated Ras, the serine/threonine kinase Raf-1 is activated, which is followed by Raf-1-mediated phosphorylation of MEK. MEK then phosphorylates and activates the MAPK isoforms Erk1/2.

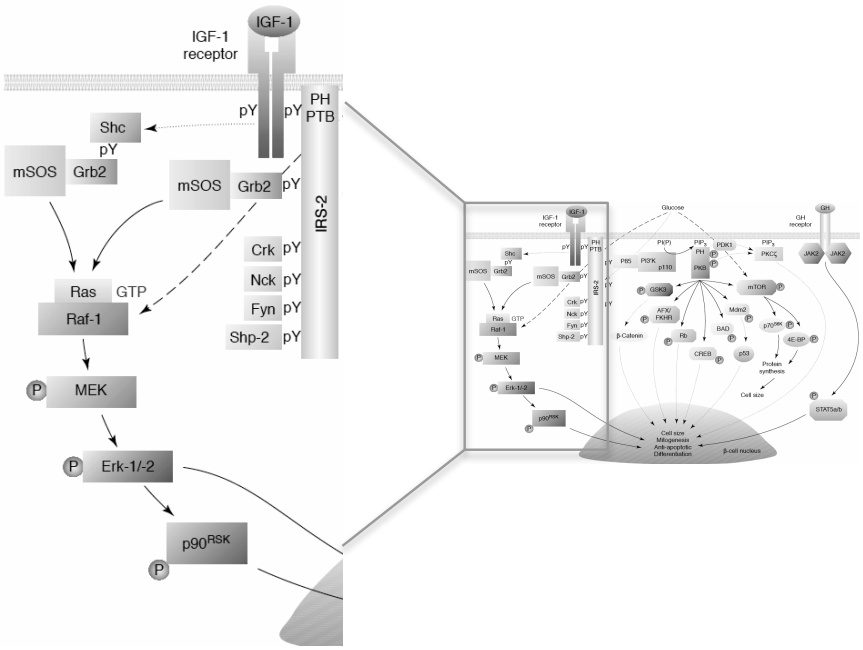

Figure 27. MAPK pathway in detail adapted from (Lingohr et al., 2002).

1. Erk1/2 phosphorylation promotes their translocation to the nucleus, where they upregulate the transcription of certain genes, including that encoding insulin. In fact, Erk1/2 mediate an essential step in the signaling cascade through which glucose regulates insulin gene transcription, with actions on at least five factors (Beta2, E47, MafA, C/EBP-B, PDX1) that bind to the most glucose-sensitive regions of the insulin gene promoter (Khoo et al., 2003; Lawrence et al., 2005).

2. Additionally, activated Erk1/2 catalyzes the phosphorylation of transcription factors and some of their regulators. Erk1/2 nuclear targets include the ternary complex factor (TCF) family of transcription factors. These proteins play a major role in inducing the expression of the immediate early genes (IEGs). The

immediate early gene products such as c-Fos and c-Myc induce late-response genes that promote cell survival, cell division, and cell motility. The Erk1/2 cascade also regulates transcriptional repression and chromatin remodeling.

The Erk1/2 family of protein kinases can also activate other proteins and more than 50 cytoplasmic substrates have been identified, such as p90RSK (Roskoski, 2012). The 90-kDa ribosomal S6 kinase family of proteins is a group of protein-serine/threonine kinases that regulates transcription and cell survival by mediating the phosphorylation of a number of transcription factors including:

3. The cAMP response element binding protein (CREB), which is directly phosphorylate at serine 133 by activated RSK, and required to initiate transcription of targets genes such as Bcl-2 and Irs2 (Qiao et al., 2003);

4. The transcriptional inhibitor IkB, which degradation is triggered by phosphorylation of two serine residues, Ser32 and Ser36; p90rsk1 phosphorylates IkBa at Ser32, liberating NFkB of the inhibitory effect of IkB and allowing its translocation to the nucleus, where it promotes cell survival (Schouten et al., 1997);

5. RSK1/2 also promote G1-phase progression of the cell cycle by catalyzing the phosphorylation and inhibition of the cyclin-dependent kinase inhibitor p27Kip cell growth, motility, proliferation, and survival.

6. Activated RSK enzymes also catalyze the phosphorylation of several ribosome-associated proteins that enhance protein synthesis. These include ribosomal protein S6 and eukaryotic initiation factor 4B (eIF4B).

7. One possibility that RSK mediates cell survival is through the inactivation of pro-apoptotic proteins including Bad and death-associated protein kinase (DAPK) (Shimamura et al., 2000). The apoptotic Bad, which was reported to be phosphorylated at Serine 112 after activation of the MAP kinase pathway (Bonni, 1999).Indeed, Bad represent a point of convergence of several different signal transduction pathways that are activated by survival factors and inhibit apoptosis in mammalian cells (Lizcano et al., 2000) (Fig.28).

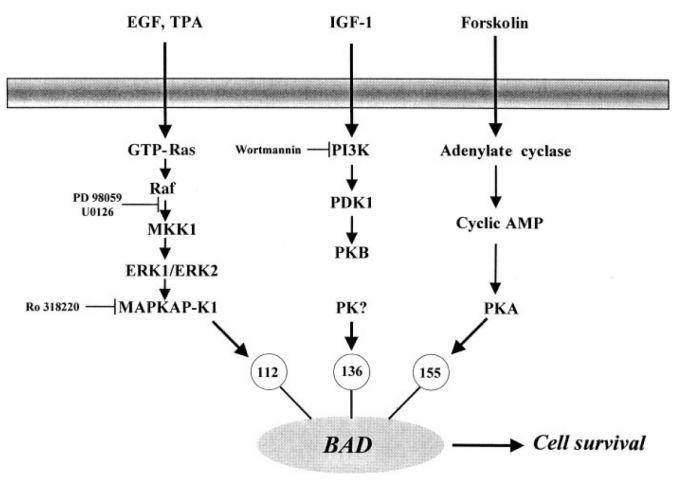

Figure 28. Bad is phosphorylated at different sites in response to agonists that activate distinct signal-transduction pathways (Lizcano et al., 2000).

Recently, it has been shown that multiple crosstalk points exists between Ras/Erk and PI3K/Akt pathways, which involve multiple signaling nodes and routes and whose coordinated action determines the cell fate interactions. Therefore the traditional schemes of growth factor, hormone and cytokine receptor signaling networks, which display PI3K/Akt and Ras/Erk as two independent parallel pathways, should be carefully interpreted (Aksamitiene et al., 2012).

In conclusion, the PI3K/Akt and MAP kinase pathways (and also the cAMP-dependent kinase PKA not described here), regulate the phosphorylation state of a variety of effector molecules implicated in apoptotic regulation. This offers the cell a sensitive combinatorial means by which it can regulate the triggering of the apoptotic program (Shimamura et al., 2000) (Fig.29).

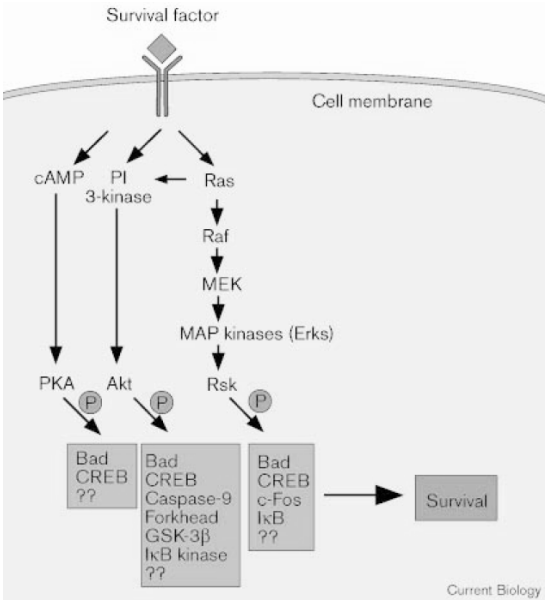

Figure 29. The trigger of the apoptotic program or of cell survival is regulated by distinct signal-transduction pathways (Shimamura et al., 2000).

6.4 Phenotypes of global knockout/transgenic animals

Targeted deletions of the components of insulin signaling *in vivo* using homologous recombination have yielded some insight into the complexity of these mechanisms. Although some single defects in the insulin-signaling pathway, such as knockout of the insulin receptor, Irs2 or Akt2, can produce diabetes, knockout of the p85 subunit of PI(3)K or IRS-1 does not. Taken together, these knockouts underscore the crucial importance of insulin and IGF itself and signaling in the overlapping regulatory functions of metabolism and growth in mice and humans.

Table 6: Partial list of phenotypes and references of global knockout/transgenics of insulin and IGF-1 genes and proteins in the insulin receptor/IGF-1 signaling pathway.

Protein	Phenotype
Insulin	Intrauterine growth retardation, Neonatal lethality, Ketoacidosis, Liver steatosis
IGF-1	Dwarfism, Variable survival
IGF-II (overexpressor)	Islet hyperplasia, organ overgrowth
Insulin receptor	Neonatal lethality, Ketoacidosis
IGF-1 receptor	Dwarfism Neonatal lethality
IRS-1	Post-natal growth retardation Insulin resistance Islet hyperplasia Insulin secretory defect
IRS-2	Insulin resistance Diabetes Islet hypoplasia
IRS-3	Relatively normal
IRS-4	Mild glucose intolerance
PI 3-kinase isoforms	
p85α	Increased insulin sensitivity, Hypoglycemia
p85β	Increased insulin sensitivity, Hypoglycemia
p50α/p55α	Increased insulin sensitivity
Akt1	Growth retardation, Increased apoptosis, Normal glucose tolerance.
Akt2	Insulin resistance in liver and muscle, Increased islet mass.
P70S6kinase	Hypoinsulinemia, Glucose intolerance, and Reduced beta-cell size.
Insulin receptor-related receptor	Normal phenotype

6.5 Identification of Insulin signaling elements in Human β-Cells

Many studies used rodent islets to explore the role of insulin and proteins belonging to the insulin-signaling pathway in the regulation of islet function and in its role in diabetes. The specific expression and function of insulin signaling pathway elements was also determined in human islets and single β-cells, concluding that the insulin signal transduction cascade isoforms were expressed in the whole islets and also in human β-cells (Fig.30).

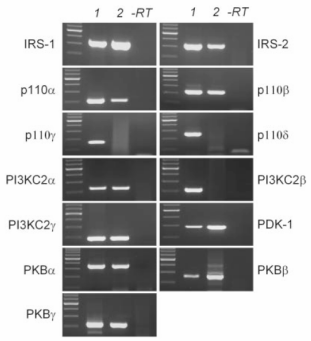

Figure 30. IR-associated gene expression in single human β-cells. Products that were amplified from single β-cells are shown in lane 2 and compared with those amplified using human islet cDNA under the same experimental conditions (lane 1). -RT indicates the absence of product formation when single-cell mRNA is used instead of single-cell cDNA templates (Muller et al., 2006).

Interestingly, their results also showed that the mRNAs coding for Irs1 and Irs2, which are proposed to be the major insulin-stimulated tyrosine phosphoproteins, were expressed in only 50 and 33% of the β-cell population. The frequency of expression of PKBα, PKBβ, and PKBγ, which represent the end point of the insulin-signaling cascade and mediate the majority of the effects triggered by insulin, was high. Indeed, 66% of the tested β-cells were found to express PKBα and all β-cells tested expressed PKBβ and PKBγ. Interestingly, although it is generally accepted that members of the first class of the PI3K enzymes mediate the majority of the insulin effects in their target tissues, the mRNAs coding for PI3KC2α and PI3KC2γ, two members of the class II PI3K family, were expressed with the highest frequency in the β-cell population (75%). In contrast, only 28 and 50% of the tested human β-cells expressed the PI3K class I catalytic subunits p110α and p110β, and none of them expressed p110γ and p110δ (Muller et al., 2006). The expression frequencies of INSR-B, IRS1, IRS2 and AKT2 were higher in β-cells than in α- and δ-cells, which confirm previous reports showing the critical roles played by these genes in β-cells. This data is consistent with the study published in 2005 by Gunton *et al*. In this report, they found that among the insulin signaling genes, insulin-receptor, *IRS2* and *Akt2* mRNA were significantly lower in diabetic subjects, which could likely lead to impaired insulin signaling in diabetic islets (Gunton et al., 2005). In contrast, there was no significative difference in the expression of PI3K or Akt1 between the two groups. These data showed that pancreatic islets from patients with type 2 diabetes display important alterations in gene expression, which are likely to be important in β-cell dysfunction in humans with T2D (Muller et al., 2007).

6.6 β-cell apoptosis

Evidence from both human disease and mouse models has shown β-cell apoptosis is a common feature of type 1 and type 2 diabetes. β-cell apoptosis is difficult to detect in vivo, due to the slow kinetics of the inflammatory process and the rapid clearance of the dead cell debris by host macrophages and neighboring cells. Nevertheless, apoptotic β-cells have been detected in situ morphologically and by TUNEL staining in various studies (Cnop et al., 2005). Because of the difficulty in obtaining specimens from patients before or after the onset of diabetes, much of what is known about β-cell apoptosis comes from animal models of both type 1 and type 2 diabetes.

In T1D, β-cell mass is reduced by 70-80% at the time of diagnosis and β-cells are destroyed by immunological mechanisms (Kloppel et al., 1985). In T2D, abnormal levels of metabolic factors contribute to β-cell failure and subsequent apoptosis. In type 2 diabetic subjects, initial pathological studies suggested a β-cell loss of 25%-50% (Kloppel et al., 1985). Irrespective of the exact mediators, highly conserved intracellular pathways of apoptosis are triggered (Cnop et al., 2005).

Apoptosis is coordinated by a family of cysteine proteases, the caspases, which are activated upon receipt of divergent pro-apoptotic stimuli. There are two major pathways leading to apoptosis of mammalian cells, the 'extrinsic' (death receptor-induced) and 'intrinsic' (Bcl-2-regulated or mitochondrial) pathways (Fig.31). However, there is now evidence that the two pathways are linked and that molecules in one pathway can influence the other. There is an additional pathway that involves T-cell mediated cytotoxicity and perforin-granzyme dependent killing of the cell.

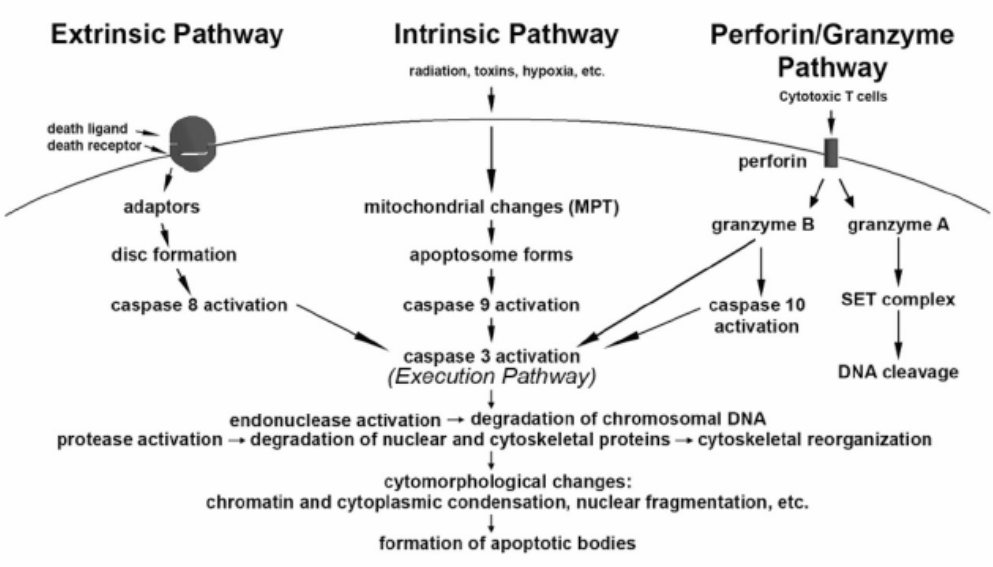

Figure 31: Schematic representation of apoptotic events. The two main pathways of apoptosis are extrinsic and intrinsic as well as a perforin/granzyme pathway. Each requires specific triggering signals to begin an energy-dependent cascade of molecular events. Each pathway activates its own initiator caspase (8, 9, 10), which in turn will activate the executioner caspase-3.

The extrinsic and intrinsic pathways converge on the same terminal, or execution pathway. This pathway is initiated by the cleavage of caspase-3 and results in DNA fragmentation, degradation of cytoskeletal and nuclear proteins, crosslinking of proteins, formation of apoptotic bodies, expression of ligands for phagocytic cell receptors and finally uptake by phagocytic cells.

6.6.1 The extrinsic pathway

The extrinsic pathway is triggered by ligands of so-called death receptors, which include members of the tumor necrosis factor (TNF) receptor gene superfamily, such as FasR or TNFR. Activation of these receptors facilitates recruitment and cleavage of initiator caspases (such as caspase-8) (Kischkel et al., 1995). Once caspase-8 is activated, the execution phase of apoptosis is triggered.

6.6.2 The intrinsic pathway

The intrinsic signaling pathway that initiate apoptosis involve a diverse array of non-receptor-mediated stimuli that produce intracellular signals that act directly on targets within the cell and are mitochondrial-initiated events. The stimulus that initiates the intrinsic pathway can be cell stress, such as growth factor or hormones withdrawal, application of chemotherapeutic drugs. All of these stimuli cause changes in the inner mitochondrial membrane that results in an opening of the mitochondrial permeability transition (MPT) pore, loss of the mitochondrial transmembrane potential and release of pro-apoptotic cytochrome c, which is normally sequestered, from the intermembrane space into the cytosol (Saelens et al., 2004). Cytochrome c together with other proteins activates the caspase dependent mitochondrial pathway: Cytochrome c binds and activates Apaf-1 as well as procaspase-9, forming an “apoptosome”, and the clustering of procaspase-9 in this manner leads to caspase-9 activation (Hill et al., 2004). The intrinsic pathway reaches the point of no return when the outer mitochondrial membrane is disrupted, leading to release of cytochrome c and downstream caspase activation (Gross et al., 1999) (Garcia-Saez, 2012).

The intrinsic pathway is regulated by the balance between pro- and antiapoptotic members of the B-cell lymphoma 2 (Bcl-2) protein family (Garcia-Saez, 2012; Gross et al., 1999). The Bcl-2 family of proteins governs mitochondrial membrane permeability and can be either pro-apoptotic or antiapoptotic. To date, more than twenty genes have been identified in the Bcl-2 family. Some of the anti-apoptotic proteins include Bcl-2, Bcl-x, Bcl-XL, Bcl-XS, Bcl-w, Bag, and some of the pro-apoptotic proteins include Bcl-10, Bax, Bak, Bid, Bad, Bim, Bik, Noxa, Puma and Blk. These proteins have special significance since they can determine if the cell commits to apoptosis or aborts the process. It is thought that the main mechanism of action of the Bcl-2 family of proteins is the regulation of cytochrome c release from the mitochondria via alteration of mitochondrial membrane permeability. A few possible mechanisms have been studied but none have been proven definitively. Serine phosphorylation of Bad is associated with 14-3-3, a member of a family of multifunctional phosphoserine binding molecules. When Bad is phosphorylated, it is trapped by 14-3-3 and

sequestered in the cytosol but once Bad is unphosphorylated, it will translocate to the mitochondria to release cytochrome C (Datta et al., 2000; Gross et al., 1999; Martinou and Youle, 2011; Tan et al., 2000). Bad can also heterodimerize with Bcl-Xl or Bcl-2, neutralizing their protective effect and promoting cell death (Yang et al., 1995). When not sequestered by Bad, both Bcl-2 and Bcl-Xl interact with Bax to inhibit apoptosis and inhibit the release of cytochrome C from the mitochondria (Fig. 32).

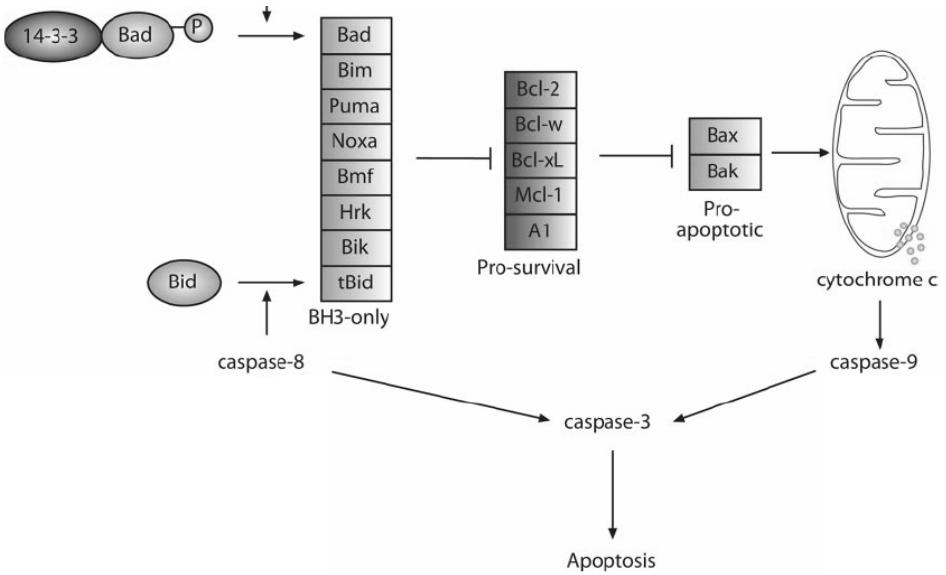

Figure 32: Model of apoptotic and survival signaling pathways involving Bad and Bcl-2 members. Sequestering members of the prosurvival group of Bcl-2 proteins by BH3-only members relieves inhibition of Bax/Bak leading to downstream caspase activation (Thomas and Biden, 2009).

6.6.3 The Execution Pathway

The extrinsic and intrinsic pathways both end at the point of the execution phase, considered the final pathway of apoptosis. It is the activation of the execution caspases that begins this phase of apoptosis. Execution caspases activate cytoplasmic endonuclease, which degrades nuclear material, and proteases that degrade the nuclear and cytoskeletal proteins. Caspase-3, caspase-6, and caspase-7 function as effector or "executioner" caspases, cleaving various substrates that ultimately cause the morphological and biochemical changes seen in apoptotic cells.

Caspase-3 is considered to be the most important of the executioner caspases and is activated by any of the initiator caspases (caspase-8, caspase-9, or caspase-10) (Slee et al., 2001). Caspase-3 specifically activates the endonuclease CAD, which then degrades chromosomal DNA within the nuclei and causes chromatin condensation. Caspase-3 also induces cytoskeletal reorganization and disintegration of the cell into apoptotic bodies.

6.6.4 Role of Bcl-2 family proteins

The pro- and antiapoptotic members of the Bcl-2 family are central regulators involved in β-cell fate decision between life and death in response to physiological insults. Their role in β-cells and their individual contribution to the glucose homeostasis remains controversial. The study by Zhou et al. was the first to provide proof of concept that overexpression of Bcl-xL in β-cells blunted stressed-induced apoptosis (Zhou et al., 2000). Unexpectedly, one of the transgenic lines expressing high levels of Bcl-xL also displayed severe hyperglycemia. In addition, another study reported increased amounts of phosphorylated BAD in islets of Zucker fatty rats, which coincided with increased β-cell survival and enhanced β-cell mass before development of obesity and hyperinsulinemia (Jetton et al., 2005). Also, data in human islets suggested that high glucose might modulate the balance of proapoptotic and antiapoptotic Bcl proteins toward apoptosis, thus favoring β-cell death (Federici et al., 2001). Indeed, the antiapoptotic gene Bcl-2 was unaffected by glucose change, whereas Bcl-xl was reduced upon treatment with high glucose. On the other hand, proapoptotic genes Bad, Bid, and Bik were overexpressed in the islets maintained in high glucose.

Recent studies cautioned that Bcl-2 protein family members might not only be involved in regulating apoptosis but also be implicated in a day-to-day control of cellular function (Danial et al., 2008). Nonetheless, other studies have tended to argue against the role of these proteins in glucose metabolism. Indeed, transgenic mice either overexpressing Bcl-2 or bearing a deletion in the Bcl-xL gene specifically in β-cells were not reported to display any aberrant alterations in glucose metabolism (Allison et al., 2000; Carrington et al., 2009) . Thus, the relative contributions of antiapoptotic versus alternative functions of Bcl-2 and Bcl-xL for overall β-cell survival and performance remain controversial. Notwithstanding, a recent study demonstrated that Bcl-2 or Bcl-xL dampens glucose-induced insulin secretion and highlight the role of these prosurvival proteins as critical physiological integrators balancing life and death with metabolism secretion coupling in the β-cell (Luciani et al., 2013).

7 INSULIN RECEPTOR SUBSTRATE PROTEINS

7.1 Structure of the IRS proteins

IRS proteins lack intrinsic catalytic activity but are composed of multiple interaction domains and phosphorylation motifs. At least three IRS proteins occur in humans and mice, including IRS1/Irs1 and IRS2/Irs2, which are widely expressed, and IRS4/Irs4, which is limited to the thymus, brain, and kidney and possibly β-cells. Rodents also express Irs3, which is largely restricted to adipose tissue and displays activity similar to Irs1.

All IRS proteins are characterized by the presence of a highly conserved NH2-terminal pleckstrin homology (PH) domain adjacent to a phosphotyrosine-binding domain (PTB), followed by a variable-length COOH-terminal tail that contains numerous tyrosine and serine phosphorylation sites. The PH and PTB domains mediate specific interactions with the insulin and IGF-I receptor kinases. The COOH-terminal end of each IRS protein contains a set of tyrosine phosphorylation sites that act as on/off switches to recruit and regulate various downstream signaling proteins, including the regulatory subunit of the lipid PI3K, Grb2, nck, and SHP2. Phylogenetic analysis reveals a close evolutionary relation between IRS1/ Irs1 and IRS2/Irs2 from humans and mice, which might have diverged from IRS4/Irs4 (Fig. 33) (White, 2002) (Thirone et al., 2006).

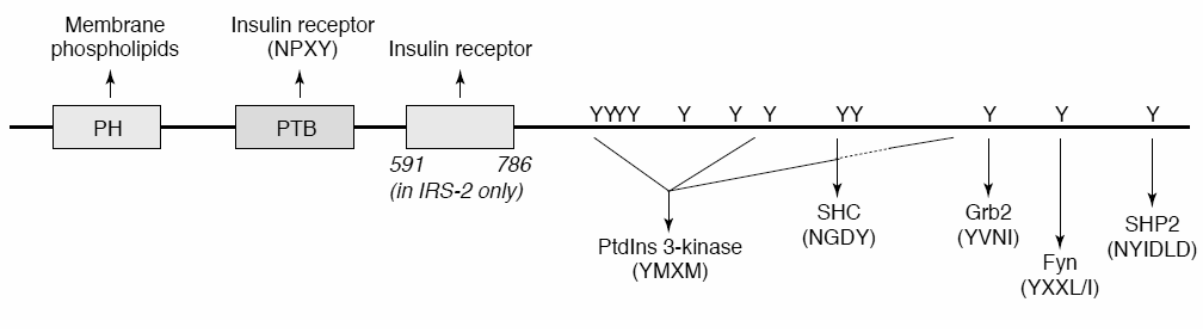

Figure 33. Structure of the mouse IRS protein (Thirone et al., 2006).

Thus, IRS proteins couple insulin/IGF receptors to the PI3-kinase and extracellular signal-regulated kinase cascades(White, 1998). As described above, activation of the PI3K/Erk cascades are important insulin/IGF-regulated pathways.

7.2 IRS signaling in the control of β-cell mass

IRS proteins regulate many biological processes, including the control of glucose metabolism, protein synthesis, and cell survival, growth and transformation (White, 2002). Although not all insulin signals are mediated by the IRS-proteins, major physiological responses to insulin/IGF are probably absent without them.

Although the IRS proteins are highly homologous and possess many similar tyrosine-phosphorylation motifs, studies in knockout mice and knockout cell lines indicate that the various IRS proteins serve complementary, rather than redundant, roles in insulin/IGF1 signaling (Fig.34).

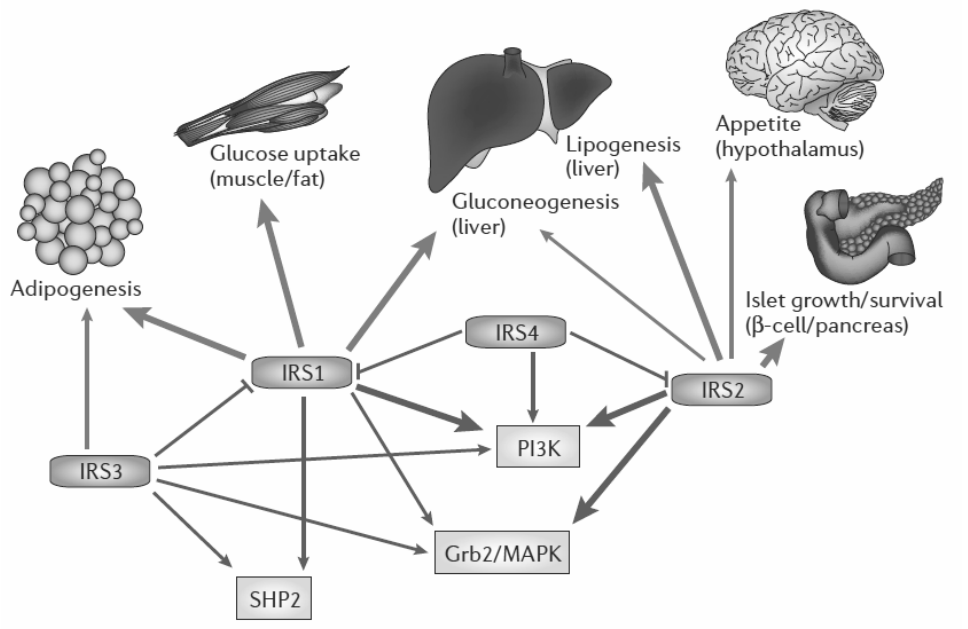

Figure 34. Isoform-specific functions of IRS proteins and their relative contribution to the biological actions that are regulated by insulin (purple arrows), as determined by knockdown and knockout studies. The thickness of the arrows is proportional to the intensity of the signal that is mediated by the IRS proteins.

Signal transduction via IRS2 is critical for β-cell growth and survival (Burks and White, 2001). Perhaps the best evidence of this is in the *Irs1*$^{-/-}$ and *Irs2*$^{-/-}$ transgenic mouse models, which also demonstrate the balance between β-cell mass and insulin resistance in relation to the pathogenesis of type 2 diabetes . IRS1 and IRS2 are key adaptor molecules in insulin signal transduction pathways in insulin target tissues (i.e., liver, muscle and fat) that act as an interface between the insulin receptor and downstream signaling elements(White, 1998). Therefore, in the absence of IRS1 and/or IRS2 expression, as in *Irs1*$^{-/-}$ and *Irs2*$^{-/-}$ transgenic mice, there is severe insulin resistance. However, the *Irs1*$^{-/-}$ mice do not become diabetic, because the β-cell mass expands in compensation for the insulin resistance, as seen in nondiabetic obesity (Kadowaki et al., 1996; Tamemoto et al., 1994). In contrast, the *Irs2*$^{-/-}$ mice become profoundly diabetic, because the β-cell mass does not expand in compensation for the insulin resistance, and the mice are insulin insufficient (Takamoto et al., 2008) (Withers et al., 1998) (Fig. 35).

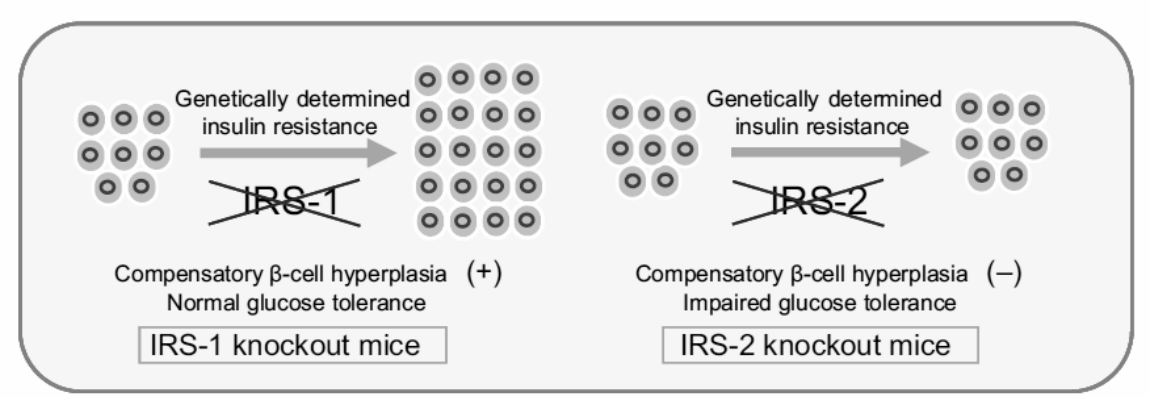

Figure 35. Schema showing the difference between IRS1 and IRS2 for compensatory β-cell hyperplasia in response to genetically determined insulin resistance (Takamoto et al., 2008).

The distinct roles of IRS1 and IRS2 illustrated in the above-mentioned studies in mice are also observed in human studies, which show a link between low IRS1 protein expression and insulin resistance in adipocytes (Rung et al., 2009). Surprisingly, such a link has not been clearly established in muscle. Furthermore, certain polymorphisms of IRS1 correlate with an elevated risk of diabetes in several populations, further supporting the importance of IRS protein in the regulation of glucose metabolism. The association between diabetes and IRS2 polymorphism is more tenuous than that of IRS1 (Thirone et al., 2006).

IRS2 (not IRS1) plays a key role in regulating β-cell mass in adaptation to the metabolic homeostasis and maintaining β-cell survival. In fact, increasing IRS2 expression in β-cells can distinctly increase the rate of glucose- and IGF-I-induced β-cell mitogenesis, implicating a significant role for IRS2 in expanding β-cell mass (Schuppin et al., 1998). However, the more pronounced effect of increasing IRS2 expression in β-cells is to promote β-cell survival, which can protect β-cells from both streptozotocin- and free fatty acid (FFA)-induced apoptosis (Hennige et al., 2003). Conversely, in the absence of IRS2 expression in β-cells, there is marked spontaneous apoptosis, and β-cell survival is dramatically reduced (Withers et al., 1999). The activation of the two major signaling pathways emerging downstream from IRS-2, the PI3K/PDK-1/PKB and Grb2/mSOS/Ras/Raf/ MEK-1/ERK pathways are the key elements promoting β-cell survival, with ERK1/2 having a more negligible contribution.

7.3 Disruption of Irs2 gene in mice

Ablation of the *Irs2* gene in male mice results in a phenotype with characteristics of type 2 diabetes: Irs2–deficient animals present defects in both insulin action and insulin production (Withers et al., 1998).

7.3.1 $Irs2^{-/-}$ mice are hyperglycemic and glucose intolerant

Only three days after birth, the levels of randomly fed sugars were elevated in $Irs2^{-/-}$ mice (166±13 mg/dl) compared with in wild-type mice (116±10 mg/dl) Between 3 and 6 weeks of age showed the development of fasting hyperglycaemia in $Irs2^{-/-}$ mice (Fig.36 a), and at 6–8 weeks of age these mice exhibited marked

glucose intolerance during an intraperitoneal glucose-tolerance test (b) (Withers et al., 1998).

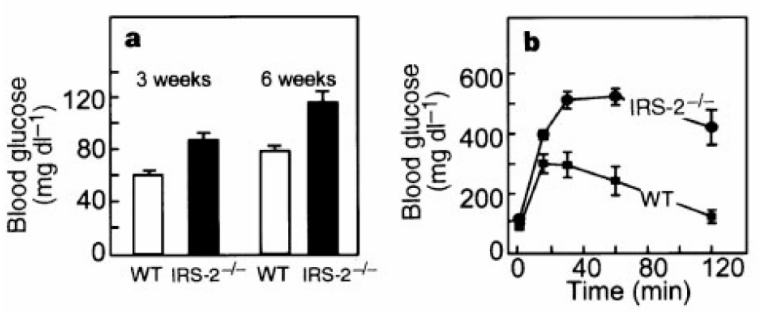

Figure 36. Adapted from (Withers et al., 1998).

At 10 weeks, *Irs2*$^{-/-}$ mice were overtly diabetic with fasting glucose levels of 323±35 mg/dl and if left untreated the levels rose progressively to 400 mg/dl at 12–16 weeks of age. Male *Irs2*$^{-/-}$ mice showed polydypsia and polyuria without ketosis, and died from dehydration and hyperosomolar coma (Withers et al., 1998); female mice do not followed a similar disease progression and rarely died from diabetes.

7.3.2 Irs2$^{-/-}$ *mice are hyperinsulinemic and insulin resistant*

Insulin levels in wild-type and *Irs2*$^{-/-}$ neonates were not significantly different, suggesting that *Irs2*$^{-/-}$ mice were slightly insulin resistant in light of their increased random glucose levels, mentioned above. After 6 weeks, *Irs2*$^{-/-}$ mice exhibited threefold higher fasting insulin levels than wild-type animals (Fig. 37c), and insulin-tolerance tests showed a significantly reduced hypoglycaemic response to exogenous insulin (d) (Withers et al., 1998).

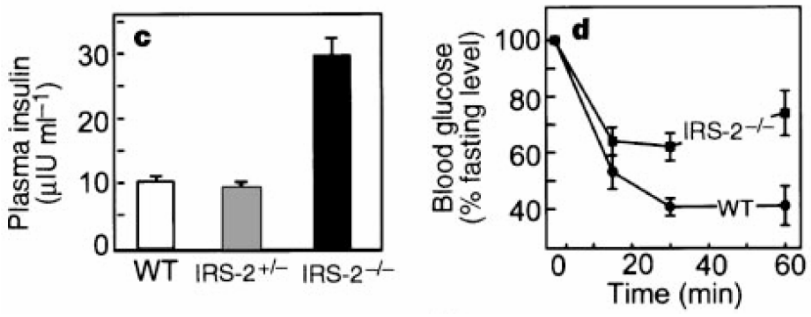

Figure 37. Adapted from (Withers et al., 1998).

Regarding insulin resistance, six-to-eight-week-old wild-type and *Irs2*$^{-/-}$ mice in the fasted state showed identical basal rates of glucose disposal and levels of production of hepatic glucose, despite the presence of hyperinsulinaemia in the *Irs2*$^{-/-}$ animals (Fig. 38e). However, low-dose insulin did not increase whole-body glucose disposal or suppress hepatic glucose release in *Irs2*$^{-/-}$ mice, although this dose of insulin markedly

enhanced these effects in wild-type and *Irs2*$^{+/-}$ mice. A higher insulin dose (20mUkg-1 min^{-1}) increased glucose disposal and suppressed hepatic glucose production in *Irs2*$^{-/-}$ mice, thus confirming that there was profound insulin resistance (Fig. 38f) (Withers et al., 1998).

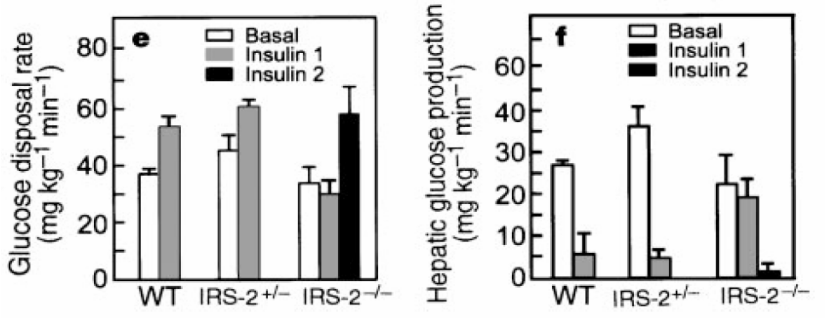

Figure 38. Adapted from (Withers et al., 1998).

Examination of signaling parameters in tissues of *Irs2*$^{-/-}$ mice implicates dysregulated PI3K activity as one molecular explanation for the insulin resistance in these animals. Studies of liver and muscle reveals impaired insulin-stimulated association of PI3K with IRS-1, elevated basal PI3K activity, and >50% inhibition of insulin-stimulated PI3K activity (Withers et al., 1998).

7.3.3 β-cell mass is reduced in Irs2$^{-/-}$ *mice*

Morphometric analysis of pancreases from mice at 4 weeks of age showed that *Irs2*$^{-/-}$ mice had significantly reduced β-cell mass compared with wild-type mice, but no significant difference in non-β endocrine-cell mass (Fig. 39) (Withers et al., 1998). In contrast, the β-cell mass of *Irs1*$^{-/-}$ mice, which have insulin resistance without diabetes, was elevated almost to the double of that of wild type mice (Hennige et al., 2005).

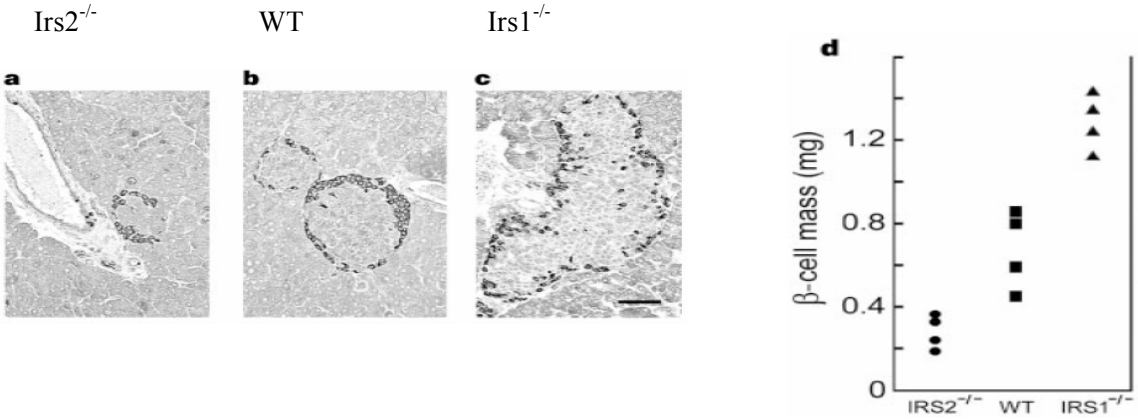

Figure 39. Adapted from (Withers et al., 1998).

Subsequent examination of neonatal *Irs2*$^{-/-}$ pancreas showed relative β-cell deficiency, suggesting that these changes are independent of long-term metabolic effects. The number of islets in *Irs2*$^{-/-}$ animals was decreased by ~50%. Additionally, islet insulin content was reduced in the *Irs2*$^{-/-}$ mouse.

7.3.4 Glucose-stimulated insulin release in Irs2$^{-/-}$

Functional assessment of insulin release *in vivo* during a glucose-tolerance test showed that 4-week-old wild-type mice (with a fasting glucose level of 79 mg/dl) exhibited a twofold increase in circulating insulin levels (from 11.75 ± 1.4 international microunits (μIU) ml^{-1} to 24.4 ± 2.7 μIU ml^{-1}; n=4) 60 minutes after glucose loading. Similarly, *Irs2*$^{-/-}$ mice (with fasting glucose levels of 106±5 mg/dl), despite fasting hyperinsulinemia, responded with a 1.9-fold increase in insulin levels 60 minutes after glucose loading (fasting, 23.5 ± 6 4.7μIU ml^{-1}; 60 min, 42.1 ± 5:8 μIU ml^{-1}; n=4). Therefore, in the early stages of the development of the diabetic phenotype, glucose-stimulated insulin release may be nearly normal. However, as the hyperglycaemia progresses glucose-stimulated insulin release is attenuated, which may be attributed to glucose toxicity towards β-cell function (Withers et al., 1998).

7.3.5 IRS2 pathways protect against apoptosis in primary β-cells

It is well described that IRS-dependent pathways mediate antiapoptotic effects of insulin IGF-1 (White, 1998). Therefore, by intercrossing *Irs2*$^{+/-}$ mice with heterozygous IGF-1 receptor (IGF1R) mice, Whiters *et al* demonstrated that Irs2 coordinates IGF-1 receptor-mediated β-cell function (Withers et al., 1999). IGF1R$^{+/-}$*Irs2*$^{-/-}$ animals displayed a severe reduction in β-cell area, with insulin-positive cells representing <2% of that seen in wild-type animals and this reduction in β-cells was much more pronounced than the 50–60% reduction observed in age-matched *Irs2*$^{-/-}$ islets. Also, they found increased numbers of apoptotic cells (measured by Fluorescent DNA fragmentation assays) within the β-cells of both *Irs2*$^{-/-}$and IGF1R$^{+/-}$*Irs2*$^{-/-}$ mice compared with wild-type animals and increased expression of Bad in the islets of these animals (Fig. 40). Moreover, they observed that the apoptotic nuclei and Bad positive cells colocalized within islets. These findings suggest that an increased apoptotic rate underlie the β-cell failure in these mice.

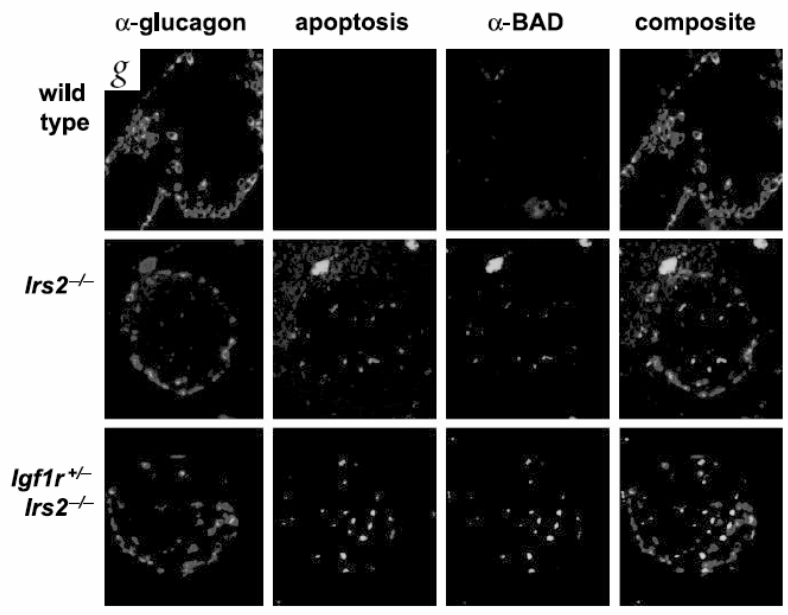

Figure 40. Adapted from (Withers et al., 1999).

As summary, *Irs2*$^{-/-}$ mice develops progressive diabetes due to reduced β-cell mass and failure of islet hyperplasia in the face of insulin resistance, indicating a crucial role for IRS2 in the regulation of β-cell survival. The combination of insulin resistance and reduced β-cell mass (which leads to diabetes in these mice) are the hallmarks of T2D, and this is why *Irs2*$^{-/-}$ mice model was considered a model that recapitulates T2D progression (White, 2002).

7.3.6 Irs2 gene disruption on Carbohydrate and Lipid Metabolism

The detailed study of the carbohydrate metabolism in *Irs2*$^{-/-}$ have confirmed that *Irs2*$^{-/-}$ are insulin resistant, as they showed a significantly attenuated response to insulin regarding whole-body glucose utilization and no significant effect of hyperinsulinemic-euglycemic clamp on the rate of endogenous glucose production (Previs et al., 2000). Following the hyperinsulinemic-euglycemic clamp, there were no significant differences in muscle glycogen. However, *Irs2*$^{-/-}$ mice had markedly reduced hepatic glycogen (0.52 ± 0.13 mmol glucose equivalents·g wet weight^{-1},$p < 0.05$ versus WT mice). In the basal state, all these parameters were similar between *Irs2*$^{-/-}$ and WT. Indeed, by using primary hepatocytes deficient for Irs2, was demonstrated that the ability of insulin to activate glycogen synthase was completely abolished compared to wild-type hepatocytes. Also, in primary wild-type hepatocytes insulin triggered a substantial inhibition of PEPCK and G6Pase mRNAs, but was incapable of suppressing it in primary hepatocytes derived from IRS-2-deficient mice. In conclusion, it was demonstrated the essential role of IRS-2 in insulin-regulated glycogen synthesis and in the expression of gluconeogenic enzymes involved in HGP. These studies implicate IRS-2 as the principal

mediator of insulin action in liver and suggest that impaired IRS-2 signaling may represent a major component of liver insulin resistance.

Regarding lipid metabolism, plasma FFA, glycerol concentrations and glycerol production were found comparable in WT and *Irs2*$^{-/-}$ mice, suggesting that basal lipolysis rates were similar. During the hyperinsulinemic-euglycemic, the concentration of plasma FFA in *Irs2*$^{-/-}$ mice suffered a minor reduction, meaning that lipid metabolism is dysregulated in these animals.

7.3.7 Prevention of T2D in Irs2$^{-/-}$ *mice*

The progression of *Irs2*$^{-/-}$ mice toward diabetes can be retarded or prevented by genetically modifying elements of the insulin/IGF-signaling cascade that promote compensatory β cell function or improve insulin sensitivity. These include: downregulation of protein tyrosine phosphatase Ptp1b, haploinsufficiency of the transcription factor Foxo1 or of the negative regulator of insulin action PTEN (Kitamura et al., 2002; Kushner et al., 2004; Kushner et al., 2005) upregulation of the pancreatic duodenal homeobox 1 (Pdx1) (Kushner et al., 2002). Also, transgenic upregulation of Irs2 in pancreatic β-cells also prevents diabetes in *Irs2*$^{-/-}$ mice obese mice, and streptozotocin-induced diabetic mice by promoting sufficient and sustained compensatory insulin secretion (Hennige et al., 2003).
The administration of Vildagliptin, an inhibitor of the enzyme dipeptidyl peptidase-4 that degrades and inactivates GLP-1 and GIP, was the only pharmacological agent shown to improved glucose tolerance in another strain of *Irs2*$^{-/-}$ mice (Sato et al., 2012), as the treatment with Exendin-4 did not shown efficacy (Park et al., 2006).

7.4 Others models of Irs2 disruption

7.4.1 Irs2 disruption on Pancreas

The critical role of pancreatic IRS2 signaling for islet endocrine cell function was demonstrated by Withers *et al* by generating a mice lacking Irs2 in the endocrine and exocrine pancreas, using the Cre system under the promotor of pancreatic and duodenal homeobox factor 1/Pdx1 (*PIrs2KO*) (Cantley et al., 2007). These mice displayed impaired glucose tolerance with reduction of β-cell mass, impaired insulin secretion, alteration in islet gene expression and beta cell calcium mobilizations, but no reductions in insulin sensitivity or body weight alterations. They demonstrated that IRS2-dependent mechanisms are required not only for β-cell compensation under conditions of increased insulin but also for maintenance of a normal postnatal beta cell mass. However, these *PIrs2KO* animals displayed normal fasting blood glucose levels and did not develop the progressive diabetes seen in *Irs2* global-null mice.

7.4.2 Liver-specific deletion of Irs2

Despite Irs2 was claimed as the principal mediator of insulin action in liver, liver-specific deletion of insulin receptor substrate 2 (LivIrs2KO) does not impair hepatic glucose and lipid metabolism in mice. Indeed, LivIrs2KO had fasting and fed blood glucose levels comparable to that seen in control animals, and tolerance to glucose was normal, as well as insulin sensitivity (Simmgen et al., 2006). Insulin regulates hepatic metabolism partly by regulating the expression of key metabolic genes in glucose and lipid metabolism. Deletion of Irs2 in the liver had no significant effect on a number of insulin-regulated transcriptional events. Detailed analysis by performing hyperinsulinaemic-euglycaemic clamps demonstrated that:

1) Whole-body glucose disposal was mildly reduced in LivIrs2KO mice and this impairment was associated with a small reduction in whole-body glycogen synthesis, which accounted for the impaired whole-body glucose utilization.

2) Endogenous glucose production and glycolysis rates were not different between LivIrs2KO and control mice.

These findings suggest that LivIrs2KO mice have a very mild defect in whole-body insulin sensitivity that does not impact on long-term glucose homeostasis.

7.4.3 Disruption of Irs2 in β-cells and brain

The conditional knockout of Irs2 in pancreatic β-cells and parts of the brain (including the hypothalamus) displayed increased appetite, lean and fat body mass, linear growth, and insulin resistance that progressed to diabetes (Lin et al., 2004). Yet, it has been shown that diabetes can be prevented in these mice by transgenic expression of *Irs2* in β-cells and by restoring sufficient β-cell function to compensate for insulin resistance in the obese mice. Thus, these findings reinforcing a primary role of the β-cell compartment in the diabetic phenotype in *Irs2*$^{-/-}$ mice. More recently, it was described that *Irs2*$^{-/-}$ animals severely diabetic (27.7 mM of fed glycemia) exhibited higher hypothalamic inflammation markers than non-diabetic or prediabetic *Irs2*$^{-/-}$ mice (11.1 mM of fed glycemia), which could represent a pathogenic factor that determines prediabetic versus diabetic outcomes in these model. Despite these understandings, it remains to be experimentally proved whether the pattern of hypothalamic inflammation revealed in this study could indeed mediate the transition from prediabetes to diabetes in the group of IRS2-deficient mice or if it is a consequence of the development of diabetes.

8 SODIUM TUNGSTATE

Sodium tungstate is the inorganic compound with the formula Na_2WO_4•2H2O and is the salt of tungstate. Tungstate is the oxoanion of tungsten (WO4) also known as wolfram, a transition metal naturally occurring as a mineral of the VI group of the periodic table of elements, with the atomic number of 74 and molecular weight of 183.85 g/mol.

As a transition metal, tungsten can be found in different oxidation states (from +2 to +6), a property that confers it the ability to replace other endogenous metals. Tungsten is similar to molybdenum in its chemical properties, and these two elements also display similar characteristics to vanadate. Indeed, they all form iso- and heteropolyanions, which present octahedral co-ordination spheres and are able to form polynucleotide complexes, but only the oxidation states +4, +5, and +6 are biologically important. It has been reported, for instance, that tungsten can replace molybdenum in Mo-containing enzymes such as xanthine oxidase and sulfite oxidase in kidneys and intestine. Moreover, it has been suggested that tungsten could replace phosphate in bone, a mimetic property, which may explain the much higher concentration found in bone tissue when compared to those of other organs.

Several studies were conducted to support the evaluation of tungstate as an antidiabetic and antiobesity therapy, without significant evidence of severe toxic effects. Overall, the toxicity of tungstate appears to be low. Some pharmacokinetic studies with sodium tungstate were also carried out in rodents (rat and mice) and beagle dog. In rat, bioavailability was high (92%), whereas it was lower in dog (approximately 65%). The elimination half-life was two times higher in dog than in rat (4h and 1.7h respectively), whereas in sheep was reported an elimination half-life of 12 to 14h. A recent study compared rats and mice exposed to tungstate and showed that the time course of tungstate in tissues from mice and rats differ. In rat tissues, the general trend from an oral tungstate dose is for tungstate to accumulate through at least the first 4 h (could accumulate for 6 or 8 h). By 24 h the tissue concentrations had decreased to about 1/10 the 4h data. In contrast to rats, the maximum concentrations in mice occur at 1-2 h for plasma and tissues, except for the femur. These data point toward a contrast in the absorption and elimination kinetics between the two species. Both the rats and mice showed tungstate distribution to each of the characterized biological compartments, indicating rapid absorption from the gastrointestinal tract and systemic distribution. After 24 h most of the rat tissues values are very close to or at baseline (endogenous) tungstate levels. Previous reports indicated that the primary elimination route for tungstate is through the urine, with more than 85% of oral doses in rats reported to be eliminated in urine by 24 h. Based on the previous animal studies, Leggett (1997) developed a kinetic model of the disposition and retention of tungstate in the human body. In that model Leggett (1997) noted that the disposition of tungstate in rats and larger mammals appears to be similar, but the rat shows more rapid excretion of tungstate than the larger mammals. The preliminary oral dose biokinetic model developed by Leggett (1997) suggested that 85% of tungstate should be eliminated by 24 h and 97% by 1 month. In that model, it was predicted that the majority of the body burden of tungstate would be retained in bone, primarily

through mechanisms of tungstate replacement of phosphate in bone as proposed by Fleshman *et al.* (1966). In previous studies by Kaye (1968) using radiolabeled tungstate in different oxidation states, it was shown that tungstate had the least retention in bone (among the tungstate forms studied).

The first proof-of-concept study on the potential effect of sodium tungstate in the treatment of obesity was recently conducted. The results of the TROTA 1 trial show that monotherapy with sodium tungstate at a dose of 200 mg/day is insufficient as an antiobesity drug. Indeed, a 6-week trial active treatment with sodium tungstate was not associated with a meaningful weight loss or body fat mass reduction (Hanzu et al., 2010).

8.1 Sodium tungstate as inhibitor of phosphatases

Phosphorylation of tyrosine residues of intracellular or membrane proteins is a fundamental cellular signal for regulating cell growth, differentiation, and proliferation. The levels of phosphotyrosine in the cell are governed by the competing actions of protein tyrosine kinases and protein tyrosine phosphatases.

In aqueous solution, sodium tungstate dissociates and forms the tungstate anion (WO_4^{-2}), with a tetrahedral structure analogous to that of phosphates (PO_4^{-2}), vanadate and molybdate. This structure seems to be an important characteristic of effective inhibitors of phosphatases, which compete with phosphate substrates of the enzyme at the catalytic unit's active site. In line with this, tetrahedral tungstate (WO_4^{-2}) was reported as a competitive inhibitor of the enzyme protein tyrosine phosphatase of *Yersinia* bacterium (Fauman et al., 1996). Another study demonstrated that tungstate complex at the catalytic site of protein phosphatase 1 (PP1), which is a serine/threonine protein phosphatase that is essential in regulating diverse cellular processes (Egloff et al., 1995). Tungstate was also described as a potent inhibitor of glucose-6-phosphatase *in vitro* acting at the catalytic unit of the system (Foster et al., 1998). Glucose-6-phosphatase catalyzes the terminal step in hepatic gluconeogenesis and glycogenolysis, resulting in the production of glucose for release into the bloodstream, and therefore plays an important role in the maintenance of blood glucose homeostasis. Related or not with this characteristic, a normoglycemic effect similar to that of vanadate was also associated with tungstate.

8.2 Normoglycemic effects of sodium tungstate

The normoglycemic effect of tungstate was first ascribed to a positive action on the liver. In a first approach, Guinovart *et al* described that both molybdate and tungstate exert effects similar to those previously reported for vanadate in isolated rat hepatocytes. All these three compounds have insulin-like effects on the glycolytic pathway, since they increase basal fructose 2,6-bisphosphate levels, counteract the effects of glucagon on fructose 2,6-bisphosphate concentrations and 6-phosphofructo-2-kinase activity, and stimulate glycolytic flux. Considering glycogen metabolism, molybdate and tungstate provoke non-insulin-like effects, since they inactivate glycogen synthase and activate glycogen phosphorylase (Fillat et al., 1992).

8.3 Sodium Tungstate effects on Liver

Posteriorly, the positive effect of sodium tungstate was confirmed in a rat model of diabetes induced by streptozotocin (Barbera et al., 1994). In this study, oral administration of tungstate was able to normalize glycaemia and glucose hepatic metabolism in diabetic rats. Like vanadate and insulin, tungstate treatment partially restored glucokinase (GK) activity in the liver of diabetic rats, contributing to a partial increase in the concentration of glucose-6-phosphate (G6P), and in this way, increased glycogen levels in diabetic rats. Regarding glycolytic/gluconeogenic pathway, 6-phosphofructo-2-kinase, L-pyruvate kinase, glycogen phosphorylasae (GPa) as well as fructose 2,6-bisphosphate activities reached levels similar to those observed in healthy animals. Moreover, mRNA levels of hepatic GK, glycogen phosphorylase, and PEPCK were also normalized. These observations, associated with discovery that tungstate was able to inhibit G6P *in vitro*, could partially explained the normoglycemic effect of sodium tungstate. The same results were obtained were STZ-induced rats were treated with sodium tungstate for 8 months.

The results obtained in STZ-induced diabetic models suggested that tungstate restores hepatic glucose metabolism in STZ-diabetic rats. After these promising results, tungstate treatment was tested in Zucker diabetic fatty (ZDF) rats, a genetic type 2 diabetes model that closely resembles the disease in humans. In this model, tungstate also improved blood glucose levels, despite these effect was not permanent and the rats eventually presented hyperglycemia (Muñoz et al., 2001). Also, tungstate treatment of these rats induced a 42% decrease in serum levels of triglycerides and normalized hepatic G6P concentrations, GPa activity, and PEPCK levels. GK activity in treated diabetic rats increased hepatic glycogen levels to 55% higher than those in untreated diabetic and healthy rats. These data suggest that tungstate administration to ZDF rats causes a considerable reduction of glycemia, mainly through a partial restoration of hepatic glucose metabolism and a decrease in lipotoxicity. Interestingly, tungstate did not significantly change the phosphotyrosine protein profile of primary cultured hepatocytes.

The first study that focused on the identification of the molecular mechanism of action of tungstate was conducted *in vitro* using CHOIR cells (Chinese hamster ovary cells that overexpress human wild type insulin receptor-IR) or primary cultured hepatocytes (Dominguez et al., 2003). These experiments showed that tungstate increased glycogen synthesis and accumulation in primary cultured hepatocytes, suggesting insulin-like actions. However, tungstate did not significantly alter the phosphorylation state of the insulin receptor β-subunit, nor did it block or delay its dephosphorylation. Therefore, this compound bypassed the IR in its mechanism of action. In contrast, at low concentrations, tungstate induced a transient strong activation of extracellular signal-regulated kinases 1 and 2 (Erk1/2) after 5–10 min of treatment, in a similar way to insulin. Despite tungstate is a potent phosphatase inhibitor, it did not significantly delay or inhibit the dephosphorylation of Erk1/2. Instead, tungstate triggered a cascade of downstream events, which included the phosphorylation of p90RSK and GSK3, which inactivates it, thus promoting glycogen deposition. Experiments with a specific inhibitor of Erk1/2 activation and kinase assays indicate that these proteins were

directly involved in the stimulation of glycogen synthase and glycogen synthesis induced by tungstate without a direct involvement of PkB/Akt. These results show a direct involvement of Erk1/2 in the mechanism of action of tungstate at the hepatic level. However, how tungstate activates Erk1/2 is still unknown. The data indicate that Erk1/2 protein kinases are not directly activated by tungstate, as they are sensitive to PD98059, a Mek1/2 inhibitor. Thus, this study proposed that tungstate acts on one or several of the components of the Ras-Raf-Mek-Erk pathway.

More recently, the action of sodium tungstate on the improvement of the diabetic state was studied *in vivo* by using STZ-induced diabetic rats. In this work, the authors reported for the first time *in vivo* that tungstate restores the phosphorylation state of Erk1/2, p90RSK and GSK3 in livers of STZ rats, thus inducing increased glycogen deposition in treated diabetic rats (Nocito et al., 2012). Furthermore, Erk1/2 increased the expression of c-fos and c-jun, which are components of the AP1 complex that decreases the expression of gluconeogenic genes, such as PEPCK. This effect may explain how this compound compromised the expression of gluconeogenic enzymes as PEPCK. Also, they demonstrated that tungstate effects on the liver of these animals were independent of PkB/Akt, because no changes were observed in the phosphorylation state of this protein, and also independent of insulin, because the effects of this compound on gluconeogenic enzymes are maintained in isolated hepatocytes cultured in the absence of insulin. Moreover, they also observed moderately increased insulinemia in tungstate-treated STZ-diabetic rats, which suggested also a possible effect of tungstate on the pancreas. Finally, the authors proposed that tungstate modulates hepatic glucose production in this model, which may contribute to ameliorating hyperglycemia in these diabetic animals.

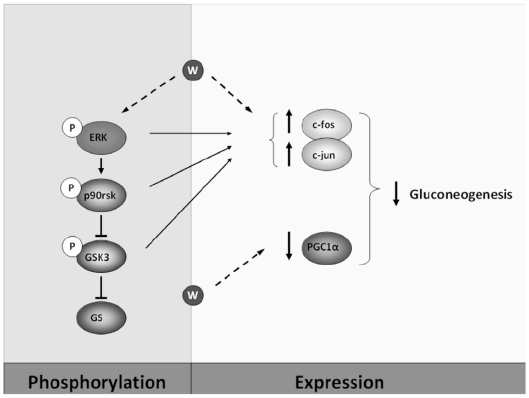

Figure 41. Schematic representation of proposed effects of tungstate on the liver (Nocito et al., 2012).

However, the authors did not explored the possible effects of tungstate on the pancreas, and did not mentionate the reason why treated diabetic rats presented blood glucose levels above 250 mg/dl at the end of the treatment. These data suggested that, despite hyperglycemia was improved after treatment with tungstate, the modulation of hepatic glucose metabolism was not sufficient to normalized glucose homeostasis in this

mice model, contrasting with previous studies with the same animal model.

Therefore, the question as to the primary target/s of tungstate action remains open. Therefore, it was recently descortinated that sodium tungstate increased the phosphorylation of Mek, Raf and Ras, and in this way, activates Erk1/2 in CHOIR cells and primary hepatocytes (Zafra et al., 2013). Moreover, by blocking Ras, the effect of tungstate on Erk phosphorylation was blocked, as well as the tungstate-induced phosphorylation of GSK3, supporting a requirement of Ras activation for tungstate-mediated effects. In addition, the involvement of G-proteins in the tungstate-mediated activation of Ras and phosphorylation of Erk was demonstrated in CHOIR cells, as well as in primary cultured rat hepatocytes. When the pre-incubated of CHOIR cells for 28 h with pertussis toxin (PTX), a G-protein inhibitor that ADP-ribosylates the alpha subunits of the heterotrimeric guanine nucleotide regulatory proteins Gai, Gao and Gat, showed a blockade of tungstate-induced Ras activation and Erk phosphorylation, and also GSK3 phosphorylation. Therefore, these study presented a new pathway to activate glycogen synthesis through which tungstate may exerts its anti-diabetic actions. This new route involves G-proteins and the subsequent activation of the Ras/Erk pathway, but it is independent of the classical insulin- activated pathway involving the insulin receptor.

8.4 Sodium Tungstate effects on Pancreas

The main action of tungstate in the STZ-induced diabetic rats (corresponding to type 1 diabetes model) appears to be the restoration of the hepatic glucose metabolism by increasing the capacity of the liver to utilize glucose through glycolysis and glycogenesis, and to decrease its potential for glucose output. However, when the neonatally injected STZ (nSTZ) rats (resembling a type 2 diabetes model) were used this does not appear to be the case; in these rats, the normoglycemic effect of tungstate cannot be attributed to the small changes observed in hepatic glucose metabolism. Moreover, the main action of tungstate appears to be correlated with an increase in insulin content and β-cell area, which leads to an improvement in the ability of β-cells to respond to glucose (Barbera et al., 1997).

Posteriorly, it was described that the normoglycaemic effects of tungstate in this model were mediated through a process of pancreatic regeneration leading to β-cell mass restoration. This new cell population was functional, allowing the decrease of glycaemia in diabetic rats, and maintaining normoglycaemia even after treatment is withdrawn. These results suggested that tungstate treatment increased extra-islet β-cell replication without modifying intra-islet β-cell replication rates. Moreover, the treatment induced increases in insulin-positive cells located close to ducts and in Pdx1 positive cells scattered in the exocrine tissue, suggesting active neogenesis. In islets from treated diabetic rats, tungstate was able to increase the phosphorylation state of Pdx1 through the activation of p38, which could be responsible for the increased insulin mRNA expression and islet content in treated animals, taking into account that Pdx1 regulates the expression of several β-cell genes, including insulin (Fernandez-Alvarez et al., 2004).

At the same time, the insulin secretory pattern elicited by tungstate was characterized at the perfused

rat pancreas. The study by *Rodríguez-Gallardo et al.* demonstrated that, in the perfused pancreas from normal rats, infusion of tungstate induces a prompt, short-lived insulin response, comparable to the early phase of glucose-induced insulin secretion. The insulinotropic effect of tungstate was dose-dependent and takes place at normal (5.5 mM) and moderately high (9 mM) glucose concentrations but not at a low glucose level (3.2 mM). The lack of influence of tungstate on glucagon release would rule out mediation of the insulinotropic effect of tungstate by a α-cell paracrine effect (Rodriguez-Gallardo et al., 2000).

Also, tungstate's effects on the insulin secretion elicited by various β-cell secretagogues were quantified *ex-vivo*. The study was performed in the perfused pancreas isolated from normal or somatostatin-depleted pancreases. In control rats, tungstate co-infusion potentiated the insulin secretory responses to glucose, arginine, exendin-4, glucagon and tolbutamide. It also inhibited the somatostatin secretory responses to the same secretagogues. In somatostatin-depleted pancreases, the stimulatory effect of tungstate on basal insulin secretion and its potentiation of arginine-induced insulin output were comparable to those found in control rats, thus suggesting an amplifying effect of tungstate on a common step in the insulin stimulus/secretion coupling process. These results supported a direct stimulatory effect of sodium tungstate on β-cell secretion that is not paracrine mediated by the inhibition of somatostanin secretion induced by this tungstate (Silvestre et al., 2005). In line with these results, cellular insulin content and basal and glucose-insulin secretion was also found increased in BRIN-BD11 β-cell line cultured with tungstate for 3 days (Liu et al., 2004). Finally, Piquer *et al*. demonstrated that tungstate treatment activates p38 and PI3K in MIN6 cells, which mediated PDX-1 translocation to the nucleus, in accordance to what was previously found in nSTZ rats treated with tungstate. However, tungstate has no effect on glucose-induced insulin secretion but stimulates basal insulin release, which is not in line with previous studies in perfused rat pancreas, in BRIN-BD11 beta cell line and in nSTZ-treated rats (Piquer et al., 2007).

Finally, Altirriba *et al.* studied pancreatic plasticity in STZ-rats treated with tungstate. In this report, morphological analysis of the pancreas demonstrated that tungstate treatment increased β-cell area and PDX-1 positive β-cells in the islets (Altirriba et al., 2009). This increased β-cell area was ascribed to a combination of a decrease in β-cell apoptosis and an increase in proliferation. This rise does not normalize β-cell area. Nevertheless, the stimulation of the treatment increased by two-fold basal insulinemia in diabetic animals. Also, differential expression analysis of the whole pancreas identified 370 differentially expressed genes. Some genes whose expression was restored by the tungstate treatment were involved in metabolism, protein modification, and oxidative stress, showing that the treatment acts on several pathways, which lead to the partial recovery of pancreatic function. Moreover, the authors conclude that tungstate effects on gene expression were independent of the decrease in glycaemia: when diabetic rats were treated with phloridzin, which leads to a decrease in glycaemia without any direct effect on pancreatic function, no significant differences in the expression of the genes resultant from microarray analysis were found between the phloridzin administrated animals and their control counterparts. Thus, the authors concluded that gene expression changes induced by the treatment were not a consequence of the decrease in glycemia observed in

the diabetic treated animals. Importantly, the authors demonstrated that tungstate and serum from tungstate treated animals induced proliferation in Ins1 cells, and correlated these findings with increased Erk1/2 phosphorylation. In conclusion, this study demonstrated that tungstate was able to partially increase β-cell area and recovered the endocrine function in STZ-rats. These improvements in pancreatic function required the combined action of several pathways, such as Wnt, TGF-b, Notch and MAPK.

8.5 Sodium Tungstate effects on Adipose Tissue

The effects of sodium tungstate on adipose tissue were studied using a rat model of diet-induced obesity. Claret *et al.* described that tungstate decreased body weight gain and adiposity of obese rats without the side effects that have been associated with the use of drugs that inhibit absorption of dietary fat (Claret et al., 2005). Also, they observed that tungstate ameliorates insulin resistance and improved lipid profile by decreasing the circulating levels of triglycerides and nonesterified fatty acids. These effects were not associated with fat malabsortion, reduced energy intake or changes in plasma leptin; instead, sodium tungstate prevented adipocyte hypertrophy and enhanced energy dissipation, by increasing fatty acid oxidation. Moreover, tungstate administration also increased the expression of UCP1 protein in brown adipose tissue, and UCP2 in white adipose tissue. The treatment with tungstate also resulted in the up-regulation several genes involved in lipid metabolism in white adipose tissue.

In summary, the authors concluded that tungstate increased whole-body energy expenditure and favored oxidative catabolism of fatty acids over anabolic pathways, without excessive free radical generation. These actions improve lipid profile and insulin sensitivity and reduce weight gain and adiposity in obese rats.

Posteriorly, a proteomics approach was used to identify proteins associated with obesity and targets of tungstate in white adipose tissue (Barcelo-Batllori et al., 2005; Barcelo-Batllori et al., 2008). Twenty-nine proteins were found differentially expressed between lean and diet-induced obese rats and tungstate treatment of obese rats reverted expression changes of 70% of the proteins modulated by obesity and another ten proteins were regulated by tungstate independently of the body weight reduction. The results suggest that tungstate antiobesity effect can be mediated by the modulation of cellular structure, metabolism, redox state and signaling processes in adipose tissue. One protein found upregulated was Raf-1. In parallel with the increased expression of Raf, tungstate activates MAPK-Erk1/2 in other models, as previously described. Regarding brown adipose tissue, the treatment with sodium tungstate identified 20 proteins as direct targets that were implicated in redox, glycolysis, Krebs cycle, electron transport and mitochondrial respiration, and fatty acid oxidation and lipolysis. Furthermore, bioinformatics analyses using Ingenuity Pathways Analysis revealed that PGC-1α could be a direct target of the tungstate antiobesity effect in brown adipose tissue.

In summary, the antiobesity effect of tungstate could result, at least in part, from the reduction of redox status and increased energy dissipation through up-regulation of PGC-1α and possibly modulation of posttranslational modifications. In addition, the *in vitro* effects of sodium tungstate on adipocyte

differentiation and mitochondrial function were described by MC Carmona *et al (Carmona et al., 2009)*. In this report, tungstate treatment of adipose cells blocks adipocyte differentiation and increases energy consumption, in total accordance with the earlier *in vivo* results in which tungstate decreased fat mass, mainly by inhibiting differentiation and increasing energy dissipation (it increases oxygen consumption of adipose cells). On the one hand, it preferentially activates the translation of a master dominant-negative regulator of adipocyte differentiation, the liver-enriched inhibitory protein (LIP).

The antiobesity effects of tungstate were completely dependent on a functional leptin system: in animals with deficiencies in the leptin system, tungstate did not reduce body weight gain, food intake or increased energy expenditure (Canals et al., 2009). Indeed, when circulating leptin levels were partially restored in mice that lack the expression of leptin (ob/ob mice), tungstate was able to exert its effects on body weight. Also, tungstate treatment induced changes in the expression levels of genes involved in energy expenditure in brown adipose tissue of mice with functional leptin system but in ob/ob mice, in agreement with previous results in diet-induce obese rats. Finally, gene expression of hypothalamic neuropeptides involved in energy homeostasis, which are classically regulated by leptin (neuropeptide Y (NPY), Agouti-related peptide (AGRP), proopiomelanocortin (POMC), and cocaine- and amphetamine-related transcript (Stull et al.)) was accessed after the treatment. Interestingly, tungstate administration modified NPY, AGRP and CART gene expression profile in lean mice but not ob/ob mice. When leptin deficiency in ob/ob mice was restored through adipose tissue transplantation, neuropeptide expression changes due to tungstate administration were similar to the ones observed in treated lean mice, thus suggesting that the effects of tungstate on body weight may be mediated centrally, via action on some of the neuropeptides involved in the regulation of energy homeostasis.

In summary, the authors demonstrated that the leptin system is essential for tungstate action because when either leptin or its receptor is absent, tungstate is ineffective. Therefore, the antiobesity activity of tungstate depends entirely on a functional leptin system. Moreover, these results indicated that tungstate promotes an adaptation of BAT to increase thermogenesis and energy expenditure, mechanism that promotes the reduction of body weight gain in a leptin-dependent manner. Also, these results suggested a hypothalamus-mediated effect of tungstate on leptin-regulated genes, by an increase in the expression of neuropeptides related to energy homeostasis regulation and modulation of food intake.

8.6 Sodium Tungstate effects on the Central Nervous System

The *in vivo* of sodium tungstate on body weight gain and food intake were mainly through increasing energy expenditure and lipid oxidation, but it also modulates hypothalamic gene expression when orally administered. Indeed, a direct effect of sodium tungstate on the central nervous system was described (Amigo-Correig et al., 2011). First of all, intraperitoneally administration of sodium tungstate to Wistar rats confirmed that it crossed the blood–brain barrier, reaching the cerebrospinal fluid. When centrally administered to the

third cerebral ventricle, sodium tungstate decreased body weight gain and food intake and increased the phosphorylation of janus kinase-2 (Jak2), and, consequently, of pStat3-Y705, the main kinases and proteins involved in leptin signaling. *In vitro*, sodium tungstate increased the phosphorylation of JAK2 and ERK1/2, but the activation of each kinase did not depend on each other. It regulated c-myc gene expression through the Jak2/Stat system and c-fos and AgRP (agouti-related peptide) gene expression through the Erk1/2 pathway simultaneously and independently. *Summarizing, sodium tungstate was able to cross the blood-brain-barrier, probably reaches the central nervous system and can eventually activate the leptin-signalling pathway of neural cells. This would regulate food intake and body weight, two major components of energy homeostasis, in part through the regulation of neuropeptide gene expression.*

Recently, another study reported that sodium tungstate effects on body weight could be associated with transcriptional and functional changes in the hypothalamus. Proteomic and immunohistochemistry results revealed that sodium tungstate modified the expression levels of proteins involved in cell morphology, axonal growth, and tissue remodeling, such as actin, and neurofilaments (essential for the maintenance of neuronal structure), and of proteins related to energy metabolism. *In vivo* magnetic resonance imaging showed that tungstate treatment can affect neuronal organization in the hypothalamus, open the possibility that sodium tungstate might also have a role in neuronal plasticity (Amigo-Correig et al., 2012).

8.7 Sodium Tungstate effects in other tissues

A few studies also attempted to address the effects of sodium tungstate in skeletal muscle. Girón *et al.* reported that diabetes decreased Glut4 expression while tungstate treatment normalized not only Glut4 protein but also Glut4 mRNA in the diabetic rats (Girón et al., 2003). Furthermore, treatment increased Glut4 protein in plasma and internal membranes, suggesting a stimulation of its translocation to the plasma membrane. The effects of sodium tungstate in in Glut4 transporters were also addressed at the molecular level using L6 differentiated myotubes. First, the authors demonstrated that tungstate treatment increases 2-deoxy-D-glucose (2-DG) transport in myotubes, through a rise in the total amount of Glut4 transporter (long-term effect) and its translocation to the plasma membrane (short-term effect). Tungstate treatment increased the total amount of Glut4 in L6 myotubes through an upregulation of *Glut4* transcription driven by MEF2 (myocyte enhancer factor 2) transcription factors. Accordingly, MEF2 levels and DNA binding activities were increased in response to the treatment. Moreover, the short-term effects of tungstate and insulin on 2-DG uptake were additive, thereby indicating distinct but convergent signaling pathways. Indeed, the tungstate-induced increase in 2-DG uptake did not involve activation of the insulin receptor and members of its amplification cascade. In addition, this increase was also independent of the phosphorylation of AMPK. These observations indicated the existence of a PI3K- and AMPK independent pathway to increase capacity for glucose uptake in muscle cells upon treatment with tungstate, that the authors latter demonstrated to be the activation of Erk1/2 pathway. In this context, tungstate-induced glucose uptake and Glut4 transcriptional activation were

dependent on the activation of extracellular signal-regulated kinases 1 and 2 (Erk1/2).
In conclusion, their results showed that tungstate treatment increased the potential for glucose transport in muscle cells by two mechanisms, translocation and increase in transcription of Glut4, both dependent of Erk1/2.

Two questions that remains unanswered are first, if these mechanisms are also present *in vivo* and second, if so, which are the physiological consequences of increased glucose uptake by the muscle when diabetic animals are treated with sodium tungstate. Indeed, when the direct impact of tungstate and other compounds (sodium selenate, selenite, vanadate) on glucose metabolism of isolated rat soleus muscle was investigated, all compounds stimulated glucose transport, but only vanadate exerted an insulin-like effect on glycogen synthesis as it stimulated muscle glycogen storage (Barbera et al., 1994). Neither selenite nor selenate or tungstate, to all of which insulin-mimetic potency has been ascribed, were capable of triggering an anabolic response in isolated rat soleus muscle. Distinct insulin mimetic effects on liver and adipocytes, respectively, have been described for selenite, selenate, and tungstate, but these report clearly indicated that these salts are not to be regarded as full insulin mimetic, since they lack direct acute stimulation of muscle glycogen storage and therefore fail to mimic the quantitatively most important effect of insulin. Lack of acute insulin like action on isolated muscle, however, does not exclude other beneficial effects of tungsten salts on muscle glucose metabolism *in vivo*, which may occur in response to chronic treatment and/or via interaction with other tissues.

II AIMS OF THE THESIS

Type 2 diabetes is characterized by changes in various metabolic parameters but the triggering factor for the transition from a prediabetic state to type 2 diabetes is β-cell failure, which involves both a critical decline of β-cell mass and/or deterioration of β-cell function. Hence, understanding how to prevent the decline and/or dysfunction of β-cells represents a critical issue in the treatment of type 2 diabetes.

The Irs2 knockout mice is a rodent model that recapitulate the pathogenesis of type 2 diabetes, as they exhibited a combination of insulin resistance and reduced β-cell mass, which are the hallmarks of type 2 diabetes. However, these mice develop progressive diabetes mainly due to β-cell failure, indicating a crucial role for IRS2 in regulating β-cell survival and expansion.

Tungstate is a powerful normoglycemic agent used to treat diabetes in several genetically induced rodent models, with demonstrated beneficial effects on hepatic glucose metabolism and/or pancreatic regeneration processes.

In this work, we aimed to contribute to the understanding of the mechanisms implicated in the progression to type 2 diabetes. Thus, tungstate was used as a tool to explore (Araki et al.) the pathophysiology of type 2 diabetes in Irs2 Knockout mice and (2) the mechanisms implicated in the progression to type 2 diabetes in these mice. We hypothesized that tungstate might affect pancreatic β-cell mass and ameliorate the diabetic phenotype of *Irs*2$^{-/-}$ mice.

Finally, we have proposed the following specific aims:

- To analyze the effect of tungstate on glucose homeostasis in *Irs*2$^{-/-}$ mice, including:
  - Whole-body glucose homeostasis
  - Hepatic glucose metabolism

- To investigate the effects of tungstate on pancreatic β-cell mass regulation, by performing:
  - Morphometric study of the pancreas

III RESEARCH DESIGN AND METHODS

1 ANIMALS

1.1 Generation of the model

Irs2 knockout mice were originally developed in the laboratory of Dr. Morris White, at Joslin Diabetes Center/HHMI, Boston (Withers et al., 1998) and generously donated by Dr. Deborah Burks to our laboratory. A targeting vector containing neomycin resistance and herpes simplex virus thymidine kinase genes was used to delete the entire insulin receptor substrate 2 gene. Homologous recombination between the normal endogenous gene and the targeting vector results in a recombined inactive gene in which exon 2 (containing the start codon) have been substituted by the neomycin-resistance gene, which also includes a stop codon (neo).

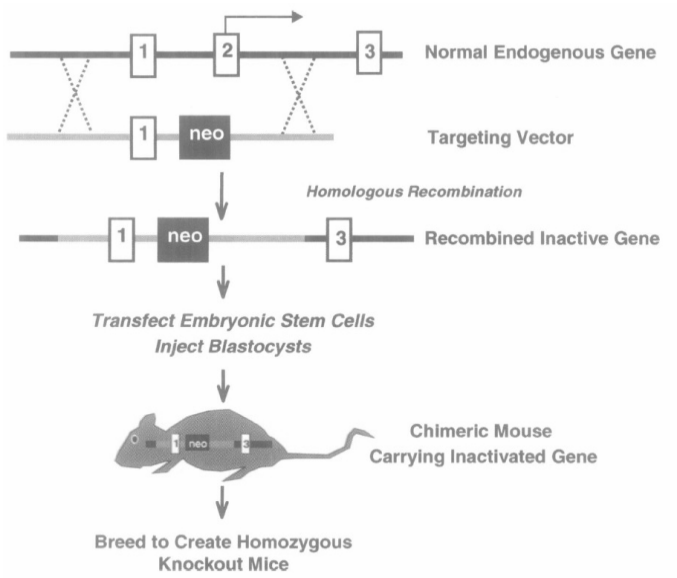

Figure 1: Gene targeting by homologous recombination.

The construct was electroporated into 129X1/SvJ x 129S1/Sv-derived R1 embryonic stem (ES) cells. In the correctly targeted ES cells, the modified gene replaced the normal endogenous gene, and they survive to neomycin selection. The properly targeted cells were then injected into C57BL/6 mouse blastocysts, which in turn are implanted into pseudo-pregnant foster mothers to complete development. The resulting chimeric animals carrying the inactivated Irs2 gene were crossed to C57BL/6 mice and breed to create homozygous knockout mice. Initially, the animals were maintained in a C57B1/129sv hybrid background, but were finally backcrossed to obtain a pure C57BL/6 background.

It is important to clarify that another *Irs2*$^{-/-}$ strain mice was generated by another group with a different background (C57B1/6 x CBA hybrid background), which results in a different and less severe diabetic

phenotype (Kubota et al., 2000).

1.2 The colony

To obtained homozygous knockout mice for Irs2, we intercrossed heterozygous (*Irs2*$^{+/-}$, HTZ) mice as *Irs2*$^{-/-}$ mice (both female and male) are majority infertile. By intercrossing *Irs2*$^{+/-}$ mice we generated wild-type (*Irs2*$^{+/+}$, WT) and *Irs2*$^{-/-}$ mice that were used in our study. The litters were of normal size (around 8 animals) but we observed that *Irs2*$^{-/-}$ mice did not born with the expected frequency (1 out of 4 animals), as in some litters no knockout animals were present. As previously described, we observed that *Irs2*$^{-/-}$ neonates were smaller than WT neonates.

1.3 Genotyping

The genotyping of the animals was done by Polymerase chain reaction (PCR) with 1cm of mouse-tail using the Fast Tissue-to-PCR kit (Fermentas #K1091). The steps for PCR cycling were described at www.jax.org the section for *Irs2*$^{-/-}$ mice model, being the annealing temperature 65ºC. The primers used were also described in www.jax.org and are the following (5'---3-):

Irs2 mutant forward: GCTATCAGGACATAGCGTTGG ---------- Final concentration: 1μM
Irs2 wild-type forward: CTTGGCTACCATGTTGTTATTGTC ------Final concentration: 0.25μM
Irs2 common: AGCTCTGGAGGTTTACTTTCCTAG---------- Final concentration: 1.33 μM

Our protocol only differs from that described in the kit in what refers to the concentration of the primers used. The mutant primer amplifies a DNA fragment of 700 base pair; the wild-type primer amplifies a DNA fragment of 550 base pairs and the common (heterozygote) primer amplifies two DNA fragments of 550 to 700 base pairs. The PCR was performed with the 3 primers at the same time and separated by gel electrophoresis on a 1.5% agarose gel.

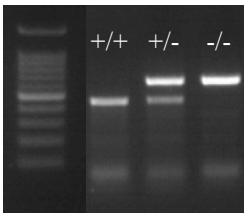

Figure 2: Electrophoresis of a PCR example.

2 THE TREATMENT WITH TUNGSTATE

Principles of laboratory animal care were followed (European and local government guidelines) and the Animal Research Committee of the University of Barcelona approved all protocols.

2.1 Including criteria

2.1.1 Age

In order to define at which age we should initiate the treatment with tungstate, we proceeded to the measurement of blood glucose levels in *Irs2*$^{-/-}$ mice at 8 weeks old, as it was previously described that these animals exhibited fasting hyperglycemia between the age of 6 and 8 weeks (Withers et al., 1998). HTZ and WT animals were also included. At the age of 8 weeks, *Irs2*$^{-/-}$ mice displayed fasting hyperglycemia relative to WT animals, whereas HTZ showed normal fasting glycaemia (Fig. 3A). In the research with rodents, the glucose tolerance test is the most widely used test to determine whether a genetically engineered (e.g., transgenic or knockout) or dietary-induced mouse is glucose intolerant or diabetic. Thus, we performed glucose tolerance test as described in section 3, at 8 weeks of age. *Irs2*$^{-/-}$ mice exhibited higher blood glucose levels during the glucose tolerance test than WT animals (Fig. 3B), showing that *Irs2*$^{-/-}$ mice were less tolerant to glucose. HTZ had similar tolerance to WT animals. However, at the age of 8 weeks, *Irs2*$^{-/-}$ mice did not exhibit marked and severe glucose intolerance as previously described (Withers et al., 1998), and therefore, we decided to wait until the age of 10 weeks in order to see more pronounce differences between *Irs2*$^{-/-}$ and WT mice. All the experiments were therefore performed with 10-weeks old WT and *Irs2*$^{-/-}$ animals and the results are displayed in the section of Results. HTZ mice were not included, as these animals did not show abnormalities in blood glucose levels or glucose intolerance.

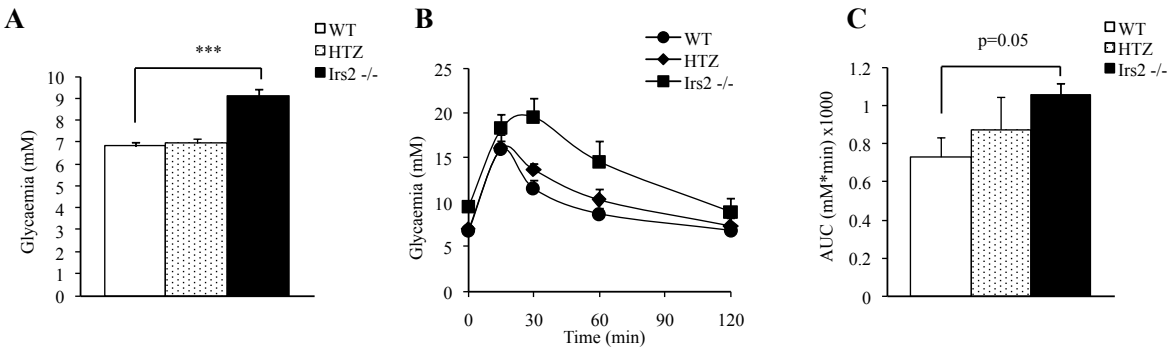

Figure 3: Fasting blood glucose levels (A) were measured in 8-week old WT (n=4), HTZ (n=4) and *Irs2*$^{-/-}$ mice (n=5). Intraperitoneal glucose tolerance test was performed in 8-week old WT (n=4), HTZ (n=4) and *Irs2*$^{-/-}$ (n=3) mice and the correspondent area under the curve (AUC) calculation is shown (C). Data are mean ± SE, ***p<0.001 indicated groups.

2.1.2 Glycaemia

At the beginning of the experiment, WT and *Irs2*$^{-/-}$ mice were randomly divided into two treatment groups, one group received distilled water as drinking water (untreated group) whilst the other received ad libitum a solution of 2mg/ml of sodium tungstate (Na2WO4 · 2H2O, Sigma-Aldrich, USA) in distilled water (treated group).

As reviewed in the introduction, the appearance of the diabetic phenotype in *Irs2*$^{-/-}$ animals occurs within a short time frame, and is highly variable between individuals, meaning that at the same age, some individuals may present moderate hyperglycemia and others may be already diabetic. Indeed, in our colony we observed this disparity of phenotype as, at the age of 10 weeks, around 25% of the animals were diabetic (basal glycemic levels superiors to ≈16mM (≈300mg/dl)), contrasting with the 75% that presented basal glycemic levels around to 10-11mM (≈200mg/dl). When diabetic *Irs2*$^{-/-}$ animals were treated with tungstate, none presented any improvement in their glycemic levels as depicted in figure 4. Additionally, 40 % of these diabetic treated *Irs2*$^{-/-}$ animals died within the first 2 weeks of treatment, and 90% died after 3 weeks of treatment. This contrasted with the 0% of mortality observed in moderately hyperglycemic *Irs2*$^{-/-}$ mice that were treated with tungstate.

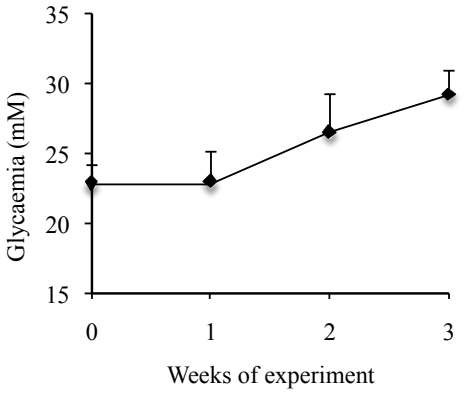

Mortality in diabetic *Ir2*$^{-/-}$ mice	
Died in 1st week of treatment	10%
Died in 2nd week of treatment	40%
Died in 3nd week of treatment	90%

Figure 4: Fasting blood glucose levels were recorded in treated *Irs2*$^{-/-}$ mice (n=10) that were severely diabetic at the time of initiation of the treatment with tungstate and mortality in diabetic *Irs2*$^{-/-}$ mice. Data are mean ± SE.

Thus, two including criteria were followed in this study regarding *Irs2*$^{-/-}$ animals: being 10-weeks old and displaying initial blood glucose levels inferior to 16mM.

2.2 Duration of the treatment

Initially the animals were treated for 4 weeks as previously described in several tungstate-related works. However, 13% of *Irs2*$^{-/-}$ animals that were left untreated died from hyperosmolar coma during the two first experiments, and 38% displayed blood glucose levels above 400 mg/dl at the end of the experiment, making almost non-viable the performance of the glucose tolerance test and the recovery of tissues. Additionally, tungstate decreased the glycaemia of *Irs2*$^{-/-}$ treated animals in the first two weeks after the onset of the treatment (Fig. 5). Thus, in order to avoid the dead of untreated *Irs2*$^{-/-}$ animals, but at the same time, maximize the differences between treated and untreated *Irs2*$^{-/-}$ animals, we decided to stop the treatment at 3 weeks.

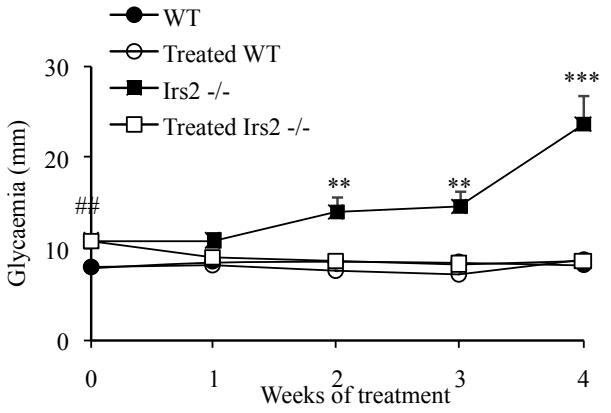

Figure 5. Effect of 1 month of treatment with tungstate in the fasting blood glucose levels of *Irs2*$^{-/-}$ mice. Fasting blood glucose level was recorded once a week during 1 month of treatment with tungstate in WT and *Irs2*$^{-/-}$ mice (n=6 for each genotype). Data are mean ± SE, ##p<0.01 between *Irs2*$^{-/-}$ and WT mice, and ***p<0.001 and **p<0.01 between treated and untreated *Irs2*$^{-/-}$ mice.

A long-term treatment with tungstate was also performed in order to confirm some results obtained with short-term 3-weeks treatment. Mice with the same characteristics of the 3-weeks treatment (10 weeks of age and moderate hyperglycemia) were treated during 20 weeks with tungstate, reaching the age of 30 weeks.

3 METABOLIC STUDIES

3.1 Basal Glycemia

Blood glucose levels were measured weekly until the time of sacrifice using a clinical glucometer and Accu-Check test strips (Roche Diagnostics, Switzerland). Blood samples were collected at the same time points with a microvette (Sarstedt).

3.2 Glucose Tolerance Test

Variables such as fasting duration, route, and amount of glucose administration, as well as state of consciousness, may have a large impact on the measured glucose tolerance in mice. In our study, we have evaluated the glucose tolerance in the mouse by administering intraperitoneally 2 g/kg body weight of glucose following 6 h of fasting, as it was demonstrated that these conditions results in more robust differences in plasma glucose and insulin levels between experimental groups (Andrikopoulos et al., 2008). Therefore, for intraperitoneal glucose tolerance tests (IGTT), 6 hour-fasted mice were injected with 2 g glucose/Kg body weight (Glucose 40%) and glycemia was measured at time 0, 15, 30, 60 and 120 minutes after glucose injection. Blood samples were collected at the same time points with a microvette (Sarstedt).

3.3 Insulin Tolerance Test

For insulin tolerance tests (ITT), animals were also fasted for 6 hours and injected with 0.75 IU insulin/Kg body weight (Actrapid, Novo Norddisk) and blood glucose levels measured as previously indicated.

3.4 Insulinemia

For insulin determination a commercial Enzyme-Linked Immunosorbent Assay (ELISA) was used (Mercodia Mouse Insulin Elisa, Sweden, 10-1247-01). Plasma from blood samples collected at the IGTT or once a week

was separated by centrifugation and kept at -80ºC and posteriorly diluted 1:2 or 1:4 in the standard solution of the assay (also used as negative control).

4 HEPATIC GLUCOSE METABOLISM

The study of the glucose metabolism was done in collaboration with Dr. Delia Zafra and Dr. Joan Guinovart from the Institute for Research in Biomedicine in Barcelona. Therefore, all the experimental protocols belong to their laboratory and will be briefly described in this section. Enzymes and biochemical reagents were from Sigma-Aldrich. All other chemicals were of analytical grade.

4.1 Enzymatic Activity and Glycogen content

Glycogen Synthase (GS) activity was determined in frozen liver samples homogenized (Polytron) in 10 volumes of ice-cold 10 mM Tris-HCl buffer (pH 7.4) containing 150 mM KF, 15 mM EDTA, 0.6 M sucrose, 1 mM phenylmethylsulfonyl fluoride, 1 mM benzamidine, 10 μg/ml leupeptin, 10 μg/ml pepstatin, 10 μg/ml aprotinin, 25 nM okadaic acid and 15 mM 2-mercaptoethanol. Whole homogenates were used for determinations. Total (T) GS activity was measured in the presence of 6.6 mM glucose-6-phosphate, active or intrinsic GS activity (I form) was measured in the absence of glucose-6-phosphate and GS I/T activity ratio (-G6P/+G6P) were measured as described (Thomas et al., 1968).

Glucokinase (GK) activity was determined by measuring the capacity of the liver sample to phosphorylate glucose into glucose-6-phosphate using a spectrophotometric assay (Kuwajima et al., 1986). 100 mg of frozen liver samples were homogenized using a polytron in 1 ml of buffer containing Tris-HCl 50 mM, KCl 100 mM, EDTA 1 mM, 10% sacarosa (p/v), β-mercaptoetanol 0,1 mM at pH 7.4.

Glycogen phosphorylase (GP) activity was measured from pulverized tissue maintained at -80 ° C, which were prepared in the same buffer and under the same conditions outlined for the determination of GS activity. This activity was determined using a radiometric assay which measures the incorporation of [14-C]-glucose-1-phosphate to glycogen, following the technique described by Gilboe (Gilboe et al., 1972) in absence or presence of different effectors. The test is based on the incubation of GP enzyme in conditions in which glycogen is synthesized instead of degraded. It is a measure of the amount of glycogen produced by the GP per unit of time and protein. The GP can be found in phosphorylated state and active (form a) and in an unphosphorylated and inactive state (form b). To determine its activity, a mixture consisting of [14-C]-glucose-1-phosphate at 75mM (0.005 mCi / mmol), KF 125mm and glycogen at 0.6% in a pH of 6.3 was used. To determine the activity of the form a (active), caffeine, which is an inhibitor of the form b, is added to the assay mixture to give a final concentration of 1 mM. and AMP. To determine the activity of the total GP enzyme (GP, form a+b), AMP, which is a activator of the form b, is added to the assay mixture to give a final concentration of 1 mM.

All enzymatic activities were expressed as specific activity (mU / mg tissue).

To measure glycogen content, protein concentration of liver extracts was first measured following the method Pierce BCA (bicinchoninic acid) protein assay. Frozen liver samples were homogenized with 4

volumes of 30% (w/v) KOH and boiled at 100 ºC for 15 min; glycogen was determined after ethanol precipitation as described (Chan and Exton, 1976).

4.2 Electrophoresis and Immunoblotting

Homogenates (20 µg of protein) were resolved by 10% SDS-PAGE. The protein was transferred onto a nitrocellulose membrane and probed with the following antibodies: an antibody against liver GS (Garcia-Rocha et al., 2001), an antibody against Phospho-liver GS (Ser 8) (Ros et al., 2009), an antibody against GP, Phospho-GP (Ser 14) and GK (de la Iglesia et al., 1999). ERK antibody was from Upstate (Waltham, MA). Phospho-GS (Ser 641) antibody was purchased from Cell Signalling (Beverly, MA). GAPDH antibody was from Ambion (Austin, USA). PEPCK antibody was a kind gift of Dr. Daryl Granner (Vanderbilt University, USA). Secondary antibodies conjugated to horseradish peroxidase against rabbit (GEHealthcare), mouse (DakoCytomation) or sheep (Dako Cytomation) immunoglobulins were used. Immunoreactive bands were visualized using an ECL plus kit (GE Healthcare), following the manufacturer's instructions.

5 IMMUNOHISTOCHEMISTRY.

5.1 Pancreas Processing and Tissue Sectioning

At the end of the treatment, the animals were sacrificed and the whole pancreas was rapidly excised, blotted, and weighed. Before weighing, the pancreas was quickly cleaned from other tissues that may have been also excised (fat, duodenum, and lymph nodes). Then the pancreas was placed in a previously weighed cassette and weighed on a scientific scale, following by an overnight fixation in 10% formalin neutral buffered solution at 4ºC, and embedded in paraffin as described (Montanya and Tellez, 2009).

5 µm longitudinal sections of paraffin blocks were sectioned in a microtome and rehydrated the day after with xylene, followed by decreasing concentrations of ethanol and finally PBS in order to deparaffinize the tissue sections (Montanya and Tellez, 2009).

5.2 Immunofluorescence for Insulin, Glucagon and Pdx1

For insulin and glucagon staining, the deparaffinized sections were permeabilized with 1% Triton X-100 in PBS for 30 min, followed by incubation with blocking solution (PBS+1%BSA). For Pdx1, the deparaffinized sections were subjected to an antigen retrieval protocol, consisting in microwaving the sections in 10mM citrate buffer (pH 6.0) for 5 minutes and twice, followed by a permeabilization step with 1% Triton X-100 in PBS for 30 min, and incubation with blocking solution of antibody diluent with background reducing components+3% Donkey serum for 40 min. All the sections were thereafter incubated overnight with primary antisera at 4ºC. Primary antibodies used was: guinea pig anti-insulin, mouse anti-glucagon and rabbit anti-Pdx1 (Table 1). Pdx1 antibody is a homemade and it was a kind gift from Dr. Jorge Ferrer's group. For Pdx1 detection, a double immunohistochemical staining with insulin was performed. Insulin and Glucagon primary antibodies were diluted in PBS+1%BSA, whereas Pdx1 was diluted in antibody diluent with background

reducing components (Dako). Cyanine 2 and Cyanine 3-labelled secondary antibodies (Jackson Immunoresearch, UK) were diluted in PBS+1%BSA, and incubated for a period of 2 hours at room temperature. Hoechst 33258 (Sigma-Aldrich), a blue fluorescent dye used to stain the DNA, was used as nuclear marker and diluted 1:1000 in PBS. Images were taken with a Leica DMR HC epifluorescence microscope.

5.3 Immunofluorescence for Caspase 3

Detection of the active form of caspase 3 was performed in order to detect apoptotic β-cells. This method was chosen as caspase 3 is activated during the early stages of apoptosis. For caspase 3 detection, a double immunohistochemical staining with insulin was performed. After the deparaffinization of the sections an antigen retrieval protocol was applied, consisting in microwaving the sections in 10mM citrate buffer (pH 6.0) for 2 minutes. The sections were then permeabilized with 1% Triton X-100 in PBS before overnight primary antisera incubation at 4ºC. The primary antibodies used a rabbit anti-caspase 3 and guinea-pig anti-insulin (Table 1) in antibody diluent with background reducing components (Dako). Cyanine 2 and Cyanine 3-labelled secondary antibodies were diluted in PBS+1%BSA, and incubated for a period of 2 hours at room temperature. Hoechst 33258 was used as nuclear marker and diluted in 1:1000 in PBS. Images were taken with a Leica DMR HC epifluorescence microscope.

5.4 Immunofluorescence for Ki67

For detection of proliferative β-cells, Ki67 immunostaining was performed. Ki67 is a nuclear antigen associated with cell proliferation and is present throughout the active cell cycle phases, but absent in resting cells. Compared with BrdU staining, the advantage of Ki67 is that no antigen must be injected to identify replication. For Ki67 detection, a double immunohistochemical staining with insulin was performed. After the deparaffinization of the sections, an antigen retrieval protocol was applied, consisting in microwaving the sections in 10mM citrate buffer (pH 6.0) for 5 minute and twice. The sections were then permeabilized with 1% Triton X-100 in PBS before overnight primary antisera incubation at 4ºC. Primary antibodies used were guinea pig anti-insulin and mouse anti-Ki67 (Table 1) in antibody diluent (Dako). Cyanine 2 and Cyanine 3-labelled secondary antibodies were diluted in PBS+1%BSA, and incubated for a period of 2 hours at room temperature. Hoechst 33258 was used as nuclear marker and diluted 1:1000 in PBS. Images were taken with a Leica DMR HC epifluorescence microscope.

Table 1: Antibodies used in immunohistochemistry analysis

Antigen	1º Antibody source	Dilution	Commercial reference	2º Antibody	Dilution
Insulin	Donkey Guinea pig	1/500	Dako A0564	Cy2 Anti-Guinea pig Jackson I.R. 706-225-148	1/500
Glucagon	Mouse	1/1000	Dako A0565	Cy3 Goat Anti-mouse GE Healthcare PA43002	1/500
Pdx1	Rabbit	1/800	----------	Cy3 Donkey Anti-rabbit Jackson I.R. 711-165-152	1/500
Cleaved Caspase 3	Rabbit	1:400	Cell signalling, 9661	Cy3 Donkey Anti-rabbit Jackson I.R. 711-165-152	1/500
Ki67	Mouse	1:50	BD Pharmigen 550609	Cy3 Goat Anti-mouse GE Healthcare PA43002	1/500

6 MORPHOMETRIC ANALYSIS

For each animal, a minimum of 3 pancreatic sections separated by at least 150µm was stained with the respective primary antibodies. Images of all islets identified in the tissue section were taken with a Leica DMR HC epifluorescence microscope and analyzed with ImageJ software. The same sections were posteriorly counter-stained with toluidine blue for the calculation of the total surveyed pancreatic area using the "Analyse-Measure" tool of Image J software.

Fractional β-cell area calculation: the perimeter of the area stained for insulin is traced in the captured image using the "Analyse-Measure" tool of Image J software, which then calculates the areas that have been traced in pixels or µm. Results were expressed as the percentage of insulin positive area relative to the total surveyed pancreatic area as described (Montanya and Tellez, 2009). A minimum of 50 islets with more than five insulin-positive cells was analysed per animal for β-cell area calculation.

Total β-cell mass: was calculated by multiplying fractional β-cell area per pancreas weight (Montanya and Tellez, 2009).

For proliferation analysis: β-cells that expressed Ki67-positive nuclei were counted and this number divided by total number of β-cells.

For apoptosis analysis: β-cells expressing cytoplasmic active caspase 3 were counted and divided by the total number of β-cells.

The results are expressed as percentage of proliferative or apoptotic β-cells relative to total number of β-cells.

The total number of β-cells was quantified by counting the number of nucleus stained with Hoechst in insulin expressing cells using the "Analyze-Analyze particles" tool of Image J software.

7 ISLET ISOLATION

WT or *Irs2*$^{-/-}$ mice were sacrificed by cervical dislocation, the abdominal cavity was open and the pancreas and common bile duct were exposed. By clamping on either side of the small-intestinal, where the bile duct drains, inflate the pancreas by inserting a 30g needle and 5 ml syringe containing 2 ml of cold collagenase solution through the bile duct (Szot et al., 2007) (Stull et al., 2012). After inflation of the pancreas is complete, it was removed from the body and placed into a falcon containing 1 ml of collagenase (Roche Diagnostics) solution to posterior digestion for 6 minutes followed by islet separation in a density gradient using Histopaque (Sigma Diagnostics) as previously described (Casas et al., 2008). Islets were handpicked under a stereomicroscope, pelleted and rapidly frozen at -80ºC for the microarray and the protein expression studies, or put in RPMI-1640 medium for culture studies.

8 ISLET CULTURE

After isolation, islets were first cultured overnight in RPMI-1640 medium (Gibco-BRL, Pisley, U.K.) containing 11.1 mmol/l glucose and supplemented with 10% FBS, 2 mmol/l l-glutamine, 100 units/ml penicillin, and 100 µg/ml streptomycin at 37°C with 5% CO2 to allow total recovery from the isolation procedure. Next day, islets were incubated with the RPMI-1640 medium (Control condition) or the RPMI-1640 medium supplemented with 100µM sodium tungstate with or without a highly selective inhibitor of both MEK1 and MEK2, the 1,4-diamino-2, 3-dicyano-1,4-bis[2-aminophenylthio] butadiene (U0126) (Sigma-Aldrich), used at a final concentration of 20µM.

9 RNA ISOLATION AND CDNA PREPARATION

Total RNA was prepared from isolated islets using the RNeasy Micro Kit (Qiagen, Venlo, Netherlands) and eluted in 12 ul of RNAse free water**.** 300 ng of RNA was retrotranscribed using Superscript III (Invitrogen, Carlsbad, CA, USA) following the manufacturer's instructions, resulting in a final cDNA concentration of 15 ng/ul, assuming that all RNA was retrotranscribed to cDNA.

10 QUANTITATIVE PCR ANALYSIS

2.5 ng of cDNA was used for amplification by Real Time PCR in a LightCycler® 480 System (Roche, Germany) using SYBR Green (Mesa Green, Eurogentec, Belgium). The final volume reaction was 10ul, and the primers were always used at a final concentration of 10µM. PCR products were verified by dissociation curve analysis. Expression levels were normalized to expression of TATA box binding protein (Tbp) gene. Primer sequences are provided in Table 2.

11 GENE EXPRESSION PROFILING

The study of the gene expressing profiling was done in collaboration with the Bioinformatics platform of IDIBAPS.

Total RNA was prepared as described from pools of approximately 200 isolated islets (2-3 animals per experimental group) and RNA integrity was assessed using the 2100 Bioanalyzer (Agilent Technologies, Santa Clara, CA, USA) in the Genomic Unit of IDIBAPS. 300 ng of total RNA was converted to cDNA as describe above. A total of 15 μg of labeled cRNA was fragmented and hybridized to oligonucleotide Affymetrix Mouse 430 2.0 whole genome arrays (representing about 14000 well-characterized mouse genes) in the Genomic Unit. In total, 12 microarrays (3 per experimental group corresponding to a total of 6-9 animals per group) were hybridized. Washes and scanning of the arrays were performed according to manufacturer instructions. Expression values were summarized after background correction and normalization steps using the RMA (Robust Multi-array Average) methodology (Irizarry et al., 2003). The results corresponding to the microarray datasets were submitted to the GEO (NCBI) repository (accession number GSE43620).

The non-supervised hierarchical clustering of the differentially expressed genes did not correctly aggregate the all the samples within the correct experimental group, and finally, 1 microarray sample per experimental group was excluded from the study.

Differential expression analysis was performed by the non-parametric approach Rank Prod (Breitling et al., 2004). The web tool David was used for the calculation of the functional over-representation statistics of the list of significant genes obtained in the Rank Prod analysis (Dennis et al., 2003). Gene Ontology Biological Process GO_BP_FAT database was considered. A FDR (false discovery rate, which is the expected proportion of false positive findings among those differential expressions) and q-values threshold (measure of significance for each probe set in terms of FDR) inferior to 0.05 was considered as valid. Therefore, all the genes presented had q-values<0.05.

Table 2: List of primer sequences used in qRT-PCR experiments.

Primer	(5'---3')	Gene ID
Caspase 3 Forward	TCATTCAGGCCTGCCGGGGT	Casp3
Caspase 3 Reverse	ACAGGAAGTCAGCCTCCACCG	Casp3
Txnip Forward	CAGAAAAGGATTCTGTGAAGGTGAT	Txnip
Txnip Reverse	GCCATTGGCAAGGTAAGTGTG	Txnip
Bad Forward	CCTCGCTGGCTCCTGCACAC	Bad
Bad Reverse	TGGGCTGCTGGTCTCCACCG	Bad
Bik Forward	AGGGTGTTCGGGCAGTTCGC	Bik
Bik Reverse	TGGGGGACCTGGTCGTGTGG	Bik
Bax Forward	TTCGGGACCCCCACATGGCA	Bax
Bax Reverse	CAGTGGGAGGCCTCAGCCCA	Bax
Bcl2 Forward	GGGATGCCTTTGTGGAACTA	Bcl2
Bcl2 Reverse	CTCACTTGTGGCCCAGGTAT	Bcl2
Bag1 Forward	AAGTCCGGCCCCGCTCTTCT	Bag
Bag1 Reverse	ACCTGGGTCCCGGTCACGTT	Bag
Puma Forward	TCAATAGCAACCCACTCGGCGG	Bbc3
Puma Reverse	CCCCGGGGGCATGAACACTC	Bbc3
Caspase 9 Forward	TGGAGGCGCTATGTGGGGGC	Casp9
Caspase 9 Reverse	TCGCTCACTAGGCGCACCCT	Casp9
Bid Forward	CTGGGGGCCGAGCACATCAC	Bid
Bid Reverse	GGCAGTTCCCGACCCAGCAC	Bid
Chop Forward	CACGGCGGGCTCTGATCGAC	Ddit3
Chop Reverse	GCGCGATGGTGCTGGGTACA	Ddit3
Apaf2 Forward	TGACCCTCCCTGGGCTGCTT	Apaf2
Apaf2 Reverse	GCACCAGGATGCCCAAGCCTTT	Apaf2
Cidea Forward	GGACTACGCGGGAGCCCTCA	Cidea
Cidea Reverse	ATCACCCCACGCCGGCTACT	Cidea
Gasdermin A Forward	GCTCCCCCACCTTTGTGCCCT	Gsdma
Gasdermin A Reverse	GAGGCTCTGTAGTGTCTTGCAGTGT	Gsdma

Primer	(5'---3')	Gene id
Reg3d2 Forward	CCTGGGCTAATGCAGAGGGGAG	Reg3d
Reg3d2 Reverse	CCGTGGTGTGCAGACATGGAGG	Reg3d
Reg3d1 Forward	CCACGCATCAGCTGTCCCCAA	Reg3d
Reg3d1Reverse	GGCAGTGGATCTCTGCATTAGCCC	Reg3d
Reg1 Forward	GGAGAGTGGCACTACAGACGCCA	Reg1
Reg1 Reverse	GCTCCAGTGCCAGCGACGATT	Reg1
Reg3a Forward	AGATGCTGCCTCACCTGGTCC	Reg3a
Reg3a Reverse	GCTGGTACGTGGAGAGGGCACT	Reg3a
Lepr Forward	TGGTGTGACGGTTGCTGTCAGA	Lepr
Lepr Reverse	TCCTTCCCTGCAGTTTGTATGTGGA	Lepr
Sycn Forward	GCGTACGTGCGCCAGACTCT	Sycn
Sycn Reverse	AGACCAGCCCGAGGGCAGAT	Sycn
Dusp6 Forward	GCCTGCGGATCAGCTCGGAC	Dusp6
Dusp6 Reverse	GTTGGACAGCGGGCTGCCAT	Dusp6
Dusp26 Forward	ACATGGCCAACAACCGCCGT	Dusp26
Dusp26 Reverse	TCATAGGCCTCGGGGGTGCC	Dusp26
Pmaip1 Forward	GGAACGCGCCAGTGAACCCA	Pmaip1
Pmaip1 Reverse	CCCAGGCATCTGCGCCAGAA	Pmaip1
p53 Forward	ATCCGCGGGCGTAAACGCTTC	Trp53
p53 Reverse	TAGGCTGGAGGCTGGAGTGAGC	Trp53
Rik Forward	CTGGGGGTCCCTGGCCCAA	Mzb1
Rik Reverse	AGCAGCGCCTCCAGATTCGC	Mzb1
Stk17b Forward	CAGTGTCCCAGACGCGGCTG	Stk17b
Stk17b Reverse	AGGCCCCTGTGAGGCGACTC	Stk17b
Tbp Forward	ACCCTTCACCAATGACTCCTATG	Tbp
Tbp Reverse	ATGATGACTGCAGCAAATCGC	Tbp

12 PROTEIN EXTRACTION

Protein extracts from isolated islets were prepared in lysis buffer (50 mmol/l Tris pH7.5, 5mmol/l EDTA, 150 mmol/l NaCl, 1% Triton X-100, 10 mmol/l sodium phosphate, 10 mmol/l sodium fluoride, 10 mmol/l sodium orthovanadate and protease inhibitors). Additionally, 3 consecutive cycles of 2 minutes with different temperatures (-20ºC and 37ºC) were applied to the islets, followed by a centrifugation of 20 minutes at -4ºC. For western blot analysis, 40 to 50 islets were used per sample. Theorically, 0.5 ug of protein can be obtained from a pancreatic islet. In our case, and regarding the *Irs2*$^{-/-}$ animals, the variability between animals and within the islet population within the same animal, did not allow us to define a proportion between number of islets and concentration of protein. However, we concluded that the yield of protein was about 50% inferior to the theoric one.

13 ANTIBODY MICROARRAY

Extracted proteins from isolated pancreatic islets of treated and untreated *Irs2*$^{-/-}$ mice were hybridized to an antibody microarray. The Cell Signaling Antibody Array (Sigma, CSAA1) contains 224 antibodies spotted on FAST™ nitrocellulose-coated slides that can detect protein levels as low as a few nanograms per ml. The antibodies spotted are specific for proteins important in various areas of cell signalling such as phosphorylation, cell cycle, apoptosis, nuclear signalling and cytoskeleton proteins.
Importantly, this array offered us a methodological advantage, as the concentration of labeled protein applied on the array is very low compared to that needed in immunoblot analysis (should be between 2-10 ug/ml).

In detail, extracts of proteins from a pool of approximately 400 islets (4 animals for untreated and treated *Irs2*$^{-/-}$ animals) were prepared using Extraction/Labelling Buffer from the kit and labelled with Cyanine 3 and Cyanine 5, respectively. After the removal of excess label, a mixture containing equal amounts of each labelled extract (3.5 μg/ml) was incubated on the array as described in the kit protocol. Unbounded protein was removed with a brief wash and the array was scanned with a fluorescence scanner Axon 4000B at the two fluorescence emission wavelengths for Cy3 (552nm) and Cy5 (650nm). To facilitate reliable interpretation of array experiments, each antibody feature is double-spotted and each of the 32 fields contains its own positive and negative control. After read the absorbance wavelengths we preceded to the calculation of the Ratio dye to Protein Molar (D/P ratio) following the instructions of the commercial protocol.

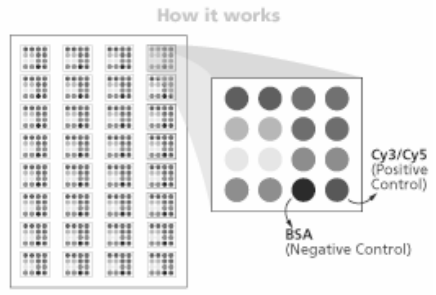

D/P ratio=(Cy3 or Cy5 concentration)/Protein concentration of sample

A D/P>2 was considered good and essential to start the array assay.

14 WESTERN BLOT

Homogenates of extracted proteins were resolved by 10-12% SDS-PAGE for 1 hour. The protein was transferred onto a PVDF membrane for 2 hours at 80-90 voltios. After 3 washes in Tbs-0.01% Tween (TbsT) and one hour of blocking with 5% of milk dissolved in TbsT, the membranes were probed overnight with the following antibodies: anti-phosphorylated Erk1/2, anti-total Erk1/2, anti-Cytochrome c, anti-phosphorylated Akt, anti-total Akt anti-phosphorylated Bad and anti-total Bad (all antibodies diluted in TbsT-5% BSA). β-actin was used as loading control. After washing in TbsT, a horseradish peroxidase-conjugated secondary antibody was added (Amersham Biosciences) for 1 h at room temperature. The complex was visualized with enhanced chemiluminescence (ECL, Amersham Biosciences) on LAS. Intensity values were obtained with Image J software.

15 STATISTICAL ANALYSIS

Quantitative data are expressed as means ± SEM and statistical significance determined by Student's t-test. $P<0.05$ was considered statistically significant.

Table 3: Antibodies used in Western Blot analysis.

Molecular weight kDa	Antigen	1º Antibody source	Dilution (TbsT)	Commercial reference	2º Antibody	Dilution
42,44	Phospho-Erk1/2	Rabbit	1:1000 5%BSA	Cell signaling 9101	Anti-rabbit IgG, peroxidase NA934	1:4000 5% milk
42,44	Erk1/2	Rabbit	1:1000 5%BSA	Cell signaling 9102	Anti-rabbit IgG, peroxidase NA934	1:4000 5% milk
60	Phospho-Akt (Ser473)	Rabbit	1:1000 5%BSA	Cell signaling 9271	Anti-rabbit IgG, peroxidase NA934	1:4000 5% milk
60	Total Akt	Rabbit	1:1000 5%BSA	Cell signaling 4691	Anti-rabbit IgG, peroxidase NA934	1:4000 5% milk
23	Phospho-Bad (Ser136)	Rabbit	1:1000 5%BSA	Cell signaling 5286	Anti-rabbit IgG, peroxidase NA934	1:4000 5% milk
23	Phospho-Bad (Ser112)	Rabbit	1:1000 5%BSA	Cell signaling 5284	Anti-rabbit IgG, peroxidase NA934	1:4000 5% milk
23	Total Bad	Rabbit	1:1000 5%BSA	Cell signaling 9239	Anti-rabbit IgG, peroxidase NA934	1:4000 5% milk
42	β-Actin	Rabbit	1:1000 5%milk	Sigma A2066	Anti-rabbit IgG, peroxidase NA934	1:4000 5% milk
17, 19	Cleaved Caspase 3	Rabbit	1:1000 5%milk	Cell signaling 9661	Anti-rabbit IgG, peroxidase NA934	1:4000 5% milk
37,39,49	Caspase 9	Rabbit	1:1000 5%milk	Cell signaling 9504	Anti-rabbit IgG, peroxidase NA935	1:4000 5% milk
14	Cytochrome c	Rabbit	1:1000 5% milk	Cell signaling 4272	Anti-rabbit IgG, peroxidase NA934	1:4000 5% milk

IV RESULTS

1 METABOLIC CHARACTERIZATION OF *IRS2*$^{-/-}$ MICE

We firstly assessed several metabolic parameters regarding whole-body glucose homeostasis in 10-weeks old *Irs2*$^{-/-}$ and WT mice, before initiate the treatment with tungstate.

1.1 10-weeks old *Irs2*$^{-/-}$ mice displayed abnormalities in glucose homeostasis

Irs2$^{-/-}$ and WT mice had equivalent body weight (Fig. 1A) and examination of fasting blood glucose levels showed that *Irs2*$^{-/-}$ mice were hyperglycemic (Fig. 1B). Following an intraperitoneal glucose challenge, *Irs2*$^{-/-}$ exhibited higher blood glucose levels than WT mice, and glucose tolerance was markedly impaired in *Irs2*$^{-/-}$ compared to WT mice (Fig. 1C), as demonstrated by the calculation of the area under the curve (AUC) (Fig. 1D).

To assess the impact of these abnormalities upon islet function, we analyzed glucose-stimulated insulin secretion (GSIS) in *Irs2*$^{-/-}$ mice *in vivo* during the glucose tolerance test. GSIS was severely perturbed with loss of insulin secretion 15 minutes after the glucose injection in *Irs2*$^{-/-}$ mice, whereas WT animals responded well to glucose challenge (Fig. 1E).

Fasting insulin levels in *Irs2*$^{-/-}$ mice were higher than in WT mice, suggesting that *Irs2*$^{-/-}$ mice were insulin resistant (Fig. 1F). Indeed, insulin tolerance tests in *Irs2*$^{-/-}$ mice showed a significantly reduced hypoglycaemic response to exogenous insulin compared to WT mice (Fig. 1G).

In summary, our results demonstrate that 10-weeks old *Irs2*$^{-/-}$ mice presented severe defects in both insulin action and insulin production, consistent with what previously described (Withers et al., 1998).

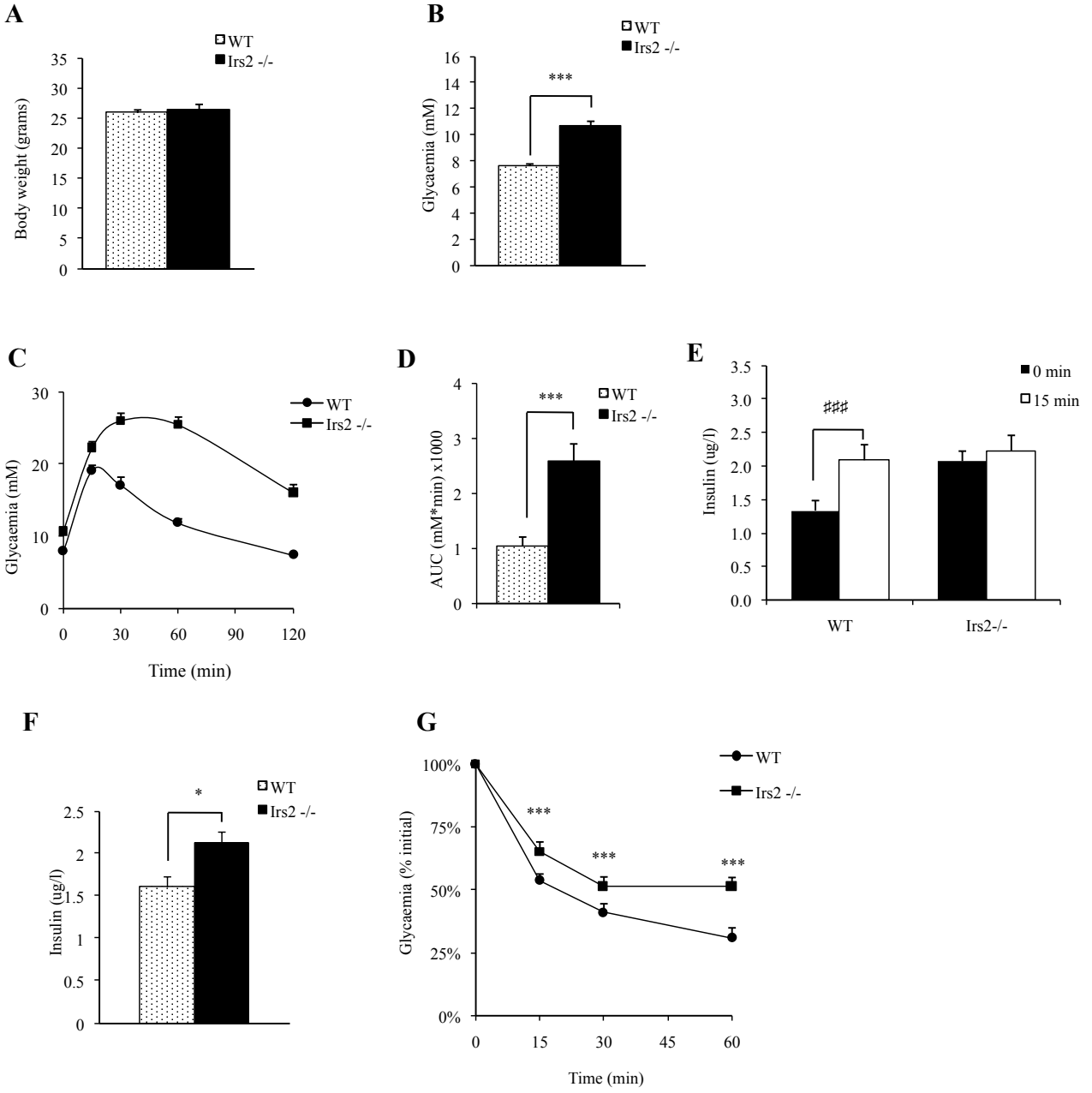

Figure 1: Metabolic characteristics of 10-week old *Irs2*$^{-/-}$ mice. Body weight (A) and fasting blood glucose levels (B) were measured in 10-week old WT and *Irs2*$^{-/-}$ mice (n=15). (C) Glucose tolerance test (GTT, n=10) was performed in 10-week old WT and *Irs2*$^{-/-}$ mice (n=15) and (D) the correspondent area under the curve (AUC) calculation is shown. (E) Plasma insulin levels were analyzed at minute 0 and 15 after glucose injection in the GTT (n=10). (F) Fasting blood insulin levels in 10-week old WT and *Irs2*$^{-/-}$ mice, (n=15) (G) Insulin tolerance test was performed in 10-week old WT and *Irs2*$^{-/-}$ mice (n=15). Data are mean ± SE, ***p<0.001, *p<0.05 and $^{###}$p<0.001, between indicated groups.

2 EFFECT OF TUNGSTATE IN *IRS2*$^{-/-}$ MICE GLUCOSE HOMEOSTASIS

Having established that 10-weeks old *Irs2*$^{-/-}$ mice exhibit marked abnormalities in glucose homeostasis, we wondered if the treatment with sodium tungstate would ameliorate it. Therefore, we divided WT and *Irs2*$^{-/-}$

animals in two experimental groups, one receiving distilled water and the other one receiving 2 mg of sodium tungstate per ml of distilled water as treatment for 3 weeks.

2.1 Treated *Irs2*$^{-/-}$ animals showed moderate increment of body weight

During the treatment with tungstate, we recorded body weight, food and water intake in order to make a detailed following of the possible changes occurring in the metabolism of the studied animals.

The body weight of *Irs2*$^{-/-}$ mice was significantly higher than that observed in treated *Irs2*$^{-/-}$ and WT mice in the second and third weeks of treatment respectively (Fig. 2A). Treated *Irs2*$^{-/-}$ animals lost weight in the first two weeks of treatment, but finally recovered the initial body weight and finished the experiment with the same weight as WT animals (Fig. 2A). We also observed that treated *Irs2*$^{-/-}$ consumed the same quantity of food and drunk the same quantity of water per day as WT animals, whereas untreated *Irs2*$^{-/-}$ ate and drunk significantly more than the other animals (Fig. 2B, C).

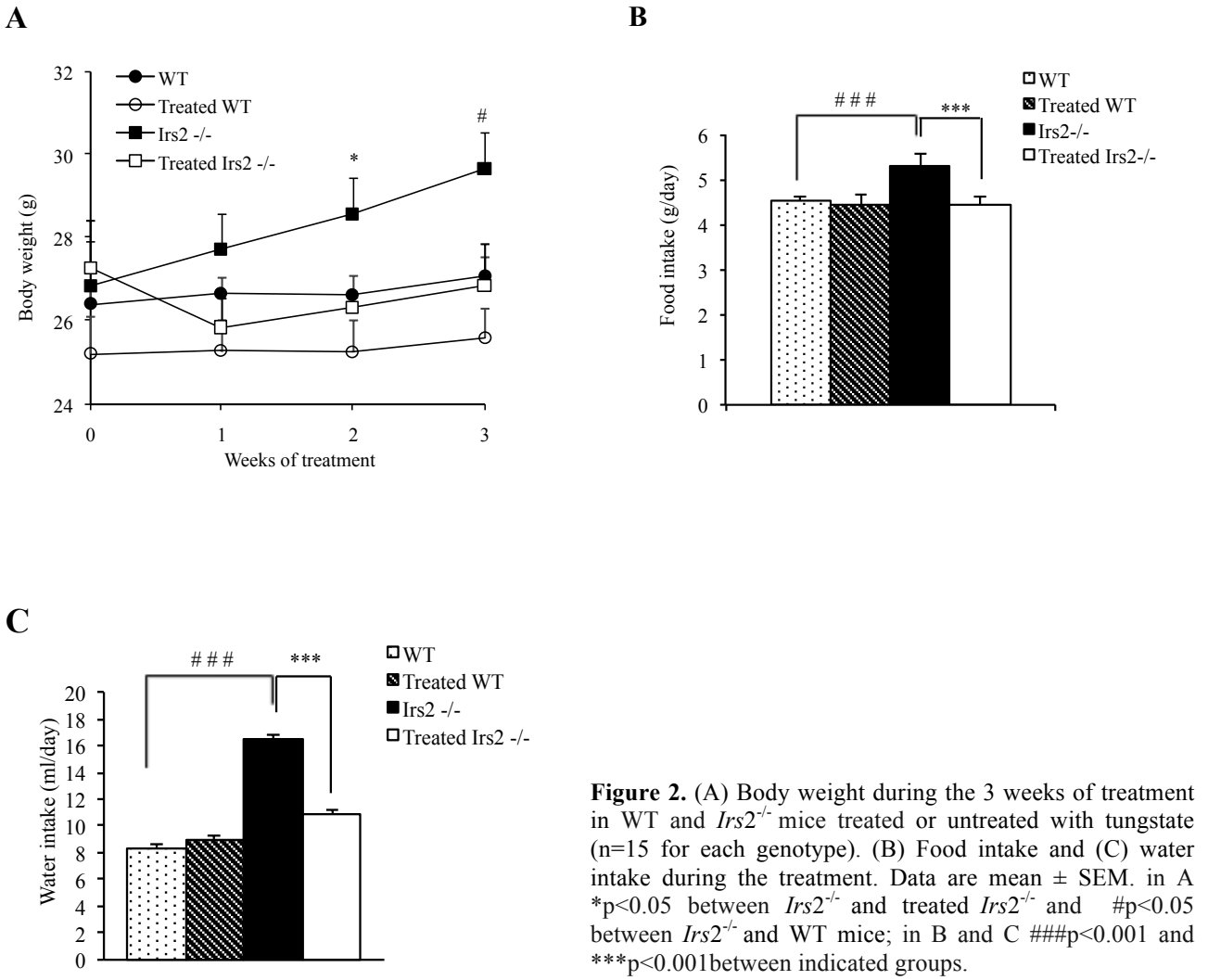

Figure 2. (A) Body weight during the 3 weeks of treatment in WT and *Irs2*$^{-/-}$ mice treated or untreated with tungstate (n=15 for each genotype). (B) Food intake and (C) water intake during the treatment. Data are mean ± SEM. in A *p<0.05 between *Irs2*$^{-/-}$ and treated *Irs2*$^{-/-}$ and #p<0.05 between *Irs2*$^{-/-}$ and WT mice; in B and C ###p<0.001 and ***p<0.001between indicated groups.

2.2 Treated *Irs2*$^{-/-}$ animals showed normal blood glucose levels

Regarding glucose metabolism, *Irs2*$^{-/-}$ mice treated with sodium tungstate experimented a gradual decrease in their blood glucose levels during the first week of treatment (Fig. 3A). This normoglycemic situation was maintained systematically in all animals until the end of the treatment (Fig. 3A, B). In contrast, the levels of fasting glucose in *Irs2*$^{-/-}$ mice that were left untreated rose progressively and these animals displayed severe hyperglycaemia at the end of the treatment (Fig. 3A, B). Of note, *Irs2*$^{-/-}$ mice that were left untreated showed polyuria and polydipsia.

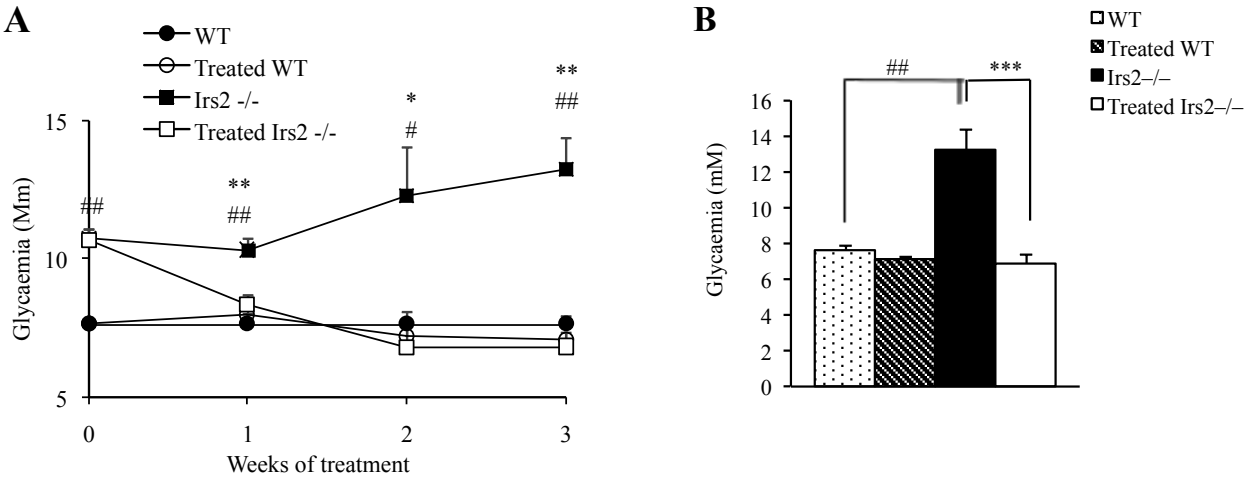

Figure 3. Tungstate normalized glycaemia in *Irs2*$^{-/-}$ mice. (A) Fasting blood glucose was recorded once a week during the 3 weeks of treatment with tungstate in WT and *Irs2*$^{-/-}$ mice treated (n=15 for each genotype) or left untreated (n=15 for each genotype). (B) Fasting blood glucose measured at the end of treatment. Data are mean ± SEM. *p<0.05, **p<0.01, ***p<0.001 between treated *Irs2*$^{-/-}$ and *Irs2*$^{-/-}$, and #p<0.05, ##p<0.01 between *Irs2*$^{-/-}$ and WT.

2.3 Treated *Irs2*$^{-/-}$ animals displayed normal glucose tolerance

After glucose administration, treated *Irs2*$^{-/-}$ mice displayed normal glucose handling and glucose tolerance was normalized, as demonstrated by the calculation of the AUC (Fig. 4A, B). In contrast, glucose tolerance was markedly impaired in *Irs2*$^{-/-}$ mice that were left untreated (Fig. 4A, B). GSIS was restored in treated *Irs2*$^{-/-}$ mice, whereas it was severely perturbed in *Irs2*$^{-/-}$ mice (Fig 4C). The treatment with tungstate did not change or improved GSIS in WT mice (Fig. 4C). Altogether, these data indicate that glucose homeostasis was improved in *Irs2*$^{-/-}$ animals treated with tungstate.

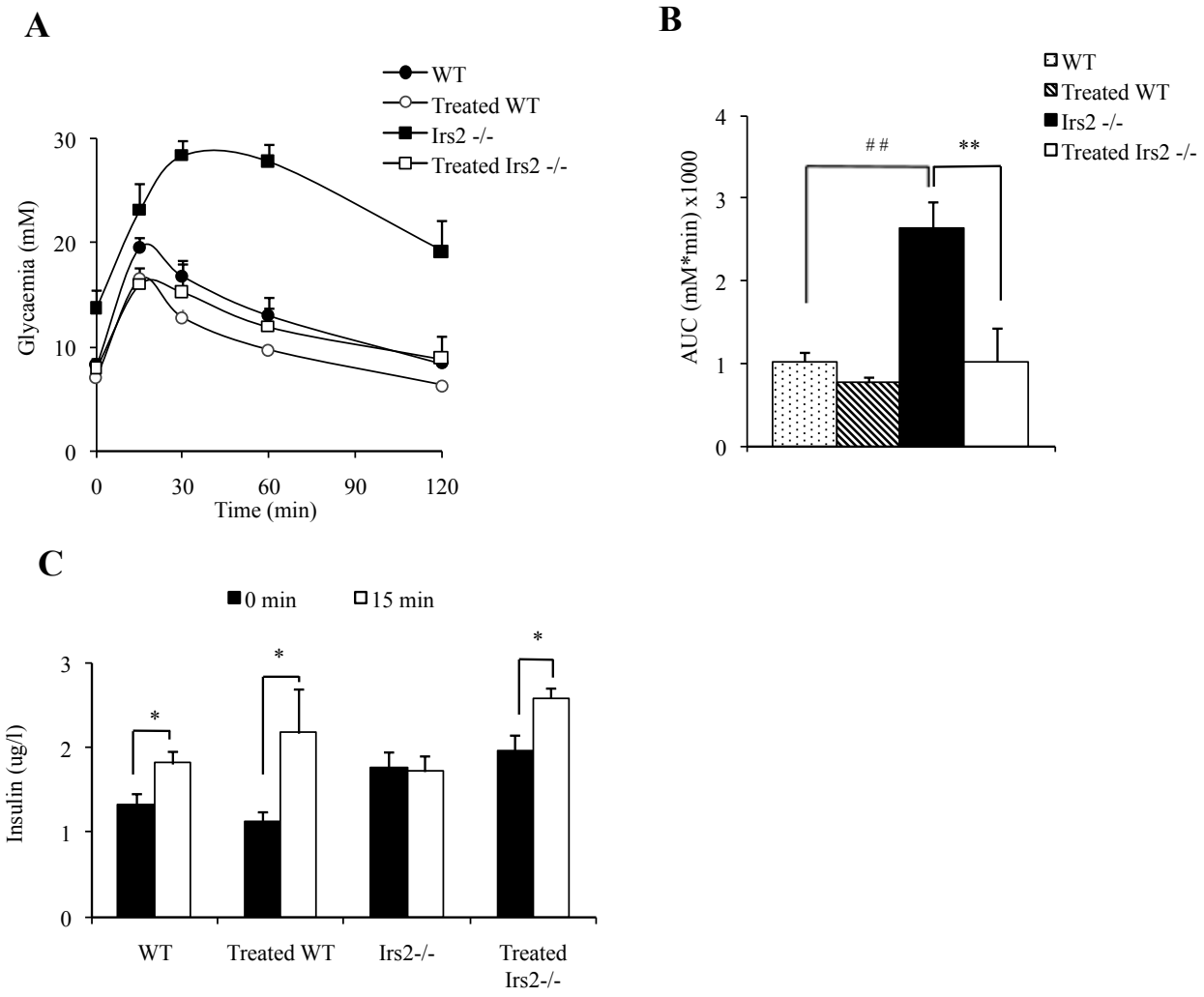

Figure 4. Tungstate improves glucose homeostasis in *Irs2*$^{-/-}$ mice. (A) Intraperitoneal glucose tolerance tests were performed in WT and *Irs2*$^{-/-}$ mice after tungstate treatment (n= 6 for each genotype). (B) Area under the curve (AUC) calculation of glucose profiles. (C) *In vivo* insulin secretion following intraperitoneal injection of glucose. Insulin levels were measured at minute 0 and 15 (n = 5 for each genotype). Data are mean ± SEM. *p<0.05, **p<0.01, and #p<0.05, ##p<0.01 between indicated groups.

2.4 Insulin resistance persisted in treated *Irs2*$^{-/-}$ animals

Fasting insulin levels in treated *Irs2*$^{-/-}$ mice were still higher than that observed in WT mice, suggesting that the treatment with tungstate did not improve insulin resistance in *Irs2*$^{-/-}$ mice (Fig. 5A). In fact, the insulin tolerance test performed at the end of the treatment revealed a reduced recovery in glucose levels after insulin administration in treated *Irs2*$^{-/-}$ mice compared to WT mice (Fig. 5B). Additionally, the insulin tolerance test showed no evidence of increased insulin sensitivity in treated *Irs2*$^{-/-}$ mice compared to *Irs2*$^{-/-}$ mice (Fig. 5B). Altogether, these data indicate that peripheral insulin action was not improved by tungstate treatment in *Irs2*$^{-/-}$ animals.

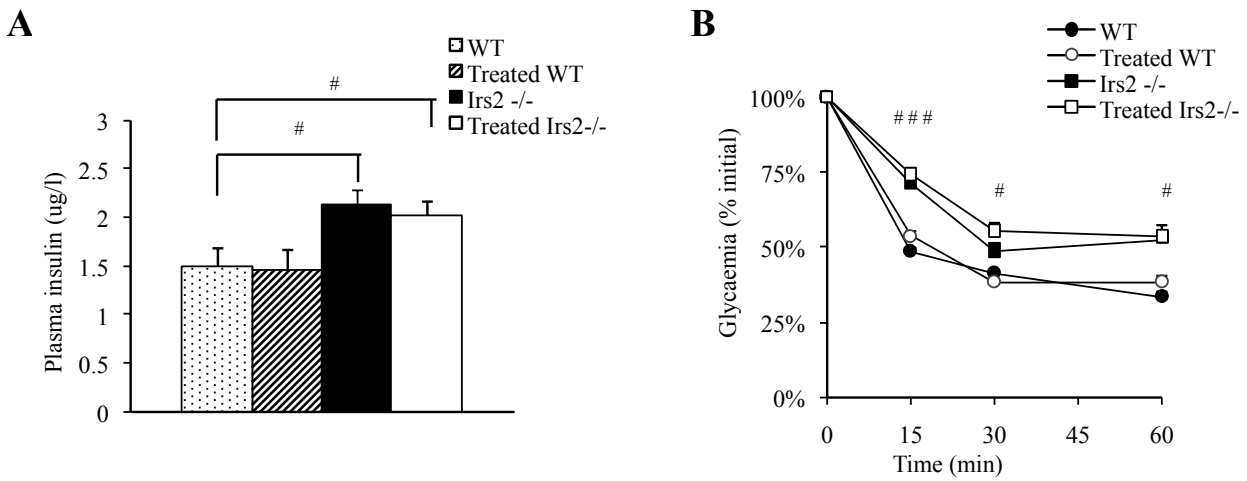

Figure 5. Tungstate did not improved peripheral insulin action in *Irs2*$^{-/-}$ mice. (A) Fasting blood insulin levels were measured in WT and *Irs2*$^{-/-}$ mice after the treatment with tungstate (n= 15 for each genotype). (B) Insulin tolerance test was performed in WT and *Irs2*$^{-/-}$ mice after tungstate treatment (n= 8-10). Data are mean ± SEM. #p<0.05 between indicated groups, except in (B) where #p< 0.05 and ###p<0.001 between treated *Irs2*$^{-/-}$ and WT mice.

3 EFFECT OF TUNGSTATE ON HEPATIC GLUCOSE METABOLISM IN *IRS2*$^{-/-}$ MICE

IRS2-dependent signaling controls the expression of enzymes involved in hepatic glucose production and insulin-regulated glycogen synthesis (Previs et al., 2000). Given that sodium tungstate has been shown to modulate glucose hepatic metabolism in some rodent models, we first determined whether tungstate improved liver function in *Irs2*$^{-/-}$ mice. We compared the expression of the key enzyme involved in hepatic gluconeogenesis and the expression and enzymatic activity of the key enzyme involved in glycogenolysis, the two metabolic processes that allow the delivery glucose to the circulation. Additionally, the expression and enzymatic activities of two key enzymes involved in glycogenesis, the main metabolic process by which the liver removes glucose from the circulation to synthetize glycogen, were also determined.

3.1 Tungstate has no major effects on PEPCK and GP protein expression

We started by checking the expression of phosphoenolpyruvate carboxykinase enzyme (PEPCK), the rate-limiting enzyme for gluconeogenesis, and the glycogen phosphorylase enzyme (GP2), which in its active form (GPA) catalyzes the removal of glucose residues from the glycogen molecule (glycogenolysis) and has been classically regarded as the 'glucose sensor' for control of hepatic glucose production.

PEPCK expression was significantly increased in *Irs2*$^{-/-}$ compared to WT animals and tungstate failed to reproducibly decrease it in all studied animals (Fig. 6A). We also observed a significant increment in the expression of the active form of GP (GPA2) in treated *Irs2*$^{-/-}$ compared to *Irs2*$^{-/-}$ and a significative decrease in the total glycogen phosphorylase expression (GP2) (Fig. 6A). However, the enzymatic activity of GPA and GP enzyme was similar between all groups (Fig. 6B), suggesting that glycogenolysis was unchanged between all experimental groups.

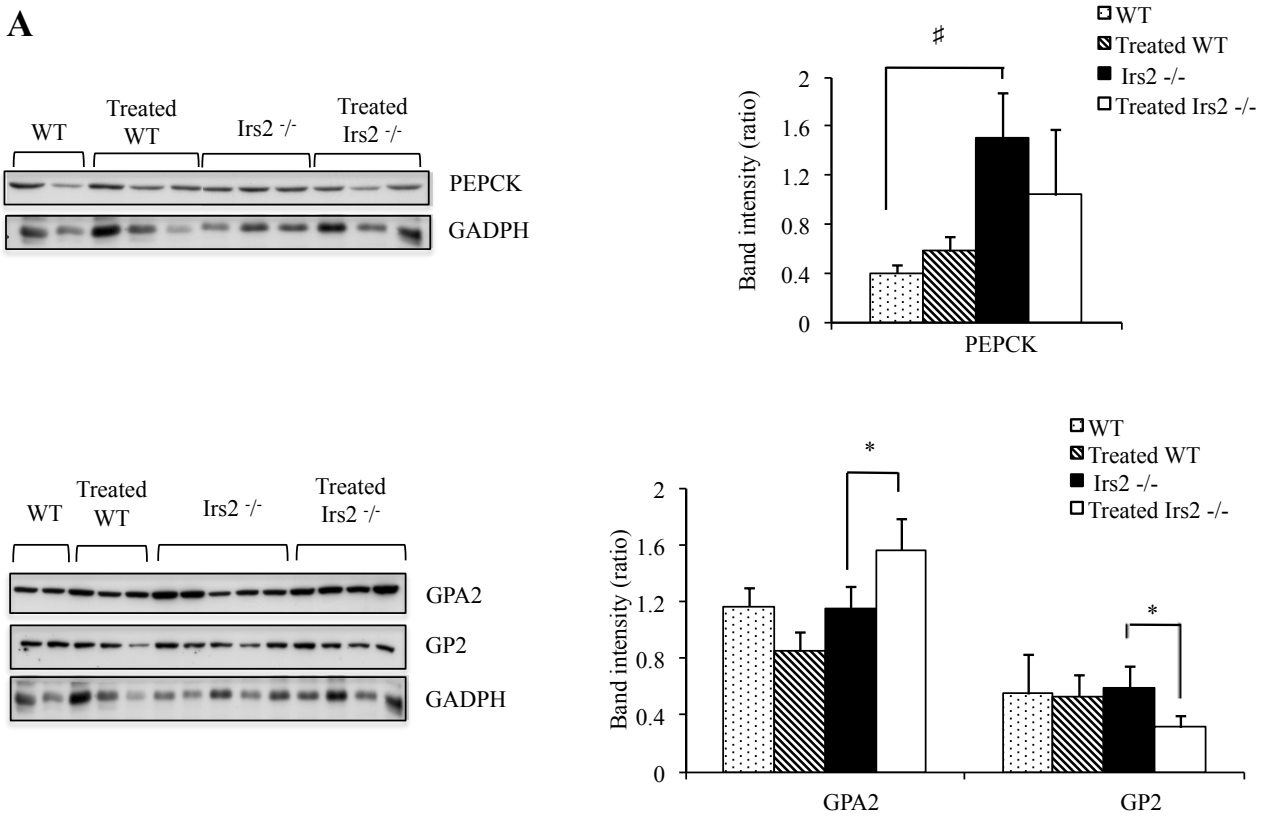

B

	GPA Activity (mU/mg)	GP Activity (mU/mg)
WT	23.9±2.4	27.4±5
Treated WT	26±3.3	26.7±2
Irs2-/-	24.4±1.8	28.1±3.1
Treated Irs2-/-	25.9±1.9	26.9±1.6

Figure 6. PEPCK and GPA expression is not normalized in treated *Irs2*$^{-/-}$mice. (A) PEPCK, GPA2 and total GP (GP2) expression levels were determined in liver lysates from WT and *Irs2*$^{-/-}$ mice after the treatment with tungstate (n = 6-8). A representative immunoblot and densitometric quantification (ratio PEPCK/GADPH signal, ratio GPA2/GP2 and GP2/GADPH signal) is shown. (B) Enzymatic activity of the active form of GP enzyme (GPA) and of the total GP was measured in liver lysates from WT and *Irs2*$^{-/-}$ mice after the treatment with tungstate (n = 6-8). Data are mean ± SEM. #p<0.05, *p< 0.05 between indicated groups.

3.2 Tungstate did not restore glycogen content in *Irs2*$^{-/-}$ mice

The synthesis of glycogen depends on several enzymes, being the more important the glucokinase (GK) that catalyzes the phosphorylation of glucose (which is a limiting factor for glycogen synthesis from glucose in the liver), and the glycogen synthase (GS) that catalyzes the last and key step in biosynthesis of glycogen.
The expression of GK enzyme was similar between WT, *Irs2*$^{-/-}$ and treated *Irs2*$^{-/-}$ animals (Fig. 7A). However, its enzymatic activity was significantly decreased in *Irs2*$^{-/-}$ compared to WT animals, and tungstate decreased it even more in treated *Irs2*$^{-/-}$ (Fig. 7B). We also measured the expression of the GS enzyme (GS), which was significantly higher in *Irs2*$^{-/-}$ compared to WT mice, and decreased in treated *Irs2*$^{-/-}$ (Fig. 7A). The phosphorylation of GS in multiple serine residues causes inactivation of this enzyme (Guinovart et al., 1979). The expression of phosphorylated GS (on serine 641) was significantly decreased in *Irs2*$^{-/-}$ and treated *Irs2*$^{-/-}$ compared to WT (Fig. 7A), suggesting that more GS in its active form was expressed in treated *Irs2*$^{-/-}$ mice. However, the measurement of the enzymatic activity revealed that total GS was significantly lower in *Irs2*$^{-/-}$ as well as in treated *Irs2*$^{-/-}$ compared to WT animals (Fig. 7A, B). In contrast, the active form of the GS (GS I) had similar enzymatic activity between experimental groups and finally, no differences were found between the ratio of activities (Fig. 7B). To further elucidate these findings, we measured glycogen content in liver of WT and *Irs2*$^{-/-}$ animals treated and untreated with tungstate. Glycogen levels were significantly inferior in *Irs2*$^{-/-}$ compared to WT mice as previously reported (Previs et al., 2000), and the treatment with tungstate did not modify them (Fig. 7C). Of note, the treatment with tungstate did not induce any significant modification in WT animals. Therefore, these data suggest that impaired glycogenesis persisted in treated *Irs2*$^{-/-}$.

A

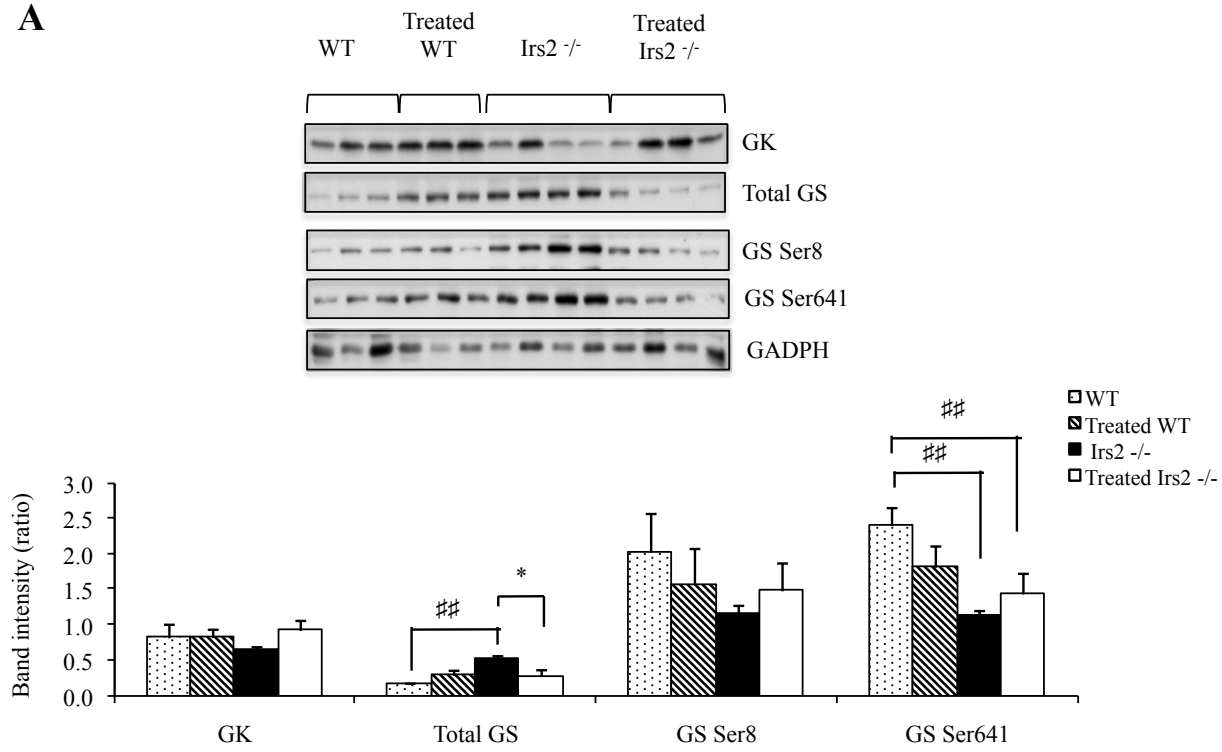

B

	GK Activity (mU/mg)	GS T Activity (mU/mg)	GS I Activity (mU/mg)	I/T Ratio
WT	39.5±3.6	1.91±0.04	0.12±0.01	0.06±0.007
Treated WT	22.1±5.9	1.85±0.21	0.12±0.02	0.06±0.005
Irs2$^{-/-}$	25±2.2##	1.52±0.06###	0.10±0.01	0.07±0.01
Treated Irs2$^{-/-}$	5.7±2.6***###	1.40±0.10##	0.09±0.01	0.07±0.005

!

C

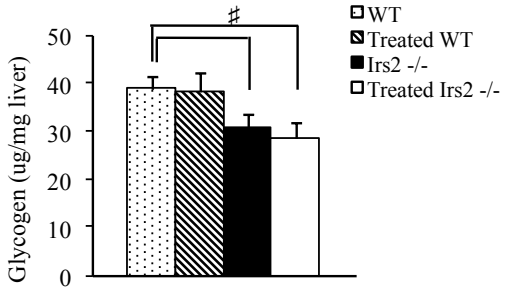

Figure 7: Glycogen content is not restored by tungstate treatment in *Irs*2$^{-/-}$mice. (A) Immunoblot analysis for the indicated proteins in liver lysates from WT and *Irs*2$^{-/-}$ mice after the treatment with tungstate (n=6 for each genotype). (B) Glucokinase enzymatic activity and Total (T), intrinsic (I) and I/T ratio glycogen synthase (GS) activity, were measured in liver lysates from WT and *Irs*2$^{-/-}$ mice (n = 6 for each genotype) after the treatment with tungstate. (C) Glycogen content was determined in liver lysates (n = 6-8 for each genotype). Data are mean ± SEM. #p< 0.05, ##p<0.01 and *p< 0.05 between indicated groups, except in B were ##p<0.01, ###p<0.001 when compared to WT and ***p< 0.001 when compared to *Irs*2$^{-/-}$ mice.

4 EFFECT OF TUNGSTATE ON THE PANCREATIC COMPARTMENT IN *IRS2*$^{-/-}$ MICE

As reviewed in the introduction, the decline in β-cell mass determines the progression to diabetes in the *Irs2*$^{-/-}$ mice model. Based on the marked improvements of glucose homeostasis without major changes in hepatic glucose metabolism or peripheral insulin sensitivity, we hypothesized that changes in β-cell mass might be involved in these effects of tungstate. To test this possibility, we performed morphometric analysis on fixed pancreatic tissue.

4.1 Increased β-cell area in treated *Irs2*$^{-/-}$ mice

Histological analysis of pancreatic islets revealed that *Irs2*$^{-/-}$ mice displayed smaller islets than WT, with obvious disruption of the normal organization of α or β-cells, whereas islet architecture was preserved in treated *Irs2*$^{-/-}$ (Fig. 8A). Morphometric analysis of fixed pancreatic tissue confirmed an important reduction in β-cell area in *Irs2*$^{-/-}$ mice compared to WT mice, consistent with was previously described in this mice model (Fig. 8B). Importantly, treated *Irs2*$^{-/-}$ mice exhibited a two-fold increase in fractional β-cell area relative to untreated *Irs2*$^{-/-}$ mice (Fig.8B), being the total pancreatic area analysed similar between all experimental groups (Fig. 8D). Regarding α-cell area, we did not find significant differences between experimental groups (Fig. 8C).

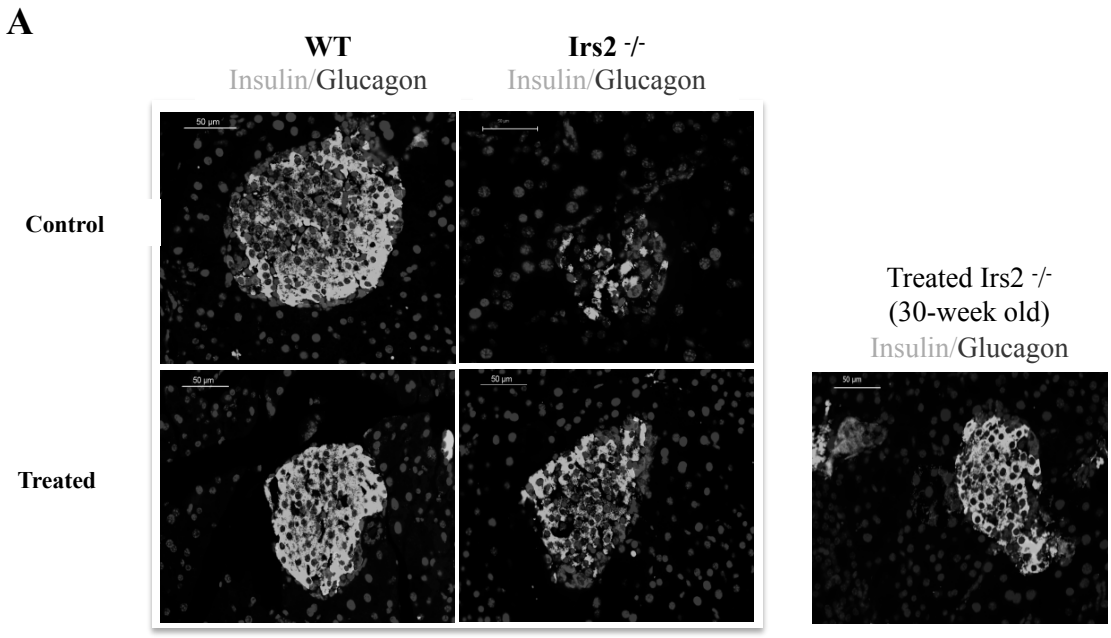

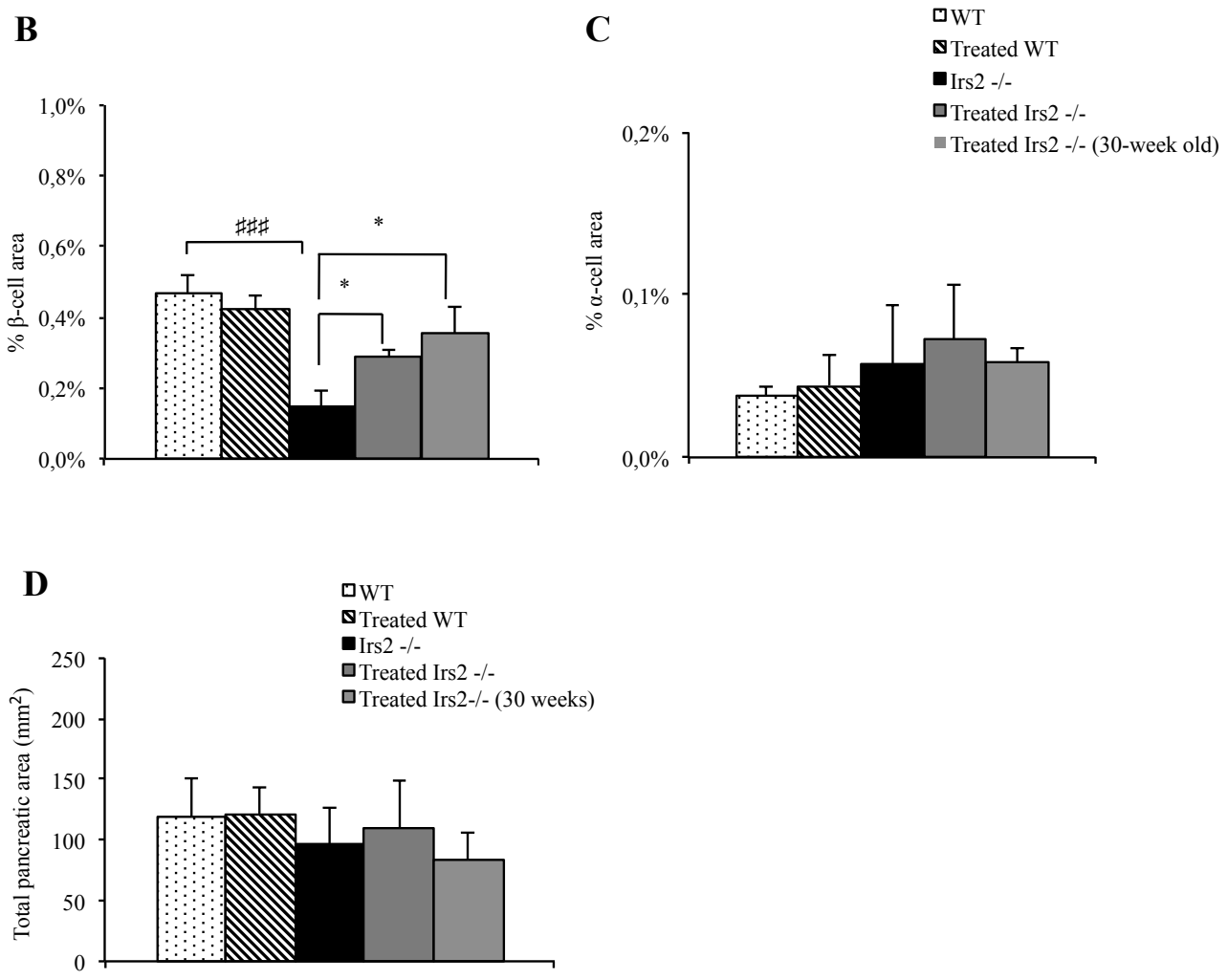

Figure 8: Tungstate increased β-cell area in *Irs2*$^{-/-}$ mice. (A) Representative images of pancreases from WT and *Irs2*$^{-/-}$ mice untreated (control) or treated with tungstate. Blue: nuclei. Scale bar: 50 μm. (B) β-cell area reported as percentage of total pancreas area. (C) α-cell area reported as percentage of total pancreas area. (D) Mean total pancreatic area analyzed per experimental group. Data was obtained from 5-8 mice per genotype, except the 30-week old mice where n=4. Data is the mean ± SEM. *$p<0.05$, $^{###}p< 0.001$ between indicated groups.

The increase in the fractional β-cell area in treated *Irs2*$^{-/-}$ mice was associated with higher number of pancreatic islets per mm^2 of pancreatic area analyzed with more β-cells compared to untreated *Irs2*$^{-/-}$ mice (Fig 9A,B).

In order to find if these improvements in pancreatic islets of treated *Irs2*$^{-/-}$ were permanent, we confirmed these results in a separate cohort of *Irs2*$^{-/-}$ animals that were treated with tungstate for the duration of 20 weeks, reaching the age of 30 weeks. Consistent with *Irs2*$^{-/-}$ animals treated for 3 weeks, these animals displayed larger islets with normal architecture (Fig. 8A), and a two and a half fold increase in β-cell area relative to untreated *Irs2*$^{-/-}$ mice (Fig. 8B) associated with a higher number of islets and β-cells (Fig. 9A, B).

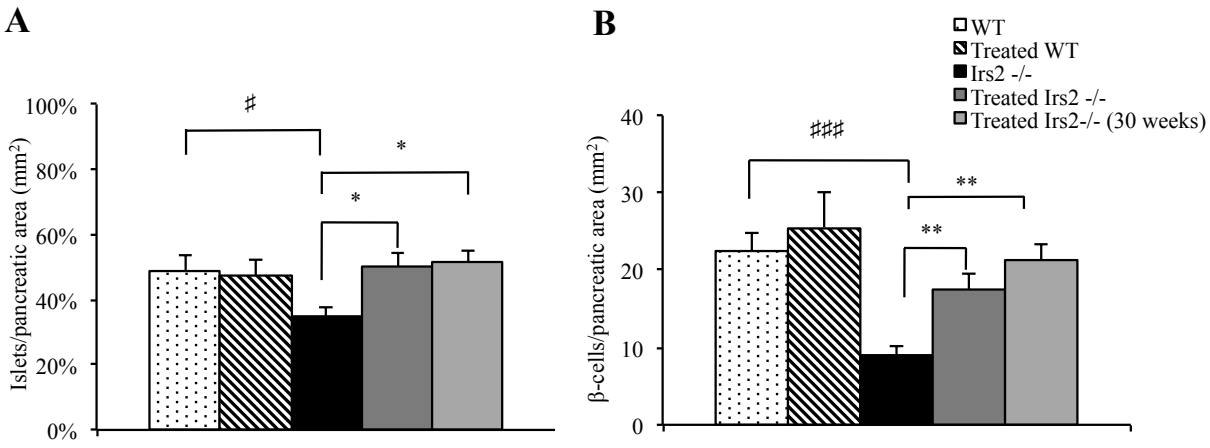

Figure 9: Treated *Irs2*$^{-/-}$ mice displayed higher number of β-cells and of islets. (A) Number of islets reported as percentage of total pancreas area (B) Number of β-cells per total pancreas area. Data is the mean ± SEM. *p<0.05, **p<0.01, $^{\#}$p< 0.05, $^{\#\#\#}$p< 0.001 between indicated groups, and was obtained from 5-8 mice per genotype, except the 30-week old mice where n=4.

4.2 Increased β-cell mass in treated *Irs2*$^{-/-}$ mice

In line with increased β-cell area, β-cell mass in treated *Irs2*$^{-/-}$ mice more than doubled that observed in *Irs2*$^{-/-}$ mice (Fig. 10A), which displayed a 60% reduction compared to WT animals (Fig. 10A). In agreement with previous reports, tungstate treatment did not induce any significant modification in WT animals (Fig. 8,9,10). However, β-cell mass of 30-weeks old *Irs2*$^{-/-}$ mice was similar to that observed in untreated *Irs2*$^{-/-}$ mice (Fig. 10A), as the pancreas of these animals weighted significantly less compared with the pancreas of the other experimental groups (Fig. 10B).

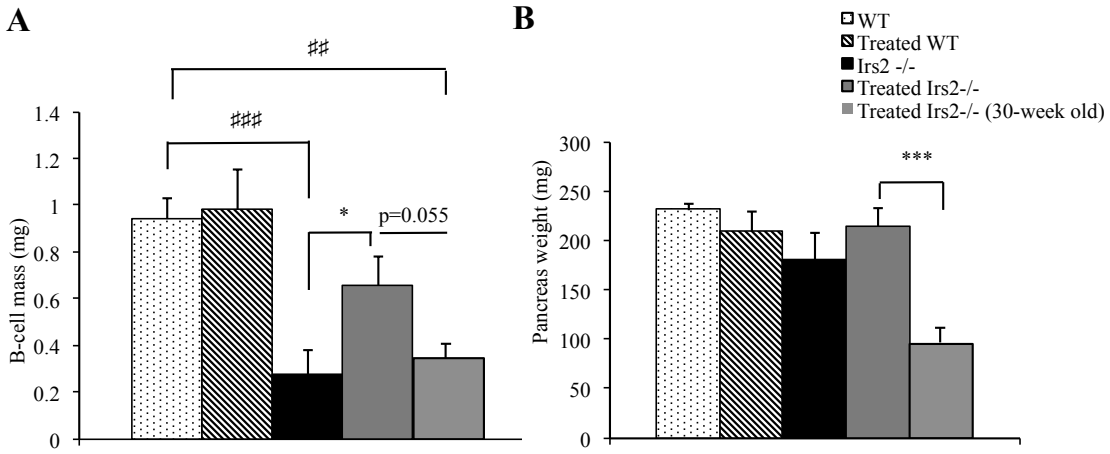

Figure 10: Tungstate increased β-cell mass in *Irs2*$^{-/-}$ mice. (A) β-cell mass. (B) Pancreatic weight. Data is the mean ± SEM. *p<0.05 and ***p<0.001, $^{\#\#}$p<0.01 and $^{\#\#\#}$p< 0.001 between indicated groups and was obtained from 5-8 mice per genotype, except the 30-week old mice where n=4.

Of note, blood glucose levels of 30-weeks old *Irs2*$^{-/-}$ mice decreased within the first 4 weeks of treatment (Fig. 11A), and were maintained in normal levels onward until the end of the treatment (Fig. 11A). This was accompanied by a decrease in body weight compared to treated WT animals (Fig. 9B), which is in line with decreased pancreatic weight (Fig. 10B).

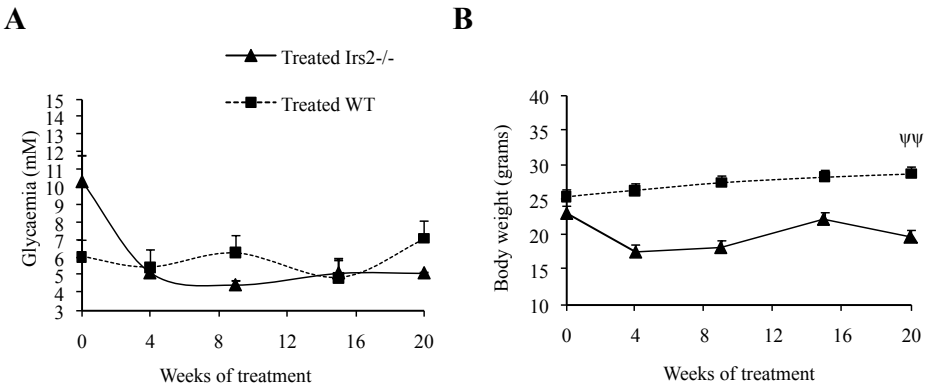

Figure 11. Fasting blood glucose levels and body weight in 30-week old *Irs2*$^{-/-}$ and 30-week old WT mice treated with tungstate for 20 weeks. Data was obtained from 4 mice per genotype. Data are mean ± SEM, $^{\Psi\Psi}p<0.01$.

4.3 Increased nuclear Pdx1 staining in treated *Irs2*$^{-/-}$ mice

We next investigated the expression levels of pancreas duodenum homeobox gene 1 (Pdx1), a key transcription factor involved in pancreatic development and in the maintenance of β-cell function, in the islets of WT and *Irs2*$^{-/-}$ mice. Immunohistochemical studies revealed Pdx1 protein to be equally expressed in the nuclei of WT and treated *Irs2*$^{-/-}$ mice, whereas nuclear expression of Pdx1 in untreated *Irs2*$^{-/-}$ mice was weak (Fig. 12A). Quantitative RT-PCR revealed the expression levels of Pdx1 mRNA to be indistinguishable between all experimental groups (Fig. 12B).

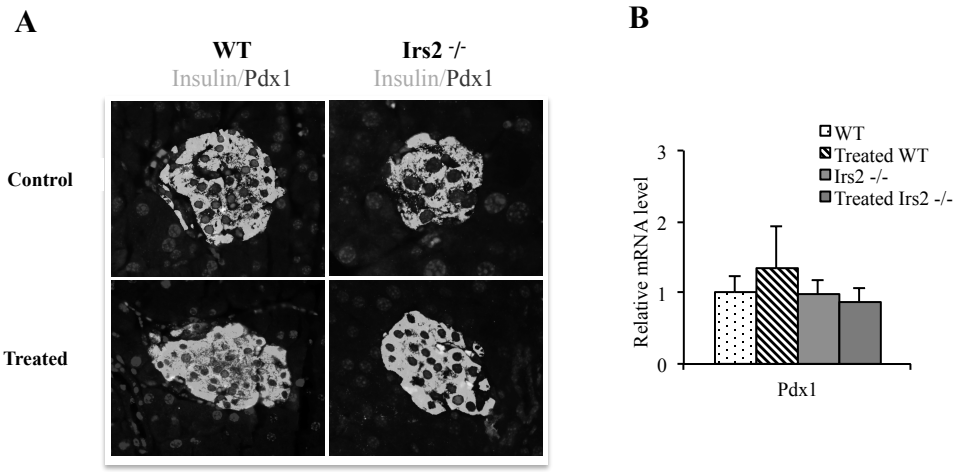

Figure 12: Pdx1 expression in *Irs2*$^{-/-}$ mice. (A) Immunohistochemical study of Pdx1 in WT and *Irs2*$^{-/-}$ mice untreated (control) or treated with tungstate. Original magnification x200. (B) qRT-PCR of Pdx1 gene. Data was obtained from 3 mice per genotype and is mean ± SEM.

4.4 Treated *Irs2*$^{-/-}$ mice display enhanced β-cell survival

β-cell mass is controlled by the equilibrium between formation of new β-cells and death of existing ones. To establish the extent to which each of these mechanisms contributed to increased β-cell mass in treated *Irs2*$^{-/-}$ animals, we determined β-cell apoptosis by double immunostaining for insulin/cleaved caspase 3, and β-cell proliferation by double immunostaining for insulin/ki67 in fixed pancreatic tissue.

4.4.1 Treated Irs2$^{-/-}$ *mice show reduced β-cell apoptosis*

β-cell apoptosis was greatly increased in *Irs2*$^{-/-}$ relative to WT mice, consistent with decreased survival of β-cells in the absence of Irs2 (Fig. 13A, B). The treatment with tungstate resulted in a nearly three-fold reduction in β-cell apoptosis in *Irs2*$^{-/-}$ mice relative to untreated *Irs2*$^{-/-}$ (Fig. 13A, B). Interestingly, 30-weeks old *Irs2*$^{-/-}$ mice exhibited an even greater decrease in β-cell apoptosis, which reached similar values to those found in WT animals (Fig. 13B).

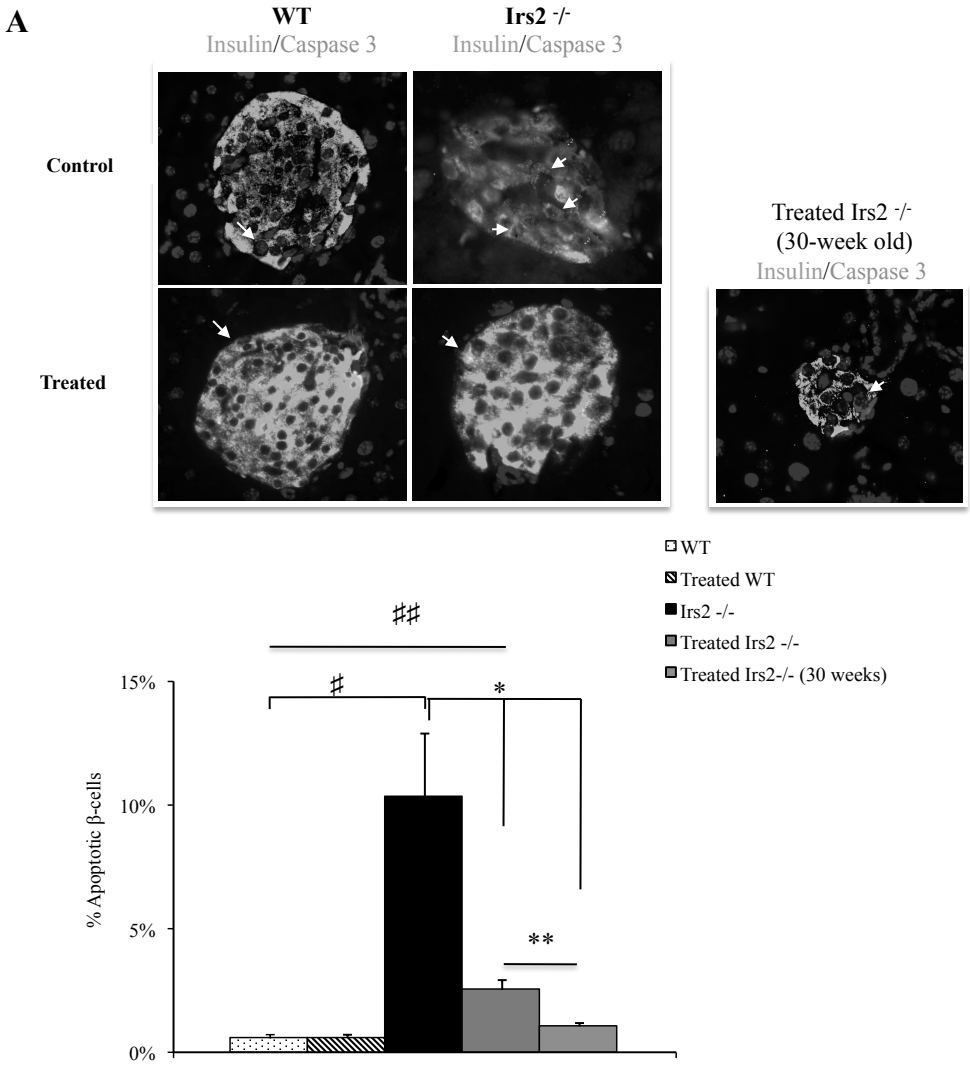

Figure 13: Tungstate decreased β-cell apoptosis in *Irs2*$^{-/-}$ mice. (A) Representative images of positive caspase 3 staining in WT and *Irs2*$^{-/-}$ mice untreated (control) or treated with tungstate. Caspase 3 positive β-cells: orange (merge between red and green) Original magnification x400 (B) β-cell apoptosis reported as percentage of cleaved caspase-3 positive β-cells divided by total β-cell number. Data is mean ± SEM, *P<0.05 and **P<0.01, #P< 0.05 and ##P< 0.01 between indicated groups. Data was obtained from 5-8 mice per genotype, except the 30-week old mice where n=4.

4.4.2 Treated Irs2$^{-/-}$ *mice show increased but minimal β-cell proliferation*

Regarding β-cell proliferation, our measurements indicate that it was increased in treated *Irs2*$^{-/-}$ but the percentage of proliferative β-cells was very low (<0.2%) (Fig. 14). Interestingly, in 30-weeks old treated *Irs2*$^{-/-}$ this difference did not reach statistical significance. Of note, the presence of proliferative β-cells was not consistent within treated *Irs2*$^{-/-}$ mice, meaning that in some animals (3/8 in treated *Irs2*$^{-/-}$ and 2/4 in 30-weeks treated *Irs2*$^{-/-}$) no Ki67-positive β-cells were found.

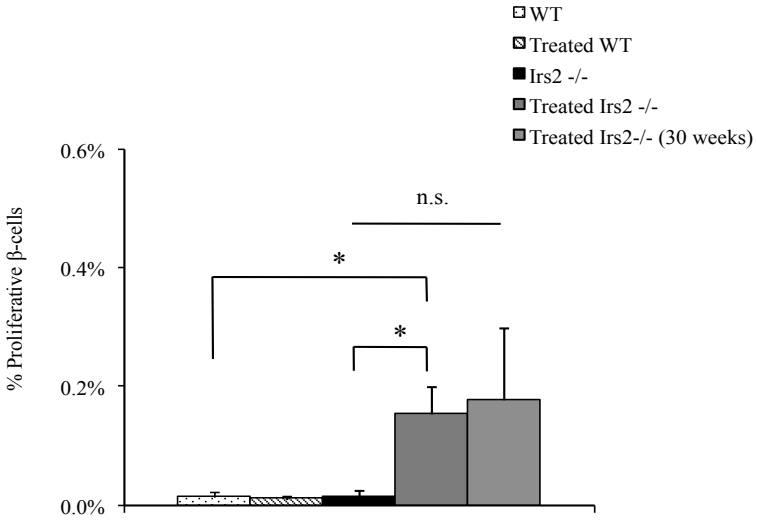

Figure 14: Tungstate had minimal effect on β-cell proliferation in *Irs2*$^{-/-}$ mice. β-cell proliferation reported as percentage of Ki67-positive β-cell nuclei divided by total β-cell number. Data are mean ± SEM, *P<0.05 between indicated groups and was obtained from 5-8 mice per genotype, except the 30-week old mice where n=4.

In summary, our data suggests that reduced apoptosis appears to be the main mechanism responsible for increased β-cell mass in *Irs2*$^{-/-}$ mice treated with tungstate.

5 THE EFFECT OF TUNGSTATE ON ISLET GENE EXPRESSION IN *IRS2*$^{-/-}$ MICE

To obtain a more comprehensive view of the changes induced by tungstate in pancreatic islets, we compared global gene expression profiles of isolated islets from treated and untreated *Irs2*$^{-/-}$ and WT animals using Affymetrix microarrays.

5.1 *Irs2*$^{-/-}$ gene expression profile

Loss of the *Irs2* gene affected the expression of 181 genes, of which 58 were induced genes and 123 were repressed. The expression results of noteworthy genes are shown in supplementary table 1 and 2. Ingenuity pathway and gene ontology analysis confirmed that the downregulated genes were primarily involved in cell signaling and molecular transport (Table 1).

Table 1: Most represented pathways and gene ontology terms of the 181 genes whose expression was significantly different between untreated *Irs*2$^{-/-}$ mice and WT.

Irs2-/- versus WT			
Ingenuity Pathway Analysis			
Cell Signalling, Molecular Transport, Vitamin and Mineral Metabolism			
Cell Death, Cellular Growth and Proliferation, Organismal Development			
Cellular Function and Maintenance			
Gene Expression, Post-translational Modification			
Gene Ontology Analysis			
Upregulated	P-value	Downregulated	P-value
GO:0006952~defense response	1.6E-08	GO:0006811~ion transport	0.006
GO:0006954~inflammatory response	3.6E-07	GO:0055085~transmembrane transport	0.022
GO:0009611~response to wounding	6.4E-06	GO:0019226~transmission of nerve impulse	7.2E-04
GO:0006955~immune response	4.6E-05	GO:0007267~cell-cell signalling	0.049
GO:0008219~cell death	0.004	GO:0006812~cation transport	0.036
GO:0002526~acute-phase response	3.4E-05	GO:0030182~neuron differentiation	0.042

Pancreatic islets in a diabetic environment have profoundly abnormal GSIS. Therefore, components of glucose metabolism pathways that are linked to secretion can be expected to be abnormal in T2D samples. Indeed, we found differential expression for several membrane transporters belonging to the solute carrier

family. For instance, the solute carrier family 2 (facilitated glucose transporter) member 2 (Slc2a2), also known as Glut2, was downregulated in the *Irs2*$^{-/-}$ samples. For the glycolytic enzymes, Pyruvate carboxylase, which is highly expressed in rodent islets and linked to insulin secretion (Dominici et al.), was also downregulated in *Irs2*$^{-/-}$. The array signal for insulin (Ins) was very high in both groups and not differentially expressed between *Irs2*$^{-/-}$ and WT animals. These signals clearly do not provide accurate information about the actual abundance of message and it seems this is particularly a problem when the message is very highly expressed. We did not find changes in the expression of the principal islet transcription factors as Pdx1 or NKX61 but we did find that MafA, a key regulator of insulin transcription, was also downregulated in *Irs2*$^{-/-}$. Concerning the upregulated genes in *Irs2*$^{-/-}$ mice compared to WT mice, they were mainly implicated in cell death and inflammatory processes (Table 1). We found that several immunoglobulins and chemokines were overexpressed in *Irs2*$^{-/-}$, and despite there was no differential expression of the major genes implicated in apoptosis, we did find upregulation of apoptosis-related genes as the cell death-inducing DNA fragmentation factor alpha subunit-like effector A (Cidea), gasdermin 1A (Gsdma) and marginal zone B and B1 cell-specific protein 1(Mzb1) genes. Two genes belonging to the regenerating islet gene family were also upregulated in *Irs2*$^{-/-}$: the Reg2 gene, which is normally expressed in islet β-cells and an autoantigen in the diabetes of nonobese diabetic (NOD) mice; the Reg3β gene, which was detected in pancreatic islets and elevated in T1D patients. However, their real roles are controversial as overexpression of Reg2 and Reg3β were also described as protective against streptozotocin-induced damage (Lu et al., 2006).

5.2 Treated *Irs2*$^{-/-}$ mice gene expression profile

5.2.1 Downregulation of inflammatory and proapoptotic genes by tungstate

Conversely, sodium tungstate treatment changed the expression of 149 genes in *Irs2*$^{-/-}$ islets (supplementary table 3) that were mostly implicated in inflammatory response and cell death, as confirmed by ingenuity pathway and gene ontology analysis (Table 2). Among these 149 genes one was an unidentified induced gene and 148 were repressed genes with fold-changes ranging from -5.25 to -1.75, encoding mainly chemokines, immunoglobulins and activators of apoptosis.

Table 2. Most represented pathways and gene ontology terms of the 149 genes whose expression was significantly different between treated *Irs2*$^{-/-}$ and untreated *Irs2*$^{-/-}$ mice.

Treated Irs2-/- versus Irs2-/-	
Ingenuity Pathway Analysis	
Inflammatory Response, Hematological System Development	
Cellular Growth and Proliferation, Cellular Development	
Cell Death, Cell-mediated Immune Response	
Cell-to-cell Signalling/Interaction, Tissue Development	
Immunological diseases	
Gene Ontology Analysis	
Downregulated	P-value
GO:0006952~defense response	1.1E-11
GO:0006954~inflammatory response	8.2E-09
GO:0006935~chemotaxis	2.6E-07
GO:0034097~response to cytokine stimulus	1.2E-06
GO:0008219~cell death	8.3E-04
GO:0042981~regulation of apoptosis	0.002

5.2.2 Tungstate reverted the expression of proinflamatory and proapoptotic genes

In this study, we were more interested in those genes whose expression was pottentially restored in *Irs2*$^{-/-}$ by sodium tungstate treatment. Therefore, we focused on the differentially expressed genes between *Irs2*$^{-/-}$ and WT animals (181 genes) and between treated and untreated *Irs2*$^{-/-}$ animals (149 genes) and overlapped these two lists, looking for possible repetitions between them. Indeed, we identified a total of 42 genes that fulfilled these criteria (Fig. 15A and Table 3). These 42 genes were of interest because they were exactly the same 42 genes upregulated in *Irs2*$^{-/-}$ mice compared to WT and downregulated in treated *Irs2*$^{-/-}$ (Fig. 15B). Gene ontology analysis identified inflammatory response and cell death as the most represented pathways among these 42 genes (Fig. 14C), which encodes mainly immunoglobulins, some transmembrane proteins and apoptosis-related proteins (Table 3).

Table 3: Common 42 genes identified in *Irs2*$^{-/-}$/WT and treated *Irs2*$^{-/-}$/untreated *Irs2* $^{-/-}$.

Query	Gene symbol	Gene Title	Fold-Change Irs2 $^{-/-}$ vs WT	Fold-Change Treated Irs2 $^{-/-}$ vs Irs2 $^{-/-}$
1418282_x_at	Serpina1b	Serine preptidase inhibitor member 1b	3.1	-2.6
1424931_s_at	Igl	Immunoglobulin lambda chain, variable 1	5.4	-4.3
1418536_at	H2-Q7	Histocompatibility 2, Q region locus 6	3.0	-2.3
1422918_at	1810009J06Rik	RIKEN cDNA 1810009J06 gene	5.3	-2.6
1435697_a_at	Cytip	Pleckstrin homology, Sec7 binding protein	3.3	-2.7
1451206_s_at	Cytip	Pleckstrin homology, Sec7 binding protein	3.0	-2.6
1441161_at	B230216G23Rik	RIKEN cDNA B230216G23 gene	3.1	-2.3
1419735_at	Csn3	Casein kappa	5.7	-2.8
1428909_at	A130040M12Rik	RIKEN cDNA A130040M12 gene	3.1	-3.4
1450689_at	Prss3	Similar to trypsinogen 15	5.8	-3.0
1422682_s_at	EG436523	Protease, serine, 1 (trypsin 1)	6.5	-3.4
1424923_at	Serpina3g	Serine peptidase inhibitor,member 3G	2.8	-2.7
1422915_at	Gast	Gastrin	5.5	-2.3
1424305_at	Igj	Immunoglobulin joining chain	3.9	-2.0
1426174_s_at	Igh-3	Immunoglobulin heavy chain	5.9	-5.3
1424631_a_at	Ighg	Immunoglobulin heavy chain	5.4	-5.2
1418652_at	Cxcl9	Chemokine (C-X-C motif) ligand 9	3.8	-3.5
1436662_at	Sorcs1	VPS10 domain receptor protein SORCS 1	4.2	-2.7
1450344_a_at	Ptger3	Prostaglandin E receptor 3 (subtype EP3)	4.2	-3.1
1427455_x_at	Gm10883	Ig kappa chain	3.7	-1.8
1423547_at	Lyz2	Lysozyme	3.2	-2.2
1416318_at	Serpinb1a	Serine (or cysteine) peptidase inhibitor, clade B, member 1a	3.2	-2.4
1418126_at	Ccl5	Chemokine (C-C motif) ligand 5	3.4	-3.1
1430523_s_at	Igl-V1	Immunoglobulin lambda chain, variable 1	5.1	-4.2
1428719_at	2010309G21Rik	RIKEN cDNA 2010309G21 gene	3.9	-2.6
1428720_s_at	2010309G21Rik	RIKEN cDNA 2010309G21 gene	3.8	-2.7
1425854_x_at	LOC665506	T-cell receptor beta, variable 13	3.1	-2.9
1427789_s_at	Gnas	Guanine nucleotide binding protein, alpha stimulating complex locus	4.4	-2.2
1426168_a_at	A130082M07Rik	T-cell receptor alpha chain	3.4	-3.2
1417956_at	Cidea	Cell death-inducing DNA fragmentation factor, alpha subunit-like effector A	4.6	-2.7
1428947_at	2010001M09Rik	RIKEN cDNA 2010001M09 gene	2.9	-2.7
1425385_a_at	Igh-6	Similar to gamma-2a immunoglobulin heavy chain	4.1	-3.7
1429381_x_at	Igh-2	Immunoglobulin heavy chain (J558 family)	3.3	-2.3
1424357_at	Tmem45b	Transmembrane protein 45b	2.8	-2.1
1452205_x_at	Gm6273	T-cell receptor beta, variable 13	3.2	-2.9
1423634_at	Gsdma	Gasdermin 1	3.1	-2.2
1436996_x_at	Lyz1	Lysozyme	3.1	-2.2
1439426_x_at	Lyz1	Lysozyme	3.7	-3.2
1449498_at	Marco	Macrophage receptor with collagenous structure	2.9	-2.3
1419388_at	Tm4sf20	Transmembrane 4 L six family member 20	4.0	-3.3
1423467_at	Ms4a4b	Membrane-spanning 4-domains, subfamily A, member 4B	3.7	-3.3

A

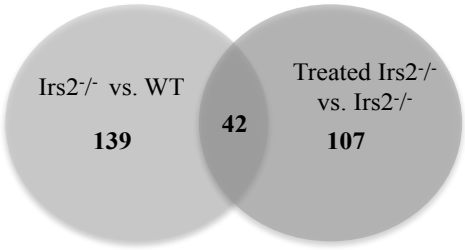

B

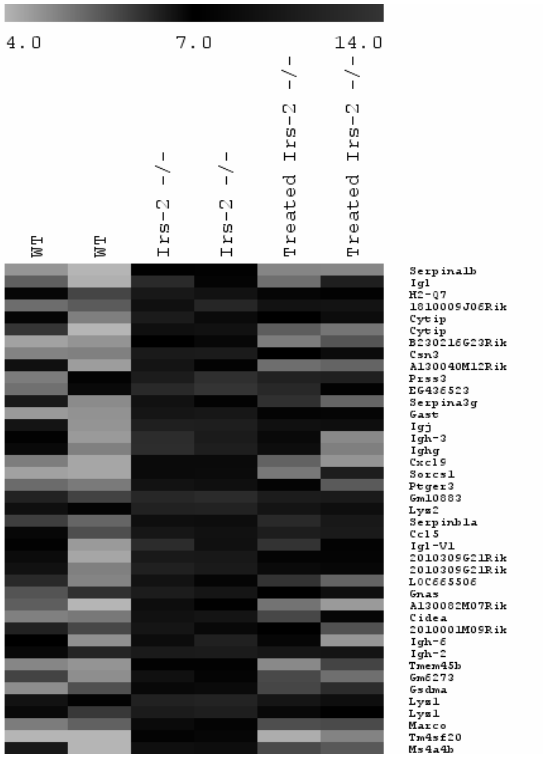

C

Gene Ontology	P-value
GO:0006952~defense response	9.38E-07
GO:0006954~inflammatory response	1.87E-04
GO:0009611~response to wounding	9.63E-04
GO:0006955~immune response	2.19E-05
GO:0008219~cell death	4.06E-04
GO:0016265~death	4.52E-04
GO:0006915~apoptosis	2.22E-02
GO:0012501~programmed cell death	2.32E-02

Figure 15. Whole-genome gene expression profiling of islets from tungstate-treated and untreated *Irs2*$^{-/-}$ and WT mice. (A) Venn diagram showing overlap between the two sets of differentially expressed genes identified in the comparisons *Irs2*$^{-/-}$ versus WT animals and treated *Irs2*$^{-/-}$ vs *Irs2*$^{-/-}$ mice. (B) Heat Diagram depicting the 42 common genes shown in A. Expression of all 42 genes was significantly upregulated in *Irs2*$^{-/-}$ mice relative to WT, and downregulated in response to tungstate treatment in *Irs2*$^{-/-}$ mice (See supplementary table 3 for complete names and fold-changes of the genes). (C) Gene ontology analysis of the common set of 42 genes.

After bibliographic research from the abovementioned list we chose three genes whose function would help us to explain the effects observed in the pancreas of tungstate treated *Irs2*$^{-/-}$ animals. They were primarily involved in apoptosis and were the: cell death-inducing DNA fragmentation factor alpha subunit-like effector A (*Cidea*), gasdermin A (*Gsdma*) and marginal zone B and B1 cell-specific protein (*Rik*) genes. We quantified their expression using islet samples isolated from treated and untreated WT and *Irs2*$^{-/-}$ mice by qRT-PCR. Despite we did not confirm the differential expression of Rik gene between treated and untreated *Irs2*$^{-/-}$ groups, we validated *Cidea* and *Gsdma* genes as significantly downregulated in isolated islets from treated *Irs2*$^{-/-}$ relative to untreated ones (Fig. 16A). Moreover, we also confirmed that these two genes were upregulated in isolated islets from *Irs2*$^{-/-}$ relative to WT, as observed in microarray analysis. These results are

of interest because they suggest that these genes could be targets of sodium tungstate (Fig. 16A).

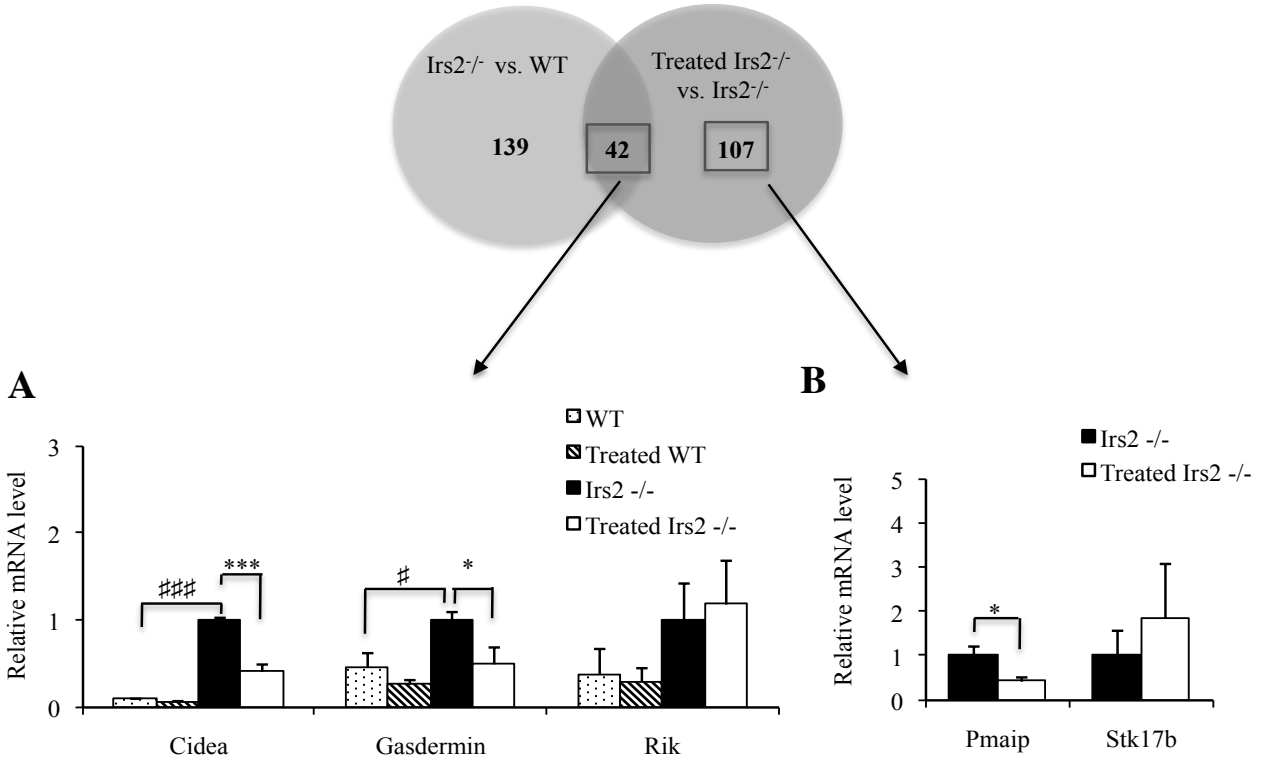

Figure 16: Whole-genome gene expression profiling of islets from tungstate-treated and untreated *Irs2*$^{-/-}$ mice. (A) Venn diagram showing overlap between the two sets of differentially expressed genes identified in the comparisons *Irs2*$^{-/-}$ vs. WT and treated *Irs2*$^{-/-}$ vs. *Irs2*$^{-/-}$ mice. (B) qRT-PCR validation of three proapoptotic genes, *Cidea*, *Gsdma and Rik,* identified in gene expression profile analysis as upregulated in *Irs2*$^{-/-}$ mice compared to WT, and downregulated in treated *Irs2*$^{-/-}$ mice compared to untreated one. qRT-PCR validation of two proapoptotic genes, *Pmaip1 and Stk17b,* identified in gene expression profile analysis as downregulated in treated *Irs2*$^{-/-}$ mice compared to untreated one. Islets of WT littermate controls (untreated and treated), *Irs2*$^{-/-}$ mice and treated *Irs2*$^{-/-}$ mice were used. Data was obtained using isolated islets from 5 to 6 mice per experimental group. Data are mean ± SEM and is expressed as fold-change relative to *Irs2*$^{-/-}$. *p<0.05, ***p<0.001 and #p<0.05, ###p<0.001 between indicated groups.

Likewise, we explored the remaining 107 genes that were downregulated in treated *Irs2*$^{-/-}$ but primarily unchanged in *Irs2*$^{-/-}$ (supplementary table 4). Interestingly, gene ontology analysis also associated these genes with inflammation and apoptosis, and we chose 2 genes of interest to be confirmed by qRT-PCR: the serine/threonine kinase 17b12 (*Stk17b*) also known as *Drac2*, which overexpression can lead to aggravated β-cell apoptosis; and the *Pmaip1* gene, which is a proapoptotic member of the Bcl2 family that regulates apoptosis. Despite we did not observe the downregulation of *Stk17b*, we did confirme *Pmaip1* gene as significantly downregulated in treated *Irs2*$^{-/-}$ relative to untreated ones (Fig. 16B).

Hence, these observations confirm that sodium tungstate primarily targets β-cell death mechanisms in *Irs2*$^{-/-}$ islets.

5.2.3 Upregulation of Reg genes

Our gene expression analysis study also indicated that the treatment with tungstate altered the expression of some genes on islets from *Irs2*$^{-/-}$ mice without any effect on treated WT animals islets profile. By comparing the gene expression profile of treated *Irs2*$^{-/-}$ and treated WT mice, a total of 178 genes appeared differentially expressed, with 53 being downregulated and 125 genes upregulated in treated *Irs2*$^{-/-}$ (supplementary tables 5 and 6). Inflammatory response and molecular function were the most represented processes concerning the upregulated genes (Table 4). The downregulated ones were associated primarily with cell signaling and molecular transport (Table 4). Eventually, some genes could be changed due to the genotype and not due to the tungstate treatment. Thus, we compare the list of differentially expressed genes between treated *Irs2*$^{-/-}$ and treated WT with the list of genes differentially expressed between *Irs2*$^{-/-}$ and WT animals without treatment. Efectivelly, by comparing the two groups of downregulated genes (53 genes in treated *Irs2*$^{-/-}$ versus treated WT and 123 genes in untreated *Irs2*$^{-/-}$ versus WT) we found that 51 genes out of the 53 list were also downregulated in untreated *Irs2*$^{-/-}$. This means that they were changed due to the genotype and not due to the treatment with tungstate. The two genes that were not in common were the par-6 partitioning defective 6 homolog gamma (Pard6g) gene and an unidentified gene 9130023H24Rik. However, we excluded these two genes of the study because they presented a high q-value equal to 0.05.

Table 4. Most represented pathways and gene ontology terms of the 178 genes whose expression was significantly different between treated *Irs2*$^{-/-}$ and treated WT mice.

Treated Irs2-/- versus Treated WT			
Ingenuity Pathway Analysis			
Cell Signaling, Molecular Transport, Vitamin and Mineral Metabolism Cellular Movement, Cellular Growth and Proliferation, Cell Death Organ Development, Organ Morphology, Gene Expression Cellular Growth and Proliferation, Hematological System Development and Function, Inflammatory Response Cancer, Cell Cycle, Developmental Disorder			
Gene Ontology Analysis			
Upregulated	P-value	Downregulated	P-value
GO:0032101~regulation of response to external stimulus	1.05E-06	GO:0006811~ion transport	9.49E-04
GO:0050727~regulation of inflammatory response	2.19E-04	GO:0019226~transmission of nerve impulse	0.0063
		GO:0007267~cell-cell signaling	0.0124
		GO:0007155~cell adhesion	0.0137
GO:0009611~response to wounding	4.37E-04		
		GO:0022610~biological adhesion	0.0137
GO:0006952~defense response	0.002		
GO:0009725~response to hormone stimulus	0.0108		
GO:0044093~positive regulation of molecular function	0.0052		
GO:0043085~positive regulation of catalytic activity	0.0024		

By comparing the two groups of upregulated genes (125 genes in treated *Irs2*$^{-/-}$ versus treated WT and 58 genes in untreated *Irs2*$^{-/-}$ versus WT) we found that 24 out of 125 genes were also upregulated in untreated *Irs2*$^{-/-}$ relative to WT animals. Therefore, we focused our attention in the remaining 101 genes that were upregulated only in treated *Irs2*$^{-/-}$ versus treated WT (Fig. 17A, and supplementary table 7). Among these 101 genes we focused our attention to those belonging to the regenerating islet gene family: Reg3a, Reg1, and islet neogenesis-associated protein (Ingap, also known as Reg3d). The roles of Reg family of proteins continue to be intriguing but poorly understood. Reg1 has been implicated in β-cell growth by association and by administration of the peptide, and a knockout resulted in reduced islet mass (Lu et al., 2006). However, Reg1 has also been found in the β-cells of mice with new onset T1D. Reg3a has been reported to have mitogenic and anti-apoptotic functions and, with Ingap, are candidates for inducing neogenesis (Lu et al., 2006). The expression of Reg3a, Reg1 and Red3d was quantified by qRT-PCR performed on islet samples from five treated *Irs2*$^{-/-}$ and five treated WT mice. However, the result was disappointing as no differential expression was found for these genes between the treated *Irs2*$^{-/-}$ and treated WT mice (Fig. 17B), excluding these genes as important for our study.

We also chose other upregulated genes in treated *Irs2*$^{-/-}$ versus treated WT that we consider of interest to be validated by qRT-PCR, as the: Leptin Receptor (*Lepr*), which activation in pancreatic β-cells inhibits insulin secretion and proinsulin gene expression; Syncollin (*Sycn*), which is involved in exocytosis; two dual specificity phosphatase proteins, the *Dusp6* and *Dusp26*, which are involved in the regulation of embryogenesis, placental development and immune responses (Pulido and Hooft van Huijsduijnen, 2008). However, we only confirmed Dusp26 as significantly increased in treated *Irs2*$^{-/-}$ relative to treated WT, excluding the other genes of our study.

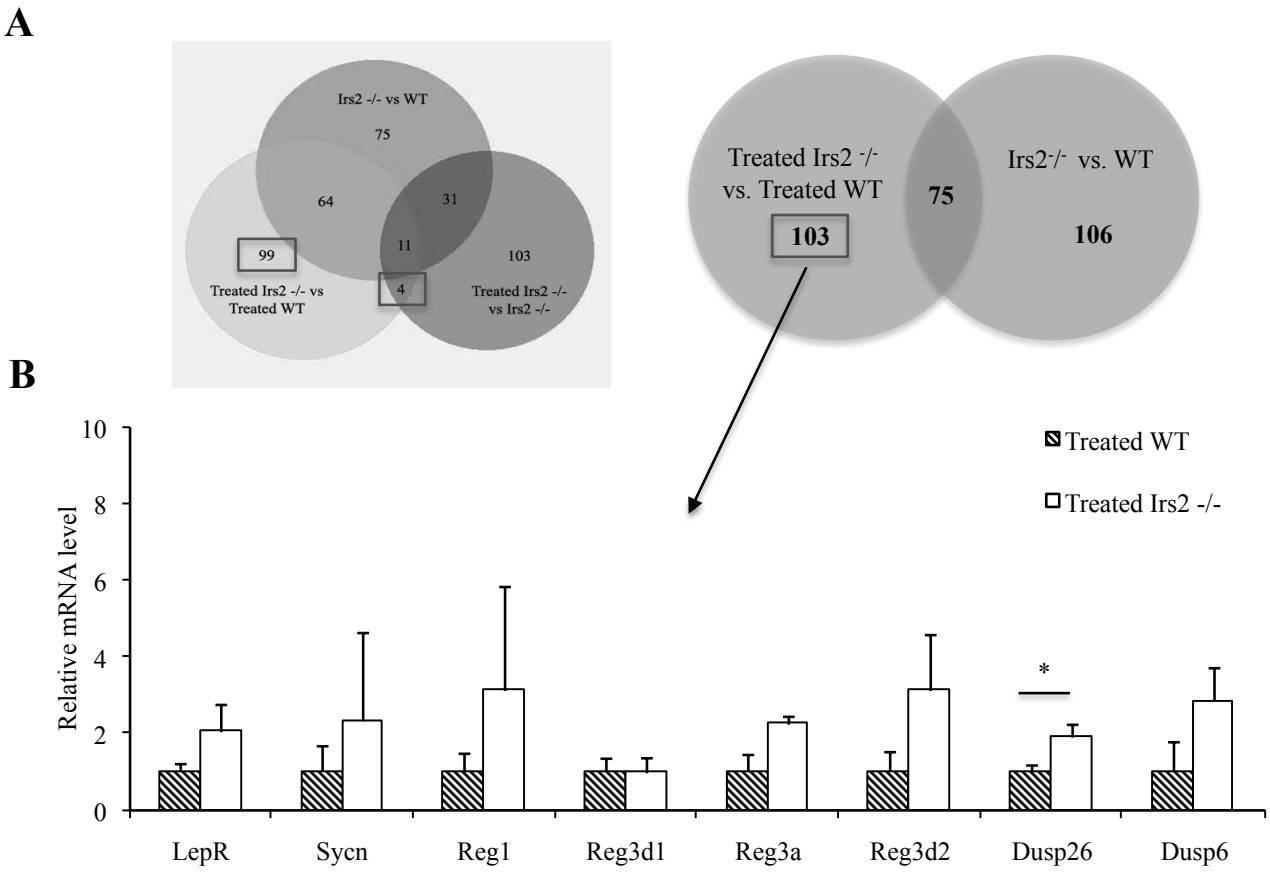

Figure 17: 103 genes were exclusively upregulated in tungstate-treated *Irs2*$^{-/-}$ mice compared to treated WT mice in the gene expression profile study. (A) Venn diagram showing overlap between the three sets of differentially expressed genes identified in the comparisons *Irs2*$^{-/-}$ vs WT animals, treated *Irs2*$^{-/-}$ vs *Irs2*$^{-/-}$ mice and treated *Irs2*$^{-/-}$ vs treated WT mice. (B) qRT-PCR validation of eight genes identified in the group of 103 genes upregulated in treated *Irs2*$^{-/-}$ mice compared to treated WT. Islets of treated *Irs2*$^{-/-}$ and treated WT mice were used. Data was obtained using isolated islets from 5 to 6 different mice per experimental group. Data are mean ± SEM and is expressed as fold-change relative to treated WT, *p<0.05 between indicated groups.

5.3 The effect of tungstate on islet gene expression of WT mice

Tungstate treatment changed the expression of 12 genes, all of them repressed in treated WT relative to WT, and the majority coding for matrix proteins and for the chaperone heat shock protein 1B (supplementary table 8).". Ingenuity pathway and gene ontology analysis confirmed that the downregulated genes were primarily involved in connective tissue disorders or post-translational mechanisms (Table 4). Other 16 genes resulted induced in treated WT, but only 4 were identified genes, and the fold-changes were to low to be considered as upregulated genes (supplementary table 9). As the changes in WT treated animals were minimal, we did not focus our study in this group of genes.

Table 5. Most represented pathways and gene ontology terms of the 12 genes whose expression was significantly downregulated in treated WT compared to WT mice.

Treated WT versus WT
Ingenuity Pathway Analysis
Connective Tissue Disorders, Genetic Disorder, Post-Translational Modification
Genetic Disorder, Metabolic Disease, Carbohydrate Metabolism
Psychological Disorders, Carbohydrate Metabolism, Drug Metabolism

6 DIFFERENTIAL PROTEIN EXPRESSION IN TREATED *IRS2*$^{-/-}$ ISLETS

We next aimed at determining the molecular mechanisms underlining the effects of tungstate on β-cell death pathways in *Irs2*$^{-/-}$ mice. We first performed hybridization of extracted proteins from isolated pancreatic islets of treated and untreated *Irs2*$^{-/-}$ mice to an antibody microarray for a screening of signaling pathways that could be altered in treated *Irs2*$^{-/-}$ mice. This array was designed to investigate alterations in several biological pathways (as signal transduction and apoptosis) and, for some of the protein targets, it can detect the phosphorylated and non-phosphorylated forms of the target protein. Importantly, this array offered us a methodological advantage, as it allowed us to investigate several signaling pathways simultaneously with a small quantity of protein compared to that needed in immunoblot analysis. This analysis showed that several proteins implicated in signal transduction were upregulated in *Irs2*$^{-/-}$ treated mice, which suggest an overall improvement in intracellular signaling in these animals (Table 6). Of note, the two phosphorylated forms of Focal adhesion kinase (FAK) protein were upregulated in *Irs2*$^{-/-}$ treated mice. These proteins were recently implicated in promoting β-cell survival via Akt signaling. Also, the phosphorylation status of Erk1/2 was increased by 2-fold as consequence of tungstate treatment. In contrast, several proteins implicated in apoptosis were downregulated in *Irs2*$^{-/-}$ treated mice (Table 6 and Fig.18). Among these proteins we identified several caspases, including caspase 9 (decreased by 3-fold), caspase 12 (decreased by 5-fold) and active caspase 3 (decreased by 1.6 fold) (Table 6). Similarly, a mitochondrial protein called Smac that, along with Cytochrome c promotes apoptosis by activating caspases, was also found to be less expressed in *Irs2*$^{-/-}$ treated mice. Other proteins involved in apoptosis, such as the death receptor Fas (which forms the death-inducing signaling complex DISC) and the adaptor molecule FADD, were also downregulated in *Irs2*$^{-/-}$ treated mice. These evidences suggested a general decrease in apoptotic events in *Irs2*$^{-/-}$ treated animals. These results prompted us to examine in more detail the expression of key proteins potentially involved in tungstate effect in *Irs2*$^{-/-}$ islets by immunoblot analysis.

Table 6: Protein expression in *Irs2*$^{-/-}$ treated mice compared to untreated ones resulting from Panorama Antibody Microarray. The expression signal for each protein was normalized to actin signal and the fold-changes were calculated by divided the signal for treated *Irs2*$^{-/-}$ for the corresponding signal of *Irs2*$^{-/-}$ untreated mice. Proteins with FC above 1.5 were considered as upregulated, and below 0.5 as downregulated in treated *Irs2*$^{-/-}$ animals relative to untreated *Irs2*$^{-/-}$.

Upregulated (FC>1.5)	Area	FC	Downregulated (FC<0.5)	Area	FC
PKC β	Signal Transduction	6.1	Phosphotyrosine	Signal Transduction	0.4
PKC γ		4.4	GRB-2		0.4
MAP Kinase activated phosphotyrosine		**3.2**	PKC α		0.3
FAK Phospho (pY^{577})		**3.1**	EGF receptor		0.2
Phospho-Pyk2 (pY$^{579/580}$)		2.8	GRP1 (ARNO3 Cytohesin-3)		0.0
Pyk2		2.6	IkB α		0.4
FAK phospho (pY397)		**2.5**	p57^{kip2}	Cell Cycle /Nuclear	0.4
MAPK non phosphorylated ERK		2.4	Cyclin A		0.4
PTEN		2.1	Cdk6		0.3
MAP Kinase (ERK1+ERK2)		**2.0**	HAT1 (Histone acetyltransferase)		0.2
MAP Kinase activated phosphothrenine		**1.9**	MDM2		0.2
MAP Kinase activated (diphosphorylated MAPK)		**1.9**	Phospho-Histone H3 (pS^{10})		0.1
p38 MAPK activated (diphosphorylated p38)		1.8	HDAC 4 (Histone Deacetylase 4)		0.1
JNK activated (diphosporylated JNK)		1.6	Cyclin D2		0.1
Phospho-Tau	Neurobiology	3.9	hnRNP M3-M4		0.0
Tyrosine Hydroxylase		3.5	Cyclin B1		0.4
i-NOS		2.7			
e-NOS		2.2	**Caspase 9**	Apoptosis	**0.3**
b-Synuclein		2.1	ARTS		0.3
AP2 gamma	Nuclear	3.7	**FADD**		**0.2**
AP2 beta		3.0	Bcl-xL		0.3
AP2 alpha		2.1	**Caspase 12**		**0.2**
HSP 70	Cell Stress	3.6	**Fas (CD95/Apo-1)**		**0.3**
Aop-1		3.3	**Caspase 3 – Active**		**0.6**
HSP 90		2.7	**Caspase 3**		**0.6**
Nedd 8		1.7	**SMAC/DIABLO**		**0.6**
Calcineurin	Ca Associated Protein	2.0	**Apoptosis Inducing Factor (AIF)**		**0.5**
Calmodulin		1.7			
Cytokeratin	Cytoskeleton	3.2			
p21^{Waf-1}	Cell Cycle	2.6			

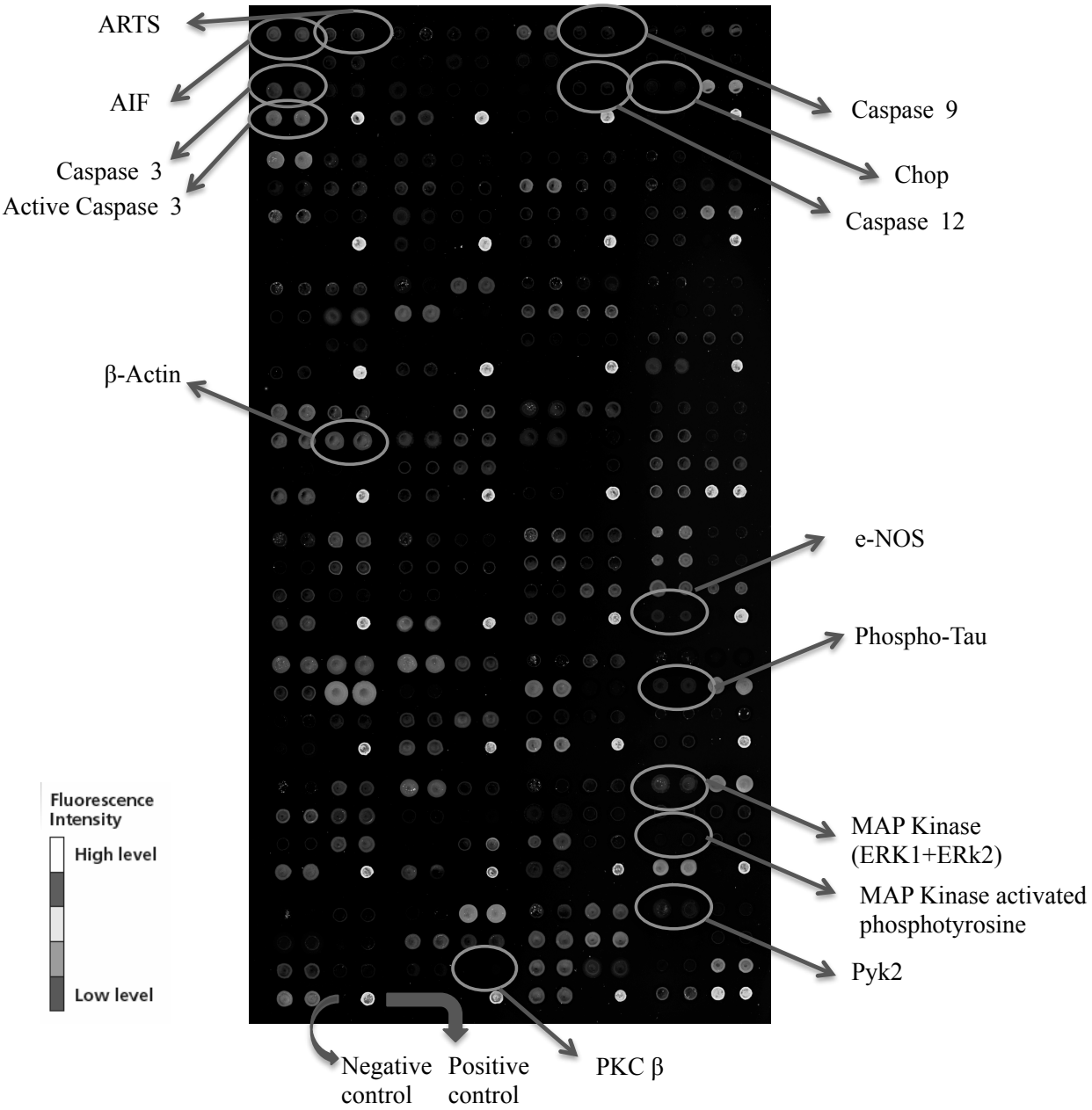

Figure 18: Protein expression in *Irs2*$^{-/-}$ treated mice compared to untreated ones resulting from Panorama Antibody Microarray. Extracts from isolated islets were prepared from treated and untreated Irs2-/- using Extraction/Labeling Buffer and labeled with Cyanine 5 (Cy5) and Cyanine 3 (Cy3), respectively. A mixture containing equal amounts of each labeled extract was incubated on the array. The slide shown is the merge between the two fluorescence emission wavelengths for Cy5 and Cy3.

6.1 Increased Erk1/2 phosphorylation in treated *Irs2*$^{-/-}$ islets

Decreased survival of *Irs2*$^{-/-}$ mice β-cells has been associated with reduced activation of the two major signaling pathways emerging downstream of Irs2, the PI3K/PKB and MAPK cascades, and of several of their downstream targets. As Erk1/2 was previously implicated as one of the possible mediators of tungstate, and was upregulated in the antibody microarray, we hypothesized that tungstate effects on β-cell apoptosis might be related to its ability to influence the phosphorylation status of this kinase in pancreatic islets. As shown in Fig. 19A and B, we found that isolated islets from treated *Irs2*$^{-/-}$ animals exhibited increased phosphorylated levels of Erk1/2 relative to untreated *Irs2*$^{-/-}$ animals, which is consistent with the antibody array results. In contrast, the phosphorylation of Akt remained unchanged between treated and untreated *Irs2*$^{-/-}$ islets, which is also in accordance to what we saw in the antibody array. No changes were found in the expression of phosphorylated Erk1/2 or phosphorylated Akt between WT and treated WT.

One mechanism by which Erk1/2 prevents apoptosis is through phosphorylation of the pro-apoptotic protein Bad (Shimamura et al., 2000). Moreover, increased expression of unphosphorylated Bad was previously associated with increased apoptosis in islets of *Irs2*$^{-/-}$ mice (Withers et al., 1999). Based on this information, we hypothesized that activation of Erk1/2 in treated *Irs2*$^{-/-}$ mice might lead to increased phosphorylation of Bad. However, Bad protein was not modified in treated versus untreated *Irs2*$^{-/-}$ islets (Fig.19A, B). Similarly, Bad was also unchanged between *Irs2*$^{-/-}$ and WT mice, but it was less phosphorylated on serine 136 in treated *Irs2*$^{-/-}$ compared to WT mice. Interestingly, Bad was more phosphorylated on serine 112 in treated WT compared to WT.

During the intrinsic pathway of apoptosis, mitochondrial cytochrome C allows downstream activation of execution caspases. Further corroborating that apoptosis was decreased in treated *Irs2*$^{-/-}$ was our finding that the expression of the proapoptotic Cytochrome c was significantly lowered in isolated islets from treated relative to untreated *Irs2*$^{-/-}$ mice (Fig. 19C). However, we were not able to detect active caspase 3 or caspase 9 expression in our islets extracts by immunobloting analysis.

All together, these data point at activation of Erk1/2 and inhibition of the intrinsic pathway of apoptosis as implicated in the antiapoptotic effects of tungstate on pancreatic islets of *Irs2*$^{-/-}$ mice.

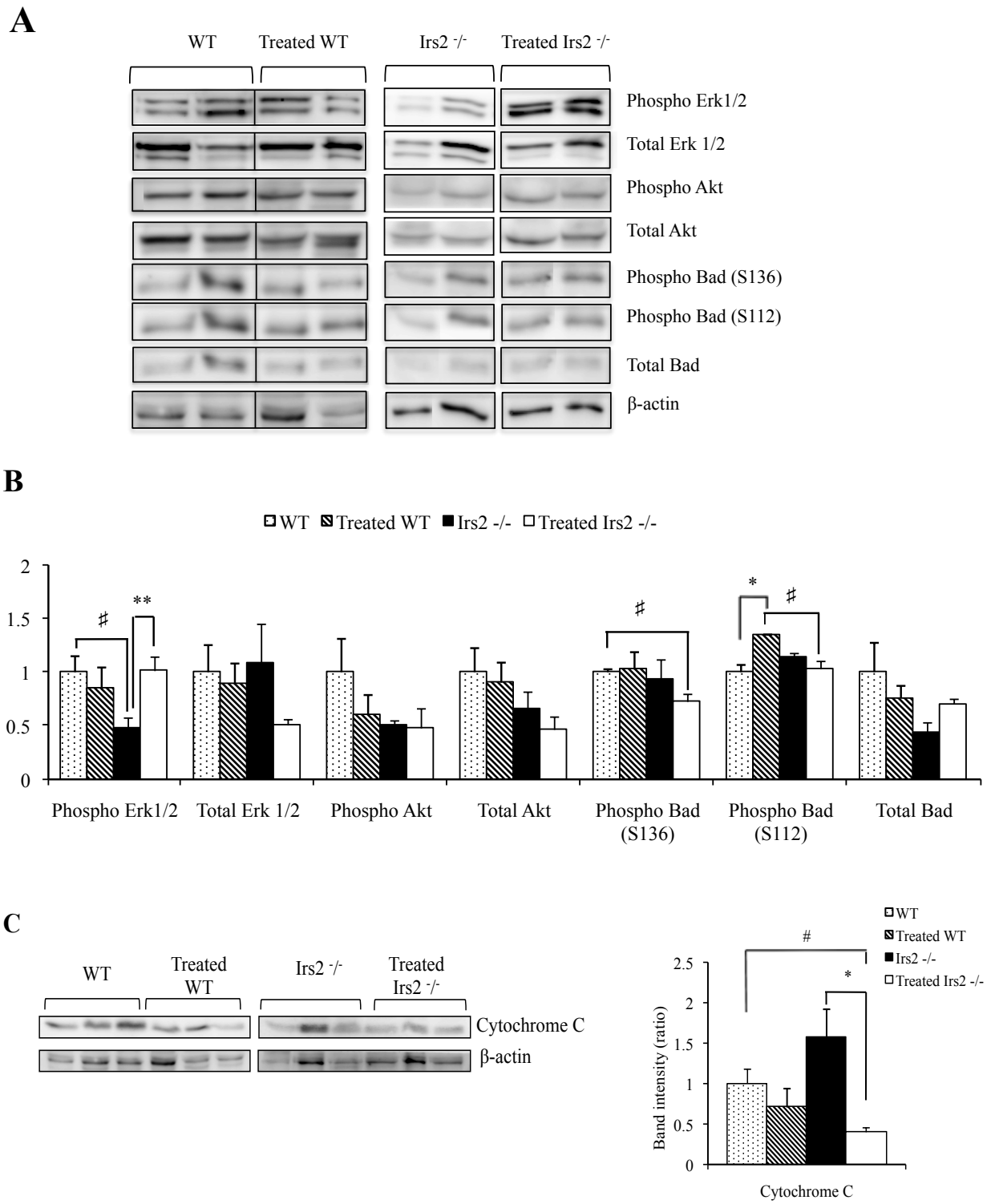

Figure 19: Increased Erk1/2 phosphorylation and decrease Cytochrome C expression in treated *Irs2*$^{-/-}$ mice. (A) Immunoblot analysis for the indicated proteins in lysates prepared from isolated islets from untreated and tungstate-treated WT and *Irs2*$^{-/-}$ mice. (B) Densitometric analysis of immunoblot bands calculated using the relative ratio of the phosphorylated protein normalized to the correspondent total protein signal. Total Ekr1/2, Total Akt and Total Bad were normalized to β-actin signal. Data corresponding to isolated islets from 4-5 different mice for Bad proteins and Akt proteins, and 9 animals for Erk1/2 proteins (C) Cytochrome C levels were determined in lysates prepared from isolated islets, data corresponding to isolated islets from 3 different mice. Data are mean ± SEM and is expressed as fold-change relative to WT. *p< 0.05, **p< 0.01 and $^{\#}$p<0.05 between indicated groups.

7 TUNGSTATE MODIFIES APOPTOSIS-RELATED GENE EXPRESSION IN ISOLATED *IRS2*$^{-/-}$ ISLETS

7.1 Direct effect of tungstate on pancreatic islets

Prior work by our group had shown that tungstate could directly affect Erk1/2 phosphorylation in a rodent β-cell line (Altirriba et al., 2009). Here we examined if tungstate had similar effects in isolated islets from WT animals. After an overnight incubation with normal culture medium, we divided the islets in two culture conditions: a control condition with normal medium and a second condition of culture with normal medium containing 100 uM of sodium tungstate. After a period incubation of 10 minutes in these two conditions, we rapidly froze the islets to preserve their phosphorylation status. We found that tungstate increased Erk1/2 phosphorylation in WT islets (Fig. 20), thus supporting a direct effect of this compound on these kinases in primary β-cells.

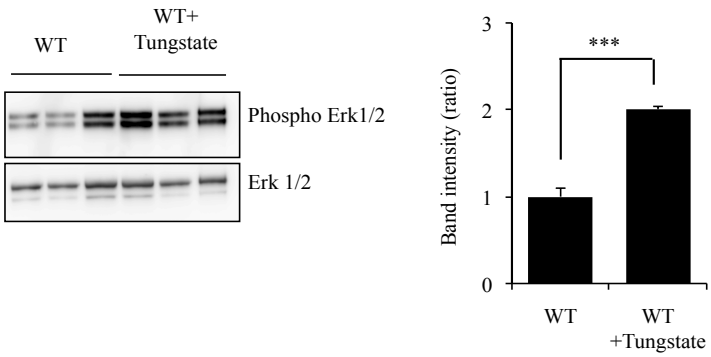

Figure 20: Erk1/2 phosphorylation is stimulated by tungstate treatment *in vitro*. Isolated islets from 8-10 weeks old WT animals were incubated with normal medium or with tungstate for 10 min and levels of phosphorylated and total Erk1/2 were measured by immunoblot analysis. Representative immunoblot and densitometric analysis showing the ratio of phosphorylated Erk1/2 relative to total Erk1/2, corresponding to isolated islets from 4 different mice. Data are mean ± SEM and is expressed as fold-change relative to basal condition, ***p<0.001 between indicated groups.

However, when we repeated the experiment using *Irs2*$^{-/-}$ islets incubated with tungstate, the same significant increase was not found despite a tendency can be observed (Fig. 21), which suggested us that possible *in vitro* effects of tungstate in *Irs2*$^{-/-}$ islets might need more time or be more moderate compared to the *in vivo* situation.

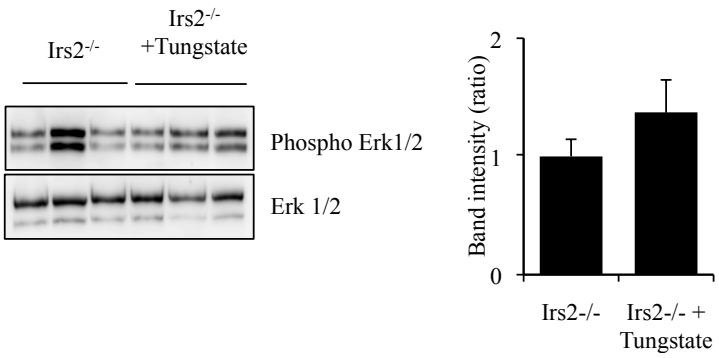

Figure 21: 10 minutes stimulation of *Irs2*$^{-/-}$ islets with tungstate. Isolated islets from 8-10 weeks-old *Irs2*$^{-/-}$ animals were incubated with normal medium or with tungstate for 10 min and levels of phosphorylated and total Erk1/2 were measured by immunoblot analysis. Representative immunoblot and densitometric analysis showing the ratio of phosphorylated Erk1/2 relative to total Erk1/2, corresponding to isolated islets from 12 different mice. Data are mean ± SEM of 3 independent experiments and is expressed as fold-change relative to basal condition.

Finally, we asked whether tungstate could directly modify the expression of apoptosis-related genes in isolated *Irs2*$^{-/-}$ islets. To this aim, we cultured *Irs2*$^{-/-}$ islets with normal medium containing sodium tungstate for 48 h and determined gene expression levels for several apoptosis-related genes by qRT-PCR. We observed that tungstate significantly reduced the expression of mRNAs encoding Caspase 3 *(Casp3)*, Bcl-2-interacting killer *(Bik),* BCL2 Binding component 3 *(Bbc3)* also known as *Puma*, and DNA-damage inducible transcript 3 (Ddit3) also known as *Chop* genes (Fig. 22A). Remarkably, tungstate also reduced expression of the *Cidea* and *Gsdma* genes, two of the genes identified in our microarray analysis as significantly modified by tungstate treatment *in vivo* (Figure 16A). *p53* gene, which controls the expression of *Chop* gene, was also downregulated with tungstate treatment (Fig. 22A). In contrast, expression of other genes implicated in the mitochondrial apoptotic pathway was not affected by tungstate (Fig. 22A). Lastly, we examined the potential contribution of Erk1/2 in the tungstate effects. To this aim, we cultured *Irs2*$^{-/-}$ islets with normal medium containing sodium tungstate or normal medium containing sodium tungstate plus an inhibitor of Mek1/2, the UO126. Next, we determined gene expression levels for the genes previously changed by tungstate. We found that the MEK inhibitor UO126 abolished the effects of tungstate on *Casp3* and *Chop* mRNAs but had no effect in any of the other tested genes (Fig. 22B). Together, these evidences show that tungstate can directly regulate expression of apoptosis-related genes in *Irs2*$^{-/-}$ islets and that Erk1/2 is involved in some but not all of these changes, indicating that sodium tungstate action is not exclusively exerted via the MAPK signaling pathway.

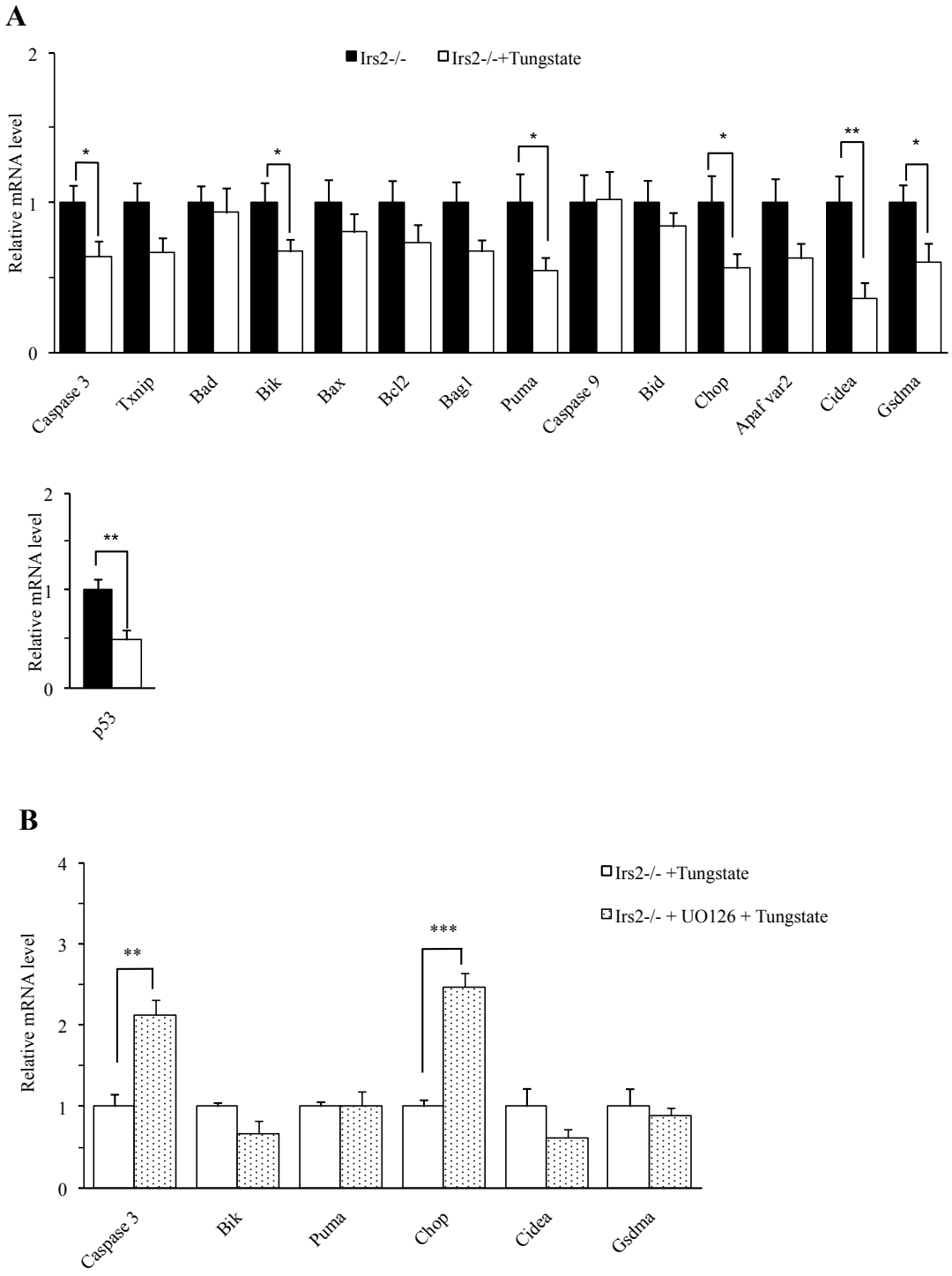

Figure 22: Sodium tungstate alters expression of apoptosis-related genes in *Irs2*$^{-/-}$ isolated islets. (A) Isolated islets from 8-10-week old *Irs2*$^{-/-}$ mice were cultured in the absence or presence of sodium tungstate for 48h. Total RNA was extracted and expression of several genes was quantitated by qRT-PCR, corresponding to islets isolated from 10 different mice. (B) Isolated islets from 10-week old *Irs2*$^{-/-}$ mice were cultured with sodium tungstate only or with the MEK1-2 inhibitor UO126 for 48h. Total RNA was extracted and expression of the indicated proapoptotic genes was determined by qRT-PCR, corresponding to isolated islets from 6 different mice. Data are mean ± SEM of 3 independent experiments and is expressed as fold-change, *p<0.05 and ***p<0.001 between indicated groups.

V DISCUSSION

1 RATIONALE

The pathogenesis of type 2 diabetes is complex, involving impaired effectiveness of insulin action and insulin deficiency. Together, these abnormalities result in increased rates of glucose release mainly by the liver, as well as decreased clearance of glucose from the circulation. Both defects are present before the development of hyperglycemia and the clinical diagnosis of diabetes. The loss of metabolic homeostasis in T2D is often associated with obesity and insulin resistance. However, some obese individuals who are insulin-resistant do not develop impaired glucose tolerance or progress to T2D. This fact denotes the ability of β-cells to adapt insulin secretion to changes in secretory demand imposed by insulin resistance in order to maintain normal glucose tolerance. In contrast, in the subset of insulin-resistant individuals that progress to T2D, this feedback between insulin-sensitive tissues and β-cells is disrupted. In fact, the progression from impaired glucose tolerance to T2D is preceded by a deterioration of β-cell function without any further deterioration in tissue sensitivity to insulin (Matthews et al., 1998). Thus, several studies have demonstrated that T2D does not develop in the absence of a significant β-cell dysfunction and that the triggering factor for the transition from an obese/insulin-resistant state to T2D is β-cell failure. The functional impairments of β-cell that characterize T2D are likely the result of the combination of cellular dysfunction and a reduction in β-cell mass, as they are both present in T2D patients and definitely very related one with each other. The relative contribution of each process and try to distinguish which one precede the other remains however a controversial issue. Both T1D and T2D are characterized by deficiencies in the number of pancreatic β-cell, with ≈99% deficit in long-standing T1D and ≈65% deficit in long-standing T2D (Meier, 2008). β-cell mass is also decreased in non-diabetic individuals with impaired fasting glucose, suggesting that β-cell loss may be an early contributor to the development of T2D. Hence, developing therapeutic strategies aimed at preventing the loss and/or enhancing survival of β-cells may reflect the most rational approaches for prevention and management of T2D.

In this thesis, we used the Irs2 knockout mice, which recapitulates the pathogenesis of T2D, in that diabetes arises only when insulin resistance and β-cell function are both impaired. Interestingly, islets isolated from T2D patients exhibit severely reduced IRS2 mRNA levels relative to non-diabetic controls, which suggests that altered IRS2-dependent signaling may contribute to β-cell dysfunction in human T2D. As IRS2-mediated insulin/IGF signaling plays a pivotal role in coordinating survival and regulating β-cell mass in adaptation to the metabolic homeostasis, the Irs2 knockout mice is a suitable model for the study of β-cell failure.
Additionally, sodium tungstate was used as a pharmacological tool to explore the pathophysiology of T2D in *Irs*2$^{-/-}$ mice, taking in advantage the expertise of our group about the normoglycemic action of this compound.

Our first and main question was whether tungstate would have any normoglycemic effect on the severe diabetes that *Irs*2$^{-/-}$mice develop. We hypothesized that tungstate might ameliorate it by affecting the

pancreatic β-cells, as failure of β-cells determines de progression to diabetes in this mice. However, as a beneficial effect of tungstate on liver was also demonstrated, and *Irs*2$^{-/-}$ mice display abnormalities in hepatic glucose homeostasis, this organ was also included as a possible target of tungstate in this mice model.

Our results show that tungstate significantly decreased β-cell apoptosis in this model, thereby preserving β-cell mass. Furthermore, these effects on β-cell mass led to the recovery from hyperglycemia and glucose intolerance, as tungstate did not have a major impact on hepatic glucose metabolism or insulin resistance.
This findings demonstrates that the targeting of β-cell mass is sufficient and crucial to prevent diabetes in this mice model. Taking into account the pivotal role of IRS2 in β-cell survival, our results also reveal that β-cell mass preservation is possible and normoglycemia can be maintained independently of the IRS2 protein. Hence, our work reinforces the idea of targeting β-cell apoptosis as a potential approach for the management of T2D.

2 PRESERVED B-CELL MASS IMPROVED GLUCOSE TOLERANCE IN *IRS2*$^{-/-}$ TREATED WITH TUNGSTATE

Sodium tungstate was established as a normoglycemic agent in neonatally STZ rats through a beneficial effect on endocrine pancreas, leading to a partial recovery in β-cell mass and improvements in β-cell function (Altirriba et al., 2009; Barbera et al., 1997; Fernandez-Alvarez et al., 2004). In agreement, in the present study we found that sodium tungstate treatment improved whole body glucose homeostasis in *Irs*2$^{-/-}$ mice, which we associated with increased β-cell mass and improved ability of β-cells to secrete insulin in response to a glucose challenge, as no major alterations in hepatic glucose metabolism or peripheral insulin sensitivity were observed. However, other reports clearly demonstrated that the normoglycemic capacity of sodium tungstate could also be ascribed to its effects on the hepatic glucose metabolism (Barberà et al., 2001; Barbera et al., 1994; Domínguez et al., 2003; Nocito et al., 2012; Zafra et al., 2013). In addition, *Irs*2$^{-/-}$ displays profound insulin resistance in liver, as both glucose disposal and hepatic glucose production are impaired in these animals (Dong et al., 2006; Taniguchi et al., 2005; Withers et al., 1998). Therefore, the liver was included as a possible target of sodium tungstate and analyzed in this study.

Regarding gluconeogenesis, we did find increased PEPCK expression in *Irs*2$^{-/-}$, which is in accordance with the attenuated capacity of insulin to suppress PEPCK expression in the absence of Irs2 (Previs et al., 2000). However, PEPCK expression in treated *Irs*2$^{-/-}$ liver extracts was not different from that found in untreated *Irs*2$^{-/-}$ (Fig. 6A). Indeed, and despite a tendency to lower PEPCK expression can be observed in treated *Irs*2$^{-/-}$ compared to *Irs*2$^{-/-}$, PEPCK expression was not consistently inferior in treated *Irs*2$^{-/-}$ individuals. Additionally, the enzymatic activity of GP, which catalyzes the removal of glucose residues from the glycogen molecule, was similar between *Irs*2$^{-/-}$ and treated *Irs*2$^{-/-}$, and protein level of the active form was actually increased in treated *Irs*2$^{-/-}$ (Fig. 6A, B). As PEPCK enzyme, the rate-limiting step in gluconeogenesis, and GP enzyme, the “glucose sensor” for control of hepatic glucose production, were not normalized in

treated *Irs*2$^{-/-}$, these findings suggests that hepatic glucose production persisted as impaired in treated *Irs*2$^{-/-}$.

Tungstate was also described to partially restore GK activity and increase glycogen levels in STZ diabetic rats. In our study, GK enzymatic activity was decreased in treated and untreated *Irs*2$^{-/-}$, which is in line with decreased glycogen content in both mice (Fig. 7). Accordingly, the active form of glycogen synthase (GS I) had similar enzymatic activity between experimental groups, which is in accordance with previous data of tungstate on nSTZ-rats published by Barberà *et al*. These findings demonstrate that the treatment with tungstate did not restore the synthesis of glycogen in *Irs*2$^{-/-}$ mice, and contrast to prior data demonstrating beneficial effects of tungstate on hepatic glucose metabolism in other diabetic rodent models. Thus, tungstate was shown to strongly modulate glucose hepatic metabolism in STZ-diabetic rats, a type 1 diabetic model, and it also affected, albeit more modestly, liver function in other T2D rodent models (Barbera et al., 1997; Muñoz et al., 2001). In fact, restoration of hepatic glucose metabolism by sodium tungstate was the main responsible for the normoglycemic effects of tungstate in STZ-diabetic rats, despite alterations in endocrine pancreas were also observed in this model. In contrast, the changes induced by tungstate in hepatic metabolic state in Zucker diabetic fatty rats or neonatally STZ-diabetic rats could hardly be responsible for the observed normalization of hyperglycaemia. While the reasons for these discrepancies remain elusive, they indicate that the hepatic effects of tungstate are likely model-specific. Therefore, although we cannot completely disregard the possible contribution of liver to the improvement of glucose metabolism in *Irs*2$^{-/-}$ mice, no major alterations in hepatic glucose metabolism were detected after the treatment with tungstate. Consistent with this conclusion was the finding that insulin resistance persisted in treated *Irs2*$^{-/-}$. Therefore, it was expected that insulin-stimulated hepatic glucose metabolism was still impaired in treated *Irs2*$^{-/-}$.

Our present findings supports the increasing body of evidence that indicates that targeting β-cell mass decline is crucial to improve whole body glucose tolerance in the *Irs*2$^{-/-}$ background. Consistent with this idea, a recent study has revealed that restoration of hepatic insulin signaling is not enough to completely normalize glucose tolerance and overcome the reduction of β-cell mass in *Irs*2$^{-/-}$ mice (Gonzalez-Rodriguez et al., 2010). Likewise, glucose tolerance is not completely restored and diabetes cannot be prevented in *Irs*2$^{-/-}$: *PTP1b*$^{-/-}$ mice because of insufficient β-cell expansion despite increased peripheral insulin sensitivity (Kushner et al., 2004). Interestingly, of the two models used in these studies, the *Irs*2$^{-/-}$ mice treated with resveratrol is the most similar to our model, as both resveratrol and tungstate were administered to adult *Irs*2$^{-/-}$, when hyperglycemia is already present as well as islet damage. Thus, despite resveratrol improved systemic insulin sensitivity by restoring hepatic insulin signaling, decreased PTP1B levels and phosphatase activity in *Irs*2$^{-/-}$ mice liver, it failed to restore glucose tolerance consistent with a failure to improve islet morphology or β-cell mass (Gonzalez-Rodriguez et al., 2010). In any case, we cannot forget that tungstate can act as an inhibitor of phosphatases that can participate in several cellular processes. Still, the only study that accessed this property of tungstate *in vivo* showed that it did not significantly change the phosphotyrosine protein profile of primary cultured hepatocytes. Also, in CHOIR cells, tungstate did not significantly delay or inhibit the dephosphorylation of Erk1/2. Therefore, its possible action as inhibitor of phosphatase remains as an open

question.

In addition to enhancing β-cell mass, tungstate prevented excessive body weight gain in *Irs2*$^{-/-}$ mice. This result is in agreement with previous data from our group describing antiobesity actions of this compound (Amigo-Correig et al., 2011; Claret et al., 2005). The contributions of energy homeostasis or reduced body weight gain to the improvement in glucose homeostasis of treated *Irs2*$^{-/-}$ mice were not addressed and cannot be fully disregarded. Our observation that tungstate normalized food intake in *Irs2*$^{-/-}$ mice suggests that tungstate may impact energy homeostasis. Indeed, previous findings by our group showed that tungstate could affect body weight mainly through increasing energy expenditure and by modulating hypothalamic gene expression. However, the available data demonstrated that peripheral insulin action is not improved with the treatment, which makes unlikely that the beneficial effects of tungstate on glucose homeostasis were related to reduced body weight gain. In the same line, *Irs2*$^{-/-}$ body weight was not different before or after the treatment, which made us think that possibly defects in whole-body energy balance are not a determinant factor in the development of diabetes in *Irs2*$^{-/-}$ mice. Nevertheless, further research would be needed to completely disregard the effects of tungstate on central nervous system and energy homeostasis in the *Irs2*$^{-/-}$ mice. Yet, it has been shown that hyperglycemia can be prevented in mice with conditional deletion of the *Irs2* gene in β-cells and the brain by transgenic expression of *Irs2* in β-cells (Lin et al., 2004), reinforcing a primary role of the β-cell compartment in the diabetic phenotype in *Irs2*$^{-/-}$ mice.

In line with this concept that β-cell failure, and not peripheral insulin resistance, is the major cause of diabetes in in *Irs2*$^{-/-}$ mice, are the reports where the progression of *Irs2*$^{-/-}$ mice toward diabetes was prevented by genetically targeting β-cell mass decline. For instance, the transgenic expression of Irs2 itself in pancreatic β-cells prevents diabetes in *Irs2*$^{-/-}$ mice by promoting β-cell growth and survival (Hennige et al., 2003). Furthermore, changes that mimic the effects of Irs2 signaling prevent the early onset of diabetes in *Irs2*$^{-/-}$ mice. For example, haploinsufficiency for Foxo1 avoided β-cell failure in *Irs2*$^{-/-}$ mice through partial restoration of β-cell proliferation (Kitamura et al., 2002), and upregulation of Pdx1 restored β-cell mass and function in *Irs2*$^{-/-}$ mice, as Pdx1 promotes the expression of genes that mediates glucose-sensitive insulin secretion and survival (Kushner et al., 2002). In the same line, our present data demonstrate that the effect of tungstate on β-cell mass was sufficient to prevent diabetes appearance in the Irs2-deficient background, and thus, we propose that preserved β-cell mass is the likely explanation for the improved glucose tolerance observed in Irs2-deficient mice treated with tungstate.

3 TUNGSTATE PRESERVES B-CELL MASS OF *IRS2*$^{-/-}$ BY CONFERRING PROTECTION AGAINST APOPTOSIS

β-cell mass in adults is maintained through a tight balance between β-cell birth (by replication or neogenesis) and β-cell death (mainly apoptosis). The disruption of this balance is determinant in the progression to diabetes. Patients with T2D have decreased β-cell mass, but the etiology of this reduction is not totally clear, as only a few studies were performed with human pancreatic species, which resulted in some controversy (Butler et al., 2003). The analysis of autopsy pancreatic specimens from both lean and obese subjects with normal glucose tolerance, impaired glucose tolerance or T2D, demonstrated that the frequency of β-cell apoptosis was increased in those with T2D and that the frequency of new islet formation (neogenesis), while being higher in obese individuals, was not different between T2D subjects and their matched normal glucose tolerant controls (Butler et al., 2003; Thomas et al., 2009). They also reported that the frequency of replication was very low and its contribution to β-cell mass in humans may be less significant than it contribution in rodents. Therefore, one might predict that the principal mechanism for the decreased β-cell mass in T2D is the increase in β-cell apoptosis, rather than changes in replication or neogenesis. *Irs*2$^{-/-}$ mice show reduced β-cell mass at birth that remains inadequate to compensate for peripheral insulin resistance, leading to the progression to diabetes. Moreover, IRS-dependent pathways mediate the antiapoptotic effects of insulin and IGF-1 and thus, islets of *Irs*2$^{-/-}$ mice show increased numbers of apoptotic cells, demonstrating that IRS2 protein protect β-cells from apoptosis (Withers et al., 1999). Consequently, decreased survival of β-cells represents the main mechanism underlying β-cell mass loss in *Irs*2$^{-/-}$ mice**.**

We propose that tungstate preserved β-cell mass of *Irs*2$^{-/-}$ by conferring protection against apoptosis (measured as reduction of cleaved Caspase 3 levels) rather than by stimulating proliferation of remaining β-cells. Although certain contribution of this latter mechanism cannot be completely ruled out, the low proliferation rates (0.15%, or 1.5 β-cells per each 1000) and the fact that we did not detect proliferative cells in all treated *Irs*2$^{-/-}$ animals, suggest that this mechanism is not associated with the consistent increment in β-cell mass observed in the pancreases from all *Irs*2$^{-/-}$ treated animals. Indeed, only 5 out of 8 treated *Irs*2$^{-/-}$ mice presented ki67-positive β-cells (Fig.14). Contrastingly, the rate of β-cell apoptosis was consistently reduced to the same level (around 2.5%) in all *Irs*2$^{-/-}$ treated animals (Fig. 13). Moreover, when *Irs*2$^{-/-}$ animals were treated for 20 weeks, the rate of β-cell apoptosis was even more reduced, reaching similar levels to those found in WT animals, suggesting that long-term treatment with tungstate affected mainly β-cell apoptosis. In contrast, the rate of β-cell proliferation was unchanged in long-term treated *Irs*2$^{-/-}$ animals due to high variability between animals: only 2 out of the 4 pancreas analyzed presented Ki67-positive β-cells. Interestingly, the administration of tungstate for 20 weeks lead to increased β-cell area, extending the lifespan of *Irs*2$^{-/-}$ mice to 30 weeks, whereas the normal lifespan is 12-16 weeks (Fig. 8). Despite the cohort of animals was modest, this data reveals that the impact of tungstate on β-cell loss is a sustained effect rather than a transient one. However, the increment in β-cell area did not associate with increased β-cell mass, as the

pancreas of these animals weighted less, which we associate with lower body weight as β-cell mass expansion and body weight follow a linear correlation throughout life (Montanya et al., 2000).

In addition to any reduction in β-cell mass, a functional defect in β-cell function has also to be present in the development of T2D. We observed that *Irs2*$^{-/-}$ mice displayed impaired GSIS during the glucose tolerance test, and that tungstate treatment improved it. This improvement in β-cell function was also supported by increased nuclear expression of Pdx1 in islets from treated *Irs2*$^{-/-}$ mice, observed by immunohistochemical analysis, as Pdx1 is required for maintenance of the β-cell phenotype, including expression of insulin and Glut2. Curiously, genes associated with insulin secretion and transcription (*Glut2*, *Pc* and *MafA*) found downregulated in *Irs2*$^{-/-}$ islets were not differentially expressed between treated *Irs2*$^{-/-}$ and WT animals, suggesting a possible improvement in β-cell functionality in treated *Irs2*$^{-/-}$ mice. GSIS in the *Irs2*$^{-/-}$ mice is still controversial. Some authors reported that *Irs2*$^{-/-}$ mice display blunted GSIS, whereas others reported increased GSIS, as their islets may secrete more insulin as a mechanism of adaptation to a scenario of insulin resistance. It seems that in the early stages of the development of the diabetic phenotype, GSIS may be nearly normal. However, as the hyperglycaemia progress, GSIS is attenuated, which may be attributed to glucose toxicity towards β-cell function. However, the mice lacking Irs2 in the endocrine and exocrine pancreas also display impaired insulin secretion despite the absence of hyperglycemia, suggesting that Irs2 is also important for normal insulin secretion. In any case, the same mechanisms by which tungstate promotes β-cell survival and allows the maintenance of β-cell mass in *Irs2*$^{-/-}$ mice would eventually lead to an improvement in insulin secretion, as β-cell function and β-cell mass are closely related and can be barely distinguishable. Nevertheless, we purpose that the arrest of β-cell apoptosis by tungstate was the crucial mechanisms by which glucose homeostasis was normalized in treated *Irs2*$^{-/-}$. Supporting this conviction is the study where Exendin 4 was administered to *Irs2*$^{-/-}$. In this report, despite a delay in the progression of diabetes was obtained by promoting insulin secretion from the remaining islets, these animals finally developed fatal diabetes, as Exendin 4 largely failed to inhibit β-cell apoptosis (Park et al., 2006).

Gene expression profiling of *Irs2*$^{-/-}$ islets from untreated and treated animals provides further support to the notion that tungstate has a broad impact on cell death pathways in this model. Inflammation processes were also present in *Irs2*$^{-/-}$ mice islets and targeted by tungstate treatment. Indeed, the decreased expression of chemokines and immunoglobulins genes in the profile of treated *Irs2*$^{-/-}$ could indicate the decreased presence of macrophages involved in elimination of a small number of apoptotic cells. However, the interpretation of the microarray data has to be done cautiously, as the increment in the number of β-cells would eventually lead to increased expression of β-cell specific genes. Also, we do not exclude a component of T1D in the diabetic phenotype of *Irs2*$^{-/-}$ mice, as both proinflamatory genes and Reg genes, normally associated with T1D, were also overexpressed in *Irs2*$^{-/-}$ islets. Several studies reveal that Irs2-dependent signaling is ultimately transmitted to a hierarchy of transcription factors, which regulate differentiation and maintenance of β-cells. It is of considerable interest that two particular proapototic genes, *Gsdma* and *Cidea*, were found significantly upregulated in *Irs2*$^{-/-}$ mice islets compared to WT and downregulated in islets from treated *Irs2*$^{-/-}$ mice, whiwh

was also confirmed by quantitative RT-PCR (Fig.16). The *Gsdma* gene is involved in apoptosis induction and is regulated by TGF-β signaling, which has been related with β-cell function and glucose homeostasis (Brown and Schneyer, 2010; Lin et al., 2009; Saeki et al., 2007). Interestingly, however in the opposite way, the ligand 3 of TGF-β signaling pathway was found upregulated in the pancreas of diabetic rats treated with tungstate. In the same line, suppression of the *Cidea* gene, which is regulated by the peroxisome proliferator-activated receptor family, has been shown to protect against β-cell loss in a T2D mice model (Omae et al., 2012; Viswakarma et al., 2007). However, further studies are needed to reveal the precise mechanisms by which tungstate downregulated *Cidea* and *Gsdma* in β-cells and to clarify the precise contribution of downregulation of these genes for the prevention of pancreatic β-cell loss in *Irs*2$^{-/-}$ treated animals.

Another proapoptotic gene of interest found downregulated in treated *Irs*2$^{-/-}$mice compared to WT animals (but unchanged in *Irs*2$^{-/-}$mice) was *Pmaip1,* also known as *Noxa.* Interestingly, *Pmaip1* encodes a Bcl-2 homology 3 (BH3) only member of the Bcl-2 family of proteins. When ectopically expressed, *Pmaip1* underwent BH3 motif-dependent localization to mitochondria and interacted with anti-apoptotic Bcl-2 family members, resulting in the activation of caspase 9. The transcription of *Pmaip1* can be regulated in a p53-dependent pathway, but also in a p53-independent manner, involving the binding of FoxO1 and FoxO3 proteins to its promoter region. Curiously, the promotor of *Pmapi1* is also a target of the activating transcription factor 3 (ATF3), a pro-apoptotic stress-inducible gene that downregulates Irs2 expression, providing a mechanistic insight to the pro-apoptotic action of ATF3 in pancreatic β-cells, and upregulates the expression of Pmaip1, providing another potential explanation for the ability of ATF3 to promote β-cell death. In addition, transgenic mice expressing ATF3 in the pancreatic β-cells have reduced β-cells mass. Because it is a transcription factor, ATF3 must exert its action, at least in part, by regulating downstream target genes, thus implicating them in β-cells dysfunction. Therefore, the fact that *Pmaip1* is downregulated in treated *Irs*2$^{-/-}$ mice compared to treated WT, but not in *Irs*2$^{-/-}$mice, suggest us that it could be playing a role in the antiapoptotic action of tungstate on *Irs*2$^{-/-}$mice. However, this mechanism should be properly elucidated. In contrast to *Irs*2$^{-/-}$mice, tungstate did not have a major action on pancreatic islets from WT animals, as only a few genes were altered by the treatment. These findings are in accordance with our results that tungstate does not altered glucose homeostasis in WT animals and is also in line with previous findings that tungstate do not have significant effects on healthy animals.

The changes in the rate of β-cell turnover resulting in reduced β-cell mass can also be related to toxic factors such as islet amyloid deposits, increased glucose levels or elevated lipid concentrations. The *Irs*2$^{-/-}$ mice is a genetic model of β-cell dysfunction, and therefore, the reduction of β-cell mass is primary the result of the ablation of Irs2 in the β-cells. However, the contribution of external toxic factors cannot be excluded. Indeed, chronic hyperglycemia (glucotoxicity) and increased exposure to free fatty acids can result in β-cell dysfunction, resulting in a loss of responsiveness to glucose stimulation, that ultimately lead to apoptosis. However, studies in T2D patients revealed that a portion of the deleterious effect of hyperglycemia on insulin secretion is reversible. Also, diminished β-cell function was observed in healthy subjects with high risk of

developing diabetes despite they do not yet have hyperglycemia. Therefore, these toxic factors certainly participates in the pathogenesis of T2D, but if they do so as initiating factors or exacerbates the decline of β-cell function is still controversial. In this way, the deleterious contributions of external factors in exacerbating β-cell dysfunction in *Irs*2$^{-/-}$ mice, as well as the possible effect of tungstate on reducing these factors cannot be completely ruled out. However, it was previously observed by our group that tungstate effects on pancreatic gene expression were independent of the decrease in glycaemia (Altirriba et al., 2009).

4 ERK1/2 IS ONE POSSIBLE MEDIATOR OF THE ANTIAPOPTOTIC EFFECTS OF TUNGSTATE IN *IRS2*$^{-/-}$ PANCREATIC ISLETS

Insulin and IGF-1 play important roles in the regulation of metabolism and growth of virtually all tissues, protecting cells from apoptosis mainly through activation of PI3K/Akt and Ras/MAPK signaling pathways. Our data implicate Erk1/2 as one likely mediator of the effects of tungstate on β-cell survival in *Irs*2$^{-/-}$ animals, as Erk1/2 but not Akt exhibit changes in their phosphorylation status in treated relative to untreated *Irs*2$^{-/-}$ islets. Activation of MAPK has often been implicated in protection from apoptosis (Lin et al., 1997; Parrizas et al., 1997) and phosphorylation of several downstream proteins involved in cell survival mechanisms has been implicated in the antiapoptotic effects of MAPK pathway (Bonni, 1999; Roskoski, 2012; Shimamura et al., 2000). In line with our findings, the effects of tungstate in liver of STZ-rats and cultured myotubes were demonstrated to be independent or to be possible without a direct involvement of Akt. However, we cannot exclude the possibility that additional protein/s located downstream of Akt in the Akt-signaling pathway are altered by tungstate and participate in the protective effects of this compound against β-cell apoptosis, as Akt and Erk1/2 signaling have multiple crosstalk points and common downstream targets. Supporting our data about the increase in phosphorylated Erk1/2 are the findings that tungstate restores the phosphorylation state of Erk1/2 in several cell types, as described in introduction. However, it is the first time that an increase in phosphorylated Erk1/2 is reported in pancreatic islets. Interestingly, tungstate was recently shown to increase the phosphorylation state of Ras, Raf and Mek, and in this way, activates Erk1/2 (Zafra et al., 2013). Thus, despite Erk1/2 does not seem to be its primary target, tungstate definitely have the potential to activate MAPK pathway.

Activated Erk1/2 can exerted their functions in the cytoplasm or it can translocate to the nucleus and upregulate the transcription of some genes, including insulin, through the phosphorylation of crucial transcription factors as Beta2, Pdx1 and MafA. For instance, once Pdx1 is phosphorylated, it translocate to the nucleus where it binds to insulin gene promoter. Pdx1 was reported to be severely reduced in islets from *Irs*2$^{-/-}$ mice (Suzuki et al., 2003). Therefore, we can speculate that the observed increase in phosphorylated Erk1/2 could eventually lead to an increase in β-cell survival and/or function through the phosphorylation of Pdx1, which is in line with the observed increase in nuclear expression of Pdx1 in treated *Irs*2$^{-/-}$ mice. However,

hyperglycemia can downregulate Pdx1 expression (Harmon et al., 1999), and therefore, the increased Pdx1 expression in treated *Irs2*$^{-/-}$ mice could also be secondary to the normalization of glycaemia observed in this animals.

In addition, several cytoplasmic substrates of Erk1/2 that have been linked to cellular survival could potentially mediate the blockade of β-cell apoptosis by tungstate. One direct downstream target of Erk1/2 is the p90rsk, which was found to be more phosphorylated in the liver of tungstate treated STZ-rats (Nocito et al., 2012). Based on these findings, we choose to look more downstream in the MAPK cascade for changes induced by tungstate. p90rsk can mediate cell survival by phosphorylating and inactivating the pro-apoptotic protein Bcl2-associated death promoter (Bad). An increase in unphosphorylated Bad expression was observed in *Irs2*$^{-/-}$ islets along with increased numbers of apoptotic cells (Withers et al., 1999). In addition, another study reported increased amounts of phosphorylated Bad, which coincided with increased β-cell survival and enhanced β-cell mass (Jetton et al., 2005). Thus, we hypothesized that increased activation of Erk1/2 would eventually lead to increased levels of phosphorylated Bad. However, we failed to detect relevant changes in Bad expression or phosphorylation between treated and untreated *Irs2*$^{-/-}$ islets. Curiously, we also failed to detect changes in phosphorylated Bad between *Irs2*$^{-/-}$ and WT islets. The reason for these discrepancies are unclear at present but at least two possible explanations can be plausible. First, Bad's apoptotic activity is regulated by an extensive array of separate signaling pathways and second, Bad expression levels are difficult to be detected in endocrine pancreas (Kitada et al., 1998). In line with these findings, we observed that phosphorylated levels of Bad were comparable low in *Irs2*$^{-/-}$ as in WT animals. Moreover, as 40-60 islets per sample were used in the western blot analysis, we do not exclude a methodological limitation to detect Bad expression in our conditions. Nevertheless, we did find that the expression of cytochrome c was significantly lower in treated *Irs2*$^{-/-}$ compared to untreated *Irs2*$^{-/-}$ islets. Cytochrome c is released as consequence of the disruption of integrity of the outer mitochondrial membrane when the mitochondrial or Bcl2-regulated apoptotic pathway is activated. Therefore, this finding suggest that Bcl2-regulated apoptotic pathway is less active in treated *Irs2*$^{-/-}$ islets, despite no changes were detected in the expression of Bad. The Bcl2-regulated apoptotic pathway converges on the activation of cysteine proteases of the caspase family, including caspase 3. Despite we were unable to detected caspase 3 by immunoblot analysis, our immunohistochemical analysis did demonstrate lower staining for active/cleaved caspase 3 in treated versus untreated *Irs2*$^{-/-}$ islets. Furthermore, several caspases were found downregulated in treated *Irs2*$^{-/-}$ animals when we performed the protein microarray analysis, corroborating that cell death pathways are decreased in islets from treated *Irs2*$^{-/-}$ animals. Thus, one question that remains unanswered is how increased Erk1/2 signaling is linked to reduced β-cell apoptosis in these animals.

It has been previously suggested that caspase 3 activation is essential for β-cell apoptosis and that *in vivo* loss of caspase-3 protected β-cells from apoptosis and from STZ-induced diabetes (Radziszewska et al., 2009), thus supporting the notion that caspase 3 is a critical mediator of apoptosis in β-cells. Additionally, the accumulation of cleaved caspase 3 was associated with decreased growth and survival of *Irs2*$^{-/-}$ β-cells. Our

immunohistochemical analysis demonstrated that tungstate reduced the levels of cleaved caspase 3 in treated *Irs*2$^{-/-}$ animals, resulting in increased β-cell mass. Intringuingly, our results show that tungstate also reduced C*asp3* gene expression in *Irs*2$^{-/-}$ islets *in vitro*, at least partly through activation of Erk1/2, suggesting that tungstate-induced stimulation of MAPK signaling may directly affect β-cell survival at the gene transcription level. The *Chop* gene was also downregulated by tungstate in *Irs*2$^{-/-}$ islets in vitro, and this regulation seems to be also dependent of Erk1/2 activation. Interestingly, it has been shown that Erk1/2 represses *Chop* expression in β-cells through the modulation of MafA and C/EBP-B, and that targeted disruption of *Chop* gene can prevent diabetes in Akita by decreasing ER stress–mediated apoptosis in β-cells (Lawrence et al., 2007; Oyadomari et al., 2002), suggesting that the effects of tungstate through Erk1/2 on *Chop* gene may be contributing to increased β-cell survival in treated *Irs*2$^{-/-}$ animals. *Chop* expression can be induced by inflammatory cytokines via the nitric oxide signaling or via stress signals from the endoplasmic reticulum (ER) that promote β-cell death. Thus, downregulation of *Chop* gene could also suggests a protective effect of tungstate against β-cell ER stress.

In addition to *Casp3* and *Chop*, tungstate modified the expression of other apoptosis-related genes in isolated islets. Interestingly, the *Gsdma* and *Cidea* genes, which were downregulated by tungstate *in vivo*, were also repressed by this compound *in vitro*, suggesting that a direct effect of tungstate on pancreatic islets is conceivable. However, repression of *Gsdma* and *Cidea,* as well as repression of the mitochondrial genes *Puma* and *Bik* genes by tungstate did not appear as Erk1/2-dependent. *Puma* and *Bik* genes belong to the same proapoptotic family as *Bad*, which are believed to act by sequestering the antiapoptotic members Bcl2 and Bcl-xl, that in turn relieves inhibition of Bax and Bak (proapoptotic), leading to downstream caspase activation. However, the relative contribution of these pro- and antiapoptotic proteins for overall beta-cell survival and function remains controversial. Indeed, some studies implicated Bcl2 protein family members not only in the regulation of apoptosis but also in the control of cellular function (Soria and Gauthier, 2013). Nonetheless, other studies tended to argue against the critical role of these proteins for survival (Carrington et al., 2009) (Allison et al., 2000). Therefore, whether decreased expression of these genes would provide advantage for *Irs*2$^{-/-}$ β-cells remains to be answered.

All together, our findings implicate Erk1/2 as an important player in supporting β-cell survival in *Irs*2$^{-/-}$, probably through activation of mechanisms leading to decreased caspase 3 activation, despite a direct inhibitory role on *Casp3* gene expression cannot be disregarded. However, further studies will be needed to reveal the precise mechanisms by which Erk1/2 activation inhibits apoptosis in *Irs*2$^{-/-}$ β-cells. Moreover, the implication of MAPK pathway does not exclude that other signal transduction pathways, which were not addressed in this study, can also be playing a role in supporting β-cell survival in treated *Irs*2$^{-/-}$ islets.

5 PRESERVATION OF B-CELL MASS IN A SCENARIO OF COMPROMISED IRS2-MEDIATED INSULIN/IGF SIGNALING

Several findings point to a critical role of the IRS2-mediated insulin-signaling pathway in β-cell survival: IRS2 expression in β-cells stimulates the rate of glucose- and IGF-I-induced β-cell mitogenesis, implicating a significant role of IRS2 in expanding β-cell mass (Schuppin et al., 1998); the overexpression of IRS2 in β-cells protect them from both streptozotocin- and free fatty acid (FFA)-induced apoptosis (Hennige et al., 2003); in the absence of IRS2, β-cell survival is dramatically reduced (Withers et al., 1999; Withers et al., 1998). However, the effects of tungstate on β-cell mass preservation in *Irs2*$^{-/-}$ mice appear to bypass the *IRS2* protein. Furthermore, we show that β-cell death is evaded in a scenario of compromised IRS2-dependent signaling. Others demonstrated that the treatment with vildagliptin, an inhibitor of dipeptidylpeptidase-4 enzyme that degrades GLP1, might have the potential to suppress β-cell apoptosis and preserve β-cell mass by Irs-2-independent pathways (Sato et al., 2012). However, the *Irs2*$^{-/-}$ mice used in their study had a different genetic background from our *Irs2*$^{-/-}$ mice. Indeed, in that study, untreated *Irs2*$^{-/-}$ mice did not reach blood glucose levels superior to 160mg/dl, and therefore, the abnormalities in glucose homeostasis were only modest. Contrastingly, our *Irs2*$^{-/-}$ mice model display severe diabetic phenotype, with completely damaged β-cells and shorter lifespan than the other model. Therefore, the comparisons between the two models can lead to wrong assumptions.

The effects of tungstate on GSIS in *Irs2*$^{-/-}$ mice appear to be also independent of *IRS2* protein. Other compounds are able to increase the capacity of *Irs2*$^{-/-}$ islets to secrete insulin as exendin 4, which retards the progress toward diabetes in *Irs2*$^{-/-}$ mice by enhancing GSIS (Park et al., 2006). However, in contrast to tungstate, exendin 4 fails to promote β-cell survival in *Irs2*$^{-/-}$ mice, which is essential for its long-term beneficial effects upon glucose tolerance and prevention of diabetes in other mice models. The reason for this is that Irs2 signaling is essential for the long-term effects of exendin 4, probably through an increase in the expression of Pdx1, which promotes β-cell function and improves glucose tolerance in diabetic rodents. Indeed, in a normal situation, increased activation of the transcription factor CREB (cAMP response element-binding protein) by exendin 4 would strongly stimulates Irs2 gene expression, activating the PI3K-Akt cascade with the logical consequences in β-cell growth and survival. Therefore, the potential to increase *Irs2* have to exist in order to exendin 4 prevent diabetes. In spite of this, exendin 4 stimulates Erk1/2 phosphorylation in the absence of *Irs2* in Min6 β-cell line (Park et al., 2006). Also, signaling by Erk1/2 is not required for insulin secretion, as fusion and release of vesicles containing insulin granules occurs normally even if Erk1/2 is blocked (Khoo and Cobb, 1997). Additionally, it was suggested that activation of the PI3K branch of IRS mediated signal-transduction pathways was more important than that leading to MAPK activation in terms of increased β-cell proliferation in response to IGF-1 in *Irs2*$^{-/-}$ mice. However, Erk1/2 is a significant regulator of nuclear events involved in β-cell function, such as insulin biosynthesis or the transcription of other crucial genes, and phosphorylate several proteins with prosurvival functions. Thus, it is

conceivable that activation of Erk1/2 in a different biological context would result in a different outcome.

Our results further support that tungstate could be promoting β-cell survival and regulating expression of proapoptotic genes in the absence of *IRS2* protein, thus preventing T2D progression in *Irs*2$^{-/-}$ mice. Our data also support the idea that β-cell mass decline is potentially reversible in *Irs*2$^{-/-}$ mice, especially in the early stages of the disease. This concept that β-cell mass decline can be avoided even in the absence of IRS2 protein is potentially valuable of a clinical point of view as impaired insulin signaling, including lower *IRS2* mRNA expression, was described in diabetic islets (Gunton et al., 2005). However, tungstate was not effective in *Irs*2$^{-/-}$ mice that were already severely diabetic at initiation of treatment (Fig.4, section III). Thus, it is conceivable that at advanced stages of diabetes, the remaining β-cell mass is no longer recoverable and β-cell apoptosis unstoppable, suggestive of a point of no return in β-cell failure (Weir and Bonner-Weir, 2004).

In summary, treatment with tungstate attenuated β-cell apoptosis in *Irs*2$^{-/-}$ mice, leading to increase β-cell mass and restoration of glucose homeostasis in this knockout model. Taking into account the pivotal role of IRS2 in β-cell survival, our results reveal that β-cell mass preservation is possible and normoglycemia can be maintained independently of the IRS2-mediated Insulin/IGF signaling. As far as we know, our study is the first one demonstrating that a pharmacological agent is able to protect β-cells from apoptosis in the absence of IRS2 protein in this mice model. Whether it is currently feasible to protect β-cells from apoptosis in a clinical situation where islet insulin signaling is expected to be impaired remains to be properly addressed. Indeed, protection of pancreatic β-cells is a challenge for modern medicine, which is currently facing the enormous worldwide diffusion of T2D. The epidemiological explosion of the disease is a clear demonstration that strategies to protect the β-cell implemented so far were largely inadequate. Another demonstration of the poor efficacy of protection of the β-cells is the high rate of loss of metabolic control over the years in patients with T2D. We believed that our findings open the possibility of β-cell survival-oriented therapeutic strategies aimed to circumvent IRS2-dependent signaling and further support that preserving the β-cells from decline in function and eventual failure is crucial in preventing T2D and changing the natural history of this disease.

VI CONCLUSIONS

Taking into account our results, our major conclusions are the following:

1) Tungstate was able to restore normal glycaemia and glucose tolerance in *Irs2*$^{-/-}$ mice;

2) Insulin resistance and abnormalities in hepatic glucose metabolism persisted in treated *Irs2*$^{-/-}$ mice;

3) Treated *Irs2*$^{-/-}$ mice displayed enhanced β-cell mass;

4) Reduced β-cell apoptosis was the main mechanism responsible for increased β-cell mass in *Irs2*$^{-/-}$ mice treated with tungstate;

The targeting of β-cell apoptosis by tungstate prevented the decline in β-cell mass and underlie the improvement in whole body glucose homeostasis observed in *Irs2*$^{-/-}$ mice.

5) Tungstate decreased the expression of several genes implicated in cell death and inflammation processes and of proteins involved in mitochondrial apoptosis in *Irs2*$^{-/-}$ mice;

6) Erk1/2 is one mediator of the antiapoptotic effects of tungstate in *Irs*2$^{-/-}$ pancreatic islets;

7) Bad protein is not implicated in the antiapoptotic effects of tungstate in *Irs*2$^{-/-}$ pancreatic islets;

Tungstate had a broad impact on cell death mitochondrial pathway

8) β-cell mass decline is potentially reversible and normoglycemia can be maintained in a scenario of compromised IRS2 expression;

Our findings open the possibility of β-cell survival-oriented therapeutic strategies aimed to circumvent IRS2-dependent signaling.

VII REFERENCES

A

Agius, L. (2008). Glucokinase and molecular aspects of liver glycogen metabolism. *Biochem J* **414**, 1-18.

Aksamitiene, E., Kiyatkin, A. and Kholodenko, B. N. (2012). Cross-talk between mitogenic Ras/MAPK and survival PI3K/Akt pathways: a fine balance. *Biochem Soc Trans* **40**, 139-46.

Allison, J., Thomas, H., Beck, D., Brady, J. L., Lew, A. M., Elefanty, A., Kosaka, H., Kay, T. W., Huang, D. C. and Strasser, A. (2000). Transgenic overexpression of human Bcl-2 in islet beta cells inhibits apoptosis but does not prevent autoimmune destruction. *Int Immunol* **12**, 9-17.

Altirriba, J., Barbera, A., Del Zotto, H., Nadal, B., Piquer, S., Sanchez-Pla, A., Gagliardino, J. J. and Gomis, R. (2009). Molecular mechanisms of tungstate-induced pancreatic plasticity: a transcriptomics approach. *BMC Genomics* **10**, 406.

Amigo-Correig, M., Barcelo-Batllori, S., Piquer, S., Soty, M., Pujadas, G., Gasa, R., Bortolozzi, A., Carmona, M. C. and Gomis, R. (2011). Sodium tungstate regulates food intake and body weight through activation of the hypothalamic leptin pathway. *Diabetes Obes Metab* **13**, 235-42.

Amigo-Correig, M., Barcelo-Batllori, S., Soria, G., Krezymon, A., Benani, A., Penicaud, L., Tudela, R., Planas, A. M., Fernandez, E., Carmona Mdel, C. et al. (2012). Anti-obesity sodium tungstate treatment triggers axonal and glial plasticity in hypothalamic feeding centers. *PLoS One* **7**, e39087.

Andrikopoulos, S., Blair, A. R., Deluca, N., Fam, B. C. and Proietto, J. (2008). Evaluating the glucose tolerance test in mice. *Am J Physiol Endocrinol Metab* **295**, E1323-32.

Araki, E., Lipes, M. A., Patti, M. E., BrÃ1⁄4ning, J. C., B. Haag, r., Johnson, R. S. and Kahn, C. R. (1994). Alternative pathway of insulin signalling in mice with targeted disruption of the IRS-1 gene. *Nature* **372**, 186-90.

Ashcroft, F. M. and Rorsman, P. (2012). Diabetes mellitus and the beta cell: the last ten years. *Cell* **148**, 1160-71.

Assmann, A., Ueki, K., Winnay, J. N., Kadowaki, T. and Kulkarni, R. N. (2009). Glucose Effects on Beta-Cell Growth and Survival Require Activation of Insulin Receptors and Insulin Receptor Substrate 2. *Mol Cell Biol* **29**, 3219-3228.

B

Barbera, A., Fernandez-Alvarez, J., Truc, A., Gomis, R. and Guinovart, J. J. (1997). Effects of tungstate in neonatally streptozotocin-induced diabetic rats: mechanism leading to normalization of glycaemia. *Diabetologia* **40**, 143-9.

Barberà, A., Gomis, R. R., Prats, N., Rodríguez-Gil, J. E., Domingo, M., Gomis, R. and Guinovart, J. J. (2001). Tungstate is an effective antidiabetic agent in streptozotocin-induced diabetic rats: a long-term study. *Diabetologia* **44**, 507-513.

Barbera, A., Rodriguez-Gil, J. E. and Guinovart, J. J. (1994). Insulin-like actions of tungstate in diabetic rats. Normalization of hepatic glucose metabolism. *J Biol Chem* **269**, 20047-53.

Barcelo-Batllori, S., Corominola, H., Claret, M., Canals, I., Guinovart, J. and Gomis, R. (2005). Target identification of the novel antiobesity agent tungstate in adipose tissue from obese rats. *Proteomics* **5**, 4927-35.

Barcelo-Batllori, S., Kalko, S. G., Esteban, Y., Moreno, S., Carmona, M. C. and Gomis, R. (2008). Integration of DIGE and bioinformatics analyses reveals a role of the antiobesity agent tungstate in redox and energy homeostasis pathways in brown adipose tissue. *Mol Cell Proteomics* **7**, 378-93.

Barnett, A. H., Eff, C., Leslie, R. D. and Pyke, D. A. (1981). Diabetes in identical twins. A study of 200 pairs. *Diabetologia* **20**, 87-93.

Bergman, R. N., Finegood, D. T. and Kahn, S. E. (2002). The evolution of beta-cell dysfunction and insulin resistance in type 2 diabetes. *Eur J Clin Invest* **32 Suppl 3**, 35-45.

Bollen, M., Keppens, S. and Stalmans, W. (1998). Specific features of glycogen metabolism in the liver. *Biochem J* **336 (Pt 1)**, 19-31.

Bonner-Weir, S. (2000a). Life and death of the pancreatic beta cells. *Trends Endocrinol Metab* **11**, 375-8.

Bonner-Weir, S. (2000b). Perspective: Postnatal pancreatic beta cell growth. *Endocrinology* **141**, 1926-9.

Bonni, A. (1999). Cell Survival Promoted by the Ras-MAPK Signaling Pathway by Transcription-Dependent and -Independent Mechanisms. *Science* **286**, 1358-1362.

Bouwens, L. and Rooman, I. (2005). Regulation of Pancreatic Beta-Cell Mass. *Physiological Reviews* **85**, 1255-1270.

Bratanova-Tochkova, T. K., Cheng, H., Daniel, S., Gunawardana, S., Liu, Y. J., Mulvaney-Musa, J., Schermerhorn, T., Straub, S. G., Yajima, H. and Sharp, G. W. (2002). Triggering and augmentation mechanisms, granule pools, and biphasic insulin secretion. *Diabetes* **51 Suppl 1**, S83-90.

Breitling, R., Armengaud, P., Amtmann, A. and Herzyk, P. (2004). Rank products: a simple, yet powerful, new method to detect differentially regulated genes in replicated microarray experiments. *FEBS Lett* **573**, 83-92.

Brown, M. L. and Schneyer, A. L. (2010). Emerging roles for the TGFbeta family in pancreatic beta-cell homeostasis. *Trends Endocrinol Metab* **21**, 441-8.

Bruce, D. G., Chisholm, D. J., Storlien, L. H. and Kraegen, E. W. (1988). Physiological importance of deficiency in early prandial insulin secretion in non-insulin-dependent diabetes. *Diabetes* **37**, 736-44.

Burks, D. J. and White, M. F. (2001). IRS proteins and beta-cell function. *Diabetes* **50 Suppl 1**, S140-5.

Butler, A. E., Janson, J., Bonner-Weir, S., Ritzel, R., Rizza, R. A. and Butler, P. C. (2003). Beta-cell deficit and increased beta-cell apoptosis in humans with type 2 diabetes. *Diabetes* **52**, 102-10.

C

Cabrera, O., Berman, D. M., Kenyon, N. S., Ricordi, C., Berggren, P. O. and Caicedo, A. (2006). The unique cytoarchitecture of human pancreatic islets has implications for islet cell function. *Proc Natl Acad Sci U S A* **103**, 2334-9.

Calles-Escandon, J. and Robbins, D. C. (1987). Loss of early phase of insulin release in humans impairs glucose tolerance and blunts thermic effect of glucose. *Diabetes* **36**, 1167-72.

Canals, I., Carmona, M. C., Amigo, M., Barbera, A., Bortolozzi, A., Artigas, F. and Gomis, R. (2009). A functional leptin system is essential for sodium tungstate antiobesity action. *Endocrinology* **150**, 642-50.

Cantley, J., Choudhury, A. I., Asare-Anane, H., Selman, C., Lingard, S., Heffron, H., Herrera, P., Persaud, S. J. and Withers, D. J. (2007). Pancreatic deletion of insulin receptor substrate 2 reduces beta and alpha cell mass and impairs glucose homeostasis in mice. *Diabetologia* **50**, 1248-56.

Carmona, M. C., Amigo, M., Barcelo-Batllori, S., Julia, M., Esteban, Y., Moreno, S. and Gomis, R. (2009). Dual effects of sodium tungstate on adipocyte biology: inhibition of adipogenesis and stimulation of cellular oxygen consumption. *Int J Obes (Lond)* **33**, 534-40.

Carrington, E. M., McKenzie, M. D., Jansen, E., Myers, M., Fynch, S., Kos, C., Strasser, A., Kay, T. W., Scott, C. L. and Allison, J. (2009). Islet beta-cells deficient in Bcl-xL develop but are abnormally sensitive to apoptotic stimuli. *Diabetes* **58**, 2316-23.

Casas, S., Novials, A., Reimann, F., Gomis, R. and Gribble, F. M. (2008). Calcium elevation in mouse pancreatic beta cells evoked by extracellular human islet amyloid polypeptide involves activation of the mechanosensitive ion channel TRPV4. *Diabetologia* **51**, 2252-62.

Chan, T. M. and Exton, J. H. (1976). A rapid method for the determination of glycogen content and radioactivity in small quantities of tissue or isolated hepatocytes. *Anal Biochem* **71**, 96-105.

Chen, L., Magliano, D. J. and Zimmet, P. Z. (2012). The worldwide epidemiology of type 2 diabetes mellitus--present and future perspectives. *Nat Rev Endocrinol* **8**, 228-36.

Claret, M., Corominola, H., Canals, I., Saura, J., Barcelo-Batllori, S., Guinovart, J. J. and Gomis, R. (2005). Tungstate decreases weight gain and adiposity in obese rats through increased thermogenesis and lipid oxidation. *Endocrinology* **146**, 4362-9.

Cnop, M., Igoillo-Esteve, M., Hughes, S. J., Walker, J. N., Cnop, I. and Clark, A. (2011). Longevity of human islet alpha- and beta-cells. *Diabetes Obes Metab* **13 Suppl 1**, 39-46.

Cnop, M., Welsh, N., Jonas, J. C., Jorns, A., Lenzen, S. and Eizirik, D. L. (2005). Mechanisms of pancreatic beta-cell death in type 1 and type 2 diabetes: many differences, few similarities. *Diabetes* **54 Suppl 2**, S97-107.

Cohen, P. and Goedert, M. (2004). GSK3 inhibitors: development and therapeutic potential. *Nat Rev Drug Discov* **3**, 479-87.

D

Danaei, G., Finucane, M. M., Lu, Y., Singh, G. M., Cowan, M. J., Paciorek, C. J., Lin, J. K., Farzadfar, F., Khang, Y. H., Stevens, G. A. et al. (2011). National, regional, and global trends in fasting plasma glucose and diabetes prevalence since 1980: systematic analysis of health examination surveys and epidemiological studies with 370 country-years and 2.7 million participants. *Lancet* **378**, 31-40.

Danial, N. N., Walensky, L. D., Zhang, C. Y., Choi, C. S., Fisher, J. K., Molina, A. J., Datta, S. R., Pitter, K. L., Bird, G. H., Wikstrom, J. D. et al. (2008). Dual role of proapoptotic BAD in insulin secretion and beta cell survival. *Nat Med* **14**, 144-53.

Datta, S. R., Dudek, H., Tao, X., Masters, S., Fu, H., Gotoh, Y. and Greenberg, M. E. (1997). Akt phosphorylation of BAD couples survival signals to the cell-intrinsic death machinery. *Cell* **91**, 231-41.

Datta, S. R., Katsov, A., Hu, L., Petros, A., Fesik, S. W., Yaffe, M. B. and Greenberg, M. E. (2000). 14-3-3 proteins and survival kinases cooperate to inactivate BAD by BH3 domain phosphorylation. *Mol Cell* **6**, 41-51.

de la Iglesia, N., Veiga-da-Cunha, M., Van Schaftingen, E., Guinovart, J. J. and Ferrer, J. C. (1999). Glucokinase regulatory protein is essential for the proper subcellular localisation of liver glucokinase. *FEBS Lett* **456**, 332-8.

DeFronzo, R. A. (2004). Pathogenesis of type 2 diabetes mellitus. *Med Clin North Am* **88**, 787-835, ix.

Defronzo, R. A. (2009). Banting Lecture. From the triumvirate to the ominous octet: a new paradigm for the treatment of type 2 diabetes mellitus. *Diabetes* **58**, 773-95.

DeFronzo, R. A. (2010). Current issues in the treatment of type 2 diabetes. Overview of newer agents: where treatment is going. *Am J Med* **123**, S38-48.

Demeterco, C., Hao, E., Lee, S. H., Itkin-Ansari, P. and Levine, F. (2009). Adult human beta-cell neogenesis? *Diabetes Obes Metab* **11 Suppl 4**, 46-53.

Dennis, G., Jr., Sherman, B. T., Hosack, D. A., Yang, J., Gao, W., Lane, H. C. and Lempicki, R. A. (2003). DAVID: Database for Annotation, Visualization, and Integrated Discovery. *Genome Biol* **4**, P3.

Dickson, L. M. and Rhodes, C. J. (2004). Pancreatic β-cell growth and survival in the onset of type 2 diabetes: a role for protein kinase B in the Akt? *American Journal of Physiology - Endocrinology And Metabolism* **287**, E192-E198.

Dominguez, J. E., Munoz, M. C., Zafra, D., Sanchez-Perez, I., Baque, S., Caron, M., Mercurio, C., Barbera, A., Perona, R., Gomis, R. et al. (2003). The antidiabetic agent sodium tungstate activates glycogen synthesis through an insulin receptor-independent pathway. *J Biol Chem* **278**, 42785-94.

Domínguez, J. E., Muñoz, M. C., Zafra, D., Sánchez-Pérez, I., Baqué, S., Caron, M., Mercurio, C., Barberà, A., Perona, R., Gomis, R. et al. (2003). The Antidiabetic Agent Sodium Tungstate Activates Glycogen Synthesis through an Insulin Receptor-independent Pathway. *Journal of Biological Chemistry* **278**, 42785-42794.

Dominici, F. P., Arostegui Diaz, G., Bartke, A., Kopchick, J. J. and Turyn, D. (2000). Compensatory alterations of insulin signal transduction in liver of growth hormone receptor knockout mice. *J Endocrinol* **166**, 579-90.

Dong, X., Park, S., Lin, X., Copps, K., Yi, X. and White, M. F. (2006). Irs1 and Irs2 signaling is essential for hepatic glucose homeostasis and systemic growth. *J Clin Invest* **116**, 101-14.

E

Egloff, M. P., Cohen, P. T., Reinemer, P. and Barford, D. (1995). Crystal structure of the catalytic subunit of human protein phosphatase 1 and its complex with tungstate. *J Mol Biol* **254**, 942-59.

F

Fauman, E. B., Yuvaniyama, C., Schubert, H. L., Stuckey, J. A. and Saper, M. A. (1996). The X-ray crystal structures of Yersinia tyrosine phosphatase with bound tungstate and nitrate. Mechanistic implications. *J Biol Chem* **271**, 18780-8.

Federici, M., Hribal, M., Perego, L., Ranalli, M., Caradonna, Z., Perego, C., Usellini, L., Nano, R., Bonini, P., Bertuzzi, F. et al. (2001). High glucose causes apoptosis in cultured human pancreatic islets of Langerhans: a potential role for regulation of specific Bcl family genes toward an apoptotic cell death program. *Diabetes* **50**, 1290-301.

Fernandez-Alvarez, J., Barbera, A., Nadal, B., Barcelo-Batllori, S., Piquer, S., Claret, M., Guinovart, J. J. and Gomis, R. (2004). Stable and functional regeneration of pancreatic beta-cell population in nSTZ-rats treated with tungstate. *Diabetologia* **47**, 470-7.

Fillat, C., Rodriguez-Gil, J. E. and Guinovart, J. J. (1992). Molybdate and tungstate act like vanadate on glucose metabolism in isolated hepatocytes. *Biochem J* **282 (Pt 3)**, 659-63.

Fonseca, V. A. (2009). Defining and characterizing the progression of type 2 diabetes. *Diabetes Care* **32 Suppl 2**, S151-6.

Foster, J. D., Young, S. E., Brandt, T. D. and Nordlie, R. C. (1998). Tungstate: a potent inhibitor of multifunctional glucose-6-phosphatase. *Arch Biochem Biophys* **354**, 125-32.

G

Garcia-Rocha, M., Roca, A., De La Iglesia, N., Baba, O., Fernandez-Novell, J. M., Ferrer, J. C. and Guinovart, J. J. (2001). Intracellular distribution of glycogen synthase and glycogen in primary cultured rat hepatocytes. *Biochem J* **357**, 17-24.

Garcia-Saez, A. J. (2012). The secrets of the Bcl-2 family. *Cell Death Differ* **19**, 1733-40.

Gardete-Correia, L., Boavida, J. M., Raposo, J. F., Mesquita, A. C., Fona, C., Carvalho, R. and Massano-Cardoso, S. (2010). First diabetes prevalence study in Portugal: PREVADIAB study. *Diabet Med* **27**, 879-81.

Garvey, W. T. and Birnbaum, M. J. (1993). Cellular insulin action and insulin resistance. *Baillieres Clin Endocrinol Metab* **7**, 785-873.

Gerich, J. E. (1998). The genetic basis of type 2 diabetes mellitus: impaired insulin secretion versus impaired insulin sensitivity. *Endocr Rev* **19**, 491-503.

Gilboe, D. P., Larson, K. L. and Nuttall, F. Q. (1972). Radioactive method for the assay of glycogen phosphorylases. *Anal Biochem* **47**, 20-7.

Girón, M. D., Caballero, J. J., Vargas, A. M., Suárez, M. D., Guinovart, J. J. and Salto, R. (2003). Modulation of glucose transporters in rat diaphragm by sodium tungstate. *FEBS Lett* **542**, 84-88.

Gonzalez-Rodriguez, A., Mas Gutierrez, J. A., Sanz-Gonzalez, S., Ros, M., Burks, D. J. and Valverde, A. M. (2010). Inhibition of PTP1B restores IRS1-mediated hepatic insulin signaling in IRS2-deficient mice. *Diabetes* **59**, 588-99.

Gross, A., McDonnell, J. M. and Korsmeyer, S. J. (1999). BCL-2 family members and the mitochondria in apoptosis. *Genes Dev* **13**, 1899-911.

Guinovart, J. J., Salavert, A., Massague, J., Ciudad, C. J., Salsas, E. and Itarte, E. (1979). Glycogen synthase: a new activity ratio assay expressing a high sensitivity to the phosphorylation state. *FEBS Lett* **106**, 284-8.

Gunton, J. E., Kulkarni, R. N., Yim, S., Okada, T., Hawthorne, W. J., Tseng, Y. H., Roberson, R. S., Ricordi, C., O'Connell, P. J., Gonzalez, F. J. et al. (2005). Loss of ARNT/HIF1beta mediates altered gene expression and pancreatic-islet dysfunction in human type 2 diabetes. *Cell* **122**, 337-49.

H

Hanzu, F., Gomis, R., Coves, M. J., Viaplana, J., Palomo, M., Andreu, A., Szpunar, J. and Vidal, J. (2010). Proof-of-concept trial on the efficacy of sodium tungstate in human obesity. *Diabetes Obes Metab* **12**, 1013-8.

Harmon, J. S., Gleason, C. E., Tanaka, Y., Oseid, E. A., Hunter-Berger, K. K. and Robertson, R. P. (1999). In vivo prevention of hyperglycemia also prevents glucotoxic effects on PDX-1 and insulin gene expression. *Diabetes* **48**, 1995-2000.

Hennige, A. M., Burks, D. J., Ozcan, U., Kulkarni, R. N., Ye, J., Park, S., Schubert, M., Fisher, T. L., Dow, M. A., Leshan, R. et al. (2003). Upregulation of insulin receptor substrate-2 in pancreatic β cells prevents diabetes. *Journal of Clinical Investigation* **112**, 1521-1532.

Hennige, A. M., Ozcan, U., Okada, T., Jhala, U. S., Schubert, M., White, M. F. and Kulkarni, R. N. (2005). Alterations in growth and apoptosis of insulin receptor substrate-1-deficient beta-cells. *Am J Physiol Endocrinol Metab* **289**, E337-46.

Henquin, J. C., Ishiyama, N., Nenquin, M., Ravier, M. A. and Jonas, J. C. (2002). Signals and pools underlying biphasic insulin secretion. *Diabetes* **51 Suppl 1**, S60-7.

Hill, M. M., Adrain, C., Duriez, P. J., Creagh, E. M. and Martin, S. J. (2004). Analysis of the composition, assembly kinetics and activity of native Apaf-1 apoptosomes. *EMBO J* **23**, 2134-45.

I

Imamura, M. and Maeda, S. (2011). Genetics of type 2 diabetes: the GWAS era and future perspectives [Review]. *Endocr J* **58**, 723-39.

Irizarry, R. A., Hobbs, B., Collin, F., Beazer-Barclay, Y. D., Antonellis, K. J., Scherf, U. and Speed, T. P. (2003). Exploration, normalization, and summaries of high density oligonucleotide array probe level data. *Biostatistics* **4**, 249-64.

J

Jetton, T. L., Lausier, J., LaRock, K., Trotman, W. E., Larmie, B., Habibovic, A., Peshavaria, M. and Leahy, J. L. (2005). Mechanisms of compensatory beta-cell growth in insulin-resistant rats: roles of Akt kinase. *Diabetes* **54**, 2294-304.

Jitrapakdee, S. (2012). Transcription factors and coactivators controlling nutrient and hormonal regulation of hepatic gluconeogenesis. *Int J Biochem Cell Biol* **44**, 33-45.

Juhl, K., Bonner-Weir, S. and Sharma, A. (2010). Regenerating pancreatic beta-cells: plasticity of adult pancreatic cells and the feasibility of in-vivo neogenesis. *Curr Opin Organ Transplant* **15**, 79-85.

K

Kadowaki, T., Tamemoto, H., Tobe, K., Terauchi, Y., Ueki, K., Kaburagi, Y., Yamauchi, T., Satoh, S., Sekihara, H., Aizawa, S. et al. (1996). Insulin resistance and growth retardation in mice lacking insulin receptor substrate-1 and identification of insulin receptor substrate-2. *Diabet Med* **13**, S103-8.

Kahn, S. E. (2001). Clinical review 135: The importance of beta-cell failure in the development and progression of type 2 diabetes. *J Clin Endocrinol Metab* **86**, 4047-58.

Karaca, M., Magnan, C. and Kargar, C. (2009). Functional pancreatic beta-cell mass: involvement in type 2 diabetes and therapeutic intervention. *Diabetes Metab* **35**, 77-84.

Khan, A. H. and Pessin, J. E. (2002). Insulin regulation of glucose uptake: a complex interplay of intracellular signalling pathways. *Diabetologia* **45**, 1475-83.

Khoo, S. and Cobb, M. H. (1997). Activation of mitogen-activating protein kinase by glucose is not required for insulin secretion. *Proc Natl Acad Sci U S A* **94**, 5599-604.

Khoo, S., Griffen, S. C., Xia, Y., Baer, R. J., German, M. S. and Cobb, M. H. (2003). Regulation of insulin gene transcription by ERK1 and ERK2 in pancreatic beta cells. *J Biol Chem* **278**, 32969-77.

Kischkel, F. C., Hellbardt, S., Behrmann, I., Germer, M., Pawlita, M., Krammer, P. H. and Peter, M. E. (1995). Cytotoxicity-dependent APO-1 (Fas/CD95)-associated proteins form a death-inducing signaling complex (DISC) with the receptor. *EMBO J* **14**, 5579-88.

Kitada, S., Krajewska, M., Zhang, X., Scudiero, D., Zapata, J. M., Wang, H. G., Shabaik, A., Tudor, G., Krajewski, S., Myers, T. G. et al. (1998). Expression and location of pro-apoptotic Bcl-2 family protein BAD in normal human tissues and tumor cell lines. *Am J Pathol* **152**, 51-61.

Kitamura, T. and Ido Kitamura, Y. (2007). Role of FoxO Proteins in Pancreatic beta Cells. *Endocr J* **54**, 507-15.

Kitamura, T., Nakae, J., Kitamura, Y., Kido, Y., Biggs, W. H., Wright, C. V. E., White, M. F., Arden, K. C. and Accili, D. (2002). The forkhead transcription factor Foxo1 links insulin signaling to Pdx1 regulation of pancreatic β cell growth. *Journal of Clinical Investigation* **110**, 1839-1847.

Kloppel, G., Lohr, M., Habich, K., Oberholzer, M. and Heitz, P. U. (1985). Islet pathology and the pathogenesis of type 1 and type 2 diabetes mellitus revisited. *Surv Synth Pathol Res* **4**, 110-25.

Kubota, N., Tobe, K., Terauchi, Y., Eto, K., Yamauchi, T., Suzuki, R., Tsubamoto, Y., Komeda, K., Nakano, R., Miki, H. et al. (2000). Disruption of insulin receptor substrate 2 causes type 2 diabetes because of liver insulin resistance and lack of compensatory beta-cell hyperplasia. *Diabetes* **49**, 1880-9.

Kulik, G. and Weber, M. J. (1998). Akt-dependent and -independent survival signaling pathways utilized by insulin-like growth factor I. *Mol Cell Biol* **18**, 6711-8.

Kulkarni, R. (2005). New Insights into the Roles of Insulin/IGF-I in the Development and Maintenance of β-Cell Mass. *Reviews in Endocrine and Metabolic Disorders* **6**, 199-210.

Kushner, J. A., Haj, F. G., Klaman, L. D., Dow, M. A., Kahn, B. B., Neel, B. G. and White, M. F. (2004). Islet-sparing effects of protein tyrosine phosphatase-1b deficiency delays onset of diabetes in IRS2 knockout mice. *Diabetes* **53**, 61-6.

Kushner, J. A., Simpson, L., Wartschow, L. M., Guo, S., Rankin, M. M., Parsons, R. and White, M. F. (2005). Phosphatase and tensin homolog regulation of islet growth and glucose homeostasis. *J Biol Chem* **280**, 39388-93.

Kushner, J. A., Ye, J., Schubert, M., Burks, D. J., Dow, M. A., Flint, C. L., Dutta, S., Wright, C. V., Montminy, M. R. and White, M. F. (2002). Pdx1 restores beta cell function in Irs2 knockout mice. *J Clin Invest* **109**, 1193-201.

Kuwajima, M., Newgard, C. B., Foster, D. W. and McGarry, J. D. (1986). The glucose-phosphorylating capacity of liver as measured by three independent assays. Implications for the mechanism of hepatic glycogen synthesis. *J Biol Chem* **261**, 8849-53.

L

Lawrence, M. C., McGlynn, K., Naziruddin, B., Levy, M. F. and Cobb, M. H. (2007). Differential regulation of CHOP-10/GADD153 gene expression by MAPK signaling in pancreatic beta-cells. *Proc Natl Acad Sci U S A* **104**, 11518-25.

Lawrence, M. C., McGlynn, K., Park, B. H. and Cobb, M. H. (2005). ERK1/2-dependent activation of transcription factors required for acute and chronic effects of glucose on the insulin gene promoter. *J Biol Chem* **280**, 26751-9.

Leahy, J. L. (2005). Pathogenesis of type 2 diabetes mellitus. *Arch Med Res* **36**, 197-209.

Lillioja, S., Mott, D. M., Zawadzki, J. K., Young, A. A., Abbott, W. G., Knowler, W. C., Bennett, P. H., Moll, P. and Bogardus, C. (1987). In vivo insulin action is familial characteristic in nondiabetic Pima Indians. *Diabetes* **36**, 1329-35.

Lin, H. M., Lee, J. H., Yadav, H., Kamaraju, A. K., Liu, E., Zhigang, D., Vieira, A., Kim, S. J., Collins, H., Matschinsky, F. et al. (2009). Transforming growth factor-beta/Smad3 signaling regulates insulin gene transcription and pancreatic islet beta-cell function. *J Biol Chem* **284**, 12246-57.

Lin, T. H., Chen, Q., Howe, A. and Juliano, R. L. (1997). Cell anchorage permits efficient signal transduction between ras and its downstream kinases. *J Biol Chem* **272**, 8849-52.

Lin, X., Taguchi, A., Park, S., Kushner, J. A., Li, F., Li, Y. and White, M. F. (2004). Dysregulation of insulin receptor substrate 2 in β cells and brain causes obesity and diabetes. *Journal of Clinical Investigation* **114**, 908-916.

Lingohr, M. K., Buettner, R. and Rhodes, C. J. (2002). Pancreatic ²-cell growth and survival a role in obesity-linked type 2 diabetes? *Trends in molecular medicine* **8**, 375-384.

Liu, H. K., Green, B. D., McClenaghan, N. H., McCluskey, J. T. and Flatt, P. R. (2004). Long-term beneficial effects of vanadate, tungstate, and molybdate on insulin secretion and function of cultured beta cells. *Pancreas* **28**, 364-8.

Lizcano, J. M., Morrice, N. and Cohen, P. (2000). Regulation of BAD by cAMP-dependent protein kinase is mediated via phosphorylation of a novel site, Ser155. *Biochem J* **349**, 547-57.

Lu, Y., Ponton, A., Okamoto, H., Takasawa, S., Herrera, P. L. and Liu, J. L. (2006). Activation of the Reg family genes by pancreatic-specific IGF-I gene deficiency and after streptozotocin-induced diabetes in mouse pancreas. *Am J Physiol Endocrinol Metab* **291**, E50-8.

Luciani, D. S., White, S. A., Widenmaier, S. B., Saran, V. V., Taghizadeh, F., Hu, X., Allard, M. F. and Johnson, J. D. (2013). Bcl-2 and Bcl-xL suppress glucose signaling in pancreatic beta-cells. *Diabetes* **62**, 170-82.

Luco, R. F., Maestro, M. A., del Pozo, N., Philbrick, W. M., de la Ossa, P. P. and Ferrer, J. (2006). A conditional model reveals that induction of hepatocyte nuclear factor-1alpha in Hnf1alpha-null mutant beta-cells can activate silenced genes postnatally, whereas overexpression is deleterious. *Diabetes* **55**, 2202-11.

M

Manning, B. D. and Cantley, L. C. (2007). AKT/PKB signaling: navigating downstream. *Cell* **129**, 1261-74.

Marte, B. M. and Downward, J. (1997). PKB/Akt: connecting phosphoinositide 3-kinase to cell survival and beyond. *Trends in Biochemical Sciences* **22**, 355-358.

Martin, B. C., Warram, J. H., Krolewski, A. S., Bergman, R. N., Soeldner, J. S. and Kahn, C. R. (1992). Role of glucose and insulin resistance in development of type 2 diabetes mellitus: results of a 25-year follow-up study. *Lancet* **340**, 925-9.

Martinou, J. C. and Youle, R. J. (2011). Mitochondria in apoptosis: Bcl-2 family members and mitochondrial dynamics. *Dev Cell* **21**, 92-101.

Matheny, R. W., Jr. and Adamo, M. L. (2009). Current perspectives on Akt Akt-ivation and Akt-ions. *Exp Biol Med (Maywood)* **234**, 1264-70.

Matschinsky, F. M. (2002). Regulation of pancreatic beta-cell glucokinase: from basics to therapeutics. *Diabetes* **51 Suppl 3**, S394-404.

Matthews, D. R., Cull, C. A., Stratton, I. M., Holman, R. R. and Turner, R. C. (1998). UKPDS 26: Sulphonylurea failure in non-insulin-dependent diabetic patients over six years. UK Prospective Diabetes Study (UKPDS) Group. *Diabet Med* **15**, 297-303.

Matveyenko, A. V. and Butler, P. C. (2008). Relationship between beta-cell mass and diabetes onset. *Diabetes Obes Metab* **10 Suppl 4**, 23-31.

Meier, J. J. (2008). Beta cell mass in diabetes: a realistic therapeutic target? *Diabetologia* **51**, 703-13.

Montanya, E., Nacher, V., Biarnes, M. and Soler, J. (2000). Linear correlation between beta-cell mass and body weight throughout the lifespan in Lewis rats: role of beta-cell hyperplasia and hypertrophy. *Diabetes* **49**, 1341-6.

Montanya, E. and Tellez, N. (2009). Pancreatic remodeling: beta-cell apoptosis, proliferation and neogenesis, and the measurement of beta-cell mass and of individual beta-cell size. *Methods Mol Biol* **560**, 137-58.

Muller, D., Huang, G. C., Amiel, S., Jones, P. M. and Persaud, S. J. (2006). Identification of insulin signaling elements in human beta-cells: autocrine regulation of insulin gene expression. *Diabetes* **55**, 2835-42.

Muller, D., Huang, G. C., Amiel, S., Jones, P. M. and Persaud, S. J. (2007). Gene expression heterogeneity in human islet endocrine cells in vitro: the insulin signalling cascade. *Diabetologia* **50**, 1239-42.

Muñoz, M. C., Barberà, A., Domínguez, J., Fernàndez-Alvarez, J., Gomis, R. and Guinovart, J. J. (2001). Effects of Tungstate, a New Potential Oral Antidiabetic Agent, in Zucker Diabetic Fatty Rats. *Diabetes* **50**, 131-138.

Myers, M. G., Jr. and White, M. F. (1996). Insulin signal transduction and the IRS proteins. *Annu Rev Pharmacol Toxicol* **36**, 615-58.

N

Nocito, L., Zafra, D., Calbo, J., Dominguez, J. and Guinovart, J. J. (2012). Tungstate reduces the expression of gluconeogenic enzymes in STZ rats. *PLoS One* **7**, e42305.

Nuttall, F. Q., Ngo, A. and Gannon, M. C. (2008). Regulation of hepatic glucose production and the role of gluconeogenesis in humans: is the rate of gluconeogenesis constant? *Diabetes Metab Res Rev* **24**, 438-58.

O

Omae, N., Ito, M., Hase, S., Nagasawa, M., Ishiyama, J., Ide, T. and Murakami, K. (2012). Suppression of FoxO1/cell death-inducing DNA fragmentation factor alpha-like effector A (Cidea) axis protects mouse beta-cells against palmitic acid-induced apoptosis. *Mol Cell Endocrinol* **348**, 297-304.

Oyadomari, S., Koizumi, A., Takeda, K., Gotoh, T., Akira, S., Araki, E. and Mori, M. (2002). Targeted disruption of the Chop gene delays endoplasmic reticulum stress–mediated diabetes. *Journal of Clinical Investigation* **109**, 525-532.

P

Park, S., Dong, X., Fisher, T. L., Dunn, S., Omer, A. K., Weir, G. and White, M. F. (2006). Exendin-4 uses Irs2 signaling to mediate pancreatic beta cell growth and function. *J Biol Chem* **281**, 1159-68.

Parrizas, M., Saltiel, A. R. and LeRoith, D. (1997). Insulin-like growth factor 1 inhibits apoptosis using the phosphatidylinositol 3'-kinase and mitogen-activated protein kinase pathways. *J Biol Chem* **272**, 154-61.

Perley, M. J. and Kipnis, D. M. (1967). Plasma insulin responses to oral and intravenous glucose: studies in normal and diabetic sujbjects. *J Clin Invest* **46**, 1954-62.

Piquer, S., Barcelo-Batllori, S., Julia, M., Marzo, N., Nadal, B., Guinovart, J. J. and Gomis, R. (2007). Phosphorylation events implicating p38 and PI3K mediate tungstate-effects in MIN6 beta cells. *Biochem Biophys Res Commun* **358**, 385-91.

Prentki, M. and Nolan, C. J. (2006). Islet beta cell failure in type 2 diabetes. *J Clin Invest* **116**, 1802-12.

Previs, S. F., Withers, D. J., Ren, J. M., White, M. F. and Shulman, G. I. (2000). Contrasting effects of IRS-1 versus IRS-2 gene disruption on carbohydrate and lipid metabolism in vivo. *J Biol Chem* **275**, 38990-4.

Pugazhenthi, S., Nesterova, A., Sable, C., Heidenreich, K. A., Boxer, L. M., Heasley, L. E. and Reusch, J. E. (2000). Akt/protein kinase B up-regulates Bcl-2 expression through cAMP-response element-binding protein. *J Biol Chem* **275**, 10761-6.

Pulido, R. and Hooft van Huijsduijnen, R. (2008). Protein tyrosine phosphatases: dual-specificity phosphatases in health and disease. *FEBS J* **275**, 848-66.

Q

Qiao, L., Han, S. I., Fang, Y., Park, J. S., Gupta, S., Gilfor, D., Amorino, G., Valerie, K., Sealy, L., Engelhardt, J. F. et al. (2003). Bile acid regulation of C/EBPbeta, CREB, and c-Jun function, via the extracellular signal-regulated kinase and c-Jun NH2-terminal kinase pathways, modulates the apoptotic response of hepatocytes. *Mol Cell Biol* **23**, 3052-66.

R

Radziszewska, A., Schroer, S. A., Choi, D., Tajmir, P., Radulovich, N., Ho, J. C., Wang, L., Liadis, N., Hakem, R., Tsao, M. S. et al. (2009). Absence of caspase-3 protects pancreatic {beta}-cells from c-Myc-induced apoptosis without leading to tumor formation. *J Biol Chem* **284**, 10947-56.

Rodriguez-Gallardo, J., Silvestre, R. A., Egido, E. M. and Marco, J. (2000). Effects of sodium tungstate on insulin and glucagon secretion in the perfused rat pancreas. *Eur J Pharmacol* **402**, 199-204.

Rorsman, P. and Renstrom, E. (2003). Insulin granule dynamics in pancreatic beta cells. *Diabetologia* **46**, 1029-45.

Ros, S., Garcia-Rocha, M., Dominguez, J., Ferrer, J. C. and Guinovart, J. J. (2009). Control of liver glycogen synthase activity and intracellular distribution by phosphorylation. *J Biol Chem* **284**, 6370-8.

Roskoski Jr, R. (2012). ERK1/2 MAP kinases: Structure, function, and regulation. *Pharmacological Research* **66**, 105-143.

Roskoski, R., Jr. (2012). ERK1/2 MAP kinases: structure, function, and regulation. *Pharmacol Res* **66**, 105-43.

Rung, J., Cauchi, S., Albrechtsen, A., Shen, L., Rocheleau, G., Cavalcanti-Proenca, C., Bacot, F., Balkau, B., Belisle, A., Borch-Johnsen, K. et al. (2009). Genetic variant near IRS1 is associated with type 2 diabetes, insulin resistance and hyperinsulinemia. *Nat Genet* **41**, 1110-5.

S

Saeki, N., Kim, D. H., Usui, T., Aoyagi, K., Tatsuta, T., Aoki, K., Yanagihara, K., Tamura, M., Mizushima, H., Sakamoto, H. et al. (2007). GASDERMIN, suppressed frequently in gastric cancer, is a target of LMO1 in TGF-beta-dependent apoptotic signalling. *Oncogene* **26**, 6488-98.

Saelens, X., Festjens, N., Vande Walle, L., van Gurp, M., van Loo, G. and Vandenabeele, P. (2004). Toxic proteins released from mitochondria in cell death. *Oncogene* **23**, 2861-74.

Saltiel, A. R. and Kahn, C. R. (2001). Insulin signalling and the regulation of glucose and lipid metabolism. *Nature* **414**, 799-806.

Sato, K., Nakamura, A., Shirakawa, J., Muraoka, T., Togashi, Y., Shinoda, K., Orime, K., Kubota, N., Kadowaki, T. and Terauchi, Y. (2012). Impact of the dipeptidyl peptidase-4 inhibitor vildagliptin on glucose tolerance and beta-cell function and mass in insulin receptor substrate-2-knockout mice fed a high-fat diet. *Endocrinology* **153**, 1093-102.

Scaglia, L., Cahill, C. J., Finegood, D. T. and Bonner-Weir, S. (1997). Apoptosis participates in the remodeling of the endocrine pancreas in the neonatal rat. *Endocrinology* **138**, 1736-41.

Scaglia, L., Smith, F. E. and Bonner-Weir, S. (1995). Apoptosis contributes to the involution of beta cell mass in the post partum rat pancreas. *Endocrinology* **136**, 5461-8.

Schouten, G. J., Vertegaal, A. C., Whiteside, S. T., Israel, A., Toebes, M., Dorsman, J. C., van der Eb, A. J. and Zantema, A. (1997). IkappaB alpha is a target for the mitogen-activated 90 kDa ribosomal S6 kinase. *EMBO J* **16**, 3133-44.

Schuppin, G. T., Pons, S., Hugl, S., Aiello, L. P., King, G. L., White, M. and Rhodes, C. J. (1998). A specific increased expression of insulin receptor substrate 2 in pancreatic beta-cell lines is involved in mediating serum-stimulated beta-cell growth. *Diabetes* **47**, 1074-85.

Shaw, J. E., Sicree, R. A. and Zimmet, P. Z. (2010). Global estimates of the prevalence of diabetes for 2010 and 2030. *Diabetes Res Clin Pract* **87**, 4-14.

Shimamura, A., Ballif, B. A., Richards, S. A. and Blenis, J. (2000). Rsk1 mediates a MEK-MAP kinase cell survival signal. *Curr Biol* **10**, 127-35.

Silvestre, R. A., Egido, E. M., Hernandez, R. and Marco, J. (2005). Tungstate stimulates insulin release and inhibits somatostatin output in the perfused rat pancreas. *Eur J Pharmacol* **519**, 127-34.

Simmgen, M., Knauf, C., Lopez, M., Choudhury, A. I., Charalambous, M., Cantley, J., Bedford, D. C., Claret, M., Iglesias, M. A., Heffron, H. et al. (2006). Liver-specific deletion of insulin receptor substrate 2 does not impair hepatic glucose and lipid metabolism in mice. *Diabetologia* **49**, 552-61.

Slee, E. A., Adrain, C. and Martin, S. J. (2001). Executioner caspase-3, -6, and -7 perform distinct, non-redundant roles during the demolition phase of apoptosis. *J Biol Chem* **276**, 7320-6.

Soria, B. and Gauthier, B. R. (2013). Dual Trade of Bcl-2 and Bcl-xL in islet physiology: balancing life and death with metabolism secretion coupling. *Diabetes* **62**, 18-21.

Soriguer, F., Goday, A., Bosch-Comas, A., Bordiu, E., Calle-Pascual, A., Carmena, R., Casamitjana, R., Castano, L., Castell, C., Catala, M. et al. (2012). Prevalence of diabetes mellitus and impaired glucose regulation in Spain: the Di@bet.es Study. *Diabetologia* **55**, 88-93.

Steiner, D. J., Kim, A., Miller, K. and Hara, M. (2010). Pancreatic islet plasticity: interspecies comparison of islet architecture and composition. *Islets* **2**, 135-45.

Stoffers, D. A., Kieffer, T. J., Hussain, M. A., Drucker, D. J., Bonner-Weir, S., Habener, J. F. and Egan, J. M. (2000). Insulinotropic glucagon-like peptide 1 agonists stimulate expression of homeodomain protein IDX-1 and increase islet size in mouse pancreas. *Diabetes* **49**, 741-8.

Stull, N. D., Breite, A., McCarthy, R., Tersey, S. A. and Mirmira, R. G. (2012). Mouse islet of Langerhans isolation using a combination of purified collagenase and neutral protease. *J Vis Exp*.

Suzuki, R., Tobe, K., Terauchi, Y., Komeda, K., Kubota, N., Eto, K., Yamauchi, T., Azuma, K., Kaneto, H., Taguchi, T. et al. (2003). Pdx1 expression in Irs2-deficient mouse beta-cells is regulated in a strain-dependent manner. *J Biol Chem* **278**, 43691-8.

Szot, G. L., Koudria, P. and Bluestone, J. A. (2007). Murine pancreatic islet isolation. *J Vis Exp*, 255.

T

Takamoto, I., Terauchi, Y., Kubota, N., Ohsugi, M., Ueki, K. and Kadowaki, T. (2008). Crucial role of insulin receptor substrate-2 in compensatory beta-cell hyperplasia in response to high fat diet-induced insulin resistance. *Diabetes Obes Metab* **10 Suppl 4**, 147-56.

Tamemoto, H., Kadowaki, T., Tobe, K., Yagi, T., Sakura, H., Hayakawa, T., Terauchi, Y., Ueki, K., Kaburagi, Y., Satoh, S. et al. (1994). Insulin resistance and growth retardation in mice lacking insulin receptor substrate-1. *Nature* **372**, 182-6.

Tan, Y., Demeter, M. R., Ruan, H. and Comb, M. J. (2000). BAD Ser-155 phosphorylation regulates BAD/Bcl-XL interaction and cell survival. *J Biol Chem* **275**, 25865-9.

Taniguchi, C. M., Ueki, K. and Kahn, C. R. (2005). Complementary roles of IRS-1 and IRS-2 in the hepatic regulation of metabolism. *Journal of Clinical Investigation* **115**, 718-727.

Thirone, A. C., Huang, C. and Klip, A. (2006). Tissue-specific roles of IRS proteins in insulin signaling and glucose transport. *Trends Endocrinol Metab* **17**, 72-8.

Thomas, H. E. and Biden, T. J. (2009). Bad news for beta-cell apoptosis. *Diabetes* **58**, 1725-7.

Thomas, H. E., McKenzie, M. D., Angstetra, E., Campbell, P. D. and Kay, T. W. (2009). Beta cell apoptosis in diabetes. *Apoptosis* **14**, 1389-404.

Thomas, J. A., Schlender, K. K. and Larner, J. (1968). A rapid filter paper assay for UDPglucose-glycogen glucosyltransferase, including an improved biosynthesis of UDP-14C-glucose. *Anal Biochem* **25**, 486-99.

V

Vague, P. and Moulin, J. P. (1982). The defective glucose sensitivity of the B cell in non insulin dependent diabetes. Improvement after twenty hours of normoglycaemia. *Metabolism* **31**, 139-42.

Viswakarma, N., Yu, S., Naik, S., Kashireddy, P., Matsumoto, K., Sarkar, J., Surapureddi, S., Jia, Y., Rao, M. S. and Reddy, J. K. (2007). Transcriptional regulation of Cidea, mitochondrial cell death-inducing DNA fragmentation factor alpha-like effector A, in mouse liver by peroxisome proliferator-activated receptor alpha and gamma. *J Biol Chem* **282**, 18613-24.

W

Wang, Q., Li, L., Xu, E., Wong, V., Rhodes, C. and Brubaker, P. L. (2004). Glucagon-like peptide-1 regulates proliferation and apoptosis via activation of protein kinase B in pancreatic INS-1 beta cells. *Diabetologia* **47**, 478-87.

Weir, G. C. and Bonner-Weir, S. (2004). Five Stages of Evolving Beta-Cell Dysfunction During Progression to Diabetes. *Diabetes* **53**, S16-S21.

Weir, G. C., Marselli, L., Marchetti, P., Katsuta, H., Jung, M. H. and Bonner-Weir, S. (2009). Towards better understanding of the contributions of overwork and glucotoxicity to the beta-cell inadequacy of type 2 diabetes. *Diabetes Obes Metab* **11 Suppl 4**, 82-90.

Weyer, C., Bogardus, C., Mott, D. M. and Pratley, R. E. (1999). The natural history of insulin secretory dysfunction and insulin resistance in the pathogenesis of type 2 diabetes mellitus. *J Clin Invest* **104**, 787-94.

White, M. F. (1996). The IRS-signalling system in insulin and cytokine action. *Philos Trans R Soc Lond B Biol Sci* **351**, 181-9.

White, M. F. (1998). The IRS-signalling system: a network of docking proteins that mediate insulin action. *Mol Cell Biochem* **182**, 3-11.

White, M. F. (2002). IRS proteins and the common path to diabetes. *Am J Physiol Endocrinol Metab* **283**, E413-22.

Wild, S., Roglic, G., Green, A., Sicree, R. and King, H. (2004). Global prevalence of diabetes: estimates for the year 2000 and projections for 2030. *Diabetes Care* **27**, 1047-53.

Withers, D. J., Burks, D. J., Towery, H. H., Altamuro, S. L., Flint, C. L. and White, M. F. (1999). Irs-2 coordinates Igf-1 receptor-mediated beta-cell development and peripheral insulin signalling. *Nat Genet* **23**, 32-40.

Withers, D. J., Gutierrez, J. S., Towery, H., Burks, D. J., Ren, J. M., Previs, S., Zhang, Y., Bernal, D., Pons, S., Shulman, G. I. et al. (1998). Disruption of IRS-2 causes type 2 diabetes in mice. *Nature* **391**, 900-4.

Y

Yang, E., Zha, J., Jockel, J., Boise, L. H., Thompson, C. B. and Korsmeyer, S. J. (1995). Bad, a heterodimeric partner for Bcl-XL and Bcl-2, displaces Bax and promotes cell death. *Cell* **80**, 285-91.

Yenush, L. and White, M. F. (1997). The IRS-signalling system during insulin and cytokine action. *Bioessays* **19**, 491-500.

Z

Zafra, D., Nocito, L., Dominguez, J. and Guinovart, J. J. (2013). Sodium tungstate activates glycogen synthesis through a non-canonical mechanism involving G-proteins. *FEBS Lett* **587**, 291-6.

Zhou, Y. P., Pena, J. C., Roe, M. W., Mittal, A., Levisetti, M., Baldwin, A. C., Pugh, W., Ostrega, D., Ahmed, N., Bindokas, V. P. et al. (2000). Overexpression of Bcl-x(L) in beta-cells prevents cell death but impairs mitochondrial signal for insulin secretion. *Am J Physiol Endocrinol Metab* **278**, E340-51.

VIII ANNEXES

Supplementary Table 1: 58 upregulated genes in *Irs2*$^{-/-}$ compared to WT animals.

Gene ID (Affymetrix)	Gene symbol	Gene name	q-Values	Fold-change
1422682_s_at	Prss1	protease, serine, 1 (trypsin 1)	0.010	6.5
1426174_s_at	Igh-3	Immunoglobulin heavy chain (gamma polypeptide)	0.010	5.9
1450689_at	Prss3	similar to trypsinogen 15	0.010	5.8
1419735_at	Csn3	casein kappa	0.010	5.7
1422915_at	Gast	gastrin	0.010	5.5
1424631_a_at	Ighg	Immunoglobulin heavy chain (gamma polypeptide)	0.010	5.4
1424931_s_at	Igl	immunoglobulin lambda chain, variable 1	0.010	5.4
1422918_at	1810009J06Rik	RIKEN cDNA 1810009J06 gene	0.010	5.3
1430523_s_at	Igl-V1	immunoglobulin lambda chain, variable 1	0.003	5.1
1424825_a_at	Glycam1	glycosylation dependent cell adhesion molecule 1	0.004	4.6
1417956_at	Cidea	cell death-inducing DNA fragmentation factor, alpha subunit-like effector A	0.007	4.6
1427789_s_at	Gnas	GNAS (guanine nucleotide binding protein, alpha stimulating) complex locus	0.013	4.4
1426766_at	6330403K07Rik	RIKEN cDNA 6330403K07 gene	0.016	4.3
1436662_at	Sorcs1	VPS10 domain receptor protein SORCS 1	0.016	4.2
1450344_a_at	Ptger3	prostaglandin E receptor 3 (subtype EP3)	0.015	4.2
1425385_a_at	Igh-6	similar to gamma-2a immunoglobulin heavy chain	0.025	4.1
1419388_at	Tm4sf20	transmembrane 4 L six family member 20	0.021	4.0
1424305_at	Igj	immunoglobulin joining chain	0.029	3.9
1428719_at	2010309G21Rik	RIKEN cDNA 2010309G21 gene	0.029	3.9

1448290_at	Reg3b	pancreatitis-associated protein	0.034	3.9
1418652_at	Cxcl9	chemokine (C-X-C motif) ligand 9	0.025	3.8
1428720_s_at	2010309G21Rik	RIKEN cDNA 2010309G21 gene	0.031	3.8
1454622_at	Slc38a5	solute carrier family 38, member 5	0.025	3.8
1425763_x_at	Igh-2	immunoglobulin heavy chain (J558 family	0.029	3.7
1427455_x_at	Gm10883	Ig kappa chain	0.030	3.7
1439426_x_at	Lyz1	lysozyme	0.029	3.7
1421653_a_at	Igh-2	immunoglobulin heavy chain (J558 family	0.029	3.7
1423467_at	Ms4a4b	membrane-spanning 4-domains, subfamily A, member 4B	0.030	3.7
1416139_at	Reg2	regenerating islet-derived 2	0.037	3.5
1450826_a_at	Saa3	serum amyloid A 3	0.030	3.4
1422825_at	Cartpt	CART prepropeptide	0.031	3.4
1418126_at	Ccl5	chemokine (C-C motif) ligand 5	0.030	3.4
1426168_a_at	A130082M07Rik	T-cell receptor alpha chain	0.029	3.4
1429381_x_at	Igh-2	immunoglobulin heavy chain (J558 family)	0.032	3.3
1424525_at	Grp	gastrin releasing peptide	0.035	3.3
1435697_a_at	Cytip	pleckstrin homology, Sec7 and coiled-coil domains, binding protein	0.034	3.3
1436094_at	Vgf	VGF nerve growth factor inducible	0.034	3.2
1416318_at	Serpinb1a	serine (or cysteine) peptidase inhibitor, clade B, member 1a	0.032	3.2
1423547_at	Lyz2	lysozyme	0.035	3.2
1452205_x_at	Gm6273	T-cell receptor beta, variable 13	0.034	3.2
1441161_at	B230216G23Rik	RIKEN cDNA B230216G23 gene	0.035	3.1
1423634_at	Gsdma	gasdermin 1	0.036	3.1

1436996_x_at	Lyz1	lysozyme	0.037	3.1
1418282_x_at	Serpina1b	serine (or cysteine) preptidase inhibitor, clade A, member 1b	0.036	3.1
1422694_at	Ttyh1	tweety homolog 1 (Drosophila)	0.034	3.1
1425854_x_at	LOC665506	T-cell receptor beta, variable 13	0.034	3.1
1428909_at	A130040M12Rik	RIKEN cDNA A130040M12 gene	0.036	3.1
1451206_s_at	Cytip	pleckstrin homology, Sec7 and coiled-coil domains, binding protein	0.045	3.0
1418536_at	H2-Q7	histocompatibility 2, Q region locus 6	0.036	3.0
1448789_at	Aldh1a3	aldehyde dehydrogenase family 1, subfamily A3	0.035	3.0
1428947_at	2010001M09Rik	RIKEN cDNA 2010001M09 gene	0.037	2.9
1419426_s_at	Ccl21a	chemokine (C-C motif) ligand 21a	0.046	2.9
1455582_at	---	Transcribed locus	0.047	2.9
1449498_at	Marco	macrophage receptor with collagenous structure	0.038	2.9
1416892_s_at	Fam107b	RIKEN cDNA 3110001A13 gene	0.040	2.8
1424923_at	Serpina3g	serine (or cysteine) peptidase inhibitor, clade A, member 3G	0.047	2.8
1424357_at	Tmem45b	transmembrane protein 45b	0.048	2.8
1450683_at	Tagln3	transgelin 3	0.049	2.8

Supplementary Table 2: 123 downregulated genes in *Irs2*$^{-/-}$ compared to WT animals.

Gene ID (Affymetrix)	**Gene symbol**	**Gene name**	**q-Values**	**Fold-change**
1457633_x_at	Cox6a2	cytochrome c oxidase, subunit VI a, polypeptide 2	0.000	-3.4
1416561_at	Gad1	glutamic acid decarboxylase 1	0.000	-3.4

1443969_at	Irs2	insulin receptor substrate 2	0.000	-3.1
1417607_at	Cox6a2	cytochrome c oxidase, subunit VI a, polypeptide 2	0.000	-3.1
1443413_s_at	Trpm5	transient receptor potential cation channel, subfamily M, member 5	0.002	-2.7
1435435_at	Cttnbp2	cortactin binding protein 2	0.002	-2.6
1436087_at	Dpp10	dipeptidylpeptidase 10	0.002	-2.6
1418783_at	Trpm5	transient receptor potential cation channel, subfamily M, member 5	0.002	-2.6
1430591_at	Ddc	dopa decarboxylase	0.002	-2.6
1421558_at	T2	brachyury 2	0.002	-2.5
1454768_at	Kcnf1	potassium voltage-gated channel, subfamily F, member 1	0.003	-2.5
1444769_at	Tex9	Testis expressed gene 9	0.003	-2.4
1437540_at	Mcoln3	mucolipin 3	0.003	-2.4
1430416_at	4931431B13Rik	RIKEN cDNA 4931431B13 gene	0.003	-2.4
1417030_at	Tmem206	RIKEN cDNA 2310028N02 gene	0.003	-2.4
1456402_at	A330076H08Rik	RIKEN cDNA A330076H08 gene	0.003	-2.3
1449067_at	Slc2a2	solute carrier family 2 (facilitated glucose transporter), member 2	0.004	-2.3
1453403_at	2210019I11Rik	RIKEN cDNA 2210019I11 gene	0.007	-2.3
1437782_at	Cntnap2	contactin associated protein-like 2	0.007	-2.3
1416562_at	Gad1	glutamic acid decarboxylase 1	0.009	-2.2
1437060_at	Olfm4	olfactomedin 4	0.009	-2.2
1449409_at	Sult1c2	sulfotransferase family, cytosolic, 1C, member 2	0.009	-2.2
1442037_at	---	Adult male corpora quadrigemina cDNA,	0.009	-2.2

		RIKEN full-length enriched library, clone:B230352I09 product:unclassifiable, full insert sequence		
1448552_s_at	Tmem206	RIKEN cDNA 2310028N02 gene	0.009	-2.2
1455876_at	Slc4a7	solute carrier family 4, sodium bicarbonate cotransporter, member 7	0.009	-2.2
1435858_at	Tmem215	Transcribed locus	0.009	-2.2
1446364_at	---	NA	0.011	-2.1
1437376_at	Adam32	a disintegrin and metallopeptidase domain 32	0.011	-2.1
1441439_at	Ucn3	urocortin 3	0.011	-2.1
1417443_at	Fam151a	cDNA sequence BC026682	0.011	-2.1
1417336_a_at	Sytl4	synaptotagmin-like 4	0.011	-2.0
1436092_at	---	Transcribed locus	0.012	-2.0
1449240_at	Gsbs	G substrate	0.012	-2.0
1452378_at	Malat1	metastasis associated lung adenocarcinoma transcript 1 (non-coding RNA)	0.012	-2.0
AFFX-18SRNAMur/X00686_M_at	---	NA	0.012	-2.0
1434528_at	Aard	alanine and arginine rich domain containing protein	0.015	-2.0
1429344_at	9.13E+15	hypothetical 9130022E09	0.016	-2.0
1435456_at	Ttc28	tetratricopeptide repeat domain 28	0.016	-1.9
1457528_at	Slc4a7	solute carrier family 4, sodium bicarbonate cotransporter, member 7	0.015	-1.9
1444438_at	Cib3	calcium and integrin binding family member 3	0.016	-1.9
1441991_at	Prss53	cDNA sequence BC039632	0.015	-1.9
1456741_s_at	Gpm6a	glycoprotein m6a	0.018	-1.9

1438020_at	Hapln1	hyaluronan and proteoglycan link protein 1	0.016	-1.9
1419584_at	Ttc28	tetratricopeptide repeat domain 28	0.015	-1.9
1451612_at	Mt1	metallothionein 1	0.016	-1.9
1452656_at	Zdhhc2	zinc finger, DHHC domain containing 2	0.016	-1.9
1455365_at	Cdh8	cadherin 8	0.016	-1.9
1458866_at	Tmem215	RIKEN cDNA A930001M12 gene	0.018	-1.9
1417031_at	Tmem206	RIKEN cDNA 2310028N02 gene	0.018	-1.9
1444317_at	Pcdh15	protocadherin 15	0.018	-1.9
1457273_at	Odz2	odd Oz/ten-m homolog 2 (Drosophila)	0.017	-1.9
1451991_at	Epha7	Eph receptor A7	0.017	-1.9
1459372_at	Npas4	neuronal PAS domain protein 4	0.018	-1.9
1449520_at	Ttc28	tetratricopeptide repeat domain 28	0.018	-1.8
1434354_at	Maob	monoamine oxidase B	0.018	-1.8
1444965_at	E130002L11Rik	RIKEN cDNA E130002L11 gene	0.018	-1.8
1422153_a_at	Asb11	ankyrin repeat and SOCS box-containing protein 11	0.017	-1.8
1457124_at	---	Transcribed locus	0.019	-1.8
1445579_at	---	arachidonate lipoxygenase, epidermal	0.022	-1.8
1426294_at	Hapln1	hyaluronan and proteoglycan link protein 1	0.020	-1.8
1452655_at	Zdhhc2	zinc finger, DHHC domain containing 2	0.020	-1.8
1421595_at	Fam184b	RIKEN cDNA 9630031F12 gene	0.020	-1.8
1422330_at	Glp1r	glucagon-like peptide 1 receptor	0.024	-1.8
1428414_at	Ccny	cyclin Y	0.022	-1.8
1444147_at	Pcsk2	proprotein convertase subtilisin/kexin type 2	0.020	-1.8
1416383_a_at	Pcx	pyruvate carboxylase	0.021	-1.8

1445297_at	Stxbp5l	Transcribed locus	0.022	-1.8
1427509_at	Baiap3	BAI1-associated protein 3	0.024	-1.7
1439019_at	Fras1	Fraser syndrome 1 homolog (human)	0.022	-1.7
1417051_at	Pcdh8	protocadherin 8	0.023	-1.7
1454632_at	Tmem229b	RIKEN cDNA 6330442E10 gene	0.024	-1.7
1457557_at	A330076H08Rik	RIKEN cDNA A330076H08 gene	0.030	-1.7
1426295_at	Hapln1	hyaluronan and proteoglycan link protein 1	0.027	-1.7
1427231_at	Robo1	roundabout homolog 1 (Drosophila)	0.024	-1.7
1422625_at	LOC100046207	lymphocyte antigen 6 complex, locus H	0.028	-1.7
1436661_at	Dpp10	dipeptidylpeptidase 10	0.025	-1.7
1425927_a_at	Atf5	activating transcription factor 5	0.027	-1.7
1422052_at	Cdh8	cadherin 8	0.025	-1.7
1457700_at	Cyp4f39	cytochrome P450, family 4, subfamily f, polypeptide 39	0.028	-1.7
1422798_at	Cntnap2	contactin associated protein-like 2	0.027	-1.7
1420946_at	Atrx	alpha thalassemia/mental retardation syndrome X-linked homolog (human)	0.037	-1.6
1451389_at	Dnajc24	DPH4 homolog (JJJ3, S. cerevisiae)	0.033	-1.6
AFFX-PyruCarbMur/L09192_3_at	Pcx	pyruvate carboxylase	0.037	-1.6
1446815_at	---	Transcribed locus	0.036	-1.6
1450896_at	Arhgap5	Rho GTPase activating protein 5	0.033	-1.6
1450397_at	Mtap1b	microtubule-associated protein 1 B	0.040	-1.6
1422871_at	Kcnj12	potassium inwardly-rectifying channel, subfamily J, member 12	0.037	-1.6
1434644_at	Tbl1x	transducin (beta)-like 1 X-linked	0.038	-1.6

1447825_x_at	Pcdh8	protocadherin 8	0.039	-1.6
1434051_s_at	Hspa12a	heat shock protein 12A	0.037	-1.6
AFFX-18SRNAMur/X00686_5_at	---	NA	0.041	-1.6
1449224_at	Trpm5	transient receptor potential cation channel, subfamily M, member 5	0.039	-1.6
1450112_a_at	Gas2	growth arrest specific 2	0.040	-1.6
1420955_at	Vsnl1	visinin-like 1	0.039	-1.6
1415822_at	Scd2	stearoyl-Coenzyme A desaturase 2	0.038	-1.6
1449948_at	Ero1lb	ERO1-like beta (S. cerevisiae)	0.041	-1.6
1436076_at	Dlgap1	discs, large (Drosophila) homolog-associated protein 1	0.037	-1.6
1434709_at	Nrcam	neuron-glia-CAM-related cell adhesion molecule	0.040	-1.6
1444956_at	---	NA	0.042	-1.6
1423194_at	Arhgap5	Rho GTPase activating protein 5	0.040	-1.6
1438673_at	Slc4a7	solute carrier family 4, sodium bicarbonate cotransporter, member 7	0.042	-1.6
1449429_at	Fkbp1b	FK506 binding protein 1b	0.039	-1.6
1427126_at	Hspa1b	heat shock protein 1B	0.047	-1.5
1452198_at	Kdm2b	F-box and leucine-rich repeat protein 10	0.041	-1.5
1430977_at	Fam159b	RIKEN cDNA A930021C24 gene	0.043	-1.5
1421286_a_at	Atp4a	ATPase, H+/K+ exchanging, gastric, alpha polypeptide	0.040	-1.5
1434846_at	Dennd4c	DENN/MADD domain containing 4C	0.042	-1.5
1454984_at	Lifr	expressed sequence AW061234	0.040	-1.5
1422605_at	Ppp1r1a	protein phosphatase 1, regulatory (inhibitor)	0.043	-1.5

		subunit 1A		
1440282_at	LOC100046693	RIKEN cDNA 2210038L17 gene	0.043	-1.5
1419063_at	Ugt8a	UDP galactosyltransferase 8A	0.042	-1.5
1443253_at	---	NA	0.050	-1.5
1455185_s_at	Phf16	PHD finger protein 16	0.045	-1.5
1454782_at	Bai3	brain-specific angiogenesis inhibitor 3	0.042	-1.5
1430642_at	2900001G08Rik	RIKEN cDNA 2900001G08 gene	0.046	-1.5
1444027_at	Slc30a8	solute carrier family 30 (zinc transporter), member 8	0.045	-1.5
1443926_at	---	Transcribed locus	0.048	-1.5
1418257_at	Slc12a7	solute carrier family 12, member 7	0.045	-1.5
1419402_at	Mns1	meiosis-specific nuclear structural protein 1	0.047	-1.5
1436672_at	Grk5	CDNA clone IMAGE:5720309	0.048	-1.5
1453192_at	Fam101a	RIKEN cDNA 3110032G18 gene	0.046	-1.5
1421989_s_at	Papss2	3'-phosphoadenosine 5'-phosphosulfate synthase 2	0.050	-1.5
1455695_at	St8sia1	ST8 alpha-N-acetyl-neuraminide alpha-2,8-sialyltransferase 1	0.048	-1.5

Supplementary Table 3: 149 downregulated genes in treated *Irs2*$^{-/-}$ compared to untreated *Irs2*$^{-/-}$ animals.

Gene ID (Affymetrix)	**Gene symbol**	**Gene name**	**q-Values**	**Fold-change**
1426174_s_at	Igh-3	Immunoglobulin heavy chain (gamma polypeptide)	0.000	-5.3
1424631_a_at	Ighg	Immunoglobulin heavy chain (gamma polypeptide)	0.003	-5.2
1424931_s_at	Igl	immunoglobulin lambda chain, variable 1	0.006	-4.3
1430523_s_at	Igl-V1	immunoglobulin lambda chain, variable 1	0.006	-4.2

1449434_at	Car3	carbonic anhydrase 3	0.015	-3.8
1425385_a_at	Igh-6	similar to gamma-2a immunoglobulin heavy chain	0.008	-3.7
1418652_at	Cxcl9	chemokine (C-X-C motif) ligand 9	0.006	-3.5
1428909_at	A130040M12Rik	RIKEN cDNA A130040M12 gene	0.006	-3.4
1422682_s_at	Prss1	protease, serine, 1 (trypsin 1	0.021	-3.4
1416957_at	Pou2af1	POU domain, class 2, associating factor 1	0.006	-3.3
1423467_at	Ms4a4b	membrane-spanning 4-domains, subfamily A, member 4B	0.007	-3.3
1419388_at	Tm4sf20	transmembrane 4 L six family member 20	0.008	-3.3
1426168_a_at	A130082M07Rik	T-cell receptor alpha chain	0.006	-3.2
1439426_x_at	Lyz1	lysozyme	0.010	-3.2
1417851_at	Cxcl13	chemokine (C-X-C motif) ligand 13	0.006	-3.2
1418126_at	Ccl5	chemokine (C-C motif) ligand 5	0.008	-3.1
1450344_a_at	Ptger3	prostaglandin E receptor 3 (subtype EP3)	0.012	-3.1
1417867_at	Cfd	complement factor D (adipsin)	0.032	-3.1
1450689_at	Prss3	similar to trypsinogen 15	0.030	-3.0
1452205_x_at	Gm6273	T-cell receptor beta, variable 13	0.012	-2.9
1425854_x_at	LOC665506	T-cell receptor beta, variable 13	0.013	-2.9
1448377_at	Slpi	secretory leukocyte peptidase inhibitor	0.015	-2.9
1452815_at	P2ry10	purinergic receptor P2Y, G-protein coupled 10	0.014	-2.8
1448859_at	Cxcl13	chemokine (C-X-C motif) ligand 13	0.014	-2.8
1419735_at	Csn3	casein kappa	0.014	-2.8
1436662_at	Sorcs1	VPS10 domain receptor protein SORCS 1	0.014	-2.7
1424923_at	Serpina3g	serine (or cysteine) peptidase inhibitor, clade A, member 3G	0.017	-2.7
1428720_s_at	2010309G21Rik	RIKEN cDNA 2010309G21 gene	0.014	-2.7

1423226_at	Ms4a1	membrane-spanning 4-domains, subfamily A, member 1	0.018	-2.7
1419178_at	Cd3g	CD3 antigen, gamma polypeptide	0.015	-2.7
1440837_at	H2-Ob	histocompatibility 2, O region beta locus	0.018	-2.7
1428947_at	2010001M09Rik	RIKEN cDNA 2010001M09 gene	0.018	-2.7
1435697_a_at	Cytip	pleckstrin homology, Sec7 and coiled-coil domains, binding protein	0.018	-2.7
1417956_at	Cidea	cell death-inducing DNA fragmentation factor, alpha subunit-like effector A	0.015	-2.7
1428719_at	2010309G21Rik /	RIKEN cDNA 2010309G21 gene	0.017	-2.6
1451206_s_at	Cytip	pleckstrin homology, Sec7 and coiled-coil domains, binding protein	0.018	-2.6
1422918_at	1810009J06Rik	RIKEN cDNA 1810009J06 gene	0.044	-2.6
1436329_at	Egr3	early growth response 3	0.024	-2.6
1418282_x_at	Serpina1b	serine (or cysteine) preptidase inhibitor, clade A, member 1b	0.018	-2.6
1423466_at	Ccr7	chemokine (C-C motif) receptor 7	0.024	-2.5
1455656_at	Btla	B and T lymphocyte associated	0.024	-2.5
1455530_at	Ighv14-2	immunoglobulin heavy variable V14-2	0.024	-2.5
1455269_a_at	Coro1a	coronin, actin binding protein 1A	0.021	-2.5
1416246_a_at	Coro1a	coronin, actin binding protein 1A	0.023	-2.5
1416714_at	Irf8	interferon regulatory factor 8	0.024	-2.5
1450912_at	Ms4a1	membrane-spanning 4-domains, subfamily A, member 1	0.024	-2.5
1427301_at	Cd48	CD48 antigen	0.023	-2.5
1450997_at	Stk17b	serine/threonine kinase 17b (apoptosis-inducing)	0.024	-2.4
1456014_s_at	Fermt3	cDNA sequence BC032204	0.023	-2.4

1416318_at	Serpinb1a	serine (or cysteine) peptidase inhibitor, clade B, member 1a	0.024	-2.4
1427837_at	Igk-V32	similar to Unknown (protein for MGC:103328)	0.044	-2.4
1456328_at	Bank1	B-cell scaffold protein with ankyrin repeats 1	0.031	-2.4
1419684_at	Ccl8	chemokine (C-C motif) ligand 8	0.024	-2.4
1434067_at	AI662270	expressed sequence AI662270	0.024	-2.3
1428735_at	Cd69	CD69 antigen	0.044	-2.3
1422915_at	Gast	gastrin	0.024	-2.3
1447918_x_at	Igl-V1	Immunoglobulin lambda chain, variable 1	0.024	-2.3
1441161_at	B230216G23Rik	RIKEN cDNA B230216G23 gene	0.024	-2.3
1429381_x_at	Igh-2	immunoglobulin heavy chain (J558 family	0.049	-2.3
1449498_at	Marco	macrophage receptor with collagenous structure	0.024	-2.3
1425226_x_at	LOC665506	T-cell receptor beta, variable 13	0.031	-2.3
1418536_at	H2-Q7	histocompatibility 2, Q region locus 6	0.026	-2.3
1423452_at	Stk17b	serine/threonine kinase 17b (apoptosis-inducing)	0.038	-2.3
1439956_at	Ms4a6b	membrane-spanning 4-domains, subfamily A, member 6B	0.026	-2.3
1436312_at	Ikzf1	IKAROS family zinc finger 1	0.035	-2.3
1419135_at	Ltb	lymphotoxin B	0.030	-2.3
1422124_a_at	Ptprc	protein tyrosine phosphatase, receptor type, C	0.030	-2.2
1423634_at	Gsdma	gasdermin 1	0.026	-2.2
1454169_a_at	Epsti1	epithelial stromal interaction 1 (breast)	0.031	-2.2
1455660_at	Csf2rb	colony stimulating factor 2 receptor, beta, low-affinity (granulocyte-macrophage)	0.031	-2.2
1418770_at	Cd2	CD2 antigen	0.031	-2.2
1417640_at	Cd79b	CD79B antigen	0.037	-2.2
1452087_at	Epsti1	epithelial stromal interaction 1 (breast)	0.030	-2.2

1436996_x_at	Lyz1	lysozyme	0.030	-2.2
1418203_at	Pmaip1	phorbol-12-myristate-13-acetate-induced protein 1	0.045	-2.2
1423547_at	Lyz2	lysozyme	0.030	-2.2
1417995_at	Ptpn22	protein tyrosine phosphatase, non-receptor type 22 (lymphoid)	0.037	-2.2
1435331_at	Pyhin1	hypothetical protein LOC100048304///pyrin and HIN domain family, member 1	0.030	-2.2
1427789_s_at	Gnas	GNAS (guanine nucleotide binding protein, alpha stimulating) complex locus	0.030	-2.2
1440834_at	Slc5a10	solute carrier family 5 (sodium/glucose cotransporter), member 10	0.030	-2.2
1439141_at	Gpr18	G protein-coupled receptor 18	0.031	-2.2
1436576_at	Fam26f	RIKEN cDNA A630077B13 gene	0.033	-2.2
1426772_x_at	Gm6273	T-cell receptor beta, joining region	0.033	-2.2
1427329_a_at	Igh-6	immunoglobulin heavy chain 6 (heavy chain of IgM)	0.031	-2.1
1427860_at	LOC100047162	similar to Ig kappa chain V-V region MPC11 precursor	0.035	-2.1
1460218_at	Cd52	CD52 antigen	0.036	-2.1
1424357_at	Tmem45b	transmembrane protein 45b	0.031	-2.1
1415983_at	Lcp1	lymphocyte cytosolic protein 1	0.037	-2.1
1418930_at	Cxcl10	chemokine (C-X-C motif) ligand 1	0.038	-2.1
1443783_x_at	H2-Aa	Histocompatibility 2, class II antigen A, alpha	0.035	-2.1
1460423_x_at	Gm5571	Ig kappa chain	0.038	-2.1
1417620_at	Rac2	RAS-related C3 botulinum substrate 2	0.037	-2.1
1452463_x_at	Gm10883	predicted gene, ENSMUSG00000076577	0.036	-2.1
1434068_s_at	AI662270	expressed sequence AI662270	0.038	-2.1
1419004_s_at	Bcl2a1a	B-cell leukemia/lymphoma 2 related protein A1a	0.040	-2.1

1435477_s_at	Fcgr2b	Fc receptor, IgG, low affinity IIb	0.037	-2.1
1425396_a_at	Lck	lymphocyte protein tyrosine kinase	0.039	-2.1
1436847_s_at	Cdca8	cell division cycle associated 8	0.040	-2.1
1435959_at	Arhgap15	Rho GTPase activating protein 15	0.040	-2.1
1451335_at	Plac8	placenta-specific 8	0.038	-2.1
1450241_a_at	Evi2a	ecotropic viral integration site 2a	0.039	-2.0
1419480_at	Sell	selectin, lymphocyte	0.044	-2.0
1416296_at	Il2rg	interleukin 2 receptor, gamma chain	0.041	-2.0
1448162_at	Vcam1	vascular cell adhesion molecule 1	0.038	-2.0
1427351_s_at	Igh-6	immunoglobulin heavy chain 6 (heavy chain of IgM)	0.036	-2.0
1431609_a_at	Acp5	acid phosphatase 5, tartrate resistant	0.041	-2.0
1430165_at	Stk17b	serine/threonine kinase 17b (apoptosis-inducing)	0.045	-2.0
1419481_at	Sell	selectin, lymphocyte	0.043	-2.0
1448617_at	Cd53	CD53 antigen	0.044	-2.0
1435465_at	Kbtbd11	kelch repeat and BTB (Luco et al.) domain containing 11	0.042	-2.0
1448823_at	Cxcl12	chemokine (C-X-C motif) ligand 12	0.037	-2.0
1417597_at	Cd28	CD28 antigen///similar to CD28 antigen	0.044	-2.0
1420994_at	B3gnt5	UDP-GlcNAc:betaGal beta-1,3-N-acetylglucosaminyltransferase 5	0.044	-2.0
1443687_x_at	H2-DMb2	histocompatibility 2, class II, locus Mb2	0.048	-2.0
1435560_at	Itgal	integrin alpha L	0.044	-2.0
1424305_at	Igj	immunoglobulin joining chain	0.041	-2.0
1425084_at	Gimap7	GTPase, IMAP family member 7	0.044	-2.0
1449360_at	Csf2rb2	colony stimulating factor 2 receptor, beta 2, low-affinity (granulocyte-macrophage)	0.045	-2.0

1416295_a_at	Il2rg	interleukin 2 receptor, gamma chain	0.045	-2.0
1435330_at	Pyhin1	pyrin and HIN domain family, member 1	0.044	-2.0
1434152_at	Apol7c	apolipoprotein L, 3-like	0.044	-2.0
1426113_x_at	Tcra	T-cell receptor alpha chain	0.044	-2.0
1450678_at	Itgb2	integrin beta 2	0.044	-2.0
1451780_at	Blnk	B-cell linker	0.044	-2.0
1426454_at	Arhgdib	Rho, GDP dissociation inhibitor (GDI) beta	0.044	-2.0
1450291_s_at	Ms4a4c	membrane-spanning 4-domains, subfamily A, member 4C	0.045	-2.0
1436293_x_at	Ildr2	DNA segment, Chr 1, ERATO Doi 471, expressed	0.039	-2.0
1427325_s_at	Akna	AT-hook transcription factor	0.044	-2.0
1436171_at	Arhgap30	Rho GTPase activating protein 30	0.044	-2.0
1418826_at	Ms4a6b	membrane-spanning 4-domains, subfamily A, member 6B	0.041	-2.0
1434458_at	Fst	follistatin	0.041	-2.0
1419405_at	Nmb	neuromedin B	0.041	-2.0
1415964_at	Scd1	stearoyl-Coenzyme A desaturase 1	0.044	-1.9
1436905_x_at	Laptm5	lysosomal-associated protein transmembrane 5	0.044	-1.9
1452431_s_at	H2-Aa	histocompatibility 2, class II antigen A, alpha	0.044	-1.9
1452405_x_at	Tcra	T-cell receptor alpha chain	0.048	-1.9
1428804_at	Mfap3l	microfibrillar-associated protein 3-like	0.042	-1.9
1417541_at	Hells	helicase, lymphoid specific	0.044	-1.9
1421365_at	Fst	follistatin	0.043	-1.9
1451513_x_at	Serpina1b	serine (or cysteine) preptidase inhibitor, clade A, member 1b	0.044	-1.9
1456307_s_at	Adcy7	adenylate cyclase 7	0.049	-1.9
1425738_at	LOC100047222	similar to Ig kappa chain V-III region PC 6684	0.045	-1.8

		immunoglobulin Vl chain		
1425294_at	Slamf8	SLAM family member 8	0.048	-1.8
1423954_at	C3	complement component 3	0.046	-1.8
1424528_at	Cgref1	cell growth regulator with EF hand domain 1	0.049	-1.8
1429954_at	Clec4a3	C-type lectin domain family 4, member a3	0.048	-1.8
1427455_x_at	Gm10883	Ig kappa chain/	0.048	-1.8
1430700_a_at	Pla2g7	phospholipase A2, group VII (platelet-activating factor acetylhydrolase, plasma)	0.049	-1.7

Supplementary Table 4: 107 downregulated genes in treated *Irs2*$^{-/-}$ compared to untreated *Irs2*$^{-/-}$ animals.

Gene ID (Affymetrix)	Gene symbol	Gene name	q-Values	Fold-change
1449434_at	Car3	carbonic anhydrase 3	0.015	-3.8
1416957_at	Pou2af1	POU domain, class 2, associating factor 1	0.006	-3.3
1417851_at	Cxcl13	chemokine (C-X-C motif) ligand 13	0.006	-3.2
1417867_at	Cfd	complement factor D (adipsin)	0.032	-3.1
1448377_at	Slpi	secretory leukocyte peptidase inhibitor	0.015	-2.9
1452815_at	P2ry10	purinergic receptor P2Y, G-protein coupled 10	0.014	-2.8
1448859_at	Cxcl13	chemokine (C-X-C motif) ligand 13	0.014	-2.8
1423226_at	Ms4a1	membrane-spanning 4-domains, subfamily A, member 1	0.018	-2.7
1419178_at	Cd3g	CD3 antigen, gamma polypeptide	0.015	-2.7
1440837_at	H2-Ob	histocompatibility 2, O region beta locus	0.018	-2.7
1436329_at	Egr3	early growth response 3	0.024	-2.6
1423466_at	Ccr7	chemokine (C-C motif) receptor 7	0.024	-2.5
1455656_at	Btla	B and T lymphocyte associated	0.024	-2.5
1455530_at	Ighv14-2	immunoglobulin heavy variable V14-2	0.024	-2.5
1455269_a_at	Coro1a	coronin, actin binding protein 1A	0.021	-2.5
1416246_a_at	Coro1a	coronin, actin binding protein 1A	0.023	-2.5
1416714_at	Irf8	interferon regulatory factor 8	0.024	-2.5
1450912_at	Ms4a1	membrane-spanning 4-domains, subfamily A, member 1	0.024	-2.5
1427301_at	Cd48	CD48 antigen	0.023	-2.5
1450997_at	Stk17b	serine/threonine kinase 17b (apoptosis-inducing)	0.024	-2.4
1456014_s_at	Fermt3	cDNA sequence BC032204	0.023	-2.4

1427837_at	Igk-V32	similar to Unknown (protein for MGC:103328)	0.044	-2.4
1456328_at	Bank1	B-cell scaffold protein with ankyrin repeats 1	0.031	-2.4
1419684_at	Ccl8	chemokine (C-C motif) ligand 8	0.024	-2.4
1434067_at	AI662270	expressed sequence AI662270	0.024	-2.3
1428735_at	Cd69	CD69 antigen	0.044	-2.3
1447918_x_at	Igl-V1	Immunoglobulin lambda chain, variable 1	0.024	-2.3
1425226_x_at	LOC665506	T-cell receptor beta, variable 13	0.031	-2.3
1423452_at	Stk17b	serine/threonine kinase 17b (apoptosis-inducing)	0.038	-2.3
1439956_at	Ms4a6b	membrane-spanning 4-domains, subfamily A, member 6B	0.026	-2.3
1436312_at	Ikzf1	IKAROS family zinc finger 1	0.035	-2.3
1419135_at	Ltb	lymphotoxin B	0.030	-2.3
1422124_a_at	Ptprc	protein tyrosine phosphatase, receptor type, C	0.030	-2.2
1454169_a_at	Epsti1	epithelial stromal interaction 1 (breast)	0.031	-2.2
1455660_at	Csf2rb	colony stimulating factor 2 receptor, beta, low-affinity (granulocyte-macrophage)	0.031	-2.2
1418770_at	Cd2	CD2 antigen	0.031	-2.2
1417640_at	Cd79b	CD79B antigen	0.037	-2.2
1452087_at	Epsti1	epithelial stromal interaction 1 (breast)	0.030	-2.2
1418203_at	Pmaip1	phorbol-12-myristate-13-acetate-induced protein 1	0.045	-2.2
1417995_at	Ptpn22	protein tyrosine phosphatase, non-receptor type 22 (lymphoid)	0.037	-2.2
1435331_at	Pyhin1	hypothetical protein LOC100048304///pyrin and HIN domain family, member 1	0.030	-2.2
1440834_at	Slc5a10	solute carrier family 5 (sodium/glucose cotransporter), member 10	0.030	-2.2
1439141_at	Gpr18	G protein-coupled receptor 18	0.031	-2.2
1436576_at	Fam26f	RIKEN cDNA A630077B13 gene	0.033	-2.2
1426772_x_at	Gm6273 -J	T-cell receptor beta, joining region	0.033	-2.2
1427329_a_at	Igh-6	immunoglobulin heavy chain 6 (heavy chain of IgM)	0.031	-2.1
1427860_at	LOC100047162	similar to Ig kappa chain V-V region MPC11 precursor	0.035	-2.1
1460218_at	Cd52	CD52 antigen	0.036	-2.1
1415983_at	Lcp1	lymphocyte cytosolic protein 1	0.037	-2.1
1418930_at	Cxcl10	chemokine (C-X-C motif) ligand 10///similar to Small inducible cytokine B10 precursor (CXCL10) (Interferon-gamma-induced protein CRG-2) (Gamma-IP10) (IP-10) (C7)	0.038	-2.1
1443783_x_at	H2-Aa	Histocompatibility 2, class II antigen A, alpha	0.035	-2.1
1460423_x_at	Gm5571 /// Igk-V1	Ig kappa chain	0.038	-2.1
1417620_at	Rac2	RAS-related C3 botulinum substrate 2	0.037	-2.1

1452463_x_at	Gm10883	predicted gene, ENSMUSG00000076577	0.036	-2.1
1434068_s_at	AI662270	expressed sequence AI662270	0.038	-2.1
1419004_s_at	Bcl2a1a	B-cell leukemia/lymphoma 2 related protein A1a	0.040	-2.1
1435477_s_at	Fcgr2b	Fc receptor, IgG, low affinity IIb	0.037	-2.1
1425396_a_at	Lck	lymphocyte protein tyrosine kinase	0.039	-2.1
1436847_s_at	Cdca8	cell division cycle associated 8	0.040	-2.1
1435959_at	Arhgap15	Rho GTPase activating protein 15	0.040	-2.1
1451335_at	Plac8	placenta-specific 8	0.038	-2.1
1450241_a_at	Evi2a	ecotropic viral integration site 2a	0.039	-2.0
1419480_at	Sell	selectin, lymphocyte	0.044	-2.0
1416296_at	Il2rg	interleukin 2 receptor, gamma chain	0.041	-2.0
1448162_at	Vcam1	vascular cell adhesion molecule 1	0.038	-2.0
1427351_s_at	Igh-6	immunoglobulin heavy chain 6 (heavy chain of IgM)	0.036	-2.0
1431609_a_at	Acp5	acid phosphatase 5, tartrate resistant	0.041	-2.0
1430165_at	Stk17b	serine/threonine kinase 17b (apoptosis-inducing)	0.045	-2.0
1419481_at	Sell	selectin, lymphocyte	0.043	-2.0
1448617_at	Cd53	CD53 antigen	0.044	-2.0
1435465_at	Kbtbd11	kelch repeat and BTB (Luco et al.) domain containing 11	0.042	-2.0
1448823_at	Cxcl12	chemokine (C-X-C motif) ligand 12	0.037	-2.0
1417597_at	Cd28	CD28 antigen///similar to CD28 antigen	0.044	-2.0
1420994_at	B3gnt5	UDP-GlcNAc:betaGal beta-1,3-N-acetylglucosaminyltransferase 5	0.044	-2.0
1443687_x_at	H2-DMb2	histocompatibility 2, class II, locus Mb2	0.048	-2.0
1435560_at	Itgal	integrin alpha L	0.044	-2.0
1425084_at	Gimap7	GTPase, IMAP family member 7	0.044	-2.0
1449360_at	Csf2rb2	colony stimulating factor 2 receptor, beta 2, low-affinity (granulocyte-macrophage)	0.045	-2.0
1416295_a_at	Il2rg	interleukin 2 receptor, gamma chain	0.045	-2.0
1435330_at	Pyhin1	pyrin and HIN domain family, member 1	0.044	-2.0
1434152_at	Apol7c	apolipoprotein L, 3-like	0.044	-2.0
1426113_x_at	Tcra	T-cell receptor alpha chain	0.044	-2.0
1450678_at	Itgb2	integrin beta 2	0.044	-2.0
1451780_at	Blnk	B-cell linker	0.044	-2.0
1426454_at	Arhgdib	Rho, GDP dissociation inhibitor (GDI) beta	0.044	-2.0
1450291_s_at	Ms4a4c	membrane-spanning 4-domains, subfamily A, member 4C	0.045	-2.0
1436293_x_at	Ildr2	DNA segment, Chr 1, ERATO Doi 471, expressed	0.039	-2.0
1427325_s_at	Akna	AT-hook transcription factor	0.044	-2.0
1436171_at	Arhgap30	Rho GTPase activating protein 30	0.044	-2.0

1418826_at	Ms4a6b	membrane-spanning 4-domains, subfamily A, member 6B	0.041	-2.0
1434458_at	Fst	follistatin	0.041	-2.0
1419405_at	Nmb	neuromedin B	0.041	-2.0
1415964_at	Scd1	stearoyl-Coenzyme A desaturase 1	0.044	-1.9
1436905_x_at	Laptm5	lysosomal-associated protein transmembrane 5	0.044	-1.9
1452431_s_at	H2-Aa	histocompatibility 2, class II antigen A, alpha	0.044	-1.9
1452405_x_at	Tcra	T-cell receptor alpha chain	0.048	-1.9
1428804_at	Mfap3l	microfibrillar-associated protein 3-like	0.042	-1.9
1417541_at	Hells	helicase, lymphoid specific	0.044	-1.9
1421365_at	Fst	follistatin	0.043	-1.9
1451513_x_at	Serpina1b	serine (or cysteine) preptidase inhibitor, clade A, member 1b	0.044	-1.9
1456307_s_at	Adcy7	adenylate cyclase 7	0.049	-1.9
1425738_at	LOC100047222	similar to Ig kappa chain V-III region PC 6684///similar to anti-glycoprotein-B of human Cytomegalovirus immunoglobulin Vl chain	0.045	-1.8
1425294_at	Slamf8	SLAM family member 8	0.048	-1.8
1423954_at	C3	complement component 3	0.046	-1.8
1424528_at	Cgref1	cell growth regulator with EF hand domain 1	0.049	-1.8
1429954_at	Clec4a3	C-type lectin domain family 4, member a3	0.048	-1.8
1430700_a_at	Pla2g7	phospholipase A2, group VII (platelet-activating factor acetylhydrolase, plasma)	0.049	-1.7

Supplementary Table 5: 53 downregulated genes in treated *Irs2*$^{-/-}$ compared to treated WT animals.

Gene ID (Affymetrix)	Gene symbol	Gene name	q-Values	Fold-change
1457633_x_at	Cox6a2	cytochrome c oxidase, subunit VI a, polypeptide 2	0.000	-3.0
1443969_at	Irs2	insulin receptor substrate 2	0.000	-3.0
1454768_at	Kcnf1	potassium voltage-gated channel, subfamily F, member 1	0.000	-2.7
1416561_at	Gad1	glutamic acid decarboxylase 1	0.000	-2.6
1417607_at	Cox6a2	cytochrome c oxidase, subunit VI a, polypeptide 2	0.000	-2.6
1436087_at	Dpp10	dipeptidylpeptidase 10	0.000	-2.5
1430416_at	4931431B13Rik	RIKEN cDNA 4931431B13 gene	0.000	-2.3

1416562_at	Gad1	glutamic acid decarboxylase 1	0.001	-2.1
1444317_at	Pcdh15	protocadherin 15	0.007	-1.9
1434528_at	Aard	alanine and arginine rich domain containing protein	0.008	-1.9
1453403_at	2210019I11Rik	RIKEN cDNA 2210019I11 gene	0.017	-1.9
1441991_at	Prss53	cDNA sequence BC039632	0.010	-1.9
1443413_s_at	Trpm5	transient receptor potential cation channel, subfamily M, member 5	0.013	-1.9
1421558_at	T2	brachyury 2	0.011	-1.9
1422625_at	Ly6h	similar to Lymphocyte antigen 6H precursor (Ly-6H)	0.010	-1.8
1444769_at	Tex9	Testis expressed gene 9	0.016	-1.7
1437540_at	Mcoln3	mucolipin 3	0.031	-1.7
1418783_at	Trpm5	transient receptor potential cation channel, subfamily M, member 5	0.029	-1.7
1436661_at	Dpp10	dipeptidylpeptidase 10	0.026	-1.6
1454632_at	Tmem229b	RIKEN cDNA 6330442E10 gene	0.030	-1.6
1437376_at	Adam32	a disintegrin and metallopeptidase domain 32	0.032	-1.6
1419584_at	Ttc28	tetratricopeptide repeat domain 28	0.029	-1.6
1437782_at	Cntnap2	contactin associated protein-like 2	0.033	-1.6
1444965_at	E130002L11Rik	RIKEN cDNA E130002L11 gene	0.030	-1.6
1454782_at	Bai3	brain-specific angiogenesis inhibitor 3	0.031	-1.6
1422153_a_at	Asb11	ankyrin repeat and SOCS box-containing protein 11	0.046	-1.6
1435858_at	Tmem215	Transcribed locus	0.036	-1.6
1417030_at	Tmem206	RIKEN cDNA 2310028N02 gene	0.029	-1.6
1458866_at	Tmem215	RIKEN cDNA A930001M12 gene	0.036	-1.5
1429344_at	9.13E+15	hypothetical 9130022E09	0.036	-1.5

1435435_at	Cttnbp2	cortactin binding protein 2	0.044	-1.5
1449520_at	Ttc28	tetratricopeptide repeat domain 28	0.036	-1.5
1417443_at	Fam151a	cDNA sequence BC026682	0.049	-1.5
1422871_at	Kcnj12	potassium inwardly-rectifying channel, subfamily J, member 12	0.039	-1.5
1455876_at	Slc4a7	solute carrier family 4, sodium bicarbonate cotransporter, member 7	0.037	-1.5
1422330_at	Glp1r	glucagon-like peptide 1 receptor	0.034	-1.5
1421286_a_at	Atp4a	ATPase, H+/K+ exchanging, gastric, alpha polypeptide	0.046	-1.4
1455365_at	Cdh8	cadherin 8	0.043	-1.4
1430591_at	Ddc	dopa decarboxylase	0.034	-1.4
1434709_at	Nrcam	neuron-glia-CAM-related cell adhesion molecule	0.049	-1.4
1448552_s_at	Tmem206	RIKEN cDNA 2310028N02 gene	0.042	-1.4
1419402_at	Mns1	meiosis-specific nuclear structural protein 1	0.043	-1.4
1457528_at	Slc4a7	solute carrier family 4, sodium bicarbonate cotransporter, member 7	0.036	-1.4
1435456_at	Ttc28	tetratricopeptide repeat domain 28	0.047	-1.4
1437060_at	Olfm4	olfactomedin 4	0.049	-1.4
1449224_at	Trpm5	transient receptor potential cation channel, subfamily M, member 5	0.050	-1.4
1449240_at	Gsbs	G substrate	0.033	-1.4
1449409_at	Sult1c2	sulfotransferase family, cytosolic, 1C, member 2	0.045	-1.4
1417031_at	Tmem206	RIKEN cDNA 2310028N02 gene	0.048	-1.3
1420851_at	Pard6g	par-6 partitioning defective 6 homolog gamma (C. elegans)	0.050	-1.3
1436076_at	Dlgap1	discs, large (Drosophila) homolog-associated protein 1	0.049	-1.3

1427509_at	Baiap3	BAI1-associated protein 3	0.045	-1.3
1456331_at	9130023H24Rik	RIKEN cDNA 9130023H24 gene	0.048	-1.3

Supplementary Table 6: 125 upregulated genes in treated *Irs2*$^{-/-}$ compared to treated WT animals.

Gene ID (Affymetrix)	Gene symbol	Gene name	q-Values	Fold-change
1416297_s_at	Reg3b	regenerating islet-derived 3 beta	0.000	4.0
1454638_a_at	Pah	phenylalanine hydroxylase	0.000	3.4
1416783_at	Tac1	tachykinin 1	0.002	3.2
1416203_at	Aqp1	aquaporin 1	0.004	3.0
1428664_at	Vip	vasoactive intestinal polypeptide	0.008	2.9
1427351_s_at	Igh-6	immunoglobulin heavy chain 6 (heavy chain of IgM)	0.009	2.7
1418287_a_at	Dmbt1	deleted in malignant brain tumors 1	0.011	2.7
1449368_at	Dcn	decorin	0.009	2.6
1449495_at	Reg3a	regenerating islet-derived 3 alpha	0.011	2.6
1427883_a_at	Col3a1	collagen, type III, alpha 1	0.009	2.6
1435386_at	Vwf	Von Willebrand factor homolog	0.012	2.4
1417023_a_at	Fabp4	fatty acid binding protein 4, adipocyte	0.014	2.4
1452417_x_at	2010205A11Rik	immunoglobulin kappa chain variable 21	0.022	2.4
1424009_at	Reg3d	regenerating islet-derived 3 delta	0.018	2.4
1427329_a_at	Igh-6	immunoglobulin heavy chain 6 (heavy chain of IgM)	0.023	2.4
1450857_a_at	Col1a2	collagen, type I, alpha 2	0.014	2.4
1456292_a_at	Vim	vimentin	0.023	2.3
1427660_x_at	Gm10883	immunoglobulin kappa chain variable 21	0.026	2.3
1423607_at	Lum	lumican	0.023	2.2

1430027_at	1810028F09Rik	RIKEN cDNA 1810028F09 gene	0.024	2.2
1451263_a_at	Fabp4	fatty acid binding protein 4, adipocyte	0.021	2.2
1416405_at	Bgn	biglycan	0.021	2.2
1415897_a_at	Mgst1	microsomal glutathione S-transferase 1	0.022	2.2
1437438_x_at	Pnliprp2	pancreatic lipase-related protein 2	0.023	2.2
1427371_at	Abca8a	ATP-binding cassette, sub-family A (ABC1), member 8a	0.022	2.2
1437277_x_at	Tgm2	transglutaminase 2, C polypeptide	0.022	2.2
1416266_at	Pdyn	prodynorphin	0.022	2.2
1449452_a_at	Gp2	glycoprotein 2 (zymogen granule membrane)	0.023	2.2
1460668_at	Gal	galanin	0.022	2.1
1429159_at	Itih5	inter-alpha (globulin) inhibitor H5	0.022	2.1
1437015_x_at	Pla2g1b	phospholipase A2, group IB, pancreas	0.024	2.1
1418511_at	Dpt	dermatopontin	0.022	2.1
1419573_a_at	Lgals1	lectin, galactose binding, soluble 1	0.022	2.1
1415905_at	Reg1	regenerating islet-derived 1	0.023	2.1
1456523_at	Gm2115	expressed sequence C77713	0.023	2.1
1437405_a_at	Igfbp4	insulin-like growth factor binding protein 4	0.022	2.1
1424683_at	Fam134b	family with sequence similarity 134, member B	0.021	2.1
1424007_at	Gdf10	growth differentiation factor 10	0.021	2.1
1448323_a_at	Bgn	biglycan	0.022	2.1
1424208_at	Ptger4	prostaglandin E receptor 4 (subtype EP4)	0.025	2.0
1455439_a_at	Lgals1	lectin, galactose binding, soluble 1	0.026	2.0
1438118_x_at	Vim	vimentin	0.026	2.0
1438617_at	Serpina7	serine (or cysteine) peptidase inhibitor, clade A (alpha-1 antiproteinase, antitrypsin), member 7	0.027	1.9

1423523_at	Aass	aminoadipate-semialdehyde synthase	0.028	1.9
1415938_at	Spink3	serine peptidase inhibitor, Kazal type 3	0.037	1.9
1452968_at	Cthrc1	collagen triple helix repeat containing 1	0.028	1.9
1455900_x_at	Tgm2	transglutaminase 2, C polypeptide	0.028	1.9
1450505_a_at	Fam134b	family with sequence similarity 134, member B	0.029	1.9
1448823_at	Cxcl12	chemokine (C-X-C motif) ligand 12	0.028	1.9
1435307_at	Ankrd34b	ankyrin repeat domain 34B	0.043	1.9
1448186_at	Pnliprp2	pancreatic lipase-related protein 2	0.038	1.9
1450641_at	Vim	vimentin	0.032	1.9
1448107_x_at	Klk1	kallikrein 1	0.043	1.9
1415837_at	Klk1	kallikrein 1	0.043	1.9
1416468_at	Aldh1a1	aldehyde dehydrogenase family 1, subfamily A1	0.034	1.9
1423954_at	C3	complement component 3; similar to complement component C3 prepropeptide, last	0.034	1.9
1417290_at	Lrg1	leucine-rich alpha-2-glycoprotein 1	0.034	1.8
1428434_at	Zcchc12	zinc finger, CCHC domain containing 12	0.034	1.8
1417494_a_at	Cp	ceruloplasmin	0.035	1.8
1437056_x_at	Crispld2	cysteine-rich secretory protein LCCL domain containing 2	0.035	1.8
1433428_x_at	Tgm2	transglutaminase 2, C polypeptide	0.035	1.8
1423110_at	Col1a2	collagen, type I, alpha 2	0.034	1.8
1417413_at	Cuzd1	CUB and zona pellucida-like domains 1	0.038	1.8
1448259_at	Fstl1	follistatin-like 1	0.037	1.8
1434803_a_at	Sycn	syncollin	0.043	1.8
1416778_at	Sdpr	serum deprivation response	0.038	1.8
1434728_at	Gria3	glutamate receptor, ionotropic, AMPA3 (alpha 3)	0.040	1.8

1415954_at	Try4	protease, serine, 1 (trypsin 1)	0.040	1.8
1437165_a_at	Pcolce	procollagen C-endopeptidase enhancer protein	0.039	1.7
1419663_at	Ogn	osteoglycin	0.039	1.7
1451228_a_at	Sycn	syncollin	0.045	1.7
1423407_a_at	Fbln2	fibulin 2	0.040	1.7
1421195_at	Cckar	cholecystokinin A receptor	0.042	1.7
1434141_at	Gucy1a3	guanylate cyclase 1, soluble, alpha 3	0.040	1.7
1423754_at	Ifitm3	interferon induced transmembrane protein 3	0.040	1.7
1452217_at	Ahnak	AHNAK nucleoprotein (desmoyokin)	0.042	1.7
1426278_at	Ifi27l2a	interferon, alpha-inducible protein 27 like 2A	0.040	1.7
1417495_x_at	Cp	ceruloplasmin	0.041	1.7
1448734_at	Cp	ceruloplasmin	0.043	1.7
1453523_at	Krtap17-1	keratin associated protein 17-1	0.043	1.7
1428547_at	Nt5e	5' nucleotidase, ecto	0.041	1.7
1416779_at	Sdpr	serum deprivation response	0.043	1.7
1423756_s_at	Igfbp4	insulin-like growth factor binding protein 4	0.050	1.7
1450883_a_at	Cd36	CD36 antigen	0.043	1.7
1456156_at	Lepr	leptin receptor	0.042	1.6
1442340_x_at	Cyr61	cysteine rich protein 61	0.043	1.6
1448213_at	Anxa1	annexin A1	0.044	1.6
1415834_at	Dusp6	dual specificity phosphatase 6	0.043	1.6
1441793_at	Rnf39	ring finger protein 39	0.042	1.6
1456591_x_at	Akap3	A kinase (PRKA) anchor protein 3	0.045	1.6
1423281_at	Stmn2	stathmin-like 2	0.042	1.6

1448980_at	Ghrl	ghrelin	0.043	1.6
1416168_at	Serpinf1	serine (or cysteine) peptidase inhibitor, clade F, member 1	0.043	1.6
1434369_a_at	Cryab	crystallin, alpha B	0.049	1.6
1436044_at	Scn7a	sodium channel, voltage-gated, type VII, alpha	0.045	1.6
1424254_at	Ifitm1	interferon induced transmembrane protein 1	0.045	1.6
1426617_a_at	Ttyh1	tweety homolog 1 (Drosophila)	0.045	1.6
1419298_at	Pon3	paraoxonase 3	0.045	1.6
1418990_at	Ms4a4d	membrane-spanning 4-domains, subfamily A, member 4D	0.050	1.6
1425848_a_at	Dusp26	dual specificity phosphatase 26 (putative)	0.050	1.6
1452348_s_at	Ifi203	predicted gene 2785	0.050	1.5

Supplementary Table 7: 101 genes upregulated only in treated *Irs2*$^{-/-}$ compared to treated WT animals.

Gene ID (Affymetrix)	Gene symbol	Gene name	q-Values	Fold-change
1448290_at	Reg3b	pancreatitis-associated protein	0.000	5.3
1416297_s_at	Reg3b	pancreatitis-associated protein	0.000	4.0
1422682_s_at	Prss1	protease, serine, 1 (trypsin 1	0.003	3.9
1416139_at	Reg2	regenerating islet-derived 2	0.000	3.8
1450689_at	Prss3	similar to trypsinogen 15	0.012	3.4
1454638_a_at	Pah	phenylalanine hydroxylase	0.000	3.4
1416783_at	Tac1	tachykinin 1	0.002	3.2
1422825_at	Cartpt	CART prepropeptide	0.002	3.2
1424525_at	Grp	gastrin releasing peptide	0.004	3.1
1426766_at	6330403K07Rik	RIKEN cDNA 6330403K07 gene	0.002	3.1
1422915_at	Gast	gastrin	0.003	3.1

1416203_at	Aqp1	aquaporin 1	0.004	3.0
1454622_at	Slc38a5	solute carrier family 38, member 5	0.006	2.9
1419735_at	Csn3	casein kappa	0.006	2.9
1428664_at	Vip	vasoactive intestinal polypeptide	0.008	2.9
1419426_s_at	Ccl21a	chemokine (C-C motif) ligand 21a	0.009	2.8
1427351_s_at	Igh-6	immunoglobulin heavy chain 6 (heavy chain of IgM)	0.009	2.7
1424305_at	Igj	immunoglobulin joining chain	0.012	2.7
1418287_a_at	Dmbt1	deleted in malignant brain tumors 1	0.011	2.7
1449368_at	Dcn	decorin	0.009	2.6
1449495_at	Reg3a	regenerating islet-derived 3 alpha	0.011	2.6
1427883_a_at	Col3a1	procollagen, type III, alpha 1	0.009	2.6
1422918_at	1810009J06Rik	RIKEN cDNA 1810009J06 gene	0.021	2.6
1427455_x_at	Gm10883	Ig kappa chain	0.022	2.5
1435386_at	Vwf	Von Willebrand factor homolog	0.012	2.4
1417023_a_at	Fabp4	fatty acid binding protein 4, adipocyte	0.014	2.4
1452417_x_at	2010205A11Rik LOC100047628	RIKEN cDNA 2010205A11 gene	0.022	2.4
1424009_at	Reg3d	regenerating islet-derived 3 delta	0.018	2.4
1427329_a_at	Igh-6	immunoglobulin heavy chain 6 (heavy chain of IgM)	0.023	2.4
1450857_a_at	Col1a2	procollagen, type I, alpha 2	0.014	2.4
1456292_a_at	Vim	vimentin	0.023	2.3
1427660_x_at	Gm10883	Ig kappa chain	0.026	2.3
1423607_at	Lum	lumican	0.023	2.2
1430027_at	1810028F09Rik	RIKEN cDNA 1810028F09 gene	0.024	2.2
1451263_a_at	Fabp4	fatty acid binding protein 4, adipocyte	0.021	2.2

1416405_at	Bgn	biglycan	0.021	2.2
1415897_a_at	Mgst1	microsomal glutathione S-transferase 1	0.022	2.2
1437438_x_at	Pnliprp2	pancreatic lipase-related protein 2	0.023	2.2
1427371_at	Abca8a	ATP-binding cassette, sub-family A (ABC1), member 8a	0.022	2.2
1437277_x_at	Tgm2	transglutaminase 2, C polypeptide	0.022	2.2
1416266_at	Pdyn	prodynorphin	0.022	2.2
1449452_a_at	Gp2	glycoprotein 2 (zymogen granule membrane)	0.023	2.2
1460668_at	Gal	galanin	0.022	2.1
1429159_at	Itih5	inter-alpha (globulin) inhibitor H5	0.022	2.1
1437015_x_at	Pla2g1b	phospholipase A2, group IB, pancreas	0.024	2.1
1418511_at	Dpt	dermatopontin	0.022	2.1
1448789_at	Aldh1a3	aldehyde dehydrogenase family 1, subfamily A3	0.023	2.1
1419573_a_at	Lgals1	lectin, galactose binding, soluble 1	0.022	2.1
1415905_at	Reg1	regenerating islet-derived 1	0.023	2.1
1456523_at	Gm2115	expressed sequence C77713	0.023	2.1
1437405_a_at	Igfbp4	insulin-like growth factor binding protein 4	0.022	2.1
1424683_at	Fam134b	RIKEN cDNA 1810015C04 gene	0.021	2.1
1424007_at	Gdf10	growth differentiation factor 10	0.021	2.1
1448323_a_at	Bgn	biglycan	0.022	2.1
1417956_at	Cidea	cell death-inducing DNA fragmentation factor, alpha subunit-like effector A	0.024	2.0
1422694_at	Ttyh1	tweety homolog 1 (Drosophila)	0.023	2.0
1455582_at	---	Transcribed locus	0.023	2.0
1427789_s_at	Gnas	GNAS (guanine nucleotide binding protein, alpha stimulating) complex locus	0.027	2.0

1424208_at	Ptger4	prostaglandin E receptor 4 (subtype EP4)	0.025	2.0
1455439_a_at	Lgals1	lectin, galactose binding, soluble 1	0.026	2.0
1438118_x_at	Vim	vimentin	0.026	2.0
1416892_s_at	Fam107b	RIKEN cDNA 3110001A13 gene	0.027	2.0
1438617_at	Serpina7	Serine (or cysteine) peptidase inhibitor, clade A (alpha-1 antiproteinase, antitrypsin), member 7	0.027	1.9
1423523_at	Aass	aminoadipate-semialdehyde synthase	0.028	1.9
1436094_at	Vgf	VGF nerve growth factor inducible	0.028	1.9
1450344_a_at	Ptger3	prostaglandin E receptor 3 (subtype EP3)	0.035	1.9
1415938_at	Spink3	serine peptidase inhibitor, Kazal type 3	0.037	1.9
1452968_at	Cthrc1	collagen triple helix repeat containing 1	0.028	1.9
1455900_x_at	Tgm2	transglutaminase 2, C polypeptide	0.028	1.9
1450505_a_at	Fam134b	RIKEN cDNA 1810015C04 gene	0.029	1.9
1448823_at	Cxcl12	chemokine (C-X-C motif) ligand 12	0.028	1.9
1435307_at	Ankrd34b	RIKEN cDNA 6430502M16 gene	0.043	1.9
1448186_at	Pnliprp2	pancreatic lipase-related protein 2	0.038	1.9
1450641_at	Vim	vimentin	0.032	1.9
1448107_x_at	Klk1	kallikrein 1	0.043	1.9
1415837_at	Klk1	kallikrein 1	0.043	1.9
1416468_at	Aldh1a1	aldehyde dehydrogenase family 1, subfamily A1	0.034	1.9
1423954_at	C3	complement component 3	0.034	1.9
1417290_at	Lrg1	leucine-rich alpha-2-glycoprotein 1	0.034	1.8
1428434_at	Zcchc12	zinc finger, CCHC domain containing 12	0.034	1.8
1417494_a_at	Cp	ceruloplasmin	0.035	1.8
1437056_x_at	Crispld2	cysteine-rich secretory protein LCCL domain	0.035	1.8

		containing 2		
1433428_x_at	Tgm2	transglutaminase 2, C polypeptide	0.035	1.8
1423110_at	Col1a2	procollagen, type I, alpha 2	0.034	1.8
1417413_at	Cuzd1	CUB and zona pellucida-like domains 1	0.038	1.8
1448259_at	Fstl1	follistatin-like 1	0.037	1.8
1434803_a_at	Sycn	syncollin	0.043	1.8
1416778_at	Sdpr	serum deprivation response	0.038	1.8
1436662_at	Sorcs1	VPS10 domain receptor protein SORCS 1	0.040	1.8
1434728_at	Gria3	glutamate receptor, ionotropic, AMPA3 (alpha 3)	0.040	1.8
1415954_at	Try4	trypsin 4	0.040	1.8
1437165_a_at	Pcolce	procollagen C-endopeptidase enhancer protein	0.039	1.7
1419663_at	Ogn	osteoglycin	0.039	1.7
1451228_a_at	Sycn	syncollin	0.045	1.7
1423407_a_at	Fbln2	fibulin 2	0.040	1.7
1421195_at	Cckar	cholecystokinin A receptor	0.042	1.7
1434141_at	Gucy1a3	guanylate cyclase 1, soluble, alpha 3	0.040	1.7
1423754_at	Ifitm3	interferon induced transmembrane protein 3	0.040	1.7
1452217_at	Ahnak	AHNAK nucleoprotein (desmoyokin)	0.042	1.7
1426278_at	Ifi27l2a	interferon, alpha-inducible protein 27	0.040	1.7
1417495_x_at	Cp	ceruloplasmin	0.041	1.7
1448734_at	Cp	ceruloplasmin	0.043	1.7
1453523_at	Krtap17-1	keratin associated protein 17-1	0.043	1.7
1428547_at	Nt5e	5' nucleotidase, ecto	0.041	1.7
1416779_at	Sdpr	serum deprivation response	0.043	1.7

1450683_at	Tagln3	transgelin 3	0.042	1.7
1423756_s_at	Igfbp4	insulin-like growth factor binding protein 4	0.050	1.7
1450883_a_at	Cd36	CD36 antigen	0.043	1.7
1456156_at	Lepr	leptin receptor	0.042	1.6
1442340_x_at	Cyr61	cysteine rich protein 61	0.043	1.6
1448213_at	Anxa1	annexin A1	0.044	1.6
1415834_at	Dusp6	dual specificity phosphatase 6	0.043	1.6
1441793_at	Rnf39	Ring finger protein 39	0.042	1.6
1456591_x_at	Akap3	A kinase (PRKA) anchor protein 3	0.045	1.6
1423281_at	Stmn2	stathmin-like 2	0.042	1.6
1448980_at	Ghrl	ghrelin	0.043	1.6
1416168_at	Serpinf1	serine (or cysteine) peptidase inhibitor, clade F, member 1	0.043	1.6
1434369_a_at	Cryab	crystallin, alpha B	0.049	1.6
1436044_at	Scn7a	sodium channel, voltage-gated, type VII, alpha	0.045	1.6
1424254_at	Ifitm1	interferon induced transmembrane protein 1	0.045	1.6
1426617_a_at	Ttyh1	tweety homolog 1 (Drosophila)	0.045	1.6
1419298_at	Pon3	paraoxonase 3	0.045	1.6
1418990_at	Ms4a4d	membrane-spanning 4-domains, subfamily A, member 4D	0.050	1.6
1425848_a_at	Dusp26	dual specificity phosphatase 26 (putative)	0.050	1.6
1452348_s_at	Ifi203	interferon activated gene 203	0.050	1.5

Supplementary Table 8: 12 downregulated genes in treated WT compared to WT animals.

Gene ID (Affymetrix)	Gene symbol	Gene name	q-Values	Fold-change
1449368_at	Dcn	decorin	0.010	-2.6295045
1427126_at	Hspa1b	heat shock protein 1B	0.000	-2.3803965
1454638_a_at	Pah	phenylalanine hydroxylase	0.013	-2.225725
1429159_at	Itih5	inter-alpha (globulin) inhibitor H5	0.020	-2.0930735
1427127_x_at	Hspa1b	heat shock protein 1B	0.018	-2.081439
1427883_a_at	Col3a1	procollagen, type III, alpha 1	0.027	-1.9552045
1452318_a_at	Hspa1b	heat shock protein 1B	0.022	-1.938904
1424007_at	Gdf10	growth differentiation factor 10	0.022	-1.9178645
1427371_at	Abca8a	ATP-binding cassette, sub-family A (ABC1), member 8a	0.023	-1.8355645
1423607_at	Lum	lumican	0.031	-1.7221645
1450857_a_at	Col1a2	procollagen, type I, alpha 2	0.034	-1.6898415
1456292_a_at	Vim	vimentin	0.050	-1.599411

Supplementary Table 9: 16 upregulated genes in treated WT compared to WT animals.

Gene ID (Affymetrix)	Gene symbol	Gene name	q-Values	Fold-change
1459948_at	---	Mus musculus, clone IMAGE:1511633, mRNA	0.000	1.71907
1429703_at	2900072G11Rik	RIKEN cDNA 2900072G11 gene	0.030	1.485426
1443157_at	---	product:unclassifiable, full insert sequence	0.042	1.476153
1446596_at	---	NA	0.050	1.4171085
1439123_at	---	product:unclassifiable, full insert sequence	0.045	1.309506
1445395_at	---	product:hypothetical protein, full insert sequence	0.048	1.304167

1441589_at	---	product:unclassifiable, full insert sequence	0.049	1.290338
1433184_at	6720477C19Rik	RIKEN cDNA 6720477C19 gene	0.039	1.277744
1444693_at	---	NA	0.044	1.2619885
1445963_at	---	NA	0.041	1.2609245
1443697_at	---	NA	0.049	1.2559315
1447174_at	---	product:unclassifiable, full insert sequence	0.038	1.255911
1429702_at	2900072G11Rik	RIKEN cDNA 2900072G11 gene	0.048	1.2272225
1446972_at	D15Wsu126e	DNA segment, Chr 15, Wayne State University 126, expressed	0.049	1.1816985
1446598_at	---	product:unclassifiable, full insert sequence	0.046	1.1749865
1457177_at	---	product:unclassifiable, full insert sequence	0.049	1.1709475

IX Abbreviations

Apaf1	Apoptotic peptidase activating factor 1
ATP	Adenosine triphosphate
Bad	Bcl-2-associated death promoter
Bag	BCL2-associated athanogene 1
Bax	BCL2-associated X protein
Bbc3/Puma	BCL2 binding component 3
Bcl-2	B-cell lymphoma 2
Bid	BH3 interacting domain death agonist
Bik	BCL2-interacting killer
BrdU	Bromodeoxyuridine (5-bromo-2'-deoxyuridine,
BSA	Bovine serum albumine
cAMP	Cyclic adenosine monophosphate
CHOIR	Chinese hamster ovary with insulin receptor
Cidea	Cell death-inducing DFFA-like effector a
Ddit3/Chop	DNA-damage-inducible transcript 3
DMEM	Dulbecco's Modified Eagle Medium
DNA	Deoxyribonucleic acid
Dusp	Dual specificity protein phosphatase
ECL	Enhanced chemiluminescence
ELISA	Enzyme-linked immunosorbent assay
Erk1/2	Extracellular signal-related kinases-1 and -2
FBS	Fetal bovine serum
G6P	Glucose-6-phosphate
G6Pasa	Glucose-6-phosphatase
GK	Glucokinase
GLUT	Glucose transporter
GP	Glycogen phosphorylase
GPA	Active phosphorylated Glycogen phosphorylase
GS	Glycogen synthase

Gsdma	Gasdermin A
GSIS	Glucose-stimulated insulin secretion
HGP	Hepatic Glucose Production
HOMA	Homeostatic Model Assessment
IFG	Impaired fasting glucose
IGF	Insulin-like growth factor
IGT	Impaired glucose tolerance
IGTT	Intraperitoneal glucose tolerance test
IRS	Insulin receptor substrate
ITT	Insulin tolerance tests
MAPK	Mitogen-activated protein kinases
Mzb1/Rik	Marginal zone B and B1 cell-specific protein
nSTZ	Neonatally Streptozotocin
P/S	Penicillin/streptomycin
p53	Transformation related protein 53
PBS	Phosphate buffered saline
PCR	Polymerase chain reaction
Pdx1	Pancreatic and duodenal homeobox 1
PEPCK	Phosphoenolpyruvate carboxylase
PFK	Phosphofructokinase
PI-3 Kinase	Phosphoinositol-3-kinase
PI3K	Phosphatidylinositide 3-kinases
PKB/AKT	Protein kinase B
Pmaip1/Noxa	Phorbol-12-myristate-13-acetate-induced protein 1
PVDF	Polyvinylidene fluoride
Reg	Regenerating islet-derived
RNA	Ribonucleic acid
RPMI 1640	Roswell park Memorial Institute medium 1640
SDS-PAGE	Sodium dodecyl sulfate polyacrylamide gel electrophoresis
SEM	Standard error mean

Stk17b	Serine/threonine kinase 17b (apoptosis-inducing)
T1D	Type 1 Diabetes
T2D	Type 2 Diabetes
TbsT	Tris buffered saline-tween
Tris	Tris(hidroximetil)aminometano
Txnip	Thioredoxin interacting protein